TECHNISCHE UNIVERSITÄT MÜNCHEN
Department Chemie

Functional analysis and biotechnological applications of silaffin peptides

Carolin Lechner

Vollständiger Abdruck der von der Fakultät für Chemie der Technischen Universität München zur Erlangung des akademischen Grades eines Doktors der Naturwissenschaften (Dr. rer. nat.) genehmigten Dissertation.

Vorsitzender: Univ.-Prof. Dr. Michael Groll

Prüfer der Dissertation: 1. Univ.-Prof. Dr. Christian F. W. Becker,
Universität Wien, Österreich
2. Univ.-Prof. Dr. Dr. h. c. Bernhard Rieger
3. Univ.-Prof. Dr. Aymelt Itzen

Die Dissertation wurde am 01.10.2013 bei der Technischen Universität München eingereicht und durch die Fakultät für Chemie am 13.11.2013 angenommen.

Summary

Biomineralization processes leading to complex solid structures of inorganic material in biological systems has gained even increasing attention in biotechnological and medical research over the past decades. An outstanding example for biomineral morphogenesis is the formation of highly elaborate, nano-patterned silica shells by diatoms. Among the organic macromolecules that have been closely linked to the directed precipitation of silica in diatoms, silaffins play an extraordinary role. These peptides typically occur in complex posttranslationally modified forms and are directly involved in the silica deposition process in diatoms.

In this study, synthetic silaffin variants were characterized with respect to their silica precipitation properties and based on these findings novel approaches for silaffin-mediated silica immobilization of biomolecules for different purposes were developed.

Initially, the amino acid sequence of the unmodified silaffin R5 peptide was investigated to reveal intrinsic features of its silica precipitation activity. In this context different R5 variants were synthesized by solid phase peptide synthesis (SPPS) and their silica precipitation activity was analyzed based on particle morphology and amount of precipitated silica. The results confirmed the essential role of lysine residues in mediating condensation of silicic acid molecules and silica formation. The amino acids of the RRIL motif have to be present within the R5 sequence as well and contribute to formation of peptide assemblies, which serve as templates for silica precipitation. Altered morphologies of silica materials resulting from silaffin variants with scrambled sequences highlight the perfectly evolved amino acid sequence in terms of charges and functionalities for defined silica formation.

A series of silaffin peptides carrying different side chain modifications based on naturally occurring posttranslational modifications, such as trimethylation, polyamine attachment and phosphorylation, were obtained by SPPS and postsynthetic modification procedures. These specifically modified peptides enabled, for the first time, a systematic study of the effect of silaffin modifications on silica precipitation activity and on the morphology of the resulting silica material. The results revealed drastically altered performances in silica formation

depending on the particular modifications and emphasize the intricate interplay of attractive and repulsive electrostatic interactions between peptide side chains and silicic acid molecules during silica formation. The arrangement of different modifications in the context of the silaffin sequence leads to highly complex peptides that can self-assemble, mediate silicic acid polycondensation and play a major role in nano-patterning of diatom cell wall silica.

These new results regarding the functional analysis of silaffin silica precipitation properties contribute to unravel the intriguing process of silica biomineralization in diatoms and, in addition, these findings provide a rational basis for developing silaffins into efficient silica precipitation agents for novel biotechnological applications.

The ability to control formation and properties of silica with differently modified silaffin peptides was further exploited to achieve efficient immobilization of target biomolecules in silica matrices. Using fluorescently labeled silaffin peptides, it was verified that silaffins co-precipitate, under conditions used in this thesis, during silica formation. Therefore, silaffin peptides were subsequently developed into efficient reagents for simultaneous silica precipitation and direct incorporation of cargo molecules in the resulting silica material.

First, a general method for straightforward and selective conjugation of thiol-functionalized cargo-molecules with the silaffin peptide via a disulfide linkage was established. The ability of such silaffin-cargo conjugates for direct encapsulation of the cargo molecule during silaffin-mediated silica precipitation was demonstrated. Diffusion-based release of silaffin and cargo-conjugates was investigated over time and under different conditions. A strong dependency on the pH of the buffer medium with an increased release at acidic pH compared to neutral pH was observed. In addition, controlled release of the disulfide-linked silaffin-cargo conjugate under reducing conditions was analyzed. The cargo turned out to be rapidly cleaved from the conjugate and shows different kinetics of release from silica compared to the silaffin R5 peptide. With these findings, an important basis to set up a drug delivery system based on the autonomous formation of hybrid silica-peptide materials by using silaffin-cargo conjugates was provided.

Next, the method of expressed protein ligation was used to generate stable conjugates of target proteins with differently modified silaffin peptides. Protein-silaffin conjugates can be used for selective immobilization of sensitive proteins under mild conditions while maintaining control over silica properties by choice of different silaffin peptides. This novel

strategy for silica immobilization of proteins was exemplified with two proteins, eGFP and thioredoxin. Variants of the proteins with C-terminal thioester functionality that are required for expressed protein ligation were successfully obtained after thiol-induced cleavage of intein fusion proteins. The eGFP and thioredoxin thioester proteins were subsequently ligated to the modified silaffin variants in high yields. Silica precipitation experiments with these stable protein-silaffin conjugates clearly demonstrated an efficient and homogenous encapsulation of the protein in the silica material, highly superior to random entrapment resulting from simple co-precipitation experiments with the silaffin not covalently attached to the protein. Encapsulation of eGFP in the hybrid silica material was proven via fluorescence microscopy analysis and moreover, silica-immobilized eGFP was demonstrated to be stabilized against denaturation with SDS.

With the enzyme thioredoxin, the efficiency in loading of silica with protein was analyzed and a higher loading of silica with protein using the covalent protein-silaffin conjugates was shown. Analysis of diffusion-based release of thioredoxin from silica revealed that part of the protein became released over time. For both, entrapment and release rates, a dependency on the used silaffin variants for silica formation became apparent. Importantly, it was confirmed that silica immobilized thioredoxin retained its enzymatic activity.

In conclusion, the results presented here provide fundamental knowledge about silica precipitation activity of silaffins and contribute to decipher the silica biomineralization process in diatoms. In addition, modified silaffins were developed into efficient silica precipitation agents for advanced biotechnological applications such as drug delivery or efficient and tunable immobilization of enzymes under mild conditions.

Zusammenfassung

Als Biomineralisation wird die Bildung komplexer anorganischer Mineralien durch lebende Organismen bezeichnet. Die (bio-)chemischen Grundlagen dieser Vorgänge erlangten in den letzten Jahrzehnten vermehrt Aufmerksamkeit in der Forschung für die Entwicklung biotechnologischer und medizinischer Anwendungen. Ein herausragendes Beispiel für die Bildung und Formgestaltung von Biomineralien sind die äußerst kunstvoll aufgebauten, nano-strukturierten Silica-Schalen von Kieselalgen. In der Gruppe der organischen Makromoleküle, die in direktem Zusammenhang mit dem Prozess der Silica-Biomineralisation stehen, spielen Silaffine eine besondere Rolle. Diese Peptide, die typischerweise in einer komplex posttranslational modifizierten Form vorkommen, sind unmittelbar an der Silica-Bildung in Kieselalgen beteiligt.

In dieser Arbeit wurden synthetische Varianten der Silaffin-Peptide hinsichtlich ihrer Silica-präzipitierenden Eigenschaften charakterisiert. Basierend auf den gewonnen Erkenntnissen wurden neue Methoden für die Silaffin-gesteuerte Immobilisierung von Biomolekülen in Silica-Matrices für verschiedene Anwendungsfelder entwickelt.

Zunächst wurde die Aminosäuresequenz des unmodifizierten Silaffin R5 analysiert, um wesentliche Merkmale, die für die Silica-präzipitierende Eigenschaft dieses Peptids maßgeblich sind, zu identifizieren. Zu diesem Zweck wurden verschiedene Varianten des R5 Silaffin-Peptids mittels Festphasensynthese (SPPS) hergestellt. Im Anschluss wurde die Aktivität dieser Peptide basierend auf der Morphologie der erzeugten Silica-Partikel und der Menge an präzipitiertem Silica beurteilt. Die essentielle Rolle der Lysin-Seitenketten als Mediatoren der Kieselsäurekondensation und Bildung von Silica wurde bestätigt. Des Weiteren müssen die Aminosäuren des RRIL Motivs in der R5 Sequenz vorhanden sein. Diese Aminosäuren tragen zur Bildung von Peptidagglomeraten bei, welche als organisches Grundgerüst für die Silica-Bildung dienen. Silaffin Varianten mit veränderter Aminosäureabfolge hingegen bewirken eine Veränderung der Morphologie des entstehenden Silicas. Diese Ergebnisse verdeutlichen, dass die unterschiedlichen Ladungen und

Funktionalitäten innerhalb der Silaffin Sequenz perfekt aufeinander abgestimmt sind, um Präzipitation von Silica in definierter Form zu erreichen.

Anschließend wurden Silaffin Peptide mit verschiedenen Aminosäuremodifikationen, die auf den natürlich vorkommenden posttranlsationalen Modifikationen (PTMs) basieren, hergestellt. Mittels SPPS und Verfahren zur postsynthetischen Modifikation gelang die Synthese von Silaffin-Derivaten, die an spezifischen Aminosäureseitenketten tri-methyliert, phosphoryliert oder mit Polyaminen modifiziert sind. Mit Hilfe dieser spezifisch modifizierten Peptide war zum ersten Mal eine systematische Untersuchung des Einflusses von Silaffin-Modifikationen auf die Silica-präzipitierende Aktivität und die Morphologie des entstehenden Silica-Materials möglich. Die Ergebnisse zeigen einen sehr deutlichen Einfluss der einzelnen Modifikationen auf die Silica-Bildung. Die Präzipitation von Silica ist das Resultat eines aufwendigen Zusammenspiels elektrostatischer Wechselwirkungen zwischen Seitenketten der Peptide und den Kieselsäuremolekülen während der Bildung von Silica. Die Anordnung der verschiedenen Modifikationen im Rahmen der Silaffin-Sequenz resultiert in äußerst komplexen Peptiden, die sich zu größeren Agglomeraten zusammenlagern und die Polykondensation von Kieselsäure vermitteln können, sowie eine wichtige Rolle bei der Strukturierung der Zellwand von Kieselalgen spielen.

Diese neuen Ergebnisse, die aus der funktionelle Analyse von Silaffin-Peptiden hinsichtlich ihrer Silica-präzipitierenden Eigenschaften erhalten wurden, tragen dazu bei, den faszinierenden Prozess der Biomineralisation von Silica in Kieselalgen weiter zu entschlüsseln. Zudem wurde mit diesen Erkenntnissen eine fundierte Grundlage geschaffen, um Silaffine zu effizienten Silica-präzipitierenden Agenzien für neuartige biotechnologische Anwendungen zu entwickeln.

Diese Möglichkeit wurde im Weiteren genutzt, um mit unterschiedlich modifizierten Silaffinen die Bildung von Silica und dessen Eigenschaften zu kontrollieren und damit die effiziente Immobilisierung von Biomolekülen in Silica-Materialien zu erreichen. Mit Hilfe von fluoreszenzmarkierten Silaffin Peptiden wurde bestätigt, dass Silaffine unter den hier genutzten Bedingungen zur Bildung von Silica mit diesem co-präzipitieren. Daher wurden Silaffin-Peptide nachfolgend mit anderen Biomolekülen (Peptide und Proteine) verknüpft, was eine gleichzeitige Präzipitation von Silica und die direkte Inkorporation von Cargo-Molekülen in das resultierende Silica bewirkt.

Zunächst wurde eine generelle Methode für die einfache und selektive Verknüpfung eines Thiol-funktionalisierten Cargo-Moleküls mit einem Silaffin Peptid über eine Disulfidbindung etabliert. Das Potential dieser Silaffin-Cargo Konjugate für die direkte Verkapselung von Cargo-Molekülen während der Silaffin-vermittelten Präzipitation von Silica wurde gezeigt. Anschließend wurde die Freisetzung von Silaffin und Cargo-Konjugaten in Abhängigkeit von der Zeit und unter verschiedenen Umgebungsbedingungen untersucht. Dabei wurde eine starke Abhängigkeit vom pH-Wert des Puffers beobachtet, wobei sich eine erhöhte Freisetzung der Peptide bei saurerm pH verglichen mit neutralem pH zeigte. Zudem wurde die kontrollierte Freisetzung des Disulfid-verknüpften Silaffin-Cargo Konjugats under reduzierenden Bedingungen analysiert. Es zeigte sich, dass das Cargo-Molekül rasch vom Konjugat abgespalten wird und anschließend mit einer vom Silaffin R5 Peptid abweichenden Kinetik zügig aus den Silica Partikeln freigesetzt wird.

Diese Ergebnisse stellen eine wichtige Grundlage für die Entwicklung eines Systems für die Verabreichung und kontrollierte Freisetzung von Wirkstoffen dar, das auf der selbstinduzierten Ausbildung eines Hybridmaterials aus Silica und Peptid durch Silaffin-Cargo Konjugate beruht.

Nachfolgend wurden mit Hilfe der Methode der “Expressed Protein Ligation” stabile Konjugate bestehend aus ausgewählten Proteinen und unterschiedlich modifizierten Silaffin-Peptiden hergestellt. Mit diesen Protein-Silaffin Konjugaten kann eine selektive Immobilisierung von sensiblen Proteinen unter milden Bedingungen erreicht werden, wobei über die Wahl eines der verschieden modifizierten Silaffin-Peptide Einfluss auf die Eigenschaften des Silicas möglich ist.

Diese neuartige Strategie zur Silica-Immobilisierung von Proteinen wurde anhand von zwei Proteinen veranschaulicht, eGFP und Thioredoxin. Für die „Expressed Protein Ligation“ sind Varianten dieser Proteine erforderlich, die am C-Terminus ein Thioesterfunktion aufweisen. Diese Thioester-Proteine wurden durch Thiol-induzierte Abspaltung aus Intein Fusionsproteinen generiert. Anschließend wurden die eGFP- und Thioredoxin-Thioester Proteine in sehr hohen Ausbeuten mit den modifizierten Silaffin Varianten zu stabilen Protein-Silaffin Konjugaten ligiert und hinsichtlich ihrer Silica-präzipitierenden Eigenschaften analysiert. Dabei zeigte sich eine effiziente und homogene Verkapselung der Protein-Silaffin Konjugate im entstehenden Silica, die dem zufälligen Einbau bei Co-

Präzipitation von Proteinen, die nicht kovalenten mit Silaffinen verknüpft sind, deutlich überlegen ist. Fluoreszenzmikroskopische Analyse bestätigte den Einbau von eGFP in das entstehende Hybrid-Silica Material. Überdies konnte eine deutliche Stabilisierung des Silica-immobilisierten eGFP gegen Denaturierung mit SDS nachgewiesen werden.

Die Effizienz in der Beladung von Silica mit Proteinen wurde mit dem Enzym Thioredoxin untersucht. Dabei ergab sich, dass bei Verwendung der kovalenten Thioredoxin-Silaffin Konjugate eine größere Menge an Protein in das Silica verkapselt werden konnte im Vergleich zur zufälligen Co-Präzipitation von Thioredoxin, das nicht kovalent an Silaffin Peptide gebunden war. Untersuchungen zur Freisetzung von Thioredoxin aus dem Silica ergaben, dass ein Teil des verkapselten Proteins über die Zeit freigesetzt wird. Sowohl für die Effizienz der Verkapselung als auch für den Grad der Freisetzung konnte eine Abhängigkeit von den unterschiedlichen Silaffin-Varianten, die für die Präzipitation des Silica verwendet wurden, festgestellt werden. Überdies wurde bestätigt, dass die volle enzymatische Aktivität von Thioredoxin nach der Immobilisierung in Silica beibehalten wurde.

Die hier präsentierten Ergebnisse liefern grundlegende Fakten über die Silica-präzipitierenden Eigenschaften von Silaffin-Peptiden und tragen dazu bei, den Prozess der Biomineralisation von Silica in Kieselalgen zu entschlüsseln. Zudem konnten modifizierte Silaffin-Peptide für die effiziente und kontrollierte Präzipitation von Silica generiert werden. Mit Hilfe dieser Peptide konnten die Grundlagen für zukunftsweisende biotechnologische Anwendungen, wie z.B. für die kontrollierte Freisetzung von Wirkstoffen oder für die effektive und steuerbare Immobilisierung von Enzymen unter milden Bedingungen, geschaffen werden.

Table of contents

Chapter 1

Introduction

1.1 Silicon and silica in biological systems

Silicon is the second most abundant element in the Earth's crust and associated with oxygen, silicates and silica (SiO_2) constitute the most common compounds in the lithosphere.[1] Silicon rarely exists in its elemental form in nature. The predominant types are the crystalline silicate minerals quartz and alkali feldspars, as well as amorphous biogenic silica.[2] In contrast to the numerous different inorganic silicon-containing compounds, there are no naturally occurring bioorganic substances clearly identified that require or contain silicon. Nevertheless, silicon is supposed to be an essential element for many biological systems.[3,4]

In higher animals silicon is an essential nutrient required for proper growth and development.[5,6] The observed skeletal deformations in rats and chickens after silicon-depleted diets result from abnormalities in formation of collagen in connective tissue and of the cartilage matrix, rather than from improper bone formation.[7,8] The contribution of silicon to the structural integrity of connective tissues in terms of cross linking biopolymers, such as glycosaminoglycans and collagen is still controversially discussed.[9-11] In contrast, interaction of silicon with metal ions such as aluminum could explain the essentiality of silicon,[11,12] since formation of biologically inert hydroxyaluminosilicate counteracts the poisoning effects of aluminum due to a reduced gastrointestinal absorption.[13-15]

In higher plants, silicon content ranges from 0.1 - 10 % of the dry matter depending on the species.[16] Silicon is taken up by plants in the form of silicic acid from the soil and finally deposited as amorphous silica in various parts of the plants.[17-20] However, silicon is not

considered an essential element for plants but it is advantageous in numerous aspects. Silicon is beneficial for the growth of plants because it alleviates metal toxicity and the deposited silica provides structural support for strengthened cell walls. In addition, silica mediates resistance of plants to biotic and abiotic stress such as drought, salinity, and fungal or bacterial diseases, though the mechanisms of actions still need to be explored.[20-22]

Silicon is essential for a couple of specific biota including diatoms, siliceous sponges, radiolaria and silicoflagellates. These organisms require silicon for the production of siliceous structures, ranging from frustules, spicules and scales to various species-specific elaborate forms.[23] Exoskeletons made of silica are convenient to these organisms because they provide a large specific surface area, therefore high adsorption properties, and also a unique mechanical stability. Amongst the silica biomineralizing organisms diatoms are predominant and attract attention with their ornate silica frustules. Since silicon-deficiency not only effects diatom growth and cell wall formation but also interferes with metabolic processes,[24] silicon essentiality for diatoms is undisputed. As a consequence, the molecular mechanisms and the involved biomolecules of silica formation in diatoms are well studied.

1.2 Silica biomineralization in diatoms

Silica biomineralization, the formation and accumulation of amorphous, hydrated silica by living organisms, occurs globally on a vast scale. The amount of biogenic silica produced is estimated to be $(240 \pm 40) \times 10^{12}$ mol of silicon per year in surface waters, with the diatoms representing the most significant class of marine silica producing organisms.[25]

Moreover, silica biomineralization in diatoms substantially contributes to the marine silicon cycling. The biogeochemical cycle of silicon includes weathering of quartz and silicates to release silicic acid to the environment, which is in turn deposited as biogenic silica by diatoms. After the silica frustules have settled on the bottom as diatomaceous earth, the silica enters the sedimentary silicon pool and the cycle starts again.[2] Thus the diatoms do not only contribute to CO_2 fixation via photosynthesis and contribute to the carbon transport from surface to deep waters, they play a central role in nutrient and silicon cycling in aquatic biogeochemistry.[26]

1.2.1 Diatom biology and cell cycle

Diatoms, or formally *Bacillariophyta,* are eukaryotic, unicellular organisms taxonomically assigned to the *Stramenopiles*. The class of diatoms encompasses two major groups, the *Coscinodiscophytina* and the *Bacillariophytina* with the latter being further subdivided into *Mediophycea* and *Bacillariophycea*.[27] Diatoms are ubiquitously found in both marine and fresh water environments in all parts of the world as long as sufficient amounts of nutrients are present. Overall, there are more than 10,000 diatom species known to date, but it is estimated that more than 200,000 species exist worldwide.[28,29]

Diatoms are usually microscopic organisms with cell sizes ranging typically from 10-200 µm. Two general types can be distinguished based on shape and symmetry of the cell walls, the centric and the pennate diatoms (Figure 1-1).[30] Centric diatoms display radial symmetry and they either have a circular (radial centrics) or a multipolar, distorted center of symmetry (polar centrics). Pennate diatoms are generally elongated with bilateral symmetry and have a sternum alongside the longitudinal axis. Raphide pennates contain a slit in the sternum, the raphe, enabling movements on surfaces. Araphide pennates lack the raphe, and are nonmotile as the radial and polar centrics.

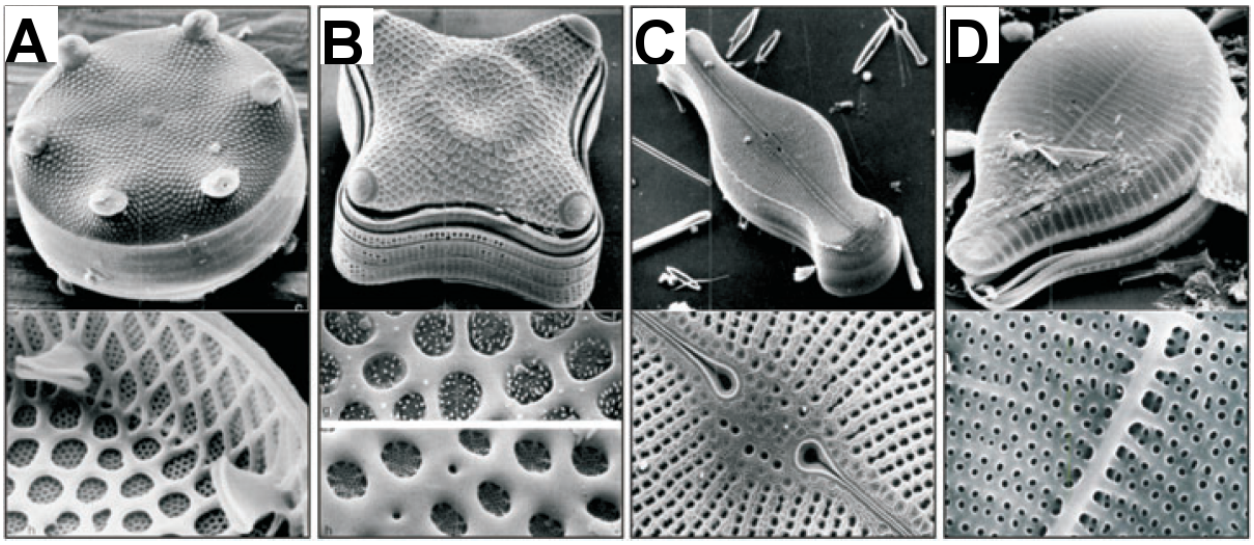

Figure 1-1 Scanning electron micrographs of different diatoms (taken from 31) **A)** *Aulacodiscus sp.*, radial centric*;* **B)** *Amphitetras sp.*, polar centric; **C)** *Didymosphenia sp.*, raphid pennate; **D)** *Podocystis sp*., araphid pennate.

The siliceous diatom cell walls are composed of two mirror-image halves, the epitheca and the hypotheca. Each theca consists of a capping valve and several girdle bands, which are silica strips running laterally along the axis of the cell. The last few girdle bands are summarized as the pleural band (Figure 1-2). The epitheca is slightly larger than the hypotheca, thus both fit into each other and together they completely enclose the protoplast. Whereas the valves generally display elaborate ornate silica architectures, the girdle bands are rather unstructured (Figure 1-1).

During their vegetative reproduction, which predominates over sexual reproduction,[30] diatoms need to build up a new silica cell wall. The required silicon for the silica formation is taken up from their aqueous habitats predominantly in the form of silicic acid.[32] The concentration of silicic acid ranges from 10-70 μM in surface waters and oceans,[25] but intracellular concentrations can reach up to several hundred millimolar.[33] Diatoms actively enrich silicic acid by specific silicic acid transporter proteins (SITs).[34-36] Sequence analysis of a variety of SIT genes have shown that the SIT proteins contain 10 transmembrane helices and a highly conserved sequence motif, GXQ (X = Q, G, R or M).[35] Based on this, a mechanistic model for the transporter protein mediated silicic acid uptake has been suggested. The highly conserved glutamine in the GXQ motif in two adjacent transmembrane domains could be directly involved in binding and transport of silicic acid. Recently, a diatom silicon transporter was heterologously expressed and reconstituted to functionality.[37] Site-directed mutagenesis of the glutamine residue in the GXQ motif will give further insights into the mechanism of silicic acid uptake into diatoms.

The intracellular transport and storage of silicic acid in diatoms is not well understood. Although silicic acid is soluble at neutral pH only until 2 mM, large pools of soluble silicon exceeding the level of silicic acid solubility have been observed in diatoms.[33] The molecular mechanisms or compounds involved to keep silicic acid soluble at high concentration and to prevent polycondensation of silicic acid to silica are unknown.

The silica deposition finally takes place in a specialized compartment, the silica deposition vesicle (SDV). The occurrence of SDVs could be shown in a variety of protists including diatoms, sponges and radiolarians, but the organelle could not yet be isolated for detailed biochemical analyses.[38] The membrane of the SDV, the silicalemma, possesses a membrane potential,[39] and the pH of the SDV lumen is acidic.[40] Association of the SDV with the

cytoskeleton, via actin microfilaments and microtubules, is important for silica molding, patterning and positioning of the SDV.[41]

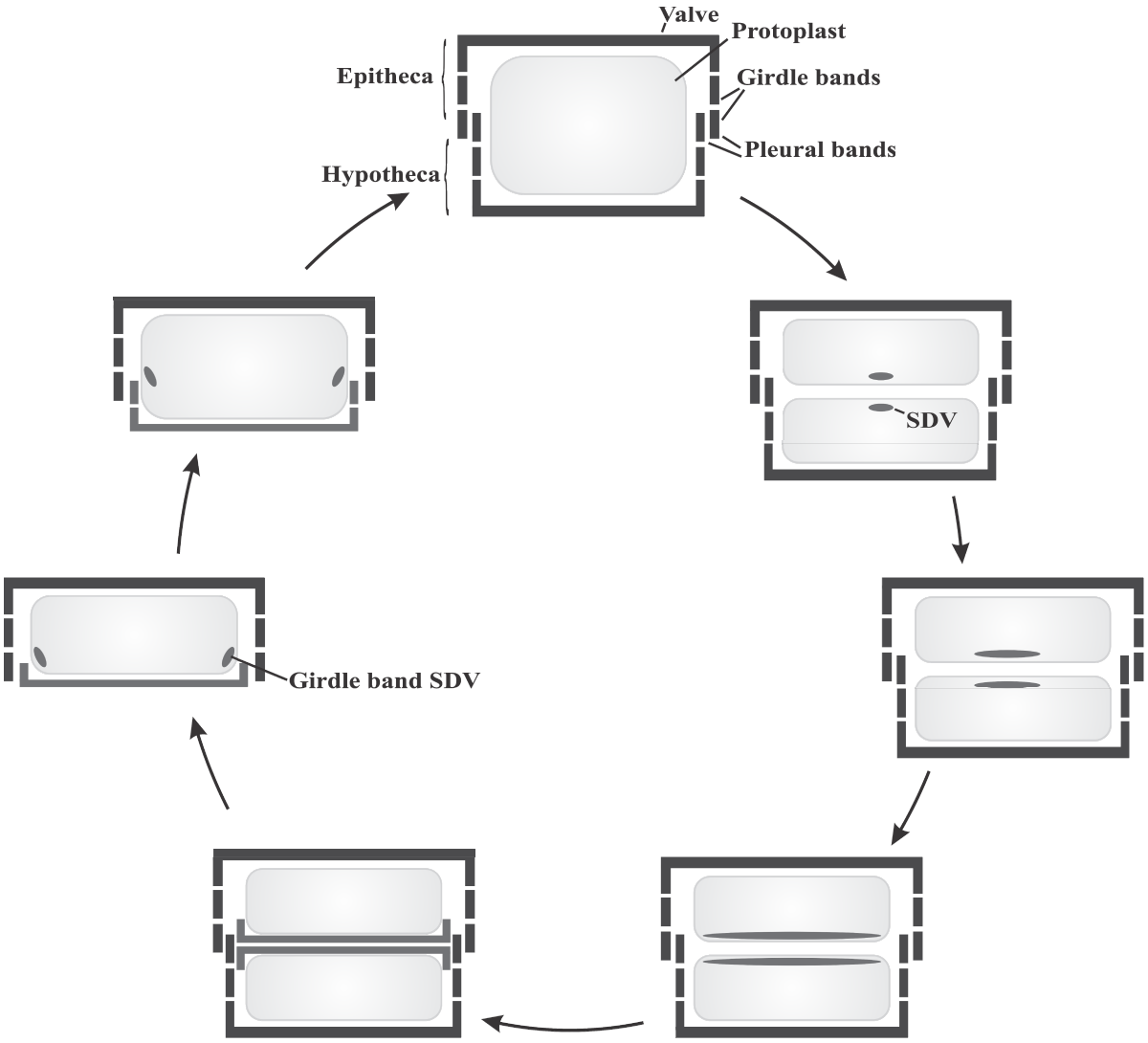

Figure 1-2 Schematic diatom cell cycle (according to 31)

The cell cycle of diatoms starts with mitosis followed by cytokinesis, resulting in the division of the protoplast in two daughter cells (Figure 1-2). However, before the daughter cells can separate, a new silica frustule has to be synthesized. The silica formation for synthesis of new valves is initiated in the SDVs. With progressing silica precipitation, the SDVs expand and once the silica synthesis is finished, the newly formed valve is deposited on the cell surface

of each protoplast by exocytosis of the SDV.[38] In addition, a stepwise synthesis of new siliceous girdle bands is necessary during cell growth to keep the protoplast enclosed in the silica shell. Depending on the species, girdle band formation can occur in different phases during cell cycle, either before or after cytokinesis.[42,43] Finally, the two sibling cells separate and during the interphase new silica girdle bands are required due to expansion of the protoplast. The girdle bands are each synthesized in separate SDVs and added to the frustule via exocytosis (Figure 1-2).

The diversity of silica nano-patterns of valves from different diatom species and the exact reproduction in each generation suggest a genomic encoding of molecular components that control silica formation and patterning. The fact of silica formation taking place in SDVs implies the occurrence of these components in the SDVs where they may act as initiators and nucleators of silica polycondensation and as structure directing molecules. To gain insight into the silica biomineralization process in diatoms, two major approaches are pursued: The analysis of diatom cell wall composition reveals organic molecules that are integral components of biosilica and potentially involved in the silica formation process (see chapter 1.2.2). In addition, sequencing and comparison of diatom genomes provides hints towards genetically encoded molecular processes of biosilicification. In this way several organic cell wall components, mainly proteins and polyamines, were identified that are associated with diatom biosilica and/or directly participate in silica formation.

1.2.2 Organic constituents of diatom cell walls and their role in silica formation

The siliceous frustules of diatoms are entirely encased in an organic matrix.[44] The initial identification of the unnatural amino acids 3,4-dihydroxyproline and *ε-N,N,N*-trimethyl-*δ*-hydroxylysine[45,46] and an overall analysis of diatom cell walls towards their amino acid content[47] clearly proved that proteins are inherent parts of diatom cell walls.

The first protein isolated from the cell wall of the diatom *Cylindrotheca fusiformis* was α1-frustulin, a glycoprotein of about 75 kDa. The frustulins were later shown to be general diatom cell wall proteins since they have been found in pennate and centric diatoms.[48,49] The

glycoproteins in the frustulin family range from 30 to 200 kDa and share multiple acidic and cysteine rich domains of about 50 amino acids (ACR domain), which show a specific affinity for Ca^{2+} ions. Frustulins are located in the organic matrix all over the cell wall, but they become associated with the silica only after silica formation and are therefore not considered to be involved in the biomineralization process.[50,51] Instead, a protective function for silica shells is suggested since silica dissolution of diatom frustules is accelerated by proteases.[52] In addition, frustulins are able to chelate cadmium and might provide a barrier against metal ion toxicity in diatoms.[53]

Another group of proteins isolated from the silica cell wall of the diatom species *C. fusiformis* are the pleuralins. The former name "HEPs" (HF extractable proteins) indicates the strong binding of these proteins to the cell wall requiring dissolution of silica with anhydrous HF for their release.[50] All pleuralins show a modular structure in which an N-terminal proline rich domain is followed by multiple repeats of the 90 amino acid PSCD domain, which is rich in proline, serine, cysteine and aspartate, followed by variable C-terminal domains. The name "pleuralins" refers to the localization of these proteins to the pleural bands of the epitheca.[43] During cell division, pleuralins are deposited to the cleavage furrow and become associated with the newly formed pleural band of the hypotheca, thus possibly providing a protection to the protoblast.

In the diatom *Thalassiosira pseudonana* proteins with biochemical similarity to the pleuralins could be identified in the girdle band region.[54] These proteins showed no sequence homologies to the pleuralins, but they are highly acidic, contain several chitin binding domains and a putative RGD cell attachment motif. The proteins show apparent molecular masses of 130 (p130) and 150 kDa (p150) and their expression was highly upregulated in copper stressed cells.[55] The morphological effect of the Cu^{2+} stress was inhibition of the cell cycle but elongation of cell bodies as a result of additional synthesized girdle bands. Therefore, a function of the stress induced cell wall proteins p130 and p150 in the girdle band region is plausible, potentially during cell division as stabilizing and shielding proteins.

Remarkably, application of advanced atomic force and ion-abrasion scanning electron microscopic techniques revealed nano- and microscale structures and the occurrence of organic matrices in the girdle band region of *T. pseudonana*.[56,57] Chitin could be proven to be a major constituent of an organic scaffold that resembles the shape of the biosilica in the

girdle band region.[58] These chitin based frameworks could serve as structural template for silica deposition[59] or as attachment site for other proteins. Notably, the stress induced cell wall proteins p130 and p150, which are also located in the girdle band region, contain multiple chitin binding domains.[54] Furthermore, another insoluble, but chitin-independent ring-shaped organic matrix, named microrings, could be identified in the girdle band region in *T. pseudonana*.[60] A class of proteins named cingulins is the integral component of these microrings. The cingulins are composed of highly repetitive structures with alternating KXXK-containing sequences, and tryptophan and/or tyrosine rich regions. Most importantly, the microrings with embedded cingulins display activity in silica formation *in vitro* and the characteristic nanopatterns of the microrings are maintained after silicification. Since the nanopatterns of the microrings also resemble characteristic silica structures in the girdle band region of *T. pseudonana*, the assumption that preassembled protein-based organic templates act in general as scaffolds for the construction of the nanostructured silica cell walls of diatoms is reasonable. Besides the cingulins, other biomolecules have been found to be associated with diatom cell walls and to be able to precipitate silica from a solution of silicic acid, the silaffins and long chain polyamines (LCPAs).

LCPAs are major components of the silica cell walls of diatoms and released only after dissolution of silica.[61] All LCPAs have a common structure of linear oligo-propylenimine chains attached to an amine-containing basis molecule, but depending on the species from which the LCPAs originate, they differ in the basis molecule and in the number and degree of methylation of propylenimine units (Figure 1-3).

The basis molecule is either putrescine, spermidine or 1,3-diaminopropane and the number of propylenimine units ranges from 6 up to 20.[61-64] The terminal nitrogen atoms of the propylenimine units are often found to be dimethylated and a positive charge is sometimes introduced by quaternary amino groups.[62,64] In centric diatoms the degree of internal *N*-methylation is much higher.[64] The inhibition of polyamine biosynthesis in *T. pseudonana* resulted in incomplete silica valve formation and a reduced thickness of the silica.[65] In contrast, the addition of native LCPAs to preparations of cingulin-microrings increased the silicification rate.[60] Together with the finding that isolated LCPAs have the ability to trigger the rapid formation of spherical silica particles from a solution of silicic acid, a direct involvement of LCPAs in silica biogenesis in diatoms is obvious.[61,66]

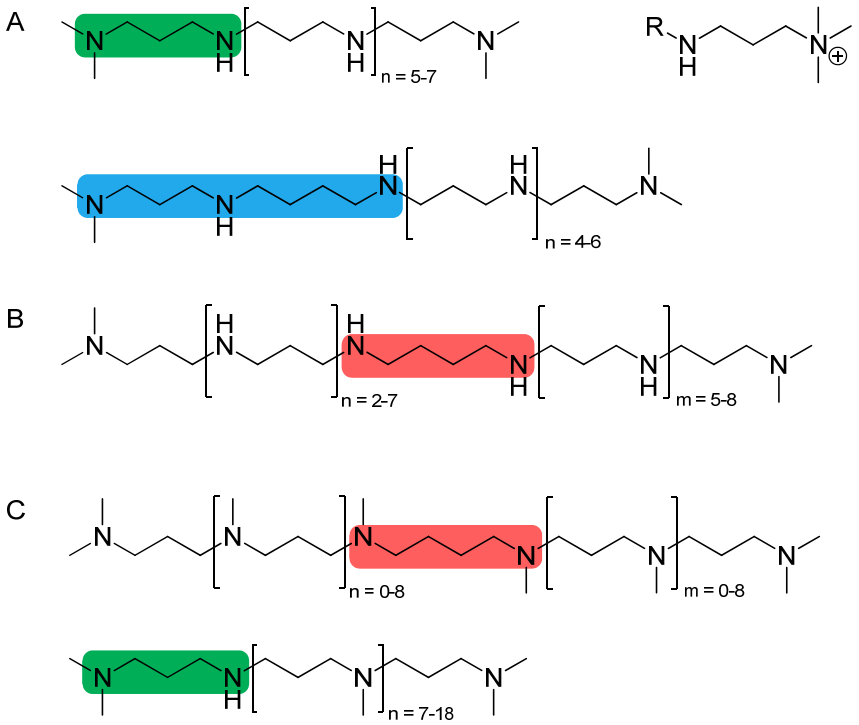

Figure 1-3 Structures of LCPAs from different diatom species: A) *T. pseudonana*, B) *C. fusiformis*, C) *S. turris*. The basis molecule is diaminopropane (green), spermidine (blue) or putrescine (red) (according to 64).

Silica precipitation activity of LCPAs *in vitro* strictly requires the presence of phosphate ions or other polyvalent anions such as pyrophosphate, sulfate or DNA in the reaction solution.[66] In addition, the species-specific LCPA structures hint towards an involvement of LCPAs not only in silica formation but also in patterning of specific silica structures in different diatom species.

Based on the cooperative action of polyamines and phosphate in silica formation, the idea of a biological phosphate-containing antagonist being present during cell wall formation in diatoms was established. Recently, this hypothesis was confirmed by the discovery of the silacidins in the diatom *T. pseudonana*.[67] The precursor protein of the silacidins is highly repetitive and upon proteolytic processing releases single peptides that are rich in aspartic and glutamic acid. The numerous serine residues within the silacidin sequence become phosphorylated converting them into strongly acidic and highly negatively charged peptides. A mixture of silacidins and polyamines from *T. pseudonana* resulted in the precipitation of silica spheres from a solution of silicic acid with the size of silica spheres directly correlating

with silacidin concentrations.[67] This effect has been described previously for phosphate ions,[66] but in contrast much lower concentrations of silacidins are required to yield comparable amounts of precipitated silica. Phosphorylation of the serine residues has been proven to be essential for activity.[68] Additionally, the expression of silacidins is distinctly increased during silicic acid starvation.[68] Therefore, a function in rescuing silica formation in silicic acid depleted habitats is proposed for silacidins.

Besides LCPAs, silaffins are the second major class of biomolecules identified from diatom cell walls. Silaffins are proteins combining both polyamine and polyanion functionalities in one molecule that fulfill a substantial function in the molecular process of silica formation in diatoms.

1.2.3 Silaffin proteins

Silaffins were initially identified from the pennate diatom *C. fusiformis*.[69] Extraction of the silica cell wall with anhydrous hydrogen fluoride to release tightly bound organic material led to isolation of high molecular weight pleuralins[50] and proteins in the mass range of 4 kDa, 8 kDa and 17 kDa. Because of their high affinity to silica, these proteins were generally named silaffins. The 4 kDa fraction was denoted silaffin-1A, the 8 kDa fraction was named silaffin-1B and the 17 kDa fraction silaffin-2. Based on preliminary sequence information of the silaffins, the corresponding gene *sil1* could be cloned from a *C. fusiformis* cDNA library. The open reading frame of *sil1* encodes a precursor protein, sil1p, of 265 amino acids (Figure 1-4).

The protein contains an *N*-terminal signal sequence for translocation into the endoplasmatic reticulum (ER) (amino acids 1-19) followed by an acidic N-terminal domain of unknown function (amino acids 20-107). The C-terminal part is strongly basic and highly repetitive (repetitive units R1-R7). Silaffin-1A and silaffin-1B both result from proteolytic processing of sil1p. Silaffin-1B derives from peptide R1, whereas silaffin-1A can be further subdivided into silaffin-$1A_1$, representing peptides R3-R7, and silaffin-$1A_2$ originating from peptide R2 (Figure 1-4).[69,70]

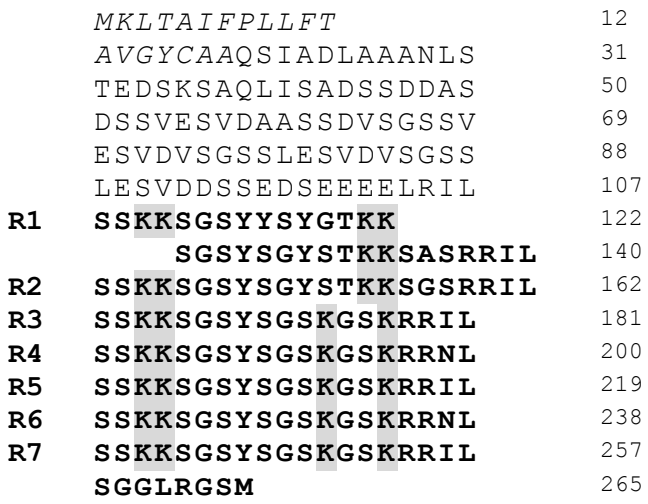

Figure 1-4 Primary structure of the silaffin precursor protein sil1p. The signal peptide 1-19 is shown in italics and the repetitive units R1-R7 in bold. The lysine clusters in the repetitive C-terminal part are highlighted in grey.[69]

The mature forms of silaffin peptides lack the C-terminal RRIL- and RRNL-sequences that are present in the repeat units R1-R7 (Figure 1-4 and 1-5). In other proteins associated with diatom silica, RXL motifs also exist in precursor proteins located at the C-terminus of individual repeats, e.g. in frustulins, cingulins or silacidins.[49,60,67] Thus the RXL-sequence may serve as a general recognition motif for a specific endopeptidase in diatoms that processes precursor polypeptides by cleavage of the RXL motifs and release of individual peptides.

However, extensive chemical analyses were necessary to finally reveal the complete chemical structure of silaffins due to numerous and extraordinary posttranslational modifications (Figure 1-4, Table 1-1).[69-71] In silaffin-$1A_1$, all lysine residues within the peptide sequence become modified. The ε-amino groups of lysine are either alkylated with *N*-methylated oligo-propylenimine residues or become di- or trimethylated.[69,70] The polyamine-modification of lysine residues resembles LCPAs that are bound to putrescine and constitutes a unique posttranslational modification.[61]

Changing the method for extraction of silaffins from diatom cell walls from HF to acidic aqueous ammonium fluoride preserved labile posttranslational modifications and gave evidence that all serine hydroxyl groups are phosphorylated. Also the trimethylated lysine residues become hydroxylated and phosphorylated at the δ-position.[71] Notably, the unique

amino acid ε-*N*,*N*,*N*-trimethyl-δ-hydroxylysine has already been previously described as organic component of diatom cell walls.[46] Together, all posttranslational modifications of silaffin-1A introduce a significant amount of both positive and negative charges rendering this peptide into a large zwitterionic molecule (Figure 1-5).

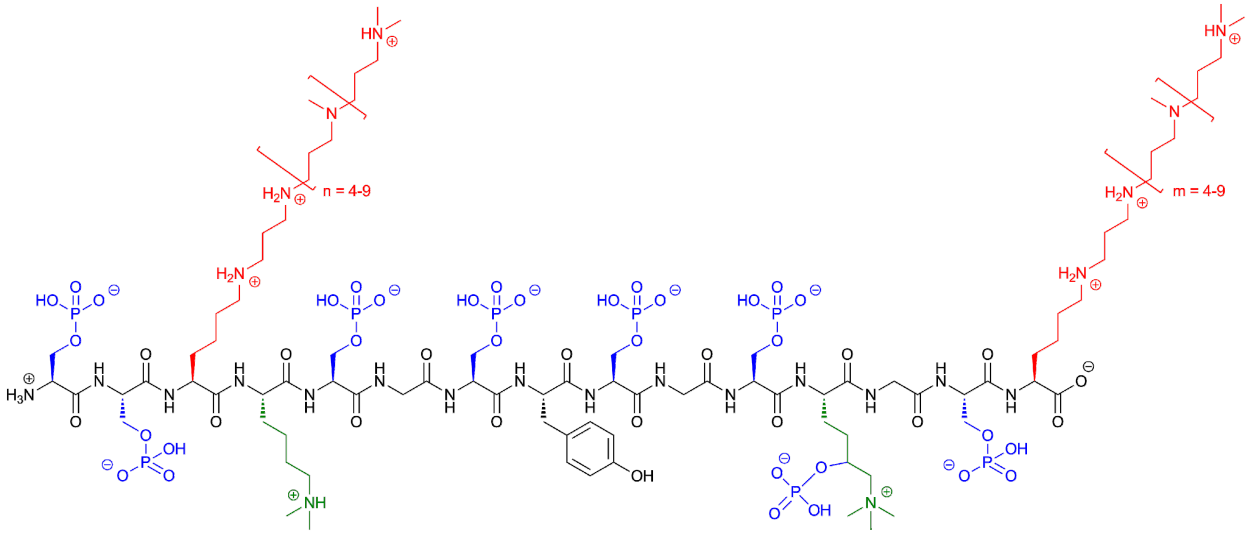

Figure 1-5 Chemical structure of native silaffin-1A$_1$ from *C. fusiformis* with annotation of putative charges at pH 5.[71]

Silaffins from *C. fusiformis* are capable of precipitating silica from a solution of silicic acid *in vitro*. The amount of precipitated silica is directly proportional to the amount of silaffin in the reaction and the silaffin peptides completely coprecipitate with the silica as long as silicic acid is present in excess.[69] The fully modified, native silaffin-1A$_1$ efficiently precipitates silica from a solution of silicic acid at pH 5.5. In contrast, silaffin-1A carrying the lysine-modifications, but lacking the serine phosphorylations, is not able to initiate silica formation under these conditions. If phosphate anions are added to the reaction solution activity could be restored and maximal activity was observed at pH 5.[71] The R5 peptide, a synthetic variant of silaffins with the sequence of the repetitive unit 5 of sil1p but lacking any posttranslational modifications (Figure 1-4), has no silica precipitation activity below pH 7. Since the pH in the SDVs is acidic, modifications of lysine residues in silaffins are essential for silica formation *in vivo*.[40]

Besides silaffin-1A and -1B, *C. fusiformis* diatoms express a third protein tightly associated with their cell walls, silaffin-2 (Table 1-1).[69] Although the complete primary structure of silaffin-2 is not known so far, the protein does not seem to be encoded by the *sil1* gene. The native form of silaffin-2 has a molecular weight of 40 kDa and is highly posttranslationally modified.[72] Besides the lysine modifications known from the silaffin-1 variants, hydroxyamino acids become phosphorylated, sulfated and glycosylated. The numerous sulfations and the abundant glucuronic acid in the carbohydrate modifications confer a strong anionic character to silaffin-2. Remarkably, and in contrast to silaffin-1A, native silaffin-2 has no activity in silica precipitation *in vitro*. This is most likely caused by the anionic modifications that overlay and inhibit the polyamine-modifications of lysine, which have been proven to be essential for silica precipitation activity.[69,72] But a mixture of native forms of silaffin-2 and silaffin-1 or LCPAs is able to precipitate silica even under phosphate-free *in vitro* conditions. More interestingly, different ratios of silaffin-2 and silaffin-1 result in silica precipitates with different morphologies and even porous silica block material could be observed.[72] Therefore, the function of silaffin-2 during cell wall biogenesis is not the direct precipitation of silica but rather regulation of silica formation and patterning.

Silaffin proteins could also be identified in other diatom species, e.g. *T. pseudonana*,[73] *E. zodiacus*[74] or *C. gracilis*[75] (Table 1-1). However, they are apparently absent from the *Coscinodiscus* species.[76] In the silaffin proteins isolated from *E. zodiacus*, additional lysine derivatives with quarternary ammonium groups were identified, e.g. lysine derivatives alkylated with an aminopropyl moiety, and trimethylated at the terminal amino group and further methylated a the ε-amino group of the lysine moiety, respectively.[74] The function of this modification is probably to increase the affinity of these silaffin peptides to the surface of formed silica.

In *T. pseudonana*, four silaffin precursor polypeptides are known, namely tpSil1p, tpSil2p, tpSil3p and tpSil4p (Table 1-1). Proteolytic processing of tpSil1p and tpSil2p results in low (20 kDa) and high (85 kDa) molecular mass isoforms.[73,77] None of these silaffin proteins have sequence similiarities to the silaffins from *C. fusiformis*, but they are also rich in hydroxyamino acids that become phosphorylated, sulfated and glycosylated. Therefore, the silaffins from *T. pseudonana* resemble the silaffin-2 protein from *C. fusiformis*. Since they

are unable to form silica *in vitro* by themselves but do so only in combination with LCPAs, they exhibit rather regulatory functions in silica formation that is comparable to silaffin-2.

Table 1-1 Overview of silaffin variants identified from different diatom species

		Posttranslational modifications		**silica precipitation activity**
diatom species	**silaffin**	**at lysine**	**at hydroxyl amino acids**	
C. fusiformis	**silaffin-1A and silaffin-1B**	methylations and polyamine modification at ε-amino group; hydroxylation and phosphorylation at δ-position	phosphorylation	yes
				yes
	silaffin-2		sulfation, glycosylation and phosphorylation	no
T. pseudonana	**tpSil1p**	methylations and polyamine modification at ε-amino group; hydroxylation and phosphorylation at δ-position	sulfation, glycosylation and phosphorylation	no
	tpSil2p			
	tpSil3p			
	tpSil4p			
E. zodiacus		methylations and polyamine modification at ε-amino group	not analyzed	not analyzed
C. gracilis		not analyzed	not analyzed	yes

A silaffin variant that is homologous to silaffin-1 from *C. fusiformis* with an ability to mediate silica formation could not be isolated from *T. pseudonana*. Yet the lysine modifications in tpSil3 are similar to those from silaffin-$1A_1$. The numerous (hydroxy-)lysine residues in tpSil3 either become dimethylated at the ε-amino group or alkylated with methylated aminopropyl units.[78] Modification of lysine with longer polyamines was not observed. Most of the lysine residues in tpSil3 are arranged in clustered tetrapeptide KXXK motifs.[78] The clustering and arrangment of lysine in KXXK motifs is also observed in silaffins and cingulins from *C. fusiformis* and might serve as a general recognition sequence for specific enzymes that transfer these extraordinary lysine modifications in a controlled

manner.[60,69,70,78] More importantly, clustering of several lysine residues in combination with phosphoserines in the tpSil3 protein was found to be crucial for targeting of silaffins to biosilica.[79] The *N*-terminal signal peptide of silaffins mediates co-translational import into the ER, together with the Golgi the location for phosphorylation and glycosylation. Indeed, a specific silaffin kinase associated with the ER and Golgi membranes was identified in *T. pseudonana*.[80] Expression of the tpSTK1 kinase, a 60 kDa protein including an *N*-terminal signal peptide for import into the ER, is significantly upregulated during silica valve formation. tpSTK1 shows specific activity in phosphorylation of silaffin substrates, but not of silacidins, indicating a preference for substrates with basic isoelectric points. Accordingly, the intracellular transport pathway of silaffins starts with co-translational import of the silaffin precursor proteins into the ER, where they become phosphorylated.[79] The location of further modification and processing, as well as transport from the ER to the SDV, where silica formation takes place, remains unclear. Finally, lysine-clusters in the silaffin sequence mediate targeting to the newly formed biosilica.[80]

1.2.4 Chemical and mechanistic aspects of the silica formation process in diatoms

Amorphous silica is formed by a complex inorganic polymerization process with orthosilicic acid as monomeric building block. The solubility of monosilicic acid $Si(OH)_4$ is limited to a concentration of 2 mM in aqueous solutions of neutral pH and deprotonation at pH values above 9 gives silicate anions $SiO(OH)_3^-$.[81] Nucleophilic substitutions between silicate anions and silicic acid molecules lead to condensation reactions, which form siloxane bonds (Si-O-Si). Silicic acid molecules react to form dimeric, trimeric and tetrameric species that further condense with monomers to form highly dense, branched polysilicic acid species. These colloidal silica particles have sizes in the nanometer range. Depending on the pH and the presence of salts or other additives, such a silica sol can undergo different further reactions (Figure 1-6). At pH values below 7, there is only weak electrostatic repulsion between the colloidal silica particles due their uncharged surfaces. Therefore, the colloidal particles aggregate to fibrillar, branched chains and form a gel. At pH values above 7, negative

charges on the surfaces of the colloidal silica particles dominate and therefore electrostatic repulsion occurs. Colloidal silica particles form a stable sol and the particles further grow by the Ostwald ripening process.[81,82] The addition of a cationic flocculant to a silica sol leads to fast precipitation of silica particles. Cationic species adsorb to silica surfaces and bring them close together resulting in coagulation of particles. Alternatively, cationic species, e.g. polyamines are suggested to stabilize the pentavalent transition state of the condensation reaction between silicic acid molecules and therefore further promote silica flocculation.[83-85]
In diatoms, the formation of silica occurs under acidic conditions in the SDV and the occurrence of colloidal silica could be proven in nascent diatom cell walls.[42,86,87] Since silica biomineralization in diatoms is much faster than abiotic silica formation, a biological flocculant is believed to assist the silica polycondensation. LCPAs and silaffins have been shown to be directly involved in the molecular processes that lead to biogenesis of the elaborate patterned silica frustules. Both, LCPAs and silaffins are highly cationic compounds, and can serve as flocculant for negatively charged silica nanoparticles.

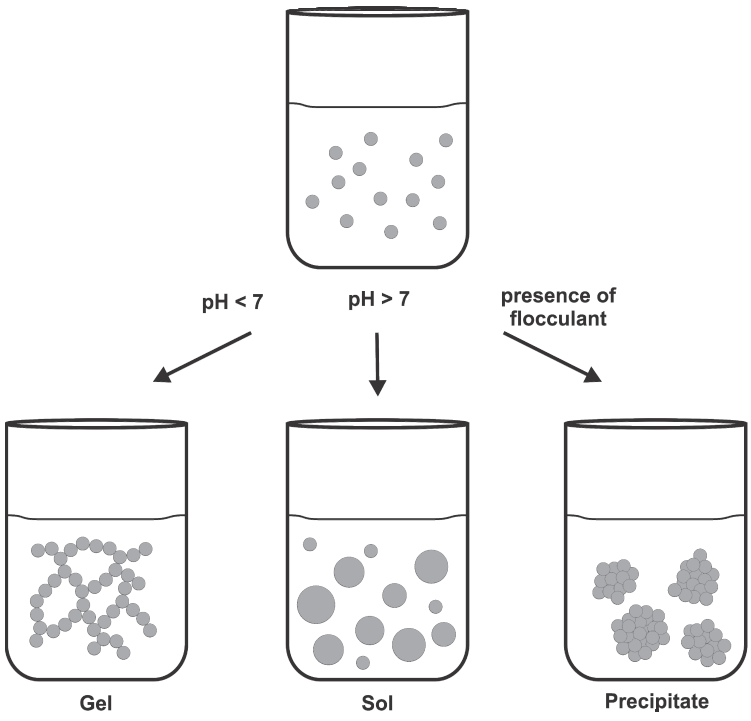

Figure 1-6 Different possibilities for development of a colloidal silica sol into a gel, a sol or a precipitate depending on the reaction conditions.

Nevertheless, deviating from the flocculant theory and based on the physicochemical properties of amphiphilic LCPAs, a phase separation model for silica formation was proposed.[76] LCPAs are able to rapidly precipitate silica from a solution of silicic acid *in vitro* but polyvalent anions, such as phosphate, are necessarily required in the reaction solution.[66] Accordingly, the LCPAs in a phosphate buffered solution can undergo a phase-separation process and form polyamine-polyanion rich microdroplets. The silicic acid in the aqueous interface between the droplets is then rapidly polymerized to silica mediated by the polyamines. Species-specific patterns observed in diatom biosilica most likely result from variations in the polyamine droplet size.[76] The microscopic phase separation of synthetic polyamines in aqueous solutions is induced by the addition of multivalent anions and essential for polyamine-mediated silica precipitation.[88] Silica precipitation with polyamines in the presence of increasing phosphate concentrations produced silica particles with increasing diameters and the process strongly depends on the pH.[66,88,89] With synthetic LCPAs that are structurally based on the native LCPAs from diatoms, a clear relationship between morphologies of silica precipitates and the structure of polyamines with respect to polyamine chain length and degree of *N*-methylation could be shown.[90] Altogether, the structure of the polyamines and the ratio of polyamine to phosphate seem to define the size of microdroplets, and thus the final size of silica spheres. In diatoms, highly acidic phosphopeptides, silacidins, could be identified as the potential native source of polyanions that assist phase separation of LCPAs *in vivo*.[67,68] Since silacidin concentration directly influences the size of the resulting silica particles, silacidins are not only serving as cross-linking polyanions that guide assembly of polyamines and assists in silica formation, but they are also involved in the control of silica morphology in diatoms.

In case of the silaffins, a model for their silica formation activity that is in agreement with the model for silica formation by LCPAs was proposed.[76] Due to the polyamine modifications and the numerous phosphorylations, native silaffin peptides are zwitterionic and self-assemble in solution via electrostatic interactions with the numerous phosphate groups serving as an intrinsic anion source.[71] Polycationic silaffins lacking the native phosphorylations require the addition of divalent anions that assist as ionic cross-linkers in the self-assembly process.[71] By means of this self-assembly of the peptides a microscopic phase separation and a high local concentration of amino groups in the aqueous solution are

induced. Since amines and polyamines have been generally shown to promote the condensation of silicic acid and thus the formation of silica,[83] the amino groups in silaffins are supposed to act as acid-base catalysts that facilitate formation of siloxane bonds in this model. Deprotonated amino groups accept a proton from a silicic acid molecule resulting in the formation of a reactive silanolate group. During the nucleophilic attack of this group to a second silicic acid molecule, protonated amino groups facilitate the release of a water molecule from the attacked molecule by protonation (Figure 1-7).[91] Advancing condensation between silicic acid monomers and the colloidal silica particles in the sol finally results in precipitation of silica. An appropriate arrangement and spacing of the amino groups in the peptidic context may stabilize the transition state in silicic acid polycondensation and therefore enhance silica formation but additionally may act as a template for silica patterning.

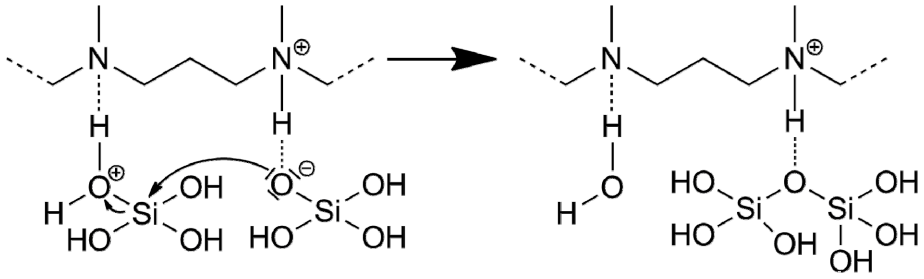

Figure 1-7 Proposed mechanism for polyamine-mediated polycondensation of silicic acid.[91]

However, only silaffin-1 from *C. fusiformis* has been proven to be able to precipitate silica from a solution of silicic acid. All other identified members from the silaffin group, i.e. silaffin-2 or the silaffins from *T. pseudonana*, are polyanionic proteins and have no intrinsic silica precipitating activity (Table 1-1). But simultaneously with the discovery of silaffins, it was noticed that a mixture of native silaffins results in a different morphology of the silica material than silaffin-1A alone.[69] Silaffin-1A led to formation of spherical, interconnected silica particles, which is the thermodynamically most stable structure. In contrast, the mixture of silaffins that also contained silaffin-2, yielded silica aggregates consisting of smaller particles. The acidic silaffin-2 is supposed to act as the internal polyanion that controls assembly of LCPAs and cationic silaffin-1A and induces phase separation. Moreover, silaffin-2 is able to influence silica structures since different mixtures of native silaffins result

in the formation of diverse nanopatterned silica morphologies.[72] Silaffin-2 as well as the silaffins identified from *T. pseudonana* are therefore called "regulatory" silaffins.
Obviously, the presence of a regulatory element leads to spatial separation and organization of the cationic silica polymerizing centers and enables formation of silica structures with higher order morphologies.
Altogether, in diatoms there is an organic matrix in the lumen of the SDV, including silaffins, LCPAs, cingulins and chitin, which serves as macroscopic template for silica formation and patterning.[58,60,61,69] Among these biomolecules, silaffin-1A is outstanding since it combines both functionalities required for silica precipitation, i.e. cationic amino and anionic phosphate groups, in one molecule and shows *in vitro* silica precipitation activity.

1.3 Biotechnological applications of silica

The scope of application of silica is tremendous due to its unique chemical and mechanical properties and its good availability. Besides more classical applications of silica as absorbent, stationary phase in liquid chromatography, catalysis or general filling material, it also finds increasing implementation as an additive in cosmetics and in the food industry since it is Generally Recognized as Safe (GRAS).[92,93] The progress in syntheses of silica materials with defined structures and properties and the development of novel routes for biomimetic silica formation have prompted the application of silica based materials particularly in biotechnology and biomedicine.[94-96]

1.3.1 Synthetic silica materials

Porous silica is a desirable material for biotechnological applications because of its chemical inertness and biocompatibility. Nevertheless, the small micropores (0.5 - 1 nm) of naturally occurring porous silica materials, such as zeolites, exclude these materials from biotechnological applications involving proteins or larger molecules. A breakthrough for biotechnological applications was made with the introduction of a novel type of highly

ordered mesoporous silica-based materials, the MCM-41 (Mobile Crystalline Material-41, Figure 1-8).[97,98] The synthesis of these kind of highly ordered mesoporous silica materials is based on the cooperative micellar self-assembly of cationic surfactants or block-copolymers and anionic silicate precursors into ordered silicate-surfactant composites. The surfactants serve as templates for the polycondensation of silicic acid and calcination of the formed silica removes the surfactant template and results in pure, mesoporous silica material. The final characteristics of the porous silica material, i.e. morphology, pore volume and diameter, are determined by varying and use of different combinations of silica sources or surfactants, pH and temperature.[99] Prominent examples of mesoporous silicas include MCM-41, MCM-48, MCM-50 or SBA-15 (Santa Barbara Amorphous-15) (Figure 1-8).[97,98,100,101] These silica materials are characterized by uniformly sized mesopores formed by amorphous silica walls and consequently a high surface area, large pore volume and tunable pore sizes.

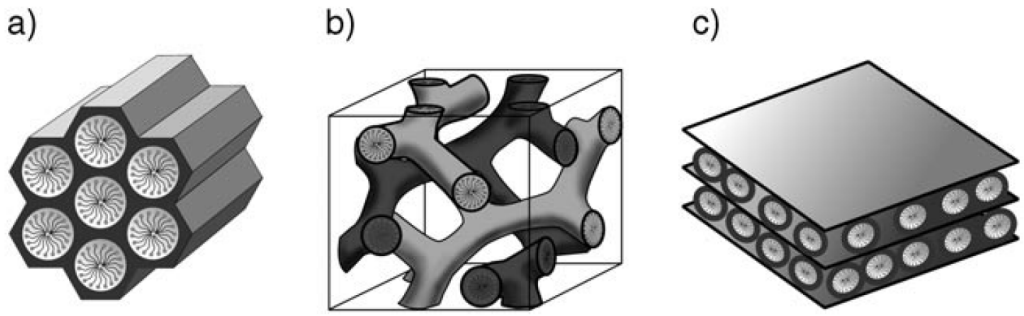

Figure 1-8 Structures of mesoporous silica materials: A) MCM-41 (2D hexagonal), B) MCM-48 (cubic) and C) MCM-50 (lamellar) (taken from [102])

Besides usage of mesoporous silicas as stationary phases in HPLC, as filling material or in catalysis,[103] an initial study has proven that MCM-41 mesoporous silica nanoparticles (MSNs) can be loaded with the anti-inflammatory drug ibuprofen and enable a sustained release of the drug.[104] This led to an enormous boost in the application of MSNs as carriers for the development of advanced drug delivery systems, further promoted by the findings that MSNs are readily and without toxic effects internalized by eukaryotic cells. Even the uptake efficiency can be tuned by morphology of the silica materials and by variable surface functionalization of the nanoparticles.[105-107]

Mesoporous silica nanoparticles can generally be loaded with a cargo molecule either by covalent linkage of the cargo to a functionalized silica surface,[108,109] or more commonly by the immersion loading method, which means that the MSNs are soaked in a solution of the cargo molecule.[110] In the latter method however, loading efficiency is dependent on various factors including the functionalization of the silica surface.[111] The possibility to generate MSNs with large pore sizes allows loading of bulky biomolecules such as peptides, proteins or even antibodies into the silica matrix.[112-114] The interaction of cargo molecules with MSNs, and therefore a fine-tuning in loading and release characteristics, can be adjusted by selective functionalization of the inner core silica or the outer particle surface.[115,116] Functionalization of a silica surface can be achieved by co-condensation of functional molecules during synthesis or by post-synthetic grafting of functionalized silanes and can result in an effective control of drug release.[116,117-119] The introduction of organic functionalities to the silica surface of MSNs facilitates additionally the attachment of targeting moieties and extends the applications of MSNs to targeted therapies. Surface modification of MSNs, e.g. with folic acid,[120,121] mannose,[122] lactobionic acid[123], the cyclic peptide RGD,[124] transferrin[125] or antibodies,[126] provided specific targeting to cancer cells. Specific targeting of drugs to their target location and a controlled release of the drug will certainly entail a reduction of the applied drug doses and reduce unwanted side effects of drugs.

Avoiding pre-mature release of loaded cargo from MSNs is possible by sealing the pores, e.g. by deposition of a lipid bilayer at functionalized MSNs to form a core-shell hybrid system.[127,128] To liberate cargos from MSNs only in response to a specific trigger effect, sophisticated stimulus-responsive systems have been developed. All of these systems have in common the containment of cargo molecules in the silica material by sealing the opening of the pores with a cap or "gatekeeper" (Figure 1-9). One prominent approach is the use of redox responsive gatekeepers, since release of cargos after endocytosis of the nanoparticles in the intracellular, reductive environment is achieved. Different gatekeepers, such as cadmium sulfide (CdS) nanoparticles,[129] collagen[130] or a cross-linked polymeric network,[131] were linked to a functionalized silica surface. Intracellular thiols readily cleave the disulfide bonds and detach the gatekeepers from the entrance of the pores, resulting in the release of the encapsulated cargo molecules (Figure 1-9 A).

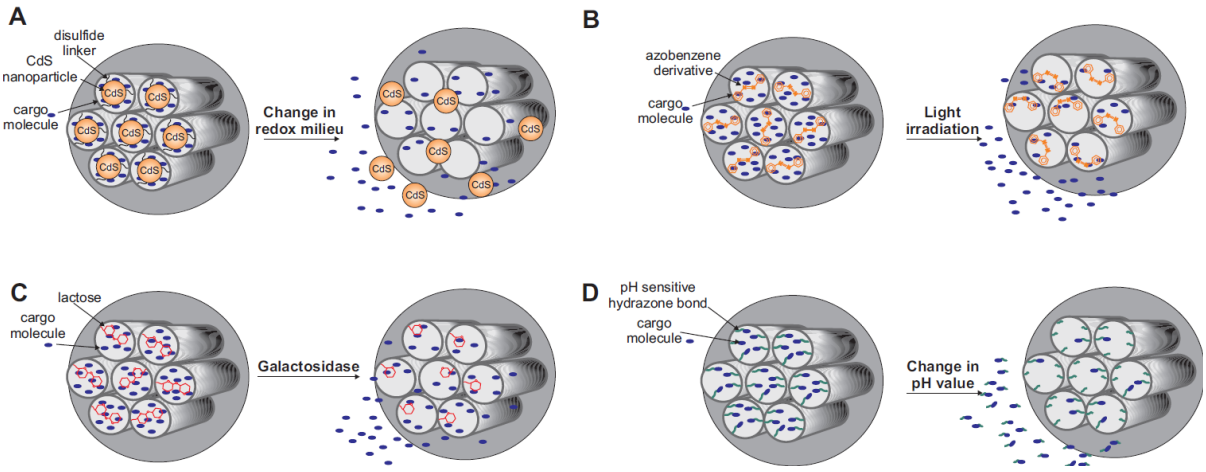

Figure 1-9 Stimulus-responsive systems for controlled release of cargo molecules from mesoporous silica nanoparticles. A) redox-responsive release (adapted from 129); B) light irradiation (adapted from 136); C) enzymatic removal of gatekeeper (adapted from 132); D) pH-sensitive release (adapted from 140).

Another strategy for stimulus responsive release is based on enzymatic removal of a gatekeeping agent, e.g. cleavage of lactose caps by β-galactosidase[132] (Figure 1-9 C), proteolysis of a peptide shell,[133] tryptic digest of avidin from a biotin-avidin cap system[134] or removal of a duplex DNA cap by endonucleases.[135] The latter two are also examples for dual stimuli-responsive systems since they allow cap removal not only enzymatically, but also via temperature shifts. Application of light-sensitive molecules as gatekeepers empowers spatiotemporal control over drug release. Examples include azobenzene derivatives as gatekeepers[136,137] (Figure 1-9 B), photosensitizers that mediate opening of a nanoparticle supported membrane[138] or a red-light based photoactivation approach.[128] Different approaches use competitive displacement[139] or changes in pH[140,141] (Figure 1-9 D) as trigger for stimulus responsive release of cargo molecules from mesoporous silica materials.

Altogether, multifunctional MSNs combining efficient cargo loading, a strategy for containment and stimulus-responsive release of cargo, and a moiety for targeting to a desired location are important for establishing an advanced drug delivery system.

Besides the wide usage of MSNs in drug delivery systems, MSNs are also excellent matrices for biosensing applications. The high porosity, the large surface area and pore sizes of mesoporous silica allows detection of larger analyte biomolecules and the incorporation of a high amount of sensors molecules into the porous matrix. These advantages lead to an

improved detection limit and, additionally, a faster diffusion of the analytes through the mesopores to the sensor molecule which yields a shorter response time. Effective sensors for glucose, H_2O_2, NO_2, ATP or neurotransmitter detection were generated by immobilization of sensor molecules on mesoporous silica materials.[142-147] The various possibilities for functionalization of mesoporous silica materials also enable development of further diagnostic or imaging applications.[124,148]

However, despite the progress in synthesis of tailored mesoporous silicas and the many examples for applications, the major disadvantages are complicated syntheses and harsh reaction conditions. Furthermore, the elaborate, hierarchically structured silica architectures observed in nature are still out of reach for chemical silica syntheses. Also the ability to form nanostructured silica under ambient conditions draws the attention to biogenic or biomimetically formed silica.

1.3.2 Diatomaceous earth and biogenic diatom silica

Geological deposits of fossilized skeletons of diatoms are referred to as diatomaceous earth, diatomite or kieselguhr. The main component is silicon dioxide besides minor quantities of aluminum and iron oxide, but the exact composition depends on the place of origin.[149] Because of the high content of diatom silica frustules, diatomaceous earth has specific properties such as low density and conductivity but a large surface area and adsorption capacity due to porosity. Owing to these characteristics, diatomaceous earth has for a long time been extensively used as adsorbent,[150] natural insecticide,[151] insulating material,[152] filter aid in wastewater treatment[153,154] or as catalyst carrier for photocatalytic reactions.[155,156]

Due to the highly porous, hierarchically nanopatterned architecture, diatom silica has a high surface area, a remarkable mechanical stability and displays photoluminescence and the properties of a photonic crystal.[157-159] Because of these properties along with its complex structures produced under physiological conditions, diatom frustules induce even more advanced applications.

Frustules of diatoms can be used as templates for the production of metal surfaces with elaborate patterned features that are valuable for surface enhanced raman spectroscopy

(SERS). Coating of purified diatom frustules with metal layers followed by dissolution of silica leaves metallic materials that reflect the exact nanopattern of the silica template.[160]

Furthermore, silica frustules of diatoms are useful templates for conversion of silica in other materials, such as nanocrystalline silicon or amorphous graphite.[161,162] Reaction of the diatom silica with gaseous magnesium and subsequent removal of the MgO with diluted hydrochloric acid at 650 °C gives nanocrystalline silicon. Otherwise, from the SiC that results from reaction of diatom biosilica with methane, the silicon can be removed with Cl_2 at 950 °C, resulting in pure carbon. In both examples, the nanoscale structures of the diatom silica are preserved.[161,162] The transformation of diatom silica templates significantly increases the specific surface area of the formed highly porous silicon or carbon materials, thus providing materials with possible applications in sensing, catalysis, (bio)chemical separation or energy storage and harvesting. Alternatively, the mineral composition of diatom frustules can be changed. GeO_2 or TiO_2 can be incorporated into the nanostructure of the silica cell wall by addition of $Ge(OH)_4$ or $TiCl_4$ to the culture medium and exploitation of diatoms as *in vivo* catalysts. Such Si-Ge composite materials could potentially be applicable in the fabrication of electroluminescent display devices, battery electrodes or dye-sensitized solar cells.[163]

Diatom shells display an efficient visible photoluminescence emission strongly dependent on the environmental conditions. This luminescence can be quenched or enhanced by several gaseous substances, thus diatom biosilica can be used as material in optical gas sensing applications.[164,165] In addition, functionalization of intact diatom frustules with an antibody was shown to enable biosensing of complimentary antigens via photoluminescence.[166]

Tethering of biomolecules to biosilica is achieved by silanization of the surface silanol groups and coupling of a heterobifunctional crosslinker followed by the attachment of the biomolecule, e.g. an antibody.[167] Other potential applications of biosilica as carrier for covalent bound antibodies include immunoprecipiation and immunoisolation[168] or the development of a diagnostic device for electrochemical detection of biomolecules.[169]

The possibility to selectively modify purified diatom biosilica with biological molecules also enables the development of silica microcapsules for targeted drug delivery. The silica shells of diatoms are highly convenient as an inert biomaterial carrier for drug delivery applications. Their hollow body structures and the micro- and nanoscale porosity allow

straightforward loading and sustained release of hydrophobic and hydrophilic cargo molecules.[170,171] Functionalization of diatom silica surfaces with different organosilanes allows tuning of the drug loading and release properties.[172,173] A possibility for magnetically guided, targeted drug delivery was demonstrated by functionalization of diatom silica with dopamine modified iron-oxide magnetic nanoparticles (Figure 1-10).[174]

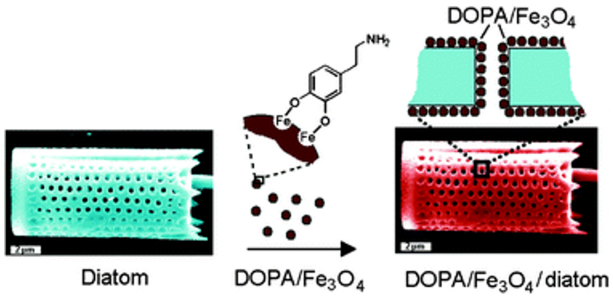

Figure 1-10 Functionalization of diatoms with dopamine modified iron oxide-nanoparticles for magnetically guided, targeted drug delivery (taken from 174).

In a different approach, living diatoms are exploited to achieve immobilization of an active enzyme in the biologically produced nanoporous silica material.[175] Silaffin proteins are involved in the silica formation process in diatoms and become tightly associated with the newly deposited frustules. Genetic fusion of a target enzyme with a silaffin gene and expression of such a fusion protein results in immobilization of the enzyme in the silica matrix. The enzyme containing biosilica can be gently purified and since the enzymes are not completely enclosed within the silica, their activity is largely retained whereas protein stability is significantly increased. This method has also proven applicable to oligomeric enzymes or enzymes that require posttranslational modifications or cofactors for activity.[176] Apparent advantages of this method include that the physiological conditions are beneficial for protein integrity and that the protein encapsulation in the nanostructured biosilica provides an ideally suited, mechanical stable and resistant matrix that ensures simultaneously substrate accessibility.

1.3.3 Biomimetic formed silica

Besides synthetic silica and biogenic silica, biomimetic silica formation has gained more attention due to the possibility to combine mild reaction conditions with control over silica structure. Approaches toward bioinspired and biomimetic silica formation were stimulated by the progress in unraveling the molecules involved in silica biomineralization processes in nature. A number of biomolecules could be identified including silaffins and LCPAs from diatoms that proved to be directly involved in the molecular processes leading to silica formation.[61,69] Investigations of their structures and their functional role in silica precipitation revealed chemical and physical prerequisites of biomolecules for activity in silica precipitation. An overall cationic character, more precisely lysine residues in case of peptides and proteins, and the ability to self-assemble in solution have been validated as required features of biomolecules that govern silica formation. Transferring these insights of biological silica formation into the lab enabled the development of routes for synthesis of novel silica materials with defined structures and properties under mild and physiological reaction conditions.

Biomolecules that fulfill the afore-mentioned requirements and have been applied and studied in biomimetic silica formation include peptides and proteins such as poly-L-lysine (PLL), poly-L-arginine (PLA), the R5 peptide, lanreotide, block-copolypeptides and lysozyme, diverse polyamines such as polyallylamine (PAA), polyethylenimine (PEI) or amine-terminated dendritic structures.

Formation of silica using biomolecules at room temperature results in amorphous silica, and therefore can adopt a large variety of morphologies. Using organic molecules as additives for silica formation, a plethora of different silica structures and morphologies could be produced (Table 1-2). Spherical silica is the thermodynamically most stable structure and is readily obtained using native silaffins,[69,71] the R5 peptide,[177] and linear or cyclic amines.[178-181] Nevertheless, the morphology of precipitated silica can be influenced by variation of the reaction conditions or by the chemical and structural nature of the mediating additive. Using the R5 peptide as a silica precipitating agent, different morphologies deviating from the common silica spheres that are obtained under static reaction conditions, e.g. fibrillar or arch-shaped structures can be achieved by keeping the reaction mixture in motion.[182] An

externally applied electrostatic or hydrodynamic force field was shown to cause the conversion from spherical shapes to fiber like structures.[183] The presence of polyhydroxy compounds, e.g. glycerol or sucrose, even prompted the formation of nanostructured sheet-like silica precipitates.[183] The effect of anionic, polyhydroxy compounds was also observed with native silaffins from diatoms. Purified cationic silaffin-1A results in the formation of spherical silica particles with diameters from 500-700 nm, but in mixture with the anionic, glycosylated silaffin-2 the silica material changes to a composite of small silica nuclei.[69] Polycationic peptides such as poly-L-lysine and poly-L-arginine are well-known to be able to precipitate silica from a solution of silicic acid.[184,185] Under static conditions PLL has been shown to trigger the formation of silica spheres and hexagons, whereas perturbation of the reaction mixture or application of electrostatic field forces change silica morphologies to fiber-like, dendrite-like or ladder shapes with periodic voids.[183,184,186] The hexagonal silica plates observed by PLL-mediated silica formation have been proven to be based on PLL chain length and self-assembly of PLL into a helical conformation in the presence of phosphate anions.[187,188] A different study showed that PLL assembles into microspheres in the presence of citrate as counterion and the surface of these microspheres can be coated with silica.[189] Activity of PLL and PLA in silica formation strongly depends on the chain length of the polypeptides and depending on the silica precursors they assist in silica polycondensation or act as flocculant.[84] Notably, application of bio-inspired, arginine-based surfactants in silica formation followed by calcination gives porous silica materials.[190]

Since self-assembly emerged to be a prerequisite for silica formation activity, different molecules were considered as structure directing silica formation agents. Block copolypeptides such as poly(L-cysteine$_{30}$-b-L-lysine$_{200}$) self-assembled into structured aggregates in solution mediate the formation of ordered silica morphologies. The oxidation state of the cysteines affects the self-assembly, and therefore the morphology of the silica material can be triggered from hard silica spheres under reducing conditions to silica in the form of packed columns resulting from oxidized copolypeptide.[191] Another peptide which is known to self-assemble into nanotubes is the synthetic octapeptide lanreotide.[192] With these peptide self-assemblies as template, double-walled silica nanotubes can be produced.[193] Also amphiphilic peptides such as A_6K or V_6K, which self-assemble into nanotubes or lamellar stacks, can be used as organic templates in biomimetic silica formation. The presence of

anions is necessary in these systems and depending on the peptide and anion composition or on external forces different silica morphologies could be obtained.[194]

Table 1-2 Overview of silica structures obtained with different silica precipitating biomolecules

	silica morphology		**conditions**
silaffin-1A	spherical particles		pH 5 – 5.5
mixture of native silaffins	cluster of small spheres		
R5 peptide	spherical particles	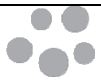	phosphate buffered solution, neutral pH, static conditions
	arch-shaped		nitrogen stream bubbling through reaction mixture
	fibrillar		mechanical shear force; electrostatic/hydrodynamic force
	sheet-like		presence of polyhydroxy compounds (e.g. glycerol)
poly-L-lysine (PLL)	spherical particles	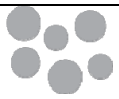	static conditions
	hexagons		phosphate induced self-assembly of long-chain PLL
	fibrous		electrostatic field, long-chain PLL
	dendrite-like		hydrodynamic field
poly(L-cysteine$_{30}$-b-L-lysine$_{200}$)	spheres		nitrogen atmosphere
	packed columns		air-oxidation
lanreotide	double-walled nanotubes		calcination of peptide template after silica formation
A_6K, V_6K	fibers		electrostatic field, flow field

Amines and polyamines are generally known to be able to precipitate silica due to their polycationic character.[83] The morphology of the silica material obtained from poly(allylamine)hydrochloride strongly depends on the reaction conditions and formation of fiber-like structures is possible under externally applied shear stress.[195,196] The size of the silica particles obtained from PAA directly correlates with concentrations of phosphate or sulfate anions in the reaction solution and depends on the pH of the reaction solution.[197,198] This effect was also observed in the case of native long chain polyamines isolated from diatoms.[66] The LCPAs isolated from diatoms are unique biomolecules in nature. Studies of the structure-function relationship of synthetic mimics of these polyamines revealed an influence of alkyl chain length, number of amino groups, and degree of methylation on silica precipitation activity and the morphology of silica material.[90,179] This understanding allowed the formation of hollow silica spheres and nonporous silica material.[179] Linear or branched polyethyleneimines (PEI) are simple polyamines, but commonly used in biomimetic silica formation. With linear PEI, almost spherical silica particles were precipitated in a phosphate containing system.[199] Perfectly monodisperse silica spheres could be obtained with polymers containing a linear PEI backbone, but in a medium containing 70 % (v/v) methanol in water.[200] Linear PEI aggregates in aqueous solutions and serves as template for silica formation. Different architectures of the PEI containing organic polymers or variation of the reaction conditions gave various silica materials in the shapes of fibrils, flowers, plates, leafs and others.[201-204] Amine-terminated dendrimers were also used as variable templates for silica formation, whereby the polypropylenimine-dendrimers (PPI) share the same momomeric units as the native LCPAs from diatoms.[205] Silica precipitating activity of amine-terminated dendrimers turned out to be dependent on the presence of phosphate anions and the size of the silica spheres can be triggered by the phosphate concentration.[206,207]

The variety of molecules with activity in silica formation, the many possibilities to steer silica structure and the mild reaction conditions let to development of diverse biotechnological applications based on biomimetic silica formation. One prominent application of biomimetically formed silica is immobilization of biomolecules such as enzymes (Figure 1-11). Generally, immobilization of biomolecules in silica matrices has the obvious advantages of stabilizing the biomolecule, therefore enabling transfer of biomolecules to non-physiological environments, and to make it reusable. Due to its

amorphous structure, mechanical stability and chemical inertness, a silica matrix, is often favorable in many applications of immobilized biomolecules such as in biosensing, biocatalysis or drug delivery. Physical immobilization of biomolecules, i.e. adsorption or entrapment of the biomolecule in a porous, insoluble matrix is often preferred over chemical immobilization via covalent attachment, since it does not as much restrict the spatial conformation of biomolecules and therefore impairs less with activity.

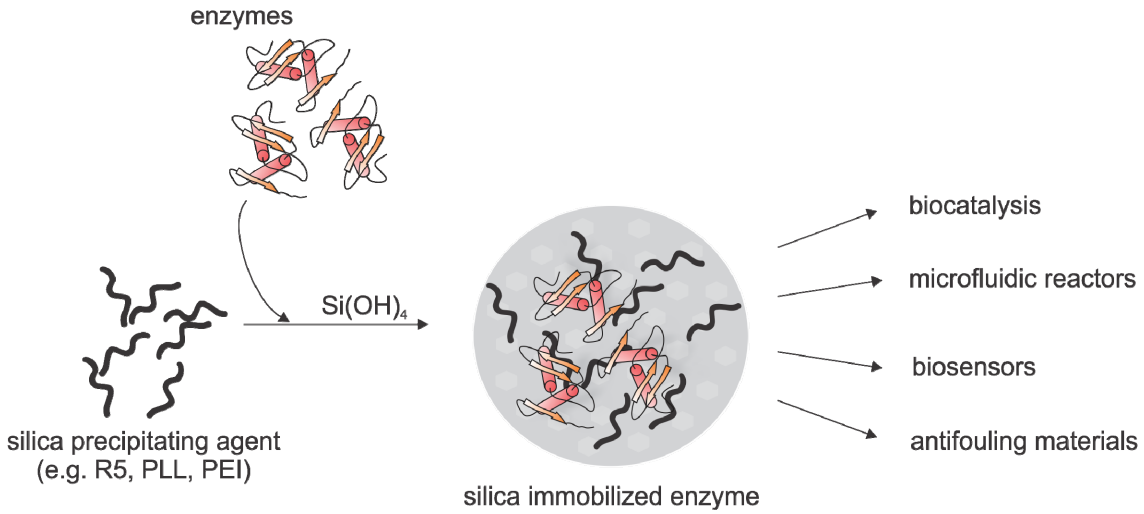

Figure 1-11 Schematic overview of enzyme immobilization via biomimetic silica formation and the application field of silica immobilized enzymes.

The route of biomimetic silica formation is suitable and advantageous especially for immobilization of sensitive enzymes in a silica matrix. Enzyme immobilization in biomimetically formed silica was achieved with different silica-precipitating agents, e.g. with PEI,[207-210] amine-terminated dendrimers,[211] lysozyme[212-215] or the R5 peptide.[216,217] The enzymes typically become entrapped in the silica material with moderate to high efficiency while preserving enzymatic activity. Silica immobilized enzymes have found different applications, e.g. as biocatalysts.[216,217] Simultaneous immobilization of multiple enzymes in silica enabled the construction of a continuous silica biocatalyst device in which one enzyme recycles the cofactor of the other enzyme.[210] In another approach two enzymes for coupled enzymatic production of hydrogen peroxide were immobilized in silica. This silica-enzyme composite material was used to develop an enzyme based, environmental friendly anti-fouling paint for ship hulls.[208] Lysozyme is a cationic protein that was shown to be able to

initiate silica formation and to become co-precipitated during silica deposition.[218,219] Silica-lysozyme biocomposites retain the antimicrobial properties of lysozyme and can be used as antifouling material.[212]

The mechanical properties of silica nanospheres facilitate the applications of enzymes in continuous flow-through reactors. Silica immobilized nitrobenzene nitroreductase was used to construct a microfluidic reactor for screening of cancer prodrug activation.[209] Another example shows immobilization of butyrylcholinesterase to screen for drug potency of cholinesterase inhibitors and was achieved with a histidine-tagged R5 peptide variant that binds to cobalt coated agarose beads and mediates the silica formation and enzyme encapsulation after addition of a silica precursor.[220]

The feasibility of silica deposition on planar surfaces has many potential practical uses. The R5 peptide has been used to deposit ordered arrays of silica nanospheres into a polymer hologram for construction of photonic devices.[221] Poly-l-lysine was also used for controlled patterned silica coating of surfaces under mild reaction conditions.[222] The integration of silica-encapsulated enzymes on planar surfaces empowers the generation of stabilized biosensors or enzyme microarrays and could be achieved with the R5 peptide or lysozyme.[214,223] The deposition of silica or a silica-enzyme layer on a gold surface mediated by lysoszyme increases the surface area and is therefore valuable for enhancing sensitivity in surface plasmon resonance sprectroscopy applications.[214] Entrapment of enzymes in carbon-nanofiber silica composites provides a conductive matrix for the enzyme and gives rise to novel electrochemical biosensor systems.[215,224,225]

The major drawback of the methods for immobilization of enzymes in silica matrices that use simple co-precipitation of the enzyme during biomimetic silica formation is that this procedure relies on random entrapment events during silica formation and may not ensure efficient or homogeneous encapsulation. These limitations can be overcome using the R5 peptide, since the peptide sequence can be genetically fused to the protein to be encapsulated in a silica matrix. Protein-silaffin chimeras can initiate silica formation and result in controlled and efficient self-entrapment in the silcica matrix.[226,227] This ability of self-entrapment of fusionproteins with the R5 peptide can also be exploited in generation of biosensors.[228,229]

1.4 Aims of this work

Silica-based materials have great potential in biotechnological and medicinal applications. Due to its unique chemical and physical properties, silica provides an ideal matrix for drug delivery applications or immobilization of sensitive biomolecules such as enzymes.

Approaches towards biomimetic silica syntheses were inspired by silica biomineralization processes that occur under mild, physiological conditions in living organisms. In diatoms, controlled formation of their elaborate nanopatterned silica frustules directly involves silaffins, a class of highly posttranslationally modified peptides.

The aim of this study is to characterize synthetic silaffin peptides in terms of their silica precipitation activity. In addition, novel approaches for silica immobilization of biomolecules for different purposes should be developed based on these silaffin peptides.

Initially, different variants of the unmodified silaffin R5 peptide will be synthesized by solid phase peptide synthesis (SPPS) and analyzed towards their silica precipitation activity and the morphology of the resulting silica materials. The will help to reveal intrinsic features of the R5 sequence that are important for its silica precipitation activity. SPPS also allows the specific introduction of amino acid modifications based on naturally occurring posttranslational modifications (PTMs). Synthesis of silaffin variants with defined modifications will enable a systematic study of the effect of each modification. Differently modified silaffin peptides are supposed to influence the properties of the resulting silica materials and therefore will provide control over properties of silica material in biotechnological applications.

Subsequently, covalent conjugates of silaffins and different cargo molecules will be synthesized to achieve formation of functionalized silica hybrid materials. First, a general route for covalent attachment a cargo molecule to the silaffin sequence via a stimulus-responsive cleavable linkage should be developed. The ability of these silaffin-conjugates to simultaneously initiate silica formation and cargo encapsulation will be explored. Moreover, the controlled release of peptides and cargo molecules will be analyzed under different conditions to establish a drug delivery system based on silaffin-conjugate induced biomimetic silica.

Next, stable conjugates of proteins and the silaffin variants carrying the defined PTMs will be generated by expressed protein ligation. The efficacy in homogenous protein encapsulation of these covalent protein-silaffin conjugates will be investigated. Analysis of silica entrapped proteins in terms of their stability and activity considering the influence of the differently modified silaffin peptides used for silica formation will promote the development of silica-immobilized, stable enzyme biocatalysts.

1.5 References

1 Wedepohl, K. H. The composition of the continental crust. *Geochimica et Cosmochimica Acta*, **1995**, *59*, 1217-1232.

2 Exley, C. Silicon in life: a bioinorganic solution to bioorganic essentiality. *J. Inorg. Biochem.* **1998**, **69**, 139-144.

3 Birchall, J. D. The essentiality of silicon in biology. *Chem. Soc. Rev*. **1995**, *24*, 351-357.

4 Nielsen, F. H. Ultratrace Elements in Nutrition. *Ann. Rev. Nutr*. **1984**, *4*, 21-41.

5 Schwarz, K.; Milne, D. B. Growth-promoting effects of silicon in rats. *Nature* **1972**, *239*, 333-334.

6 Carlisle, E. M. Silicon: An essential element for the chick. *Science* **1972**, *178*, 619-621.

7 Carlisle, E. M. *J. Nutr*. In vivo requirement for silicon in articular cartilage and connective tissue formation in the chick. **1976**, *106*, 478-484.

8 Carlisle, E. M. *J. Nutr*. A silicon requirement for normal skull formation in chicks. **1980**, *110*, 352-359.

9 Schwarz, K. A bound form of silicon in glycosaminoglycans and polyuronides. *Proc. Natl. Acad. Sci. U. S. A*. **1973**, *70*, 1608-1612.

10 Matsko, N. B.; Žnidaršič, N.; Letofsky-Papst, I.; Dittrich, M.; Grogger, W.; Štrus J.; Hofer, F. Silicon: The key element in early stages of biocalcification. *J. Struct. Biol*. **2011**, *174*, 180-186.

11 Birchall, J. D.; Bellia, J. P.; Roberts, N. B. On the mechanisms underlying the essentiality of silicon - interactions with aluminum and copper. *Coord. Chem. Rev*. **1996**, *149*, 231-240.

12 Perry, C. C.; Keeling-Tucker, T. Aspects of the bioinorganic chemistry of silicon in conjunction with the biometals calcium, iron and aluminium. *J. Inorg. Biochem*. **1998**, *69*, 181-191.

13 Birchall, J. D.; Exley, C.; Chappell, J. S.; Phillips, M.J. Acute toxicity of aluminium to fish eliminated in silicon-rich acid waters. *Nature* **1989**, *338*, 146-148.

14 Edwardson, J. A.; Moore, P. B.; Ferrier, I. N.; Lilley, J. S.; Newton, G. W. A.; Barker, J.; Templar, J.; Day, J. P. Effect of silicon on gastrointestinal absorption of aluminium. *Lancet* **1993**, *342*, 211-212.

15 Bellia, J. P.; Birchall, J. D.; Roberts, N. B. The role of silicic acid in the renal excretion of aluminium *Ann. Clin. Lab. Sci*. **1996**, 26, 227-233.

16 Hodson, M. J.; White, P. J.; Mead, A.; Broadley, M. R. Phylogenetic variation in the silicon composition of plants. *Ann. Bot*. **2005**, *96*, 1027-1046.

17 Mitani, N.; Ma, J. F. Uptake system of silicon in different plant species. *J. Exp. Bot*. **2005**, *56*, 1255-1261.

18 Ma, J. F.; Yamaji, N. Functions and transport of silicon in plants. *Cell. Mol. Life Sci*. **2008**, *65*, 3049-3057.

19 Raven J. A. The transport and function of silicon in plants. *Biol. Rev.* **1983**, *58*, 179-207.

20 Epstein E. The anomaly of silicon in plant biology. *Proc. Natl. Acad. Sci. U. S. A* **1994**, *91*, 11-17.

21 Epstein E. Silicon. *Annu. Rev. Plant Physiol. Plant Mol. Biol.* **1999**, *50*, 641-664.

22 Currie, H. A.; Perry, C. C. Silica in Plants: Biological, Biochemical and Chemical Studies. *Ann. Bot*. **2007**, *100*, 1383-1389.

23 Ehrlich, H.; Demadis, K. D.; Pokrovsky, O. S.; Koutsoukos, P. G. Modern views on desilicification: biosilica and abiotic silica dissolution in natural and artificial environments. *Chem. Rev*. **2010**, *110*, 4656-4689.

24 Lewin, J.; Reimann, B. E. Silicon and plant growth. *Ann. Rev. Plant Physiol*. **1969**, *20*, 289-304.

25 Tréguer, P.; Nelson, D. M.; Van Bennekom, A. J.; DeMaster, D. J.; Leynaert, A.; Quéguiner, B. The silica balance in the world ocean: A reestimate. *Science* **1995**, *268*, 375-379.

26 Treguer, P. Silica and the cycle of carbon in the ocean. *C.R. Geosci*. **2002**, *334*, 3-11.

27 Adl, S. M.; Simpson, A. G. B.; Farmer, M. A.; Andersen, R. A.; Anderson, O. R.; Barta, J. R.; Bowser, S. S.; Brugerolle, G.; Fensome, R. A.; Fredericq, S.; James, T. Y.; Karpov, S.; Kugrens, P.; Krug, J.; Lane, C. E.; Lewis, L. A.; Lodge, J.; Lynn, D. H.; Mann, D. G.; McCourt, R. M.; Mendoza, L.; Moestrup, O.; Mozley-Standridge, S. E.; Nerad, T. A.; Shearer, C. A.; Smirnov, A. V.; Spiegel, F. W.; Taylor, M. The new higher level classification of eukaryotes with emphasis on the taxonomy of protists. *J. Euk. Microbiol*. **2005**, *52*, 399-451.

28 Norton, T.A.; Melkonian, M.; Andersen, R. A. Algal biodiversity. *Phycologia* **1996**, *35*, 353-365.

29 Mann, D. G.; Droop, S. J. M. 3. Biodiversity, biogeography and conservation of diatoms *Hydrobiologia* **1996**, *336*, 19-32.

30 Round, F. E.; Crawford, R. M.; Mann, D. G. *The Diatoms: Biology and Morphology of the Genera*, Cambridge University Press: Cambridge, 1990; p. 747.

31 Kröger, N.; Poulsen, N. Diatoms-From Cell Wall Biogenesis to Nanotechnology. *Annu. Rev. Genet*. **2008**, *42*, 83-107.

32 Del Amo, Y.; Brzezinski, M. A. The chemical form of dissolved Si taken up by marine diatoms. *J. Phycol*. **1999**, *35*, 1162-1170.

33 Martin-Jézéquel, V.; Hildebrand, M.; Brzezinski, M. A. Silicon metabolism in diatoms: implications for growth. *J. Phycol*. **2000**, *36*, 821-840.

34 Hildebrand M.; Volcani B. E.; Gassmann W.; Schroeder, J. I. A gene family of silicon transporters. *Nature* **1997**, *20*, 688-689.

35 Thamatrakoln K.; Alverson A. J.; Hildebrand M. Comparative sequence analysis of diatom silicon transporters: toward a mechanistic model of silicon transport. *J. Phycol*. **2006**, *42*, 822-834.

36 Marron, A. O.; Alston, M. J.; Heavens, D.; Akam, M.; Caccamo, M.; Holland, P. W. H.; Walker, G. A family of diatom-like silicon transporters in the siliceous loricate choanoflagellates. *Proc. R. Soc. B* **2013**, *280*, 20122543.

37 Curnow, P.; Senior, L.; Knight, M. J.; Thamatrakoln, K.; Hildebrand, M.; Booth, P. J. Expression, purification, and reconstitution of a diatom silicon transporter. *Biochemistry* **2012**, *51*, 3776-3785.

38 Simpson, T. L.; Volcani, B. E., Eds.; *Silicon and Siliceous Structures in Biological Systems*. Springer-Verlag: New York 1981.

39 Li, C.-W.; Chu, S.; Lee, M. Characterizing the silica deposition vesicle of diatoms, *Protoplasma* **1989**, *151*, 158-163.

40 Vrieling, E. G.; Gieskes, W. W. C.; Beelen, T. P. M. Silicon deposition in diatoms: control by the pH inside the silicon deposition vesicle. *J. Phycol*. **1999**, *35*, 548-559.

41 Tesson, B.; Hildebrand, M. Extensive and intimate association of the cytoskeleton with forming silica in diatoms: control over patterning on the meso-and micro-scale. *PLoS One* **2010**, *5*, e14300.

42 Chiappino, M. L.; Volcani, B. E. Studies on the biochemistry and fine structure of silica shell formation in diatoms. *Protoplasma* **1977**, *93*, 205-221.

43 Kröger N.; Wetherbee, R. Pleuralins are involved in theca differentiation in the diatom *Cylindrotheca fusiformis*. *Protist* **2000**, *151*, 263-273.

44 Volcani, B.E. In *Biochemistry of Silicon and Related Problems*; Bendz, G., Lindquist, I., Eds.; Plenum Publishing, New York, 1978; pp 177-204.

45 Nakajima T.; Volcani, B. E. 3,4-Dihydroxyproline-a new amino acid in diatom cell wall. *Science* **1969**, *164*, 1400-1401.

46 Nakajima T.; Volcani B. E.; ε-N-trimethyl-l-δ-hydroxysine phosphate and its nonphosphorylated compound in diatom cell walls. *Biochem. Biophys. Res. Commun.* **1970**, *39*, 28-33.

47 Hecky, R. E.; Mopper, K.; Kilham, P.; Degens, T. E. The amino acid and sugar composition of diatom cell-walls. *Mar. Biol*. **1973**, *19*, 323-331.

48 Kröger, N.; Bergsdorf, C.; Sumper, M. A new calcium-binding glycoprotein family constitutes a major diatom cell wall component. *EMBO J.* **1994**, *13*, 4676-4683.

49 Kröger, N.; Bergsdorf, C.; Sumper, M. Frustulins: domain conservation in a protein family associated with diatom cell walls. *Eur. J. Biochem.* **1996**, *239*, 259-264.

50 Kröger, N.; Lehmann, G.; Rachel, R.; Sumper, M. Characterization of a 200-kDa diatom protein that is specifically associated with a silica-based substructure of the cell wall. *Eur. J. Biochem.* **1997**, *250*, 99-105.

51 van de Poll, W. H.; Vrieling, E. G.; Gieskes, W. W. C. Location and expression of frustulins in the pennate diatoms *Cylindrotheca fusiformis*, *Navicula pelliculosa*, and *Navicula salinarum* (Bacillariophyceae). *J. Phycol.* **1999**, *35*, 1044-1053.

52 Bidle, K. D.; Azam, F. Accelerated dissolution of diatom silica by marine bacterial assemblages. *Nature* **1999**, *397*, 508-512.

53 Santos, J.; Almeida, S. F. P.; Figueira, E. Cadmium chelation by frustulins: a novel metal tolerance mechanism in *Nitzschia palea* (Kützing) W. Smith *Ecotoxicology* **2013**, *22*, 166-173.

54 Davis, A. K.; Hildebrand, M.; Palenik, B. A stress-induced protein associated with the girdle band region of the diatom *Thalassiosira pseudonana* (Bacillariophyta). *J. Phycol.* **2005**, *41*, 577-589.

55 Davis, A. K.; Hildebrand, M.; Palenik, B. Gene expression induced by copper stress in the diatom *Thalassiosira pseudonana*. *Eukaryotic Cell* **2006**, *5*, 1157-1168.

56 Hildebrand, M.; Kim, S.; Shi, D.; Scott, K.; Subramaniam, S. 3D imaging of diatoms with ion-abrasion scanning electron microscopy. *J. Struct. Biol*. **2009**, *166*, 316-328.

57 Hildebrand, M.; Holton, G.; Joy, D. C.; Doktycz, M. J.; Allison, D. P. Diverse and conserved nano- and mesoscale structures of diatom silica revealed by atomic force microscopy *J. Microsc*. **2009**, *235*, 172-187.

58 Brunner, E.; Richthammer, P.; Ehrlich, H.; Paasch, S.; Ueberlein, S.; van Pee, K. H. Chitin-based organic networks: An integral part of cell wall biosilica from the diatom *Thalassiosira pseudonana*: *Angew. Chem. Int. Ed*. **2009**, *48*, 9724-9727.

59 Spinde, K.; Kammer, M.; Freyer, K.; Ehrlich, H.; Vournakis, J. N.; Brunner, E. Biomimetic silicification of fibrous chitin from diatoms. *Chem. Mater*. **2011**, *23*, 2973-2978.

60 Scheffel, A.; Poulsen, N.; Shian, S.; Kröger N. Nanopatterned protein microrings from a diatom that direct silica morphogenesis. *Proc. Natl. Acad. Sci. U. S. A* **2011**, *108*, 3175-3180

61 Kröger, N.; Deutzmann, R.; Bergsdorf, C.; Sumper, M. Species-specific polyamines from diatoms control silica morphology. *Proc. Natl. Acad. Sci. U. S. A* **2000**, *97*, 14133-14138.

62 Sumper, M.; Brunner, E.; Lehmann, G. Biomineralization in diatoms: characterization of novel polyamines associated with silica. *FEBS Lett.* **2005**, *579*, 3765-3769.

63 Sumper, M.; Lehmann, G. Silica pattern formation in diatoms: species-specific polyamine biosynthesis. *ChemBioChem* **2006**, *9*, 1419-1427.

64 Sumper, M.; Brunner, E. Learning from diatoms: nature's tools for the production of nanostructured silica. *Adv. Funct. Mat.* **2006**, *16*, 17-26.

65 Frigeri, L. G.; Radabaugh, T. R.; Haynes, P. A.; Hildebrand, M. Identification of proteins from a cell wall fraction of the diatom *Thalassiosira pseudonana* - insights into silica structure formation. *Mol. Cell. Proteomics* **2006**, *5*, 182-193.

66 Sumper, M.; Lorenz, S.; Brunner, E. Biomimetic control of size in the polyamine-directed formation of silica nanospheres. *Angew. Chem. Int. Ed.* **2003**, *42*, 5192-5195.

67 Wenzl, S.; Hett, R.; Richthammer P.; Sumper, M. Silacidins: Highly acidic phosphopeptides from diatom shells assist in silica precipitation in vitro. *Angew. Chem. Int. Ed*. **2008**, *47*, 1729-1732.

68 Richthammer, P.; Börmel, M.; Brunner, E.; van Pée, K. H. Biomineralization in diatoms: The role of silacidins. *ChemBioChem* **2011**, *12*, 1362-1366.

69 Kröger, N.; Deutzmann, R.; Sumper, M. Polycationic peptides fromdiatombiosilica that direct silica nanosphere formation. *Science* **1999**, *286*, 1129-1132.

70 Kröger, N.; Deutzmann, R.; Sumper, M. Silica-precipitating peptides from diatoms. The chemical structure of silaffin-A from *Cylindrotheca fusiformis*. *J. Biol. Chem.* **2001**, *276*, 26066-26070.

71 Kröger, N.; Lorenz, S.; Brunner, E.; Sumper, M. Self-assembly of highly phosphorylated silaffins and their function in biosilica morphogenesis. *Science* **2002**, *29*, 584-586.

72 Poulsen, N.; Sumper, M.; Kröger, N. Biosilica formation in diatoms: characterization of native silaffin-2 and its role in silica morphogenesis. *Proc. Natl. Acad. Sci. U. S. A* **2003**, *100*, 12075-12080.

73 Poulsen, N.; Kröger, N. Silica morphogenesis by alternative processing of silaffins in the diatom *Thalassiosira pseudonana*. *J. Biol. Chem.* **2004**, *279*, 42993-42999.

74 Wenzl, S.; Deutzmann, R.; Hett, R.; Hochmuth, E.; Sumper, M. Quaternary ammonium groups in silica-associated proteins. *Angew. Chem. Int. Ed.* **2004**, *43*, 5933-5936.

75 Manurung, A. I.; Pratiwi, A. R.; Syah, D.; Suhartono, M. T. Isolation and characterization of silaffin that catalyze biosilica formation from marine diatom *Chaetoceros gracilis*, *HAYATI J. Biosci.* **2007**, *14*, 119-122.

76 Sumper, M. A phase separation model for the nanopatterning of diatom biosilica. *Science* **2002**, *295*, 2430-2433.

77 Sumper, M.; Brunner, E. Silica biomineralisation in diatoms: The model organism *Thalassiosira pseudonana*. *Chembiochem* **2008**, *9*, 1187-1194.

78 Sumper, M.; Hett, R.; Lehmann, G.; Wenzl, S. A code for lysine modifications of a silica biomineralizing silaffin protein. *Ang. Chem. Int. Ed.* **2007**, *46*, 8405-8408.

79 Poulsen, N.; Scheffel, A.; Sheppard, V. C.; Chesley, P. M.; Kröger, N. Pentalysine clusters mediate silica targeting of silaffins in *Thalassiosira pseudonana*. *J. Biol. Chem*. **2013**, *288*, 20100-20109.

80 Sheppard, V.; Poulsen, N.; Kröger, N. Characterization of an endoplasmic reticulum-associated silaffin kinase from the diatom *Thalassiosira pseudonana*. *J. Biol. Chem.* **2010**, *285*, 1166-1176.

81 Iler, R. K. *The Chemistry of Silica*, Wiley: New York, 1979.

82 Ostwald, W. Studien über die Bildung und Umwandlung fester Körper. *Z. Phys. Chem*. **1897**, *22*, 289-330.

83 Mizutani, T.; Nagase, H.; Fujiwara N.; Ogoshi, H. Silicic acid polymerization catalyzed by amines and polyamines. *Bull. Chem. Soc. Jpn*. **1998**, 71, 2017-2022.

84 Coradin, T.; Durupthy, O.; Livage, J. Interactions of amino-containing peptides with sodium silicate and colloidal silica: A biomimetic approach of silicification. *Langmuir* **2002**, *18*, 2331-2336.

85 Delak, K. M.; Sahai, N. Amine-catalyzed biomimetic hydrolysis and condensation of organosilicate. *Chem. Mater*. **2005**, *17*, 3221-3227.

86 Borowitzka, M. A.; Volcani, B. E. The polymorphic diatom *Phaeodactylum tricornutum*: Ultrastructure of its morphotypes. *J. Phycol.* 1978, **14**, 10-21.

87 A. M. M.; Schulz, D. Wall morphogenesis in diatoms: Deposition of silica by cytoplasmic vesicles. *Protoplasma* **1979**, *100*, 267-288.

88 Brunner, E.; Lutz, K.; Sumper, M. Biomimetic synthesis of silica nanospheres depends on the aggregation and phase separation of polyamines in aqueous solution. *Phys. Chem. Chem. Phys.* **2004**, *6,* 854-857.

89 Lutz, K.; Gröger, C.; Sumper, M.; Brunner, E. Biomimetic silica formation: analysis of the phosphate-induced self-assembly of polyamines. *Phys. Chem. Chem. Phys.* **2005**, *7*, 2812-2815.

90 Bernecker, A.; Wieneke, R.; Riedel, R.; Seibt, M.; Geyer, A.; Steinem, C. Tailored Synthetic Polyamines for Controlled Biomimetic Silica Formation. *J. Am. Chem. Soc*. **2010**, *132*, 1023-1031.

91 Kröger, N.; Sumper, M. In *Biomineralization*; Baeuerlein, E., Ed.; Wiley-VCH, Weinheim, Germany, 2000; p. 168.

92 Berthod, A. Silica: Backbone material of liquid chromatographic column packings. *J. Chromatogr*. **1991**, *549*, 1-28.

93 Chaudhry, Q.; Scotter, M.; Blackburn, J.; Ross, B.; Boxall, A.; Castle, L.; Aitken, R.; Watkins, R. Applications and implications of nanotechnologies for the food sector. *Food Addit. Contam*. **2008**, *25*, 241-258.

94 Patwardhan, S. V. Biomimetic and bioinspired silica: recent developments and applications. *Chem. Commun*. **2011**, 47, 7567-7582.

95 Li, Z.; Barnes, J. C.; Bosoy, A.; Stoddart, J. F.; Zink, J. I. Mesoporous silica nanoparticles in biomedical applications. *Chem. Soc. Rev*. **2012**, *41*, 2590-2605.

96 Anonymus. EPA R.E.D. FACTS: Silicon dioxide and Silica Gel. **1991**, 21T-1021, 1-4.

97 Kresge, C. T.; Leonowicz, M. E.; Roth, W. J.; Vartuli, J. C.; Beck, J. S. Ordered mesoporous molecular sieves synthesized by a liquid-crystal template mechanism. *Nature* **1992**, *359*, 710-712.

98 Beck, J. S.; Vartuli, J. C.; Roth, W. J.; Leonowicz, M. E.; Kresge, C. T.; Schmitt, K. D.; Chu, C. T. W.; Olson, D. H.; Sheppard, E. W. A new family of mesoporous molecular sieves prepared with liquid crystal templates. *J. Am. Chem. Soc* **1992**, *114*, 10834-10843.

99 Wan, Y.; Zhao, D. On the controllable soft-templating approach to mesoporous silicates. *Chem.Rev.* **2007**, *107*, 2821-2860.

100 Zhao, D.; Feng, J.; Huo, Q.; Melosh, N.; Frederickson, G. H.; Chmelka, B. F.; Stucky, G. D. Triblock Copolymer Syntheses of Mesoporous Silica with Periodic 50 to 300 Angstrom Pores. *Science* **1998**, *279*, 548-552.

101 Zhao, D.; Huo, Q.; Feng, J.; Chmelka, B. F.; Stucky, G. D. Nonionic triblock and star diblock copolymer and oligomeric surfactant syntheses of highly ordered,

hydrothermally stable, mesoporous silica structures. *J. Am. Chem. Soc* **1998**, *120*, 6024-6036.

102 Hoffmann, F.; Cornelius, M.; Morell, J.; Fröba, M. Silica-based mesoporous organic-inorganic hybrid materials. *Angew. Chem. Int. Ed.* **2006**, *45*, 3216-3251.

103 Giraldo, L. F.; López, B. L.; Pérez, L.; Urrego, S.; Sierra, L.; Mesa, M. Mesoporous Silica Applications. *Macromol. Symp*. **2007**, *258*, 129-141.

104 Vallet-Regi, M.; Ramila, A.; del Real, R. P.; Perez-Pariente, J. A new property of MCM-41: Drug delivery system. *J. Chem. Mater*. **2001**, *13*, 308-311

105 Radu, D. R.; Lai, C.-Y.; Jeftinija, K.; Rowe, E. W.; Jeftinija, S.; Lin, V. S. Y. A polyamidoamine dendrimer-capped mesoporous silica nanosphere-based gene transfection reagent. *J. Am. Chem. Soc*. **2004**, *126*, 13216-13217.

106 Slowing, I.; Trewyn, B. G.; Lin, V. S. Y. Effect of surface functionalization of MCM-41-type mesoporous silica nanoparticles on the endocytosis by human cancer cells. *J. Am. Chem. Soc*. **2006**, *128*, 14792-14793.

107 Trewyn, B. G.; Nieweg, J. A.; Zhao, Y.; Lin, V. S. Y. Biocompatible mesoprous silica nanoparticles with different morphologies for animal cell membrane penetration. *Chem. Eng. J.* **2008**, *137*, 23-29.

108 Mortera, R.; Vivero-Escoto, J.; Slowing, I. I.; Garrone, E.; Onida, B.; Lin, V. S. Cell-induced intracellular controlled release of membrane impermeable cysteine from a mesoporous silica nanoparticle-based drug delivery system. *Chem. Commun.* **2009**, 3219-3221.

109 Schlossbauer, A.; Schaffert, D.; Kecht, J.; Wagner, E.; Bein, T. Click chemistry for highdensity biofunctionalization of mesoporous silica. *J. Am. Chem. Soc.* **2008**, *130*, 12558-12559.

110 Charnay, C.; Bégu, S.; Tourné-Péteilh, C.; Nicole, L.; Lerner, D. A.; Devoisselle, J. M. Inclusion of ibuprofen in mesoporous templated silica: drug loading and release property *Eur. J. Pharm. Biopharm*. **2004**, *57*, 533-540.

111 Nieto, A.; Colilla, M.; Balas, F.; Vallet-Regi, M. Surface electrochemistry of mesoporous silicas as a key factor in the design of tailored delivery devices. *Langmuir* **2010**, *26*, 5038-5049.

112 Tourne-Peteilh, C.; Lerner D. A.; Charnay, C.; Nicole, L.; Bégu, S.; Devoisselle, J. M. The potential of ordered mesoporous silica for the storage of drugs: The example of a pentapeptide encapsulated in a MSU-Tween 80. *ChemPhysChem* **2003**, *4*, 281-286.

113 Slowing, I. I.; Trewyn, B. G.; Lin, V. S. Y. Mesoporous silica nanoparticles for intracellular delivery of membrane-impermeable proteins *J. Am. Chem. Soc.* **2007**, *129*, 8845-8849.

114 Lei, C.; Liu, P.; Chen, B.; Mao, Y.; Engelmann, H.; Shin, Y.; Jaffar, J.; Hellstrom, I.; Liu, J.; Hellstrom, K. E. Local Release of Highly Loaded Antibodies from Functionalized Nanoporous Support for Cancer Immunotherapy. *J. Am. Chem. Soc.* **2010**, *132*, 6906-6907.

115 Yang, C.-M.; Lin, H.-A.; Zibrowius, B.; Spliethoff, B.; Schueth, F.; Liou, S.-C.; Chu, M.-W.; Chen, C.-H. Selective surface functionalization and metal deposition in the micropores of mesoporous silica SBA-15. *Chem. Mater.* **2007**, *19*, 3205-3211.

116 Kecht, J.; Schlossbauer, A.; Bein, T. Selective functionalization of the outer and inner surfaces in mesoporous silica nanoparticles. *Chem. Mater.* **2008**, *20*, 7207-7214.

117 Doadrio, J. C.; Sousa, E. M. B.; Izquierdo-Barba, I.; Doadrio, A. L.; Perez-Pariente, J.; Vallet-Regi, M. Functionalization of mesoporous materials with long alkyl chains as a strategy for controlling drug delivery pattern. *J. Mater. Chem.* **2006**, *16*, 462-466.

118 Popova, M.D.; Szegedi, A.; Kolev, I. N.; Mihaly, J.; Tzanikov, B. S.; Momekov, G. T.; Lambov, N.G.; Yoncheva, K.P. Carboxilic modified spherical mesoporous silica as drug delivery carriers. *Int. J. Pharm*. **2012**, *436*, 778-785.

119 Vallet-Regí, M.; Balas, F.; Arcos, D. Mesoporous Materials for Drug Delivery. *Angew. Chem. Int. Ed*. 2007, 46, 7548-7558.

120 Liong, M.; Lu, J.; Kovochich, M.; Xia, T.; Ruehm, S. G.; Nel, A. E.; Tamanoi F.; Zink, J. I. Multifunctional inorganic nanoparticles for imaging, targeting, and drug delivery. *ACS Nano*, **2008**, *2*, 889-896.

121 Rosenholm, J. M.; Meinander, A.; Peuhu, E.; Niemi, R.; Eriksson, J. E.; Sahlgren, C.; Linden, M. Targeting of porous hybrid silica nanoparticles to cancer cells. *ACS Nano* **2009**, 3, 197-206.

122 Brevet, D.; Gary-Bobo, M.; Raehm, L.; Richeter, S.; Hocine, O.; Amro, K.; Loock, B.; Couleaud, P.; Frochot, C.; Morere, A.; Maillard, P.; Garcia, M.; Durand, J. Mannose-targeted mesoporous silica nanoparticles for photodynamic therapy. *Chem. Commun*. **2009**, 1475-1477.

123 Luo, Z.; Cai, K.; Hu, Y.; Zhao, L.; Liu, P.; Duan, L.; Yang, W. Mesoporous silica nanoparticles end-capped with collagen: Redox-responsive nanoreservoirs for targeted drug delivery. *Angew. Chem. Int. Ed.* **2010**, *50*, 640-643.

124 Cheng, S. H.; Lee, C. H.; Chen, M. C.; Souris, J. S.; Tseng, F. G.; Yang, C. S.; Mou, C. Y.; Chen C. T.; Lo, L. W. Trifunctionalization of mesoporous silica nanoparticles for comprehensive cancer theranostics-the trio of imaging, targeting and therapy. *J. Mater. Chem.* **2010**, *20*, 6149-6157.

125 Ferris, D. P.; Lu, J.; Gothard, C.; Yanes, R.; Thomas, C. R.; Olsen, J. C.; Stoddart, J. F.; Tamanoi, F.; Zink, J. I. Synthesis of biomolecule-modified mesoporous silica nanoparticles for targeted hydrophobic drug delivery to cancer cells. *Small* **2011**, *7*, 1816-1826.

126 Tsai, C. P.; Chen, C. Y.; Hung, Y.; Chang, F. H.; Mou, C. Y. Monoclonal antibody-functionalized mesoporous silica nanoparticles (MSN) for selective targeting breast cancer cells. *J. Mater. Chem.* **2009**, *19*, 5737-5743.

127 Cauda, V.; Engelke, H.; Sauer, A.; Arcizet, D.; Braeuchle, C.; Raedler, J.; Bein, T. Colchicine-loaded lipid bilayer-coated 50 nm mesoporous nanoparticles efficiently induce microtubule depolymerization upon cell uptake. *Nano Letters* **2010**, *10*, 2484-2492.

128 Mackowiak, S.A.; Schmidt, A.; Weiss, V.; Argyo, C.; von Schirnding, C.; Bein, T.; Bräuchle, C. Targeted drug delivery in cancer cells with red light photoactivated mesoporous silica nanoparticles. *Nano Letters* **2013**, *13*, 2576-2483.

129 Lai, C. Y.; Trewyn, B. G.; Jeftinija, D. M.; Jeftinija, K.; Xu, S.; Jeftinija, S.; Lin, V. S. A mesoporous silica nanosphere-based carrier system with chemically removable CdS nanoparticle caps for stimuli-responsive controlled release of neurotransmitters and drug molecules. *J. Am. Chem. Soc.* **2003**, *125*, 4451-4459.

130 Luo, Z.; Cai, K.; Hu, Y.; Zhao, L.; Liu, P. Duan, L.; Yang, W. Mesoporous silica nanoparticles end-capped with collagen: Redox-responsive nanoreservoirs for targeted drug delivery. *Angew. Chem. Int. Ed.* **2010**, *50*, 640-643.

131 Liu, R.; Zhao, X.; Wu, T.; Feng, P. Tunable redox-responsive hybrid nanogated ensembles. *J. Am. Chem. Soc.* **2008**, *130*, 14418-14419.

132 Bernardos, A.; Aznar, E.; Marcos, M. D.; Martinez-Manez, R.; Sancenon, F.; Soto, J.; Barat, J. M.; Amoros, P. Enzyme-responsive controlled release using mesoporous silica supports capped with lactose. *Angew. Chem. Int. Ed.* **2009**, *48*, 5884-5887.

133 Coll, C.; Mondragon, L.; Martinez-Manez, R.; Sancenon, F.; Marcos, M. D.; Soto, J.; Amoros, P.; Perez-Paya, E. Enzyme-mediated controlled release systems by anchoring peptide sequences on mesoporous silica supports. *Angew. Chem. Int. Ed.* **2011**, *50*, 2138-2140.

134 Schlossbauer, A.; Kecht, J.; Bein, T. Biotin-avidin as a protease-responsive cap system for controlled guest release from colloidal mesoporous silica. *Angew. Chem. Int. Ed.* **2009**, *48*, 3092-3095.

135 Chen, C.; Geng, J.; Pu, F.; Yang, X.; Ren, J.; Qu, X. Polyvalent nucleic acid/mesoporous silica nanoparticle conjugates: dual stimuli-responsive vehicles for intracellular drug delivery. *Angew. Chem. Int. Ed.* **2011**, *50*, 882-886.

136 Angelos, S.; Choi, E.; Vogtle, F.; De Cola, L.; Zink, J. I. Photo-driven expulsion of molecules from mesostructured silica nanoparticles. *J. Phys. Chem. C*, **2007**, *111*, 6589-6592.

137 Ferris, D. P.; Zhao, Y. L.; Khashab, N. M.; Khatib, H. A.; Stoddart, J. F.; Zink, J. I. Light-operated mechanized nanoparticles. *J. Am. Chem. Soc.* **2009**, *131*, 1686-1688.

138 **S**chloßbauer A.; Sauer A. M.; Cauda V.; Schmidt A.; Engelke H.; Rothbauer U.; Zolghadr K.; Leonhardt H.; Bräuchle C.; Bein T. Cascaded photoinduced drug delivery to cells from multifunctional core-shell mesoporous silica. *Adv. Healthcare Mater*. **2012**, *1*, 316-320.

139 Climent, E.; Bernardos, A.; Martinez-Manez, R.; Maquieira, A.; Marcos, M. D.; Pastor-Navarro, N.; Puchades, R.; Sancenon, F.; Soto, J.; Amoros, P. Controlled delivery systems using antibody-capped mesoporous nanocontainers. *J. Am. Chem. Soc.* **2009**, *131*, 14075-14080.

140 Lee, C. H.; Cheng, S. H.; Huang, I. P.; Souris, J. S.; Yang, C. S.; Mou, C. Y.; Lo, L. W. Intracellular pH-responsive mesoporous silica nanoparticles for the controlled release of anticancer chemotherapeutics. *Angew. Chem. Int. Ed.* **2010**, *49*, 8214-8219.

141 Muhammad, F.; Guo, M.; Qi, W.; Sun, F.; Wang, A.; Guo, Y.; Zhu, G. pH-triggered controlled drug release from mesoporous silica nanoparticles via intracelluar dissolution of ZnO nanolids. *J. Am. Chem. Soc.* **2011**, *133*, 8778-8781.

142 Wei, Y.; Dong, H.; Xu, J.; Feng Q. Simultaneous immobilization of horseradish peroxidase and glucose oxidase in mesoporous sol-gel host materials. *ChemPhysChem* **2002**, *3*, 802-808.

143 Dai, Z.; Liu, S.; Ju, H.; Chen, H. Direct electron transfer and enzymatic activity of hemoglobin in a hexagonal mesoporous silica matrix. *Biosens. Bioelectron.* **2004**, *19*, 861-867.

144 Dai, Z.; Xu, X.; Ju, H. Direct electrochemistry and electrocatalysis of myoglobin immobilized on a hexagonal mesoporous silica matrix. *Anal. Biochem.* **2004**, *332*, 23-31.

145 Descalzo, A. B.; Marcos, M. D.; Martinez-Manez, R.; Soto, J.; Beltran, D.; Amoros, P. Anthrylmethylamine functionalised mesoporous silica-based materials as hybrid fluorescent chemosensors for ATP *J. Mater. Chem.* **2005**, *15*, 2721-2731.

146 Radu, D. R.; Lai, C.-Y.; Wiench, J. W.; Pruski, M.; Lin, V. S. Y. Gatekeeping layer effect: A poly(lactic acid)-coated mesoporous silica nanosphere-based fluorescence probe for detection of amino-containing neurotransmitters *J. Am. Chem. Soc.* **2004**, *126*, 1640-1641.

147 Yang, M.; Li, H.; Javadi, A.; Gong, S. Multifunctional mesoporous silica nanoparticles as labels for the preparation of ultrasensitive electrochemical immunosensors. *Biomaterials* , **2010**, *31*, 3281-3286.

148 Hurley, M. T.; Wang, Z.; Mahle, A.; Rabin, D.; Liu, Q.; English, D. S.; Zachariah, M. R.; Stein, D.; DeShong, P. Synthesis, characterization, and application of antibody functionalized fluorescent silica nanoparticles. *Adv. Funct. Mater.* **2013**, *23*, 3335-3343.

149 Calvert, R. Diatomaceous earth. *J. Chem. Edu.* **1930**, *7*. 2829.

150 Xiaohua, Q.; Mingzhu, L.; Zhenbin, C.; Rui, L. Preparation and properties of diatomite composite superabsorbent. *Polym. Adv. Technol*. **2007**, *18*, 184-193.

151 Korunic, Z. Diatomaceous Earths, a Group of Natural Insecticides. *J. Stored Prod. Res*. 1998, 34, 87-97.

152 Ivanov, S.E.; Belyakov, A.V. Diatomite and its applications. *Glass Ceram*. **2008**, *65*, 48-51.

153 Osmanlioglu, A. E. Natural diatomite process for removal of radioactivity from liquid waste. *Appl Radiat Isot* **2007**, *65*, 17-20.

154 Al-Ghouti, M. A.; Khraisheh, M. A. M.; Allen, S. J.; Ahmad, M. N. The removal of dyes from textile wastewater: a study of the physical characteristics and adsorption mechanisms of diatomaceous earth. *J. Environ. Manage*. **2003**, *69*, 229-238.

155 Hsien, K.J.; Tsai, W.T.; Su, T.Y. Preparation of diatomite-TiO_2 composite for photodegradation of bisphenol-A in water. *J. Sol-Gel Sci. Technol*. **2009**, *51*, 63-69.

156 Zhu, Q. W.; Zhang, Y. H.; Zhou, F. S.; Lv, F. Z.; Ye, Z. F.; Fan, F. D.; Chu, P. K. Preparation and characterization of Cu_2O-ZnO immobilized on diatomite for photocatalytic treatment of red water produced from manufacturing of TNT. *Chem. Eng. J.* **2011**, *171*, 61-68.

157 Hamm, C. E.; Merkel, R.; Springer, O.; Jurkojc, P.; Maier, C.; Prechtel, K.; Smetacek, V. Architecture and material properties of diatom shells provide effective mechanical protection. *Nature* **2003**, *421*, 841-843.

158 Butcher, K. S. A.; Ferris, J. M.; Philips, M. R.; Wintrebertt-Foquet, M.; Wah, J. W. J.; Jovanovic, N.; Vyverman, W.; Chepurnov, V. A luminescence study of porous diatoms *Mater. Sci. Eng. C* **2005**, *25*, 658-663.

159 Fuhrmann, T.; Landwehr, S.; El Rharbi-Kucki, M.; Sumper, M. Diatoms as living photonic crystals. *Appl. Phys. B* **2004**, *78*, 257-260.

160 Payne, E. K.; Rosi, N. L.; Xue, C.; Mirkin, C. A. Sacrificial biological templates for the formation of nanostructured metallic microshells. *Angew. Chem*. **2005**, *117*, 5192-5195.

161 Sandhage, K. H. Materials 'Alchemy': Shape-preserving chemical transformation of micro-to-macroscopic 3-D structures. *JOM* **2010**, *62*, 32-43.

162 Bao, Z. H.; Song, M. K.; Davis, S. C.; Cai, Y.; Liu, M.; Sandhage, K. H. High surface area, micro/mesoporous carbon particles with selectable 3-D biogenic morphologies for tailored catalysis, filtration, or adsorption. Energy Environm. Sci. 2011, 4, 3980-3984.

163 Jeffryes, C.; Campbell, J.; Li, H. Y.; Jiao, J.; Rorrer, G. The potential of diatom nanobiotechnology for applications in solar cells, batteries, and electroluminescent devices. *Energy Enviroment. Sci*. **2011**, *4*, 3930-3941.

164 De Stefano, L.; Rendina, I.; De Stefano, M.; Bismuto, A.; Maddalena, P. Marine diatoms as optical chemical sensors. *Appl. Phys. Lett*. **2005**, *87*, 233902.

165 Lettieri, S.; Setaro, A.; De Stefano, L.; De Stefano, M.; Maddalena, P. The gas-detection properties of light-emitting diatoms. *Adv. Funct. Mater*. **2008**, *8*, 1257-1264.

166 Gale, D. K.; Gutu, T.; Jiao, J.; Chang, C. H.; Rorrer, G. L. Photoluminescence detection of biomolecules by antibody-functionalized diatom biosilica. *Adv. Funct. Mater*. **2009**, *19*, 926-933.

167 De Stefano, L.; Larnberti, A.; Rotiroti, L.; De Stefano, M. Interfacing the nanostructured biosilica microshells of the marine diatom *Coscinodiscus wailesii* with biological matter. *Acta Biomater*. **2008**, *4*, 126-130.

168 Townley, H. E.; Parker, A. R.; White-Cooper, H. Exploitation of diatom frustules for nanotechnology: Tethering active biomolecules. *Adv. Funct. Mater*. **2008**, *18*, 369-374.

169 Lin, K. C.; Kunduru, V.; Bothara, M.; Rege, K.; Prasad, S.; Ramakrishna, B. L. Biogenic nanoporous silica-based sensor for enhanced electrochemical detection of cardiovascular biomarkers proteins. *Biosens. Bioelectron*. **2010**, *25*, 2336-2342.

170 Aw, M. S.; Simovic, S.; Addai-Mensah, J.; Losic, D. Silica microcapsules from diatoms as new carrier for delivery of therapeutics. *Nanomedicine* **2011**, *6*, 1159-1173.

171 Aw, M. S.; Simovic, S.; Yu, Y.; Addai-Mensah, J.; Losic, D. Porous silica microshells from diatoms as biocarrier for drug delivery applications. *Powder Technol*. **2012**, *223*, 52-58.

172 Aw, M. S.; Bariana, M.; Yu, Y.; Addai-Mensah, J.; Losic, D. Surface functionalized diatom microcapsules for drug delivery of water-insoluble drugs. *J. Biomater. Appl*. **2013**, *28*, 163-174.

173 Bariana, M.; Aw, M. S.; Kurkuri, M.; Losic, D. Tuning drug loading and release properties of diatom silica microparticles by surface modifications. *Int. J. Pharm.* **2013**, *443*, 230-241.

174 Losic, D.; Yu, Y.; Aw, M. S.; Simovic, S.; Thierry, B.; Addai-Mensah J. Surface functionalisation of diatoms with dopamine modified iron-oxide nanoparticles: toward magnetically guided drug microcarriers with biologically derived morphologies. *Chem. Commun*. **2010**, *46*, 6323-6325.

175 Poulsen, N.; Berne, C.; Spain, J.; Kröger, N. Silica immobilization of an enzyme through genetic engineering of the diatom *Thalassiosira pseudonana*. *Angew. Chem. Int. Ed*. **2007**, *46*, 1843-1846.

176 Sheppard, V. C.; Scheffel, A.; Poulsen, N.; Kröger, N. Live diatom silica immobilization of multimeric and redox-active enzymes. *Appl. Environ. Microbiol*. **2012**, *78*, 211-218.

177 Knecht, M. R.; Wright, D. W. Functional analysis of the biomimetic silica precipitating activity of the R5 peptide from *Cylindrotheca fusiformis*. *Chem. Commun*. **2003**, 3038-3039.

178 Annenkov, V. V.; Patwardhan, S. V.; Belton, D.; Danilovtseva, E. N.; Perry, C. C. A new stepwise synthesis of a family of propylamines derived from diatom silaffins and their activity in silicification. *Chem. Commun*. **2006**, 1521-1523.

179 Belton, D. J.; Patwardhan, S. V.; Annenkov, V. V.; Danilovtseva, E. N.; Perry, C. C. From biosilicification to tailored materials: Optimizing hydrophobic domains and resistance to protonation of polyamines. *Proc. Natl. Acad. Sci. U. S. A*. **2008**, *105*, 5963-5968.

180 Masse, S.; Laurent, G.; Chuburu, F.; Cadiou, C.; Dechamps, I.; Coradin, T. Modification of the Stöber process by a polyazamacrocycle leading to unusual core-shell silica nanoparticles *Langmuir*, **2008**, *24*, 4026-4031.

181 Masse, S.; Laurent, G.; Coradin, T. Influence of cyclic polyamines on silica formation during the Stöber process. *Phys. Chem. Chem. Phys*. **2009**, *11*, 10204-10210.

182 Naik, R. R.; Whitlock, P. W.; Rodriguez, F.; Brott, L. L.; Glawe, D. D.; Clarson, S. J.; Stone, M. O. Controlled formation of biosilica structures in vitro. *Chem. Commun*. **2003**, 238-239.

183 Rodríguez, F.; Glawe, D. D.; Naik, R. R.; Hallinan, K. P.; Stone, M. O. Study of the chemical and physical influences upon in vitro peptide-mediated silica formation. *Biomacromolecules* **2004**, 5, 261-265.

184 Patwardhan, S. V.; Mukherjee, N.; Clarson, S. J. The use of poly-L-lysine to form novel silica morphologies and the role of polypeptides in biosilicification. *J. Inorg. Organomet. Polym.* **2001**, *11*, 193-198.

185 Coradin, T.; Durupthy, O.; Livage, J. Interactions of amino-containing peptides with sodium silicate and colloidal silica: A biomimetic approach of silicification. *Langmuir* **2002**, *18*, 2331-2336.

186 Patwardhan, S. V.; Mukherjee, N.; Steinitz-Kannan, M.; Clarson, S. J. Bioinspired synthesis of new silica structures. *Chem. Commun*. **2003**, 1122-1123.

187 Tomczak, M. M.; Glawe, D. D.; Drummy, L. F.; Lawrence, C. G.; Stone, M. O.; Perry, C. C.; Pochan, D. J.; Deming, T. J.; Naik, R. R. Polypeptide-templated synthesis of hexagonal silica platelets. *J. Am. Chem. Soc*. **2005**, *127*, 12577-12582.

188 Patwardhan, S. V.; Maheshwari, R.; Mukherjee, N.; Kiick, K. L.; Clarson, S. J. Conformation and assembly of polypeptide scaffolds in templating the synthesis of silica: An example of a polylysine macromolecular "Switch". *Biomacromolecules*, **2006**, *7*, 491-497.

189 McKenna, B. J.; Birkedal, H.; Bartl, M. H.; Deming, T. J.; Stucky, G. D. Micrometer-sized spherical assemblies of polypeptides and small molecules by acid-base chemistry. *Angew. Chem. Int. Ed*. **2004**, *43*, 5652-5655.

190 Coradin, T.; Roux, C.; Livage, J. Biomimetic self-activated formation of multi-scale porous silica in the presence of arginine-based surfactants. J. *Mater. Chem*. **2002**, *12*, 1242-1244.

191 Cha, J. N.; Stucky, G. D.; Morse, D. E.; Deming, T. J. Biomimetic synthesis of ordered silica structures mediated by block copolypeptides. *Nature* **2000**, *403*, 289-292.

192 Valéry, C.; Paternostre, M.; Robert, B.; Gulik-Krzywicki, T.; Narayanan, T.; Dedieu, J. C.; Keller, G.; Torres, M. L.; Cherif-Cheikh, R.; Calvo, P.; Artzner, F. Biomimetic organization: octapeptide self-assembly into nanotubes of viral capsid-like dimension, *Proc. Natl. Acad. Sci U. S. A.* **2003**, *100*, 10258-10262.

193 Pouget, E.; Dujardin, E.; Cavalier, A.; Moreac, A.; Valéry, C.; Marchi-Artzner, V.; Weiss, T.; Renault, A.; Paternostre, M.; Artzner, F. Hierarchical architectures by synergy between dynamical template self-assembly and biomineralization, *Nat. Mater*. **2007**, *6*, 434-439.

194 Wang, Q.; Zhang, J. Y. X.; Liu, D.; Zheng, J.; Pan, Y.; Lin, Y. Controlled biosilification using self-assembled short peptides A_6K and V_6K. *RSC Adv*. **2013**, *3*, 2784-2793.

195 Patwardhan, S.V.; Mukherjee, N.; Clarson, S.J. Effect of process parameters on the polymer mediated synthesis of silica at neutral pH. *Silicon Chem*. **2002**, *1*, 47-54.

196 Patwardhan, S.V.; Mukherjee, N.; Clarson, S.J. Formation of fiber-like amorphous silica structures by externally applied shear. *J. Inorg. Organomet. Polym*. **2001**, *11*, 117-121.

197 Brunner, E.; Lutz, K.; Sumper, M. Biomimetic synthesis of silica nanospheres depends on the aggregation and phase separation of polyamines in aqueous solution. *Phys. Chem. Chem. Phys.* **2004**, *6*, 854-857.

198 Lutz, K.; Gröger, C.; Sumper, M.; Brunner, E. Biomimetic silica formation: analysis of the phosphate-induced self-assembly of polyamines. *Phys. Chem. Chem. Phys*. **2005**, *7*, 2812-2815.

199 Patwardhan, S. V.; Clarson, S. J.; Silicification and biosilicification. *Silicon Chem*. **2002**, *1*, 207-214

200 Jin, R. H.; Yuan, J. J. One-pot and rapid synthesis of uniformed silica spheres via mediation of linear poly(ethyleneimine)s and dyes. *Polym. J*. **2007**, *39*, 822-827.

201 Jin, R. H.; Yuan, J. J. Synthesis of poly(ethyleneimine)s-silica hybrid particles with complex shapes and hierarchical structures. *Chem. Commun*. **2005**, 1399-1401.

202 Yuan, J. J.; Jin, R. H. Multiply shaped silica mediated by aggregates of linear poly(ethyleneimine). *Adv. Mater*. **2005**, *17*, 885-888.

203 Jin, R. H.; Yuan, J. J. Simple synthesis of hierarchically structured silicas by poly(ethyleneimine) aggregates preorganized by media modulation. *Macromol. Chem. Phys*. **2005**, *206*, 2160-2170.

204 Yuan, J. J.; Zhu, P. X.; Fukazawa, N.; Jin, R. H. Synthesis of nanofiber-based silica networks mediated by organized poly(ethylene imine): structure, properties, and mechanism. *Adv. Funct. Mater*. **2006**, *16*, 2205-2212.

205 Knecht, M. R.; Wright, D. W. Amine-terminated dendrimers as biomimetic templates for silica nanosphere formation. *Langmuir* **2004**, *20*, 4728-4732.

206 Knecht, M. R.; Sewell, S. L.; Wright, D. W. Size control of dendrimer-templated silica. *Langmuir* **2005**, *21*, 2058-2061.

207 Neville, F.; Broderick, M. J.; Gibson, T.; Millner, P. A. Fabrication and activity of silicate nanoparticles and nanosilicate-entrapped enzymes using polyethyleneimine as a biomimetic polymer. *Langmuir* **2011**, *27*, 279-285.

208 Kristensen, J. B.; Meyer, R. L.; Poulsen, C. H.; Kragh, K. M.; Besenbacher, F.; Laursen, B. S. Biomimetic silica encapsulation of enzymes for replacement of biocides in antifouling coatings. *Green Chem.* **2010**, *12*, 387-394.

209 Berne, C.; Betancor, L.; Luckarift, H. R.; Spain, J. C. Application of a microfluidic reactor for screening cancer prodrug activation using silica-immobilized nitrobenzene nitroreductase. *Biomacromolecules* **2006**, *7*, 2631-2636.

210 Betancor, L.; Berne, C.; Luckarift, H. R.; Spain, J. C. Coimmobilization of a redox enzyme and a cofactor regeneration system. *Chem. Commun.* **2006**, 3640-3642.

211 Miller, S. A.; Hong, E. D.; Wright, D. Rapid and efficient enzyme encapsulation in a dendrimer silica nanocomposite. *Macromol. Biosci*. **2006**, *6*, 839-845.

212 Luckarift, H. R.; Dickerson, M. B.; Sandhage, K. H.; Spain, J. C. Rapid, room-temperature synthesis of antibacterial bionanocomposites of lysozyme with amorphous silica or titania. *Small* **2006**, *2*, 640-643.

213 Ramanathan, M.; Luckarift, H. R.; Sarsenova, A.; Wild, J. R.; Ramanculov, E. K.; Olsen, E. V.; Simonian, A. L. Lysozyme-mediated formation of protein-silica nano-composites for biosensing applications. *Colloids Surf., B* **2009**, *73*, 58-64

214 Luckarift, H. R.; Balasubramanian, S.; Paliwal, S.; Johnson, G. R.; Simonian, A. L. Enzyme-encapsulated silica monolayers for rapid functionalization of a gold surface. *Colloids Surf., B* **2007**, *58*, 28-33.

215 Ivnitski, D.; Artyushkova, K.; Rincon, R. A.; Atanassov, P.; Luckarift, H. R.; Johnson, G. R. Entrapment of enzymes and carbon nanotubes in biologically synthesized silica: Glucose oxidase-catalyzed direct electron transfer. *Small* **2008**, *4*, 357-364.

216 Luckarift, H. R.; Spain, J. C.; Naik, R. R.; Stone, M. O. Enzyme immobilization in a biomimetic silica support. *Nat. Biotechnol*. **2004**, *22*, 211-213.

217 Naik, R. R.; Tomczak, M. M.; Luckarift, H. R.; Spain, J. C.; Stone, M. O. Entrapment of enzymes and nanoparticles using biomimetically synthesized silica. *Chem. Commun*. **2004**, 1684-1685.

218 Coradin, T.; Coupé, A.; Livage, J. Interactions of bovine serum albumin and lysozyme with sodium silicate solutions. *Colloids Surf., B* **2003**, *29*, 189-196.

219 Cardoso, M. B.; Luckarift, H. R.; Urban, V. S.; O'Neill, H.; Johnson, G. R. Protein localization in silica nanospheres derived via biomimetic mineralization. *Adv. Funct. Mater*. **2010**, *20*, 3031-3038.

220 Luckarift, H. R.; Johnson, G. R.; Spain, J. C. Silica-immobilized enzyme reactors: application to cholinesterase-inhibition studies. *J. Chromatogr. B* **2006**, *843*, 310-316.

221 Brott, L. L.; Naik, R. R.; Pikas, D. J.; Kirkpatrick, S. M.; Tomlin, D. W.; Whitlock, P. W.; Clarson, S. J.; Stone, M. O. Ultrafast holographic nanopatterning of biocatalytically formed silica. *Nature* **2001**, *413*, 291-293.

222 Coffman, E. A.; Melechko, A. V.; Allison, D. P.; Simpson, M. L.; Doktycz, M. J. Surface patterning of silica nanostructures using bio-inspired templates and directed synthesis. *Langmuir* **2004**, *20*, 8431-8436.

223 Betancor, L.; Luckarift, H. R.; Seo, J. H.; Brand, O.; Spain, J. C. Three dimensional immobilization of β-galactosidase on a silicon surface. *Biotechnol. Bioeng*. **2008**, *99*, 261-267.

224 Vamvakaki, V.; Hatzimarinaki, M.; Chaniotakis, N. Biomimetically synthesized silica-carbon nanofiber architectures for the development of highly stable electrochemical biosensor systems. *Anal. Chem*. **2008**, *80*, 5970-5975.

225 Hatzimarinaki, M.; Vamvakaki, V.; Chaniotakis, N. Spectro-electrochemical studies of acetylcholinesterase in carbon nanofiber-bioinspired silica nanocomposites for biosensor development. *J. Mater.Chem*. **2009**, *19*, 428-433.

226 Nam, D. H.; Won, K.; Kim, Y. H.; Sang, B. I. A novel route for immobilization of proteins to silica particles incorporating silaffin domains. *Biotechnol. Progr*. **2009**, *25*, 1643-1649.

227 Marner, W. D.; Shaikh, A. S.; Muller, S. J.; Keasling, J. D. Enzyme immobilization via silaffin-mediated autoencapsulation in a biosilica support. *Biotechnol. Progr*. **2009**, *25*, 417-423.

228 Choi, O.; Kim, B. C.; An, J. H.; Min, K.; Kim, Y. H.; Um, Y.; Oh, M. K.; Sang, B. I. A biosensor based on the self-entrapment of glucose oxidase within biomimetic silica nanoparticles induced by a fusion enzyme. *Enzyme Microb. Technology* **2011**, *49*, 441-445.

229 Nam, D. H.; Lee, J. O.; Sang, B. I.; Won, K.; Kim, Y. H. Silaffin peptides as a novel signal enhancer for gravimetric biosensors. *Appl. Biochem. Biotechnol*. **2013**, *170*, 25-31.

Chapter 2

A Sequence-function analysis of the silica precipitating silaffin R5 peptide

The R5 peptide is derived from silaffin peptides naturally occurring in the diatom C. fusiformis and exhibits outstanding activity in silica precipitation. Due to its ability to cause silicification under mild conditions, several biotechnological applications based on R5-mediated biomimetic silica formation have already been reported. Yet a more detailed understanding of the R5 peptide and its intrinsic silica precipitation activity will help the rational design of R5 peptide variants as efficient agents for defined silica precipitation. The herein presented analysis of the relationship between the R5 amino acid sequence and its activity in silica precipitation emphasizes the essential role of the lysine residues in mediating silica polycondensation. Furthermore, a tetra amino acid motif (RRIL) has to be present within the R5-sequence but in contrast to previous reports we demonstrate that localization of the RRIL-motif shows minor impact on silica precipitation activity but rather on morphology of the resulting silica material. The amino acid sequence of silaffin peptides is a well-balanced arrangement in terms of positively charged side chains and different functional groups and their respective positioning. The impact of this pattern of charges and functionalities was highlighted by the disturbed morphology of silica spheres resulting from R5-variants with scrambled sequences. A detailed understanding of the evolved silaffin sequence(s) will contribute to unravel the intriguing process of silica biomineralization in diatoms.

2.1 Introduction

Biogenic formation of silica, the most abundant compound in the Earth's crust, takes place in diatoms, sponges and higher plants.[1] Diatoms are eukaryotic, unicellular microalgae and represent the major producers of amorphous silica in aqueous habitats. During their cell cycle, diatoms use special transporter proteins[2,3] to take up silicon mainly as silicic acid from their marine or fresh water environment.[4] The controlled precipitation of silica takes place in a specialized compartment, the silica deposition vesicle (SDV)[5] and the newly formed silica is finally deposited to form the exoskeleton. The highly elaborate, nano-patterned shells of diatoms are comprised of amorphous silica associated with organic matter.[1] The different classes of biomolecules identified from diatom cell walls comprise polysaccharides, e.g. poly-*N*-acetyl-D-glucosamine,[6] long chain polyamines (LCPAs)[7,8] and diverse proteins, such as frustulins,[9,10] pleuralins,[11,12] silacidins,[13,14] cingulins[15] and silaffins.[16] The latter has been proven to be located in the SDV[17] and along with LCPAs to be directly involved in the silica biomineralization process.[7,16]

Silaffins comprise a class of proteins and peptides present in most diatom species that are expressed as long precursor polypeptides and subsequently proteolytically processed and further posttranslationally modified during maturation.[18] In the diatom *C. fusiformis*, maturation of the silaffin precursor protein Sil1p results in seven silaffin peptides that show a high sequence similarity and are rich in serine and lysine residues (repetitive units R1-7).[16] The numerous serine residues in these peptides become phosphorylated and the lysine residues become hydroxylated, followed by phosphorylation at the δ-C-atom as well as methylation or alkylation with oligo-*N*-methylpropylenimine units at the ε-amino group (Figure 1-5).[19,20] The unique polyamine-modifications have been proven to be essential for the silicification activity of silaffins at acidic pH.[16] Indeed, the *in vivo* target location of silaffins, the SDV is an acidic compartment.[21,22] Nevertheless, a synthetic silaffin peptide, the repetitive unit R5 (H-SSKKSGSYSGSKGSKRRIL-OH) from *C. fusiformis* lacking any posttranslational modifications (PTMs), has been shown to efficiently precipitate silica from a phosphate buffered solution of silicic acid at neutral pH.[16,19] The proposed mechanism of silaffin- as well as R5-peptide-mediated silica precipitation involves self-assembly of these peptides. The resulting assemblies serve as templates for polycondensation of silicic acid.

Amino groups of the polyamine modifications or of the lysine residues itself mediate formation of siloxane-bonds (Figure 2-1).[16,19,23]

Due to their unique chemical and physical properties, silica-based materials have many applications, e.g. in coating, catalysis, and sensing.[24] Implementation of silica materials into biotechnology and medicine, for example in enzyme immobilization, biosensing, drug delivery and controlled release is a quickly developing field.[25-27] This fast development is based on the advantageous mild reaction conditions of biomimetic approaches for silica formation that offer an attractive alternative to common industrial silica syntheses, especially if hybrid silica materials containing sensitive biomolecules are formed.[28] Biomimetic and bioinspired silica precipitation approaches have been carried out with a number of organic additives, including polyamines,[29-32] poly-L-lysine (PLL),[33-35] block copolypeptides,[36] designed peptides,[37,38] or peptides mimicking the naturally occurring silaffins.[39-41] These molecules have been proven to be able to initiate silica formation but also to control silica morphology depending on reaction conditions, such as air oxidation, phosphate ion concentration or application of external forces (e.g. mechanical shear forces, electrostatic field, nitrogen bubbling through reaction solution).[34-36,40,42]

Based on its outstanding silica precipitating activity, several approaches towards biotechnological applications of the R5 peptide from *C. fusiformis* have been suggested, e. g. holographic nanopatterning,[43] coating,[44] and immobilization of enzymes.[45-49] The R5-sequence can be genetically fused to target proteins that should become encapsulated in a silica matrix.[47-49] Nevertheless, a thorough understanding of the silica precipitation mechanism of the R5 peptide would greatly facilitate further applications. This will not only promote the development of the R5-peptide into an efficient agent for silica precipitation in biotechnology, but will also help in further broadening the understanding of silica biomineralization in diatoms. In a previous study, Knecht *et al*. have already highlighted some key features of the R5-peptide essential for its silica precipitation activity.[41] Nevertheless, some aspects regarding the R5 sequence itself and specific amino acids were not addressed.

Here the silica precipitating activity of the silaffin R5 sequence is analyzed with special focus on the lysine residues, the C-terminal RRIL motif and the amino acid sequence.

2.2 Materials and methods

2.2.1 Materials

Fmoc-protected L-amino acids, Fmoc-Ala-Wang resin, Fmoc-Gly-Wang, Fmoc-Leu-Wang resin and 2-(1*H*-benzotriazol-1-yl)-1,1,3,3-tetramethyl-uronium hexafluorophosphate (HBTU) were purchased from Novabiochem (Nottingham, UK) and Fmoc-Lys(Boc)-Wang resin from Iris Biotech (Marktredwitz, Germany). *N*,*N*-dimethylformamide (DMF), dichloromethane (DCM) and acetonitrile (ACN) was obtained from Biosolve (Valkenswaard, The Netherlands), trifluoroacetic acid (TFA) from Roth (Karlsruhe, Germany). All other chemicals were from Sigma-Aldrich (Taufkirchen, Germany).

2.2.2 General procedure for solid phase peptide synthesis

Synthesis of all peptides was accomplished manually using fluorenylmethoxycarbonyl (Fmoc) chemistry[50] on preloaded Wang-polystyrene resins in 0.1 or 0.2 mmol scale, respectively. The Fmoc-amino acids contained the following side chain protecting groups: Arg(Pbf), Lys(Boc), Ser(tBu) and Tyr(tBu). The pseudo-proline dipeptide Fmoc-Gly-Ser($\psi^{Me,Me}$pro)-OH was used at suitable positions to improve synthesis yields[51,52] and a ninhydrin test was done occasionally to check deprotection and coupling reactions.[53] Fmoc-deprotection was achieved with 20 % piperidine in DMF with cycles of 3 and 7 min. Amino acids (2.5 eq.) were coupled using HBTU (2.38 eq.) and DIEA (5 eq.) for 30 min.

Peptides were globally deprotected and cleaved from dried resin with a mixture of TFA, triisopropylsilane and water (92.5 : 5 : 2.5) for 3 h at RT. Precipitation of crude peptides was achieved by addition of three volumes of cold diethyl ether followed by centrifugation. After washing twice with ether, precipitated peptides were dissolved in 50 % ACN in water and lyophilized.

All peptides were purified by reversed phase HPLC using a Varian Pro Star system and a C4 column (250 x 22 mm, 5 µm particle size, Protein C4, Grace Vydac) and a C18 column (250 x 10 mm, 5 µm particle size, Kromasil). Elution was achieved running linear gradients of

buffer B (ACN + 0.08 % TFA) in buffer A (ddH_2O + 0.1 % TFA). Collected fractions were analyzed by ESI-MS and pooled according to purity. All calculations of yields for purified peptides are based on the synthesis scale.

2.2.3 HPLC and mass spectrometry

Analytical HPLC analysis of peptides was performed on a Dionex Ultimate 3000 instrument using a RP-C4-column (Kromasil 300-5-C4, 150 x 4.6 mm, 5 µm particle size) at a flow rate of 1 mL/min with a linear gradient from 5 to 65% buffer B in buffer A over 30 min. Detection occurred at 214 and 280 nm wavelength.
Peptide masses were determined by electrospray ionization mass spectrometry (ESI-MS) on a Waters AutoPurification HPLC/MS System (3100 Mass Detector, 2545 Binary Gradient Module, 2767 Sample Manager and 2489 UV/Visible Detector) operating in positive ion mode.

2.2.4 *In vitro* silica precipitation

For silica precipitation assays peptides were dissolved in 50 mM potassium phosphate buffer at pH 7. Addition of silicic acid up to a final concentration of 25 mM to the peptide solution initiated silicification reactions. Silicic acid was freshly generated from tetramethoxysilane in 1 mM aqueous HCl in 4 min before each assay. Reaction mixtures were incubated at RT for 30 min, subsequently silica precipitates were separated by centrifugation (14000 rpm, 5 min) and washed twice with water.

2.2.5 Electron microscopy

For electron microscopic analysis, silica precipitates were suspended in water and suspension was applied to a *Thermanox*™ cover slip and air dried. Before analysis, samples were sputter coated with gold in high vacuum (Bal-Tec SCD 005). Electron micrographs were acquired with a scanning electron microscope (JEOL JSM 5900 LV) at 20 kV. Analysis of elemental

composition was performed with an implemented energy dispersive X-ray (EDX) detector (Röntec).

2.2.6 Quantification of precipitated silica

Silica precipitation experiments were carried out as described above. The collected silica precipitates were washed twice with ddH_2O and dissolved in 2 M NaOH for 1 h at RT. A modified β-silicomolybdate assay was used for quantification of silicon.[39,54] Briefly, a molybdate solution was produced by diluting 1.35 mL HCl (37 %) in 40.3 mL ddH_2O and mixing with a solution of 774.2 mg $(NH_4)_6Mo_7O_{24} \times 4\ H_2O$ dissolved in 9.7 mL ddH_2O. The pH was adjusted to 1.12 with 2 M NaOH. 40 µL of sample solution with dissolved silica were mixed with 160 µL ddH_2O and 800 µL of the molybdate solution and the absorbance was measured at 370 nm. The amount of silicon was calculated from a calibration curve conducted with a silicon atomic absorption standard solution. All measurements were repeated at least in triplicate.

2.3 Results and discussion

The R5 peptide (H-SSKKSGSYSGSKGSKRRIL-OH) is derived from silaffin-$1A_1$ of the diatom *C. fusiformis*, but lacking all native posttranslational modifications (PTMs).[16] The silica precipitation activity of the R5 peptide is proposed to be dependent on the ability of the peptide to self-assemble in solution into larger aggregates, which then constitute a template for silica formation.[19] The ε-amino groups of the lysine residues in the peptide act as acid-base catalysts that facilitate formation of siloxane bonds that finally result in precipitated silica (Figure 2-1).[23] However, conclusive proof that lysine residues as well as their positioning within the R5 peptide are essential in this process is not available yet. Additionally the role of the C-terminal tetrapeptide RRIL is not fully understood. The RRIL-motif is not present in native silaffins isolated from diatoms and proteolytic removal from the parent silaffin sequence by a specific protease is suggested.[20] However, the RRIL-sequence is required for silicification activity of synthetic R5.[41] Overall, little is known about the significance of the exact peptide sequence of native silaffins and the synthetic R5 peptide for their silica precipitation activity.

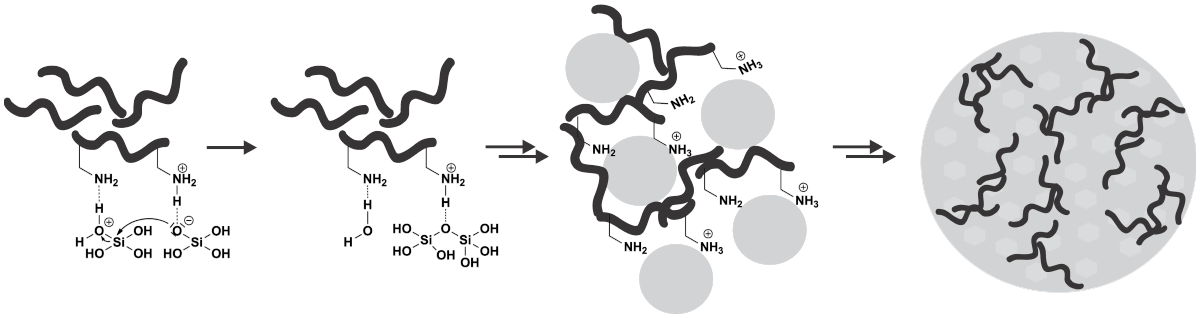

Figure 2-1 Proposed mechanism for R5 peptide-mediated polycondensation of silicic acid.

To address these points, a series of peptide variants derived from the parent R5-sequence (Table 2-1) was synthesized and analyzed in terms of their specific silica precipitation activity and morphology of resulting silica material. Peptide **1** is the R5 sequence N-terminally elongated with a cysteine residue that is able to efficiently precipitate spherical silica particles from a phosphate buffered solution of silicic acid (Figure 2-2,A).

Table 2-1 Characteristics of synthetic peptides

No.	sequence	$MW_{calc.}$	$MW^{*}_{obs.}$	Yield[a]	spec. activity[b]
1	CSSKKSGSYSGSKGSKRRIL	2115.12	2115.13	27.8 %	0.82 ± 0.02
2	SSAASGSYSGSAGSARRIL	1783.88	1784.45	22.7 %	n.d.
3	RRILSSKKSGSYSGSKGSK	2012.11	2012.32	9.0 %	0.78 ± 0.06
4	RRILSSAASGSYSGSAGSA	1783.88	1784.45	21.6 %	n.d.
5	SSKKSGSYSGSKGSK	1473.74	1473.72	53.5 %	n.d.
6	SSAASGSYSGSAGSA	1245.51	1245.46	44.0 %	n.d.
7	RRIL	556.38	556.18	97.7 %	n.d.
8	KRRIL	684.48	684.25	38.1 %	0.09 ± 0.03
9	KGSKRRIL	956.62	956.30	83.2 %	0.43 ± 0.02
10	LKSRGSKSGRYSSKSSKIG	2012.11	2012.50	33.3 %	0.82 ± 0.05
11	KYSSGSKSKSKGSGSRRIL	2012.11	2012.43	49.2 %	0.77 ± 0.02
12	SSKKSGSYRRILSGSKGSK	2012.11	2012.64	30.3 %	0.79 ± 0.02

[a] Yields based on synthesis scale

[b] Specific silica precipitation activity at pH 7.0 given in pmol silicon per min and nmol of peptide

n.d. = not detectable

***** For detailed synthesis data see chapter 2.5

To elucidate the function of lysine ε-amino groups in peptide **2** all lysine residues within the R5 sequence were replaced by alanine. Deletion of all amino groups except the N-terminal results in complete loss of silica precipitation activity (Table 2-1) This finding reflects the unique function of amino groups in silica formation. After removal of all ε-amino groups in the R5 peptide an inadequate number of basic functional groups is available to mediate polycondensation of silicic acid. The remaining two guanidine groups within the RRIL motif do not rescue silica precipitation activity. This is further emphasized when comparing silicification activities of peptides **3** and **4**. In these two peptide variants the RRIL motif was moved from C- to N-terminus and this change leads to an activity very similar to peptide **1** if all lysine residues are present as in peptide **3**. Peptide **4** with a complete lysine to alanine exchange shows no silica precipitation activity as observed for peptide **2** (Table 2-1, Figure 2-3). Positionings of the RRIL-sequence at opposing ends in peptide **1** and **3** does not influence the total amount of precipitated silica. However, morphology of the resulting silica

particles is altered and with peptide **3** imperfect spheres exhibiting surface irregularities are obtained (Figure 2-2,B).

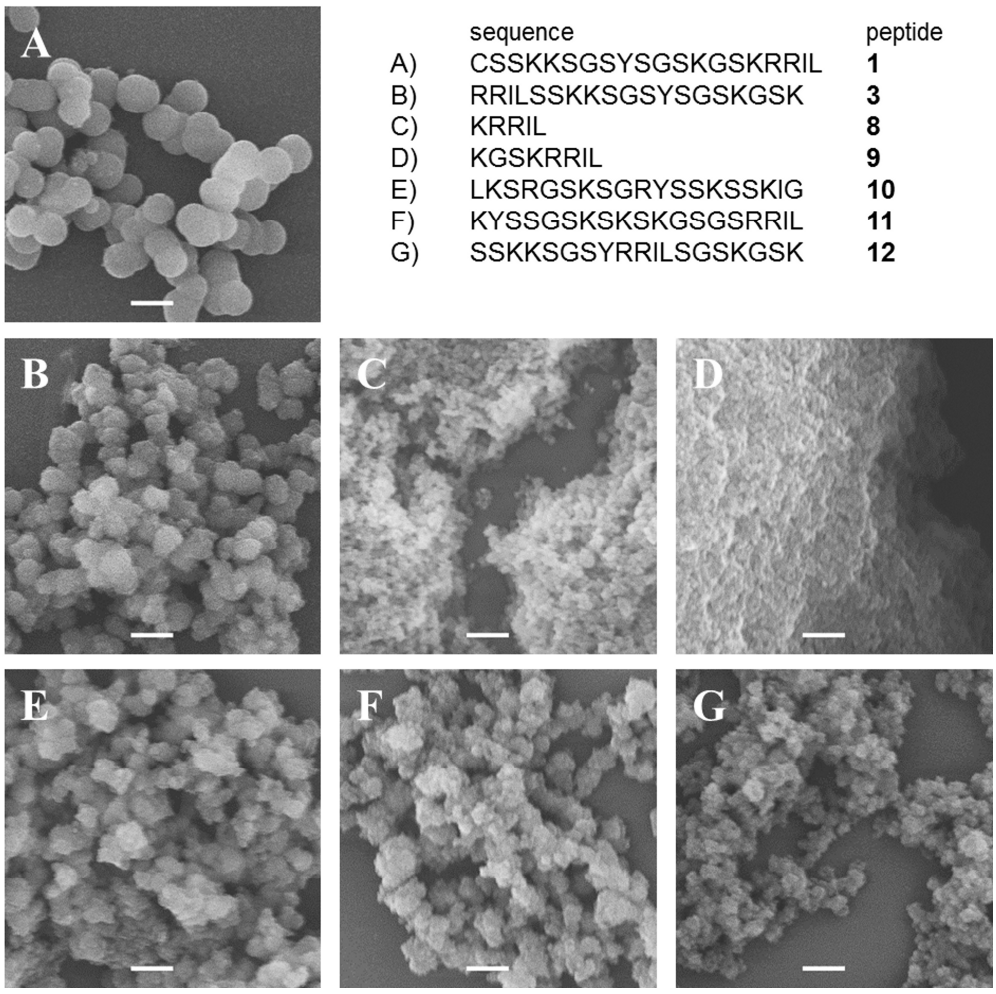

Figure 2-2 Scanning electron micrographs from silica particles resulting from (A) peptide **1**, (B) peptide **3**, (C) peptide **8**, (D) peptide **9**, (E) peptide **10**, (F) peptide **11** and (G) peptide **12**. Scale bars: 1µm.
Inset: Amino acid sequence of peptides resulting in the corresponding silica materials.

Deletion of the C-terminal RRIL-sequence from R5 leads to a complete loss of silica precipitation activity as demonstrated with peptides **5** and **6** comprising amino acids 1-15 of the native R5 sequence (Table 2-1). Neither the alanine-mutant (peptide **6**) nor the variant with four lysine residues (peptide **5**) is able to precipitate silica. Previously, a greatly reduced

activity for peptide **5** has been reported.[41] These differences might be caused by slightly different reaction conditions such as higher concentration of silicic acid and peptides applied in this study. The dramatic effect of deleting the RRIL sequence indicates an important role of this motif in silica precipitation activity, which is independent of its positioning either at the N- or C-terminus of the R5 peptide. To further elucidate RRIL importance within the R5 sequence, an RRIL tetrapeptide was synthesized and its silica precipitation activity analyzed. The isolated RRIL-peptide **7** does not precipitate silica (Table 2-1), which is in good agreement with the fact that the lysine-free R5 variant **2** is inactive as well. Therefore, two adjacent basic residues such as the arginines in RRIL cannot, independent of additional amino or guanidine groups, support silica precipitation under the reaction conditions used here.

L-Arginine alone has been shown to enhance the condensation rate of silicate monomers and the aggregation of colloidal silica particles. The guanidine group of arginine (pK 12.1) was suggested to assist in bridging between negatively charged silicate monomers or small silica nuclei at neutral pH, resulting in increased condensation rates and particle aggregation.[55] Studies with longer poly-arginine peptides provided additional proof that an increasing number of charged groups correlates with enhanced silica formation.[33] However, these systems used silicate solutions or silica sols as silica precursors with very high molar ratios of arginine or poly-arginine to silicic acid (between 0.5 and 0.1, respectively),[33,55] whereas in this study, a lower ratio of peptides to silicic acid (~ 0.02) was applied. These factors are very likely to account for the undetectable silica precipitation activity of peptide **7** under conditions applied here.

A general role of arginine residues in R5 as amino acids that direct self-assembly rather than being directly involved in silica formation has already been indicated in a previous study by Knecht and Wright.[41] The complete loss in silica precipitating activity after exchanging the arginine residues in some peptide variants into alanine, glutamate or glutamine provided proof for a pivotal role of the arginine guanidine groups. In one of the steps involved in silica precipitation (Figure 2-1), a function of the RRIL motif in self-assembly of the R5 variants in a micelle-like manner driven by the positively charged guanidinium groups and the adjacent hydrophobic amino acid isoleucine and leucine was suggested.[41] Such a micelle-like assembly is inconsistent with results obtained with peptide **3** in this study in which the RRIL

motif has been placed at the N-terminus. In this arrangement, micellar-like self-assembly of the peptides is highly unlikely. In contrast, salt-bridges between positively charged guanidine groups of arginine and negatively charged phosphate anions as the basis of R5 self-assembly still seem plausible. This hypothesis is strengthened by the facts that divalent anions such as phosphate are essential for self-assembly and silica-precipitating activity of unmodified R5 peptides[19] and that replacement of arginine with negatively charged glutamate residues obliterates the self-assembly properties of R5 variants.[41] Also mixtures of the RRIL tetrapeptide **7** with peptides **5** or **6** did not lead to precipitation of silica from a phosphate buffered solution of orthosilicic acid (data not shown). Based on this observation it is concluded that the four amino acids RRIL have to be covalently tethered to the R5 sequence to convey significant self-assembly and silica precipitation properties.

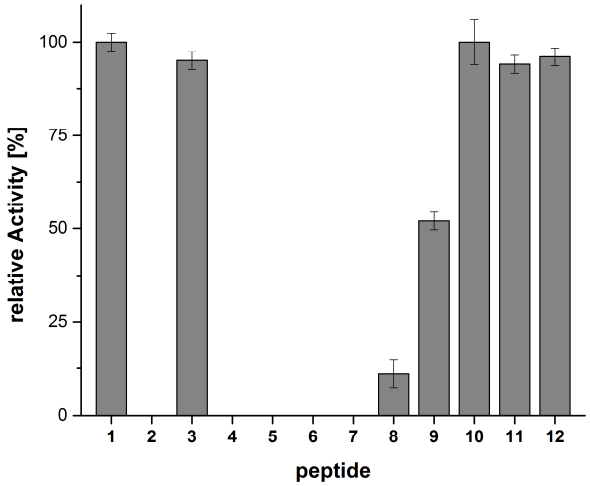

Figure 2-3 Relative silica precipitation activity of peptides **1-12**. (Peptide **1** is 100 %).

Extending the RRIL-sequence (**7**) N-terminally with one lysine residue (peptide **8**) leads to a slight recovery of silica precipitation activity (Table 2-1, Figure 2-3). Scanning electron microscopy (SEM) pictures of the obtained silica material shows small silica nanospheres assembling into larger clusters (Figure 2-2,C). Further N-terminal elongation of peptide **8** with the native sequence up to lysine residue 12 yields peptide **9** comprising the KGSK sequence and the RRIL motif. The tetrapeptide domain KXXK is a commonly observed motif of lysines in silaffin sequences of different diatom species and undergoes defined

posttranslational modification reactions.[16,56] Peptide **9** shows 50 % of the silica precipitation activity of peptide **1** (Table 2-1, Figure 2-3). The decreased specific silica precipitation activities of truncated peptides **8** and **9** compared to full length R5 variants (Table 2-1) can be explained by the reduced number of lysine residues. Studies with poly-lysine peptides with different number of lysine residues revealed increasing rates of silica formation with increasing chain length.[33]

The silica material obtained from peptide **9** closely resembles the one generated with peptide **8**, but the single nanospheres are not as distinctly visible in the fused cluster (Figure 2-2,D). This material (Figure 2-2,C and D) indicates an early stage in silica formation, a process that starts with condensation of silicic acid monomers resulting in the formation of polysilicic acid species. These colloidal silica particles grow by further condensation reactions with silicic acid monomers or colloidal silica particles aggregates and form larger silica particles (Figure 2-1). Cationic species such as polyamines have two modes of action to assist silica formation. They promote the condensation reaction of silicic acid molecules by stabilizing the transition state and they adsorb to negatively charged surfaces of colloidal silica and bring single particles close together, which results in flocculation and precipitation of silica.[30,33] The silica materials formed with peptides **8** and **9** appear to be such unstructured clusters of colloidal silica particles. Previous studies on poly-lysine mediated silica formation from silicate solutions or silica sols also gave silica materials with similar morphologies.[33,55]

Thus, although the lysine amino groups have been proven to be required for silica formation, the precipitation of silica with well-defined spherical morphologies as mediated by R5 variants depends on the exact amino acid sequence and composition.

Synthetic KXXK tetrapeptides carrying typical PTMs of silaffins, i.e. methylation and polyamine modification, have recently been shown to precipitate silica.[39] A correlation between the nature of X in the KXXK peptides and the amount and morphologies of silica precipitates became apparent. The polarity of the X residues adjacent to the C-terminal lysine residue directly influenced the size of the nanospheres in the resulting silica precipitates.[39] The KXXK peptides (also termed mini-silaffins) exhibit silica precipitation activity even in the absence of the C-terminal RRIL-sequence. The polycationic lysine modifications in the synthetic mini-silaffins assist in the self-assembly of these peptides in phosphate containing buffer just as is in native silaffins.[16,19] This finding supports the fact that the RRIL sequence

is not needed for silica precipitation activity of fully postranslationally modified silaffins, in which it is proteolytically removed.[20] Since self-assembly of native silaffins is mainly driven by their oppositely charged PTMs, they do not require the RRIL-motif for self-assembly. In contrast, unmodified R5 peptides rely on the presence of the RRIL motif and divalent anions in the reaction solution to exert their silica precipitation activity, suggesting a self-assembly of these peptides mediated by the RRIL-motif and the phosphate anions.

The large influence of amino acid sequence and of the RRIL motif in R5-mediated silica precipitation is further emphasized by the results obtained with peptides **10-12** (Table 2-1). These peptide variants represent scrambled versions of the R5 peptide, i.e. containing all native amino acids but in random order. In peptide **10**, the complete peptide sequence including the RRIL motif is scrambled, in peptide **11** the RRIL-motif is kept at its native C-terminal position but all other amino acids are randomly rearranged. Peptide **12** is an R5 variant in which the RRIL-motif is placed in the middle of the sequence. Peptide variants **10-12** exhibit similar specific silica precipitation activities at neutral pH in phosphate containing buffer as peptide **1** (Table 2-1, Figure 2-3). Morphologies of the obtained silica material resemble the grainy silica spheres also generated with peptide **3**, but with a significant decrease in particle size (Figure 2-2). These results strengthen the hypothesis that the RRIL amino acids contribute to peptide self-assembly via salt-bridging rather than via micelle formation. Although in peptide **10** the RRIL motif is disrupted and the amino acids are randomly distributed over the peptide sequence preventing mecellar self-assembly, this peptide still shows the same silica precipitating activity as peptide **1** (Figure 2-3). Proper self-assembly based on the RRIL amino acids present in the peptide sequence seems to occur independently from their sequential order or location at one of the peptide termini.

The scrambled versions of R5 used here (peptides **10-12**) also illustrate the influence of the R5 peptide sequence on the morphology of the obtained silica material. Only the native R5 sequence results in homogeneous spherical silica particles (Figure 2-2,A). Spatial organization of lysine residues and their protonated ε-amino groups, within the peptide sequence has a distinct influence on silica morphologies. For polyamine-induced silica formation, the spacing of amino groups has been shown to play an important role.[31,32] Cationic amino groups arranged in a specific pattern are thought to bring silicic acid monomers and colloidal silica particles into a close configuration which promotes

condensation reactions (Figure 2-1). In peptides **10** and **11**, distances between lysine residues are altered when compared to peptide **1** which results in fuzzy particle shapes. In both peptides, no adjacent lysine residues occur as observed in the native R5 sequence (Table 2-1). In addition, as demonstrated with synthetic KXXK mini-silaffins, the chemical nature of the amino acid side chains close to the lysine residues influences the structure of silica material.[39] This effect is also reflected in scrambled peptides **10-12**, in which the interplay of serine and lysine residues is disrupted (Figure 2-2, E-G).

2.4 Conclusion

The synthetic R5 peptide derived from the C. fusiformis silaffin-1A1 and lacking all native PTMs is a powerful tool for silica formation under mild conditions and holds great potential for biotechnological applications. For this purpose, a detailed understanding of the peptide sequence and amino acid functionalities is essential. To elucidate the impact of single amino acids and the influence of the R5 amino acid sequence, we synthesized a series of R5 variants (peptides 1-12) and observed different specific activities in silica precipitation and variable morphologies of the obtained silica material.

The amino groups of the lysine residues were confirmed as active elements in silica formation since mutations to alanine residues resulted in complete loss of function. In addition, the range of specific silica precipitation activity depends on the total number of lysine residues present in the peptide variants. The structure of the silica material turned out to be influenced by the number of lysine residues as well but also by their positioning in the peptide sequence and by the chemical nature of neighboring amino acids.

In addition it was confirmed that the amino acids of the RRIL motif have to be present in the R5 peptide, however not necessarily at the native C-terminal position or in their native order to maintain silica precipitation activity. These results suggest a contribution of the RRIL amino acids in formation of peptide assemblies, which serve as template for silica precipitation. Salt bridge formation between the guanidine groups of arginine residues and phosphate anions rather than micellar assemblies seems to be the most plausible explanation based on our data for this finding.

The sequence-function analysis of the silaffin R5 peptide emphasizes nature's sophisticated design of a biomolecule that combines functionalities for silica formation and structuring. Knowledge about key features and requirements in the R5 peptide sequence as well as modifications for silica formation can serve as basis for rational development of the R5 peptide into an efficient silica precipitating agent for a number of applications. A general advantage of the R5 peptide over other additives for biomimetic silica formation such as polyamines is the option to generate genetic fusions of the R5 sequence and a protein of interest. Such protein-R5 chimeras have great potential for efficient and homogenous silica immobilization of proteins and thus generation of stabilized biocatalysts and biosensors.[47-49]

In order to fully appreciate and understand the unique silica precipitation abilities of native silaffins and R5 in particular the impact of posttranslational modifications and their complex combinations need to be analyzed next.

2.5 Supplement: Analytical data for synthetic peptides 1-12

Peptide 1: **H-CSSKKSGSYSGSKGSKRRIL-OH**

Unmodified silaffin R5 peptide **1** was synthesized using standard SPPS procedures. Peptide **1** was purified by RP-HPLC (preparative C4, 10 mL/min flow rate, 5 % to 65 % buffer B (ACN + 0.08 % TFA) in buffer A (ddH_20 + 0.1 % TFA) in 60 min, and subsequent semipreparative C18 column, 3 mL/min flow rate, 5 % to 65 % buffer B in buffer A in 60 min) yielding 24.7 mg of peptide **1** in high purity (27.8 % yield).

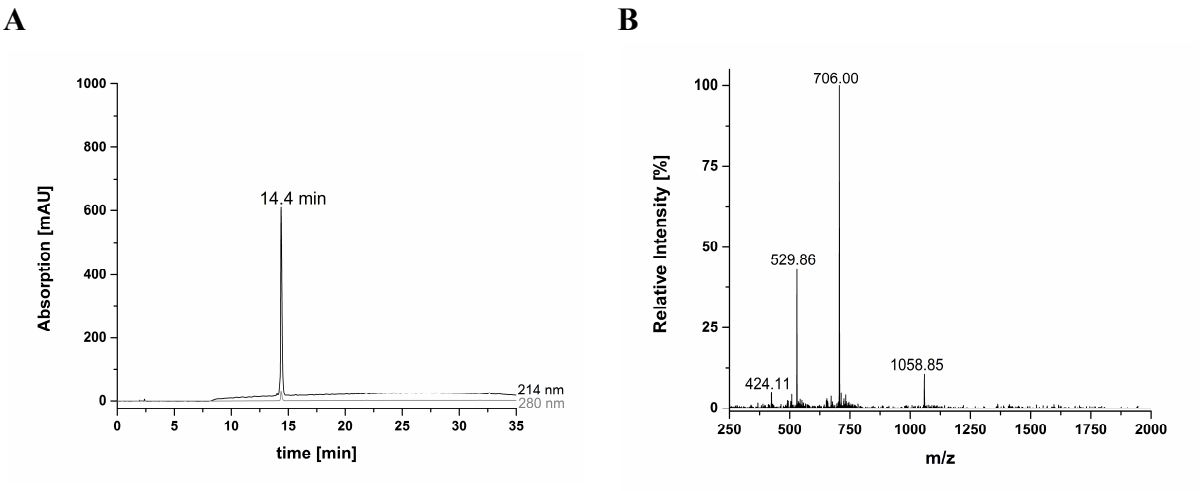

Figure 2-2 **A)** Analytical RP-HPLC chromatogram of purified peptide **1**.
B) ESI-MS of purified peptide **1**. Mass calculated for $C_{87}H_{155}N_{30}O_{29}S^+$: 2116.13 $[M+H]^+$, found: 1058.85 $[M+2H]^{2+}$, 706.00 $[M+3H]^{3+}$, 529.86 $[M+4H]^{4+}$, 424.11 $[M+5H]^{5+}$.

Peptide 2: **H-SSAASGSYSGSAGSARRIL-OH**

After synthesis of peptide **2** following standard solid phase peptide synthesis procedures, purification of crude peptide **2** was achieved by RP-HPLC using a preparative C4 column running a linear gradient from 5 to 65 % buffer B in buffer A in 60 min at a flow rate of 10 mL/min. 40.5 mg (22.7 %) of pure peptide were obtained.

A **B**

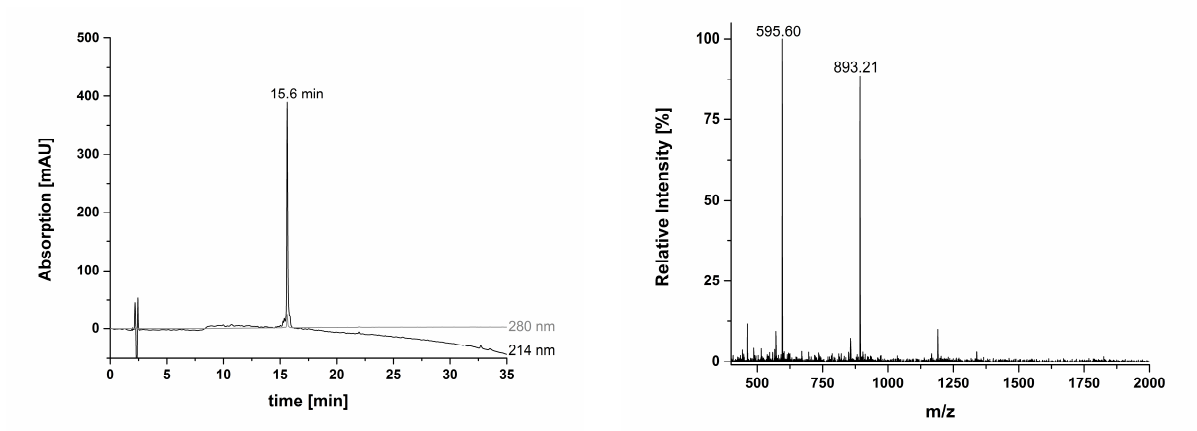

Figure 2-3 **A)** Analytical RP-HPLC chromatogram of purified peptide **2**.

B) ESI-MS of purified peptide **2**. Mass calculated for $C_{72}H_{122}N_{25}O_{28}^{+}$: 1784.89 $[M+H]^{+}$, found: 893.21 $[M+2H]^{2+}$, 595.60 $[M+3H]^{3+}$.

<u>Peptide 3:</u> **H-RRILSSKKSGSYSGSKGSK-OH**

Purification of crude peptide **3** was achieved by RP-HPLC using a C4 column running a linear gradient from 5 to 65 % buffer B in buffer A in 60 min (10 mL/min flow rate) resulting in the isolation of 6 mg peptide **3** (9 % yield).

A **B**

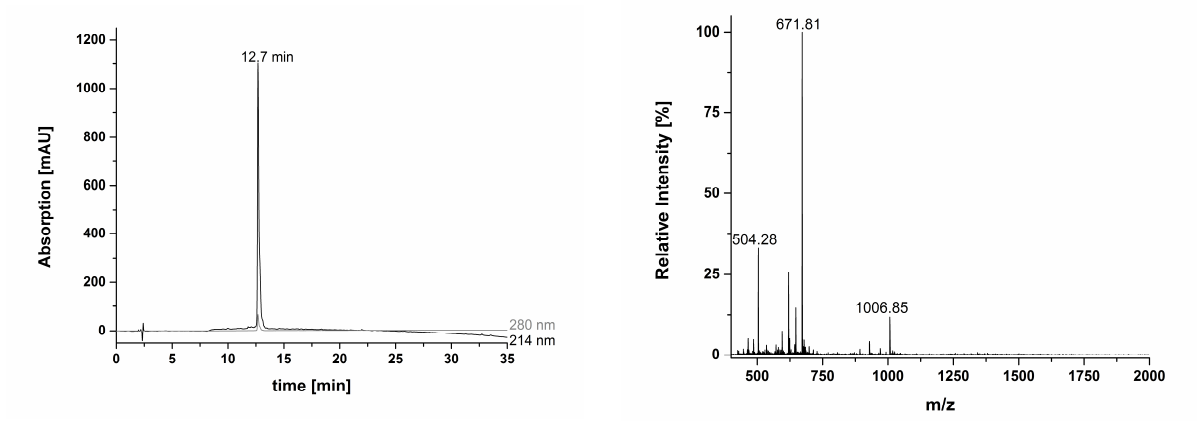

Figure 2-4 **A)** Analytical RP-HPLC chromatogram of purified peptide **3**.

B) ESI-MS of purified peptide **3**. Mass calculated for $C_{84}H_{150}N_{29}O_{28}^{+}$: 2013.12 $[M+H]^{+}$, found: 1006.85 $[M+2H]^{2+}$, 671.81 $[M+3H]^{3+}$, 504.28 $[M+4H]^{4+}$.

Peptide 4: **H-RRILSSAASGSYSGSAGSA-OH**

Peptide **4** was purified by RP-HPLC with a C4 column (10 mL/min flow rate, 5 % to 65 % buffer B in buffer A in 60 min) and subsequently with a C18 column (3 mL/min flow rate, 5 % to 65 % buffer B in buffer A in 60 min). 15 mg (21.6 %) of peptide **4** were isolated.

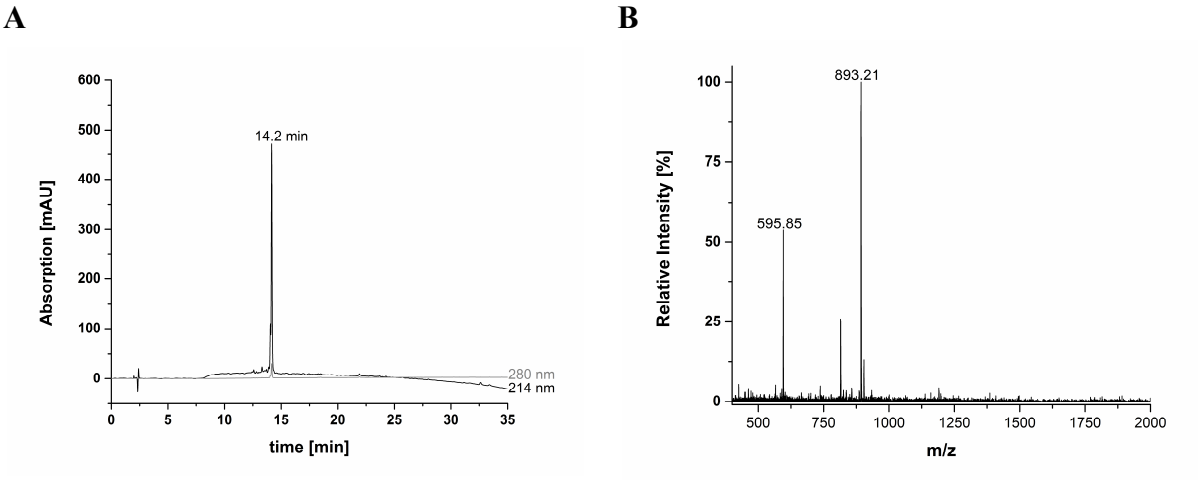

Figure 2-5 **A)** Analytical RP-HPLC chromatogram of purified peptide **4**.
B) ESI-MS of purified peptide **4**. Mass calculated for $C_{72}H_{122}N_{25}O_{28}^{+}$: 1784.89 $[M+H]^{+}$, found: 893.21 $[M+2H]^{2+}$, 595.85 $[M+3H]^{3+}$.

Peptide 5: **H-SSKKSGSYSGSKGSK-OH**

Purification of peptide **5** was achieved by RP-HPLC using a preparative C18 column running a linear gradient from 5 to 65 % buffer B in buffer A in 30 min at a flow rate of 3 mL/min yielding 10.4 mg pure peptide (53.5 %).

A **B**

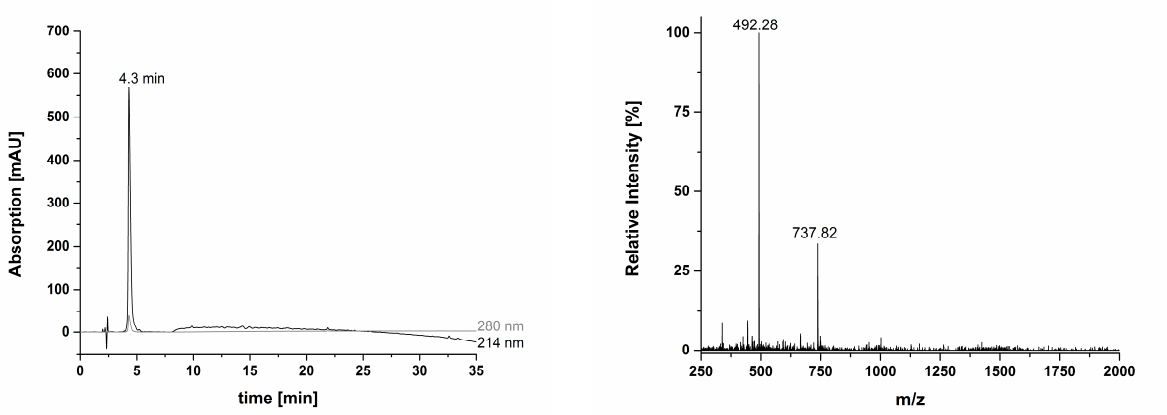

Figure 2-6 **A)** Analytical RP-HPLC chromatogram of purified peptide **5**.
B) ESI-MS of purified peptide **5**. Mass calculated for $C_{60}H_{104}N_{19}O_{24}^{+}$: 1474.75 $[M+H]^{+}$, found: 737.82 $[M+2H]^{2+}$, 492.28 $[M+3H]^{3+}$.

Peptide 6: H-SSAASGSYSGSAGSA-OH

Peptide **6** was purified by RP-HPLC with a C18 column (3 mL/min flow rate, linear gradient from 5 to 65 % buffer B in buffer A in 30 min) with a yield of 12.4 mg pure peptide (44.0 %).

A **B**

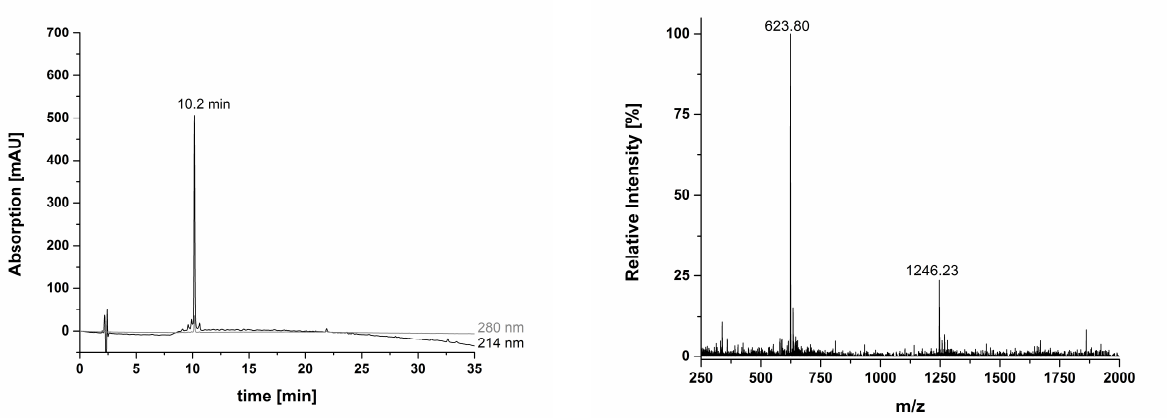

Figure 2-7 **A)** Analytical RP-HPLC chromatogram of purified peptide **6**.
B) ESI-MS of purified peptide **6**. Mass calculated for $C_{48}H_{76}N_{15}O_{24}^{+}$: 1246.52 $[M+H]^{+}$, found: 1246.23 $[M+H]^{+}$, 623.80 $[M+2H]^{2+}$.

Peptide 7: **H-RRIL-OH**

Purification of crude tetrapeptide **7** was achieved by RP-HPLC using a C4 column running a linear gradient from 20 to 65 % buffer B in buffer A in 30 min (10 mL/min flow rate). 54.4 mg pure peptide **7** were isolated (97.7 % yield).

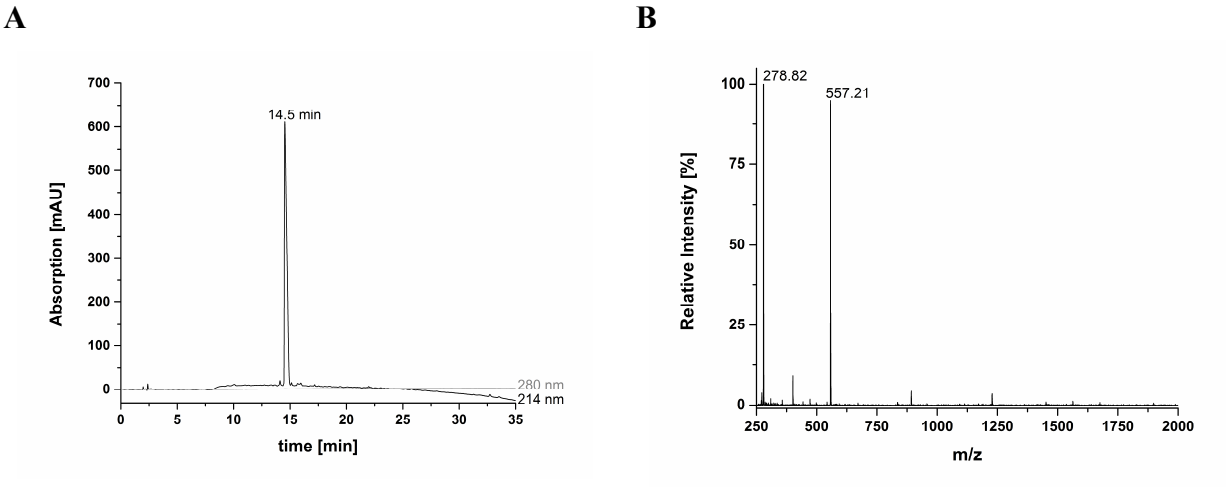

Figure 2-8 **A)** Analytical RP-HPLC chromatogram of purified peptide **7**.
B) ESI-MS of purified peptide **7**. Mass calculated for $C_{24}H_{49}N_{10}O_5^+$: 557.39 $[M+H]^+$, found: 557.21 $[M+H]^+$, 278.82 $[M+2H]^{2+}$.

Peptide 8: **H-KRRIL-OH**

For purification of crude peptide **8** a C4 column and a linear gradient from 5 to 65 % buffer B in buffer A in 60 min at a flow rate of 10 mL/min was used during RP-HPLC. 26.1 mg pure peptide were obtained (38.1 % yield).

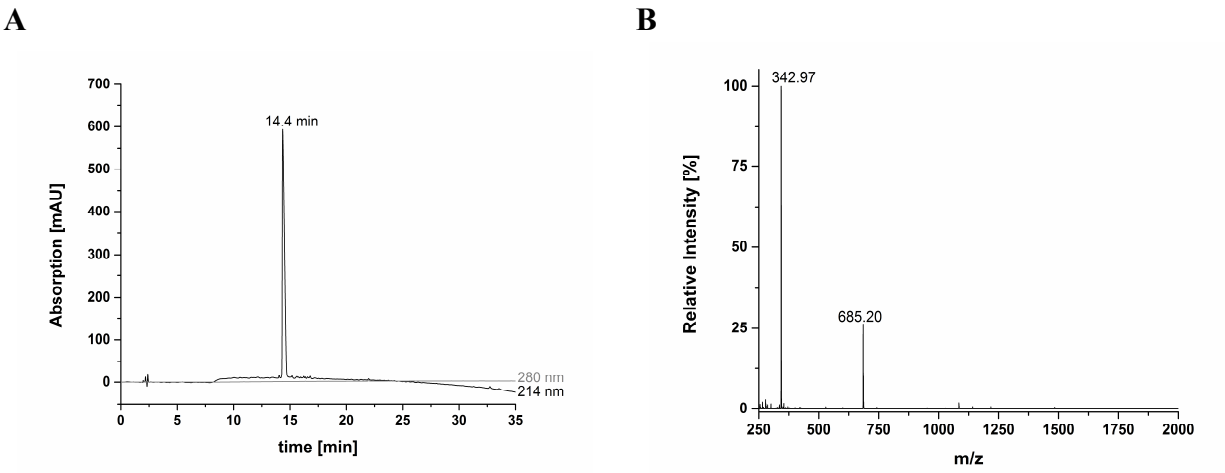

Figure 2-9 **A)** Analytical RP-HPLC chromatogram of purified peptide **8**.
B) ESI-MS of purified peptide **8**. Mass calculated for $C_{30}H_{61}N_{12}O_6^+$: 685.48 $[M+H]^+$, found: 685.20 $[M+H]^+$, 342.97 $[M+2H]^{2+}$.

Peptide 9: H-KGSKRRIL-OH

Peptide **9** was purified by RP-HPLC (preparative C4, 10 mL/min flow rate, 5 % to 65 % buffer B in buffer A in 60 min, 10 mL/min flow rate) yielding 47 mg of peptide **9** in good purity (83.2 % yield).

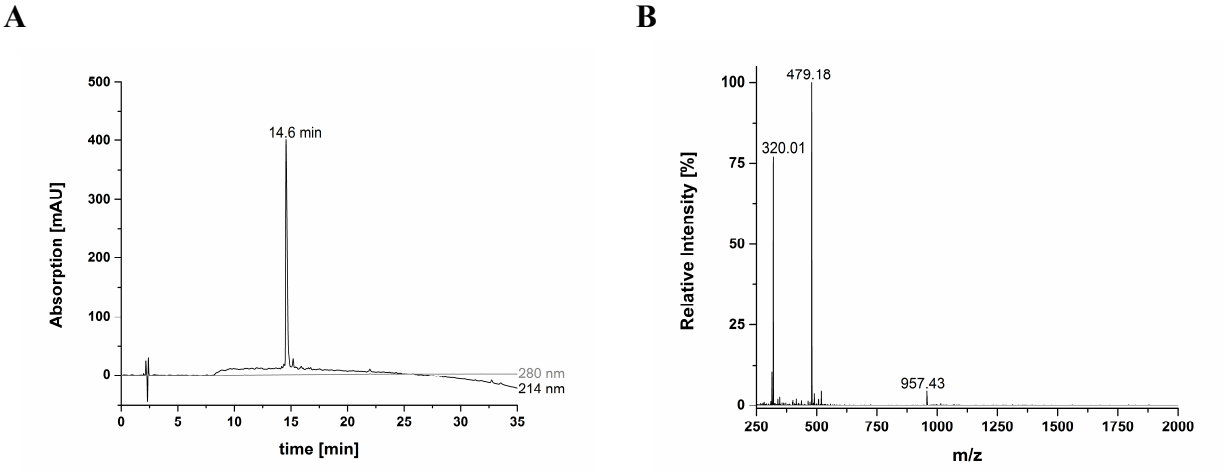

Figure 2-10 **A)** Analytical RP-HPLC chromatogram of purified peptide **9**.
B) ESI-MS of purified peptide **9**. Mass calculated for $C_{41}H_{81}N_{18}O_{10}^+$: 957.63 $[M+H]^+$, found: 957.43 $[M+H]^+$, 479.18 $[M+2H]^{2+}$, 320.01 $[M+3H]^{3+}$.

Peptide 10: **H-LKSRGSKSGRYSSKSSKIG-OH**

Purification of crude peptide **10** was achieved by RP-HPLC using a preparative C4 column running a linear gradient from 5 to 65 % buffer B in buffer A in 60 min at a flow rate of 10 mL/min. 33.5 mg (33.3 %) of peptide **10** were isolated.

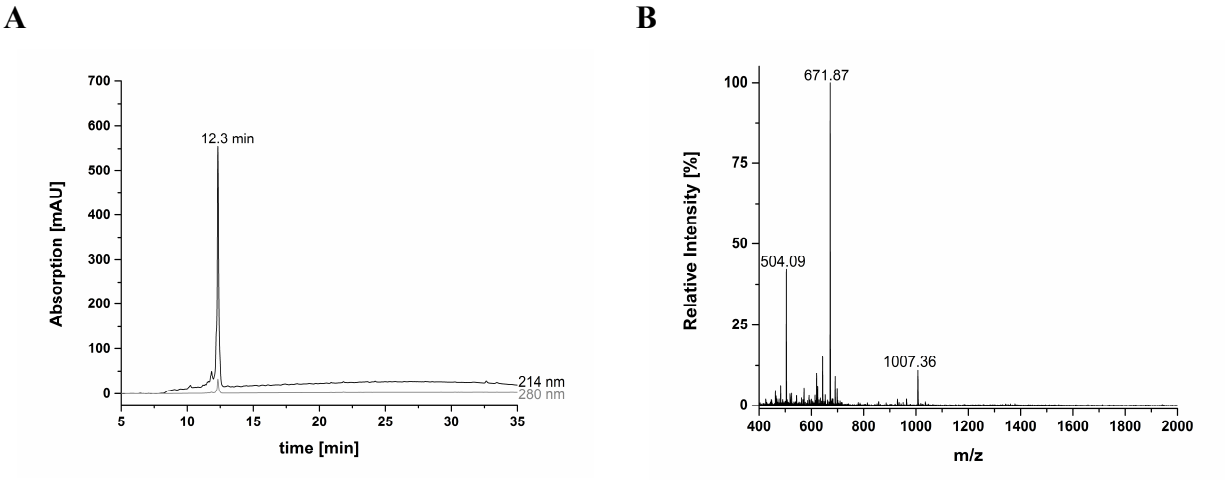

Figure 2-11 **A)** Analytical RP-HPLC chromatogram of purified peptide **10**.
B) ESI-MS of purified peptide **10**. Mass calculated for $C_{84}H_{150}N_{29}O_{28}^{+}$: 2013.12 $[M+H]^{+}$, found: 1007.36 $[M+2H]^{2+}$, 671.87 $[M+3H]^{3+}$, 504.09 $[M+4H]^{4+}$.

Peptide 11: **H-KYSSGSKSKSKGSGSRRIL-OH**

Peptide **11** was purified by RP-HPLC with a C4 column (10 mL/min flow rate, linear gradient from 5 to 65 % buffer B in buffer A in 30 min) yielding 49.5 mg pure peptide **11** (49.2 %).

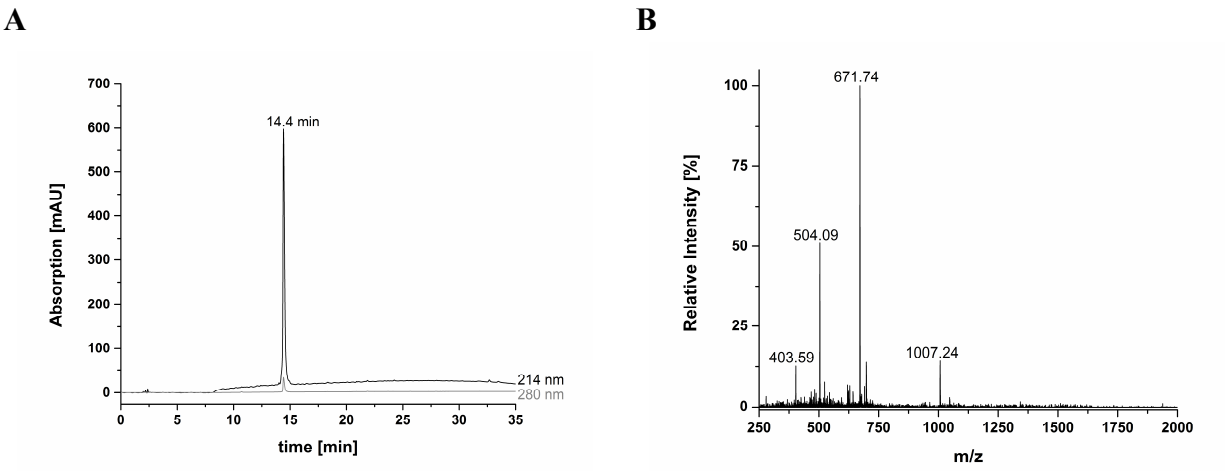

Figure 2-12 **A)** Analytical RP-HPLC chromatogram of purified peptide **11**.
B) ESI-MS of purified peptide **11**. Mass calculated for $C_{84}H_{150}N_{29}O_{28}^{+}$: 2013.12 $[M+H]^{+}$, found: 1007.24 $[M+2H]^{2+}$, 671.74 $[M+3H]^{3+}$, 504.09 $[M+4H]^{4+}$, 403.59 $[M+5H]^{5+}$.

<u>Peptide 12:</u> **H-SSKKSGSYRRILSGSKGSK-OH**

Purification of crude peptide **12** was achieved by RP-HPLC using a C4 column running a linear gradient from 5 to 65 % buffer B in buffer A in 60 min at a flow rate of 10 mL/min. 30.5 mg (30.3 %) of peptide **12** were obtained.

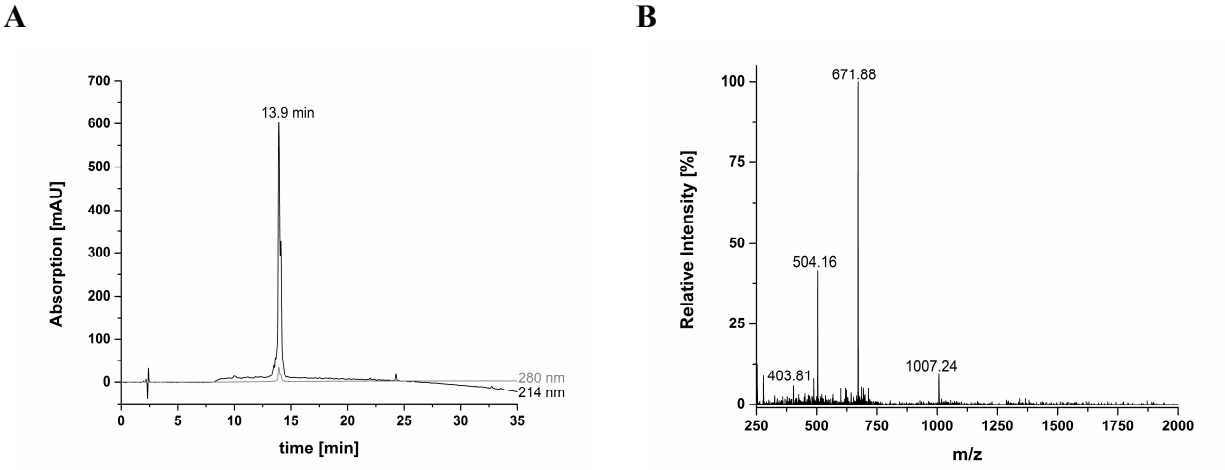

Figure 2-13 **A)** Analytical RP-HPLC chromatogram of purified peptide **12**.
B) ESI-MS of purified peptide **12**. Mass calculated for $C_{84}H_{150}N_{29}O_{28}^{+}$: 2013.12 $[M+H]^{+}$, found: 1007.24 $[M+2H]^{2+}$, 671.88 $[M+3H]^{3+}$, 504.16 $[M+4H]^{4+}$, 403.81 $[M+5H]^{5+}$.

2.6 References

1 Simpson, T.L.; Volcani, B. E. *Silicon and Siliceous Structures in Biological Systems*, Springer, New York, **1981**.

2 Hildebrand, M.; Volcani, B.E.; Gassmann, W.; Schroeder, J. I. A gene family of silicon transporters. *Nature* **1997**, *385*, 688-689.

3 Hildebrand, M.; Dahlin, K.; Volcani, B. E. Characterization of a silicon transporter gene family in *Cylindrotheca fusiformis* sequences, expression analysis, and identification of homologs in other diatoms. *Mol. Gen. Genet*. **1998**, *260*, 480-486.

4 Del Amo, Y.; Brzezinski, M.A. The chemical form of dissolved Si taken up by marine diatoms. *J. Phycol*. **1999**, *35*, 1162-1170.

5 Pickett-Heaps, J.; Schmid, M. M.; Edgar, L. A. In *Progress in Phycological Research;* Round, F. E., Chapman, D. J., Eds.; Biopress, Bristol, **1990**, *7*, pp. 1-169.

6 Brunner, E.; Richthammer, P.; Ehrlich, H.; Paasch, S.; Simon, P.; Ueberlein, S.; van Pee, K. H. Chitin-based organic networks: an integral part of cell wall biosilica in the diatom *Thalassiosira pseudonana*. *Angew. Chem. Int. Ed*. **2009**, *48*, 9724-9727.

7 Kröger, N.; Deutzmann, R.; Bergsdorf, C.; Sumper, M. Species-specific polyamines from diatoms control silica morphology. *Proc. Natl. Acad. Sci. U.S.A.* **2000**, *97*, 14133-14138.

8 Sumper, M.; Brunner, E.; Lehmann. G. Biomineralization in diatoms: Characterization of novel polyamines associated with silica. *FEBS Lett*. **2005**, *579*, 3765-3769.

9 Kröger, N.; Bergsdorf, C.; Sumper, M. A new calcium binding glycoprotein family constitutes a major diatom cell wall component. *EMBO J*. **1994**, *13*, 4676-4683.

10 Kröger, N.; Bergsdorf, C.; Sumper, M. Frustulins: domain conservation in a protein family associated with diatom cell walls. *Eur. J. Biochem*. **1996**, *239*, 259-264.

11 Kröger, N.; Lehmann, G.; Rachel, R.; Sumper, M. Characterization of a 200-kDa diatom protein that is specifically associated with a silica-based substructure of the cell wall. *Eur. J. Biochem.***1997**, *250*, 99-105.

12 Kröger, N.; Wetherbee, R. Pleuralins are involved in theca differentiation in the diatom *Cylindrotheca fusiformis. Protist* **2000**, *151*, 263-273.

13 Wenzl, S.; Hett, R.; Richthammer, P.; Sumper, M. Silacidins: highly acidic phosphopeptides from diatom shells assist in silica precipitation in vitro. *Angew. Chem.Int. Ed*. **2008**, *47*, 1729-1732.

14 Richthammer, P.; Börmer, M.; Brunner, E.; van Pee, K. H. Biomineralization in diatoms: the role of silacidins. *ChemBioChem* **2011**, *12*, 1362-1366.

15 Scheffel, A.; Poulsen, N.; Shian, S.; Kröger, N. Nanopatterned protein microrings from a diatom that direct silica morphogenesis. *Proc. Natl. Acad.Sci. U.S.A*. **2011**, *108*, 3175-3180.

16 Kröger, N.; Deutzmann, R.; Sumper, M. Polycationic peptides from diatom biosilica that direct silica nanosphere formation. *Science* **1999**, *286*, 1129-1132.

17 Poulsen, N.; Scheffel, A.; Sheppard, V. C.; Chesley, P. M.; Kröger, N. Pentalysine Clusters Mediate Silica Targeting of Silaffins in *Thalassiosira pseudonana*. *J. Biol. Chem*. **2013**, *288*, 20100-20109.

18 Kröger, N.; Poulsen, N. Diatoms - from cell wall biogenesis o nanotechnology. *Annu. Rev. Genet*. **2008**, *42*, 83-107.

19 Kröger, N.; Lorenz, S.; Brunner, E.; Sumper, M. Self-assembly of highly phosphorylated silaffins and their function in biosilica morphogenesis. *Science* **2002**, *298*, 584–86.

20 Kröger, N.; Deutzmann, R.; Sumper, M. Silica-precipitating peptides from diatoms. The chemical structure of silaffin-A from *Cylindrotheca fusiformis*. *J. Biol. Chem*. **2001**, *276*, 26066–26070.

21 Li, C. W.; Chu, S.; Lee, M. Characterizing the silica deposition vesicle of diatoms. *Protoplasma* **1989**, *151*, 158–163.

22 Vrieling, E. G.; Gieskes, W. W. C.; Beelen, T. P. M. Silicon deposition in diatoms: control by the pH inside the silicon deposition vesicle. *J. Phycol*. **1999**, *35*, 548-559.

23 Kröger, N.; Sumper, M. In *Biomineralization;* Baeuerlein, E., Ed.; Wiley-VCH: Weinheim, Germany, **2000**; p. 168.

24 Pagliaro, M. *Silica-Based Materials for Advanced Chemical Applications*, RSC Publishing, Cambridge, **2009**.

25 Slowing, I. I.; Trewyn, B. G.; Giri, S.; Lin, V. S. Y. Mesoporous silica nanoparticles for drug delivery and biosensing applications. *Adv. Funct. Mater*. **2007**, *17*, 1225-1236.

26 Liong, M.; Angelos, S.; Choi, E.; Patel, K.; Stoddard, J. F.; Zing, J. I. Mesostructured multifunctional nanoparticles for imaging and drug delivery. *J. Mater. Chem*. **2009**, *19*, 6251-6257.

27 Betancor, L.; Luckarift, H. R. Bioinspired enzyme encapsulation for biocatalysis. *Trends Biotechnol*. **2008**, *26*, 566-572.

28 Patwardhan, S. V. Biomimetic and bioinspired silica: recent developments and applications. *Chem. Commun*. **2011**, *47*, 7567-7582.

29 Sumper, M.; Lorenz, S.; Brunner, E. Biomimetic control of size in the polyamine-directed formation of silica nanospheres. *Angew. Chem. Int. Ed*. **2003**, **42**, 5192-5195.

30 Mizutani, T.; Nagase, H.; Fujiwara, N.; Ogosh, H. Silicic acid polymerization catalyzed by amines and polyamines. *Bull. Chem. Soc. Jpn*. **1998**, **71**, 2017-2022.

31 Bernecker, A.; Wieneke, R.; Riedel, R.; Seibt, M.; Geyer, A.; Steinem, C. Tailored synthetic polyamines for controlled biomimetic silica formation. *J. Am. Chem. Soc*. **2010**, *132*, 1023-1031.

32 Menzel, H.; Horstmann, S.; Behrens, P.; Bärnreuther, P.; Krueger, I.; Jahns, M. Chemical properties of polyamines with relevance to the biomineralization of silica. *Chem. Commun*. **2003**, 2994-2995.

33 Coradin, T.; Durupthy, O.; Livage, J. Interactions of amino-containing peptides with sodium silicate and colloidal silica: A biomimetic approach of silicification. *Langmuir* **2002**, *18*, 2331-2336.

34 Patwardhan, S. V.; Mukherjee, N.; Steinitz-Kannan, M.; Clarson, S. J. Bioinspired synthesis of new silica structures. *Chem. Commun*. **2003**, 1122-1123.

35 Rodriguez, F.; Glawe, D. D.; Naik, R. R.; Hallinan, K. P.; Stone, M. O. Study of the chemical and physical influences upon in vitro peptide-mediated silica formation. *Biomacromolecules* **2004**, *5*, 261-265.

36 Cha, J. N.; Stucky, G. D.; Morse, D. E.; Deming, T. J. Biomimetic synthesis of ordered silica structures mediated by block copolypeptides. *Nature* **2000**, *403*, 289-292.

37 Naik, R. R.; Brott, L. L.; Clarson, S. J.; Stone, M. O. Silica-precipitating peptides isolated from a combinatorial phage display peptide library. *J. Nanosci. Nanotech*. **2002**, *2*, 95-100.

38 Wang, Q.; Yu, J.; Zhang, X.; Liu, D.; Zheng, J.; Pan, Y.; Lin, Y. Controlled biosilification using self-assembled short peptides A_6K and V_6K. *RSC Advances* **2013**, *3*, 2784-2793.

39 Wieneke, R.; Bernecker, A.; Riedel, R.; Sumper, M.; Steinem, C.; Geyer, A. Silica precipitation with synthetic silaffin peptides. *Org. Biomol. Chem*. **2011**, *9*, 5482-5486.

40 Naik, R. R.; Whitlock, P. W.; Rodriguez, F.; Brott, L. L.; Glawe, D. D.; Clarson, S. J.; Stone, M. O. Controlled formation of biosilica structures *in vitro*. *Chem. Commun*. **2003**, 238-239.

41 Knecht, M. R.; Wright, D. W. Functional analysis of the biomimetic silica precipitating activity of the R5 peptide from *Cylindrotheca fusiformis*. *Chem. Commun*. **2003**, 3038-3039.

42 Tomczak, M. M.; Glawe, D. D.; Drummy, L. F.; Lawrence, C.G.; Stone, M. O.; Perry, C. C.; Pochan, D. K.; Deming, T. J.; Naik. R. R. Polypeptide-Templatetd synthesis of hexagonal silica platelets. *J. Am. Chem. Soc*. **2005**, *127*, 12577-12582.

43 Brott, L. L.; Naik, R. R.; Pikas, D. J.; Kirkpatrick, S. M.; Tomlin, D. W.; Whitlock, P. W.; Clarson, S. J.; Stone, M.O. Ultrafast holographic nanopatterning of biocatalytically formed silica. *Nature* **2001**, *413*, 291-293.

44 Naik, R. R.; Brott, L. L.; Rodriguez, F.; Agarwal, G.; Kirkpatrick, S. M.; Stone, M. O. Bio-inspired approaches and biologically derived materials for coatings. *Prog. Org. Coat.* **2003**, 47, 249-255.

45 Luckarift, H. R.; Spain, J. C.; Naik, R. R.; Stone, M. O. Enzyme immobilization in a biomimetic silica support. *Nat. Biotechnol*. **2004**, *22*, 211-213.

46 Naik, R. R.; Tomczak, M. M.; Luckarift, H. R.; Spain, J. C.; Stone, M. O. Entrapment of enzymes and nanoparticles using biomimetically synthesized silica. *Chem. Commun*. **2004**, 1684-1685.

47 Nam, D. H.; Won, K.; Kim, Y. H.; Sang, B. I. A novel route for immobilization of proteins to silica particles incorporating silaffin domains. *Biotechnol. Prog*. **2009**, *25*, 1643-1649.

48 Marner, W. D.; Shaikh, A. S.; Muller, S. J.; Keasling, J. D. Enzyme immobilization via silaffin-mediated autoencapsulation in a biosilica support. *Biotechnol. Prog*. **2009**, *25*, 417-423.

49 Choi, O.; Kim, B. C.; An, J. H.; Min, K.; Kim, Y. H.; Um, Y.; Oh, M. K.; Sang, B. I. A biosensor based on the self-entrapment of glucose oxidase within biomimetic silica nanoparticles induced by a fusion enzyme. *Enzyme Microb. Technol*. **2011**, *49*, 441-445.

50 Atherton, E.; Sheppard, R. C. *Solid Phase Synthesis: A Practical Approach*, IRL Press at Oxford Univ. Press, Oxford, **1989**.

51 Haack, T.; Mutter, M. Serine derived oxazolidines as secondary structure disrupting, solubilizing building blocks in peptide synthesis. *Tetrahedron Lett*. **1992**, *33*, 1589-1592.

52 Mutter, M.; Nefzi, A.; Sato, A.; Sun, X.; Wahl, F.; Wöhr, T. Pseudo-prolines (psi Pro) for accessing "inaccessible" peptides. *Peptide Res*. **1995**, *8*, 145-153.

53 Sarin, V. K.; Kent, S. B. H.; Tam, J. P.; Merrifield, R. B. Quantitative nonitoring of solid-phase peptide synthesis by the ninhydrin reaction. *Analyt. Biochem*. **1981**, *117*, 147-157.

54 Iler, R. K. *The Chemistry of Silica*, Wiley-Interscience, New York, **1979**.

55 Belton, D.; Paine, G.; Patwardhan, S. V.; Perry, C. C. Towards an understanding of (bio)silicification: the role of amino acids and lysine oligomers in silicification, *J. Mater. Chem.* **2004**, *14*, 2231-2241.

56 Sumper, M.; Hett, R.; Lehmann, G.; Wenzl, S. A code for lysine modifications of a silica biomineralizing silaffin protein. *Angew. Chem*. **2007**, *119*, 8557-8560. *Angew. Chem. Int. Ed*. **2007**, 46, 8405-8408.

Chapter 3

Effect of peptide modifications on silaffin R5 induced silica precipitation

Silaffins are peptides naturally occurring in diatoms that carry a remarkable number of posttranslational modifications. They are intimately involved in the biomineralisation process leading to the delicate nano-patterned silica shells of diatoms. Here we describe the synthesis of silaffin peptides derived from Cylindrotheca fusiformis that carry defined modifications based on naturally occurring posttranslational modifications. Their silicification activity was analysed with regard to structure and amount of precipitated silica, revealing a distinct alteration of silica precipitation activity and structure of the precipitate formed depending on the particular modifications of the silaffins

The work described in this chapter was published in
Lechner, C. C.; Becker, C. F. W. *Chem. Sci*. **2012**, *3*, 3500-3504.

DOI: 10.1039/C2SC20687K

3.1 Introduction

The silica skeletons of diatoms are one of nature's most remarkable examples for biomineral morphogenesis.[1,2] Diatoms are eukaryotic unicellular algae that use orthosilicic acid actively enriched from their aqueous habitats[3] to build up their amorphous silica cell walls.[4] Formation of this delicate nano-patterned biosilica, which exhibits an extreme mechanical stability,[5] occurs under mild physiological conditions, whereas common industrial syntheses of silica require extreme conditions of temperature, pH and pressure.[6] Therefore, a detailed understanding of the mechanisms enabling silica biogenesis and patterning in diatoms is of great interest to inspire the development of novel routes for the shape controlled synthesis of silicon-based materials.[7-9] Within the last decades numerous organic substances have been identified that occur closely associated with diatom cell walls. In contrast to frustulins,[10,11] pleuralins,[12] silacidins[13,14] and stress-induced cell wall proteins,[15] which are only embedded within the silica, cingulins,[16] long chain polyamines[17] and silaffin peptides[18] are directly involved in the molecular processes leading to silica formation. The individual silaffin peptides from *C. fusiformis* derive from a precursor protein by proteolytic processing and share a high sequence similarity (repetitive units R1-7).[18] All natural silaffin peptides carry a remarkable number of posttranslational modifications (PTMs). Besides phosphorylation of serine residues, lysine residues become hydroxylated and phosphorylated at the δ-C-atom as well as di- and trimethylated and alkylated with oligo-*N*-methyl-propyleneimine units at the ε-amino group, respectively[19,20] (Scheme 3-1, A). Both native posttranslationally modified silaffin variants as well as unmodified synthetic R5 peptide, the repetitive unit of the silaffin polypeptide from *C. fusiformis* (H-SSKKSGSYSGSKGSKRRIL-OH), have been shown to trigger precipitation of silica *in vitro*.[18] Under native conditions, silaffins show silicification activity at acidic pH and to this end the lysine modifications with *N*-methyl-propylenimine are absolutely required. In contrast, synthetic silaffin variants lacking any posttranslational modification are able to precipitate silica at neutral pH.[18,19] However, silica precipitating activity at neutral pH requires the presence of the C-terminal RRIL-sequence in synthetic silaffin R5, which is removed by proteolysis under native conditions (Scheme 3-1, A and B).[19,21] Based on the observed properties of unmodified silaffin peptides, several approaches for biotechnological applications and biomimetic silica syntheses have evolved.[22-27] Although

posttranslational modifications of native silaffins are involved in the nano-patterning of biosilica, to date there is no (bio-) technological application making use of silaffin peptides carrying such modifications or mimics thereof to steer silica precipitation and influence silica properties. No detailed studies focusing on the structure-function relationship of individual PTMs of silaffins are available other than lysine side chain modifications in minisilaffins comprising the KXXK motif (for details see below).[28] A thorough understanding of the role of such silaffin modifications would tremendously expand the scope of (bio-) technological applications for these peptides and could lead to silica materials with different biophysical properties, tailored to individual applications.

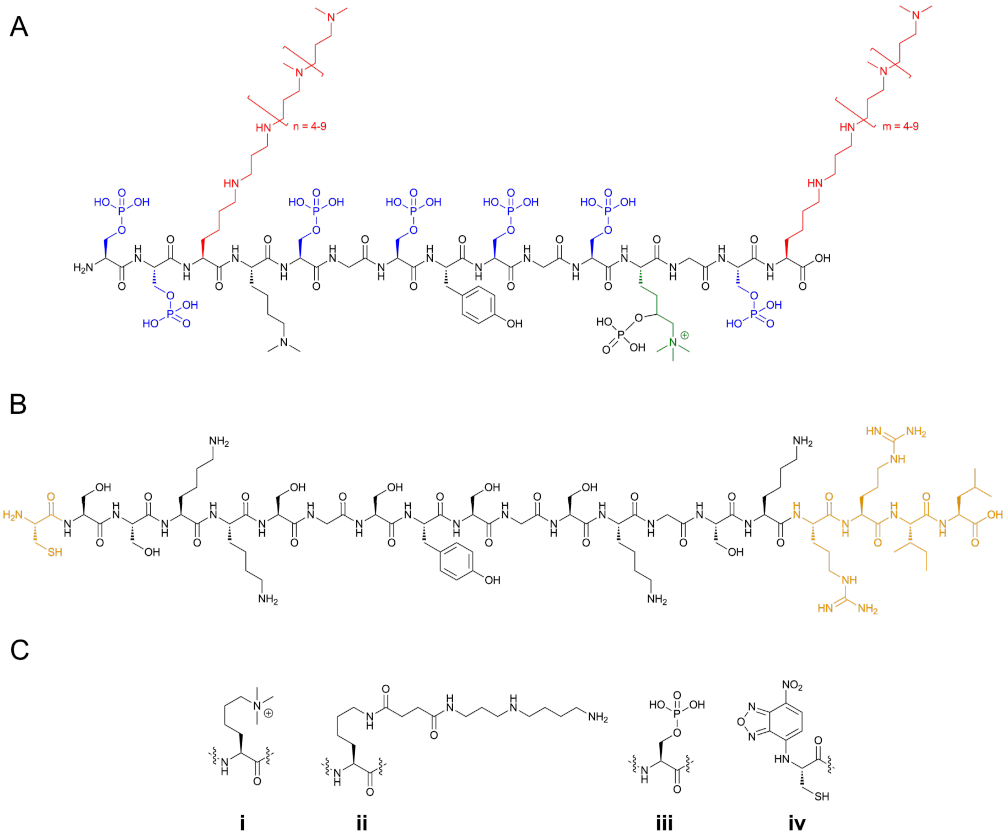

Scheme 3-1 Chemical structure of [A] the native silaffin-1A$_1$ from *C. fusiformis* with typical posttranslational modifications[20] and of [B] the unmodified synthetic silaffin peptide **A** used in this study. [C] The naturally occurring PTMs ε-*N,N,N*-trimethyllysine (i) and phosposerine (iii) were introduced in peptides **B**, **D** and **E.** ε-(4-Spermidine)succinyllysine (ii) was installed in peptide **C** to mimic native propylenimine-modified lysine residues. In peptide **F** the fluorescent probe 7-nitro-1,2,3-benzoxadiazole (NBD, iv) was introduced at the N-terminus.

In this chapter, the synthesis of silaffin R5 peptides that carry defined amino acid side chain modifications based on naturally occurring PTMs (Table 3-1) such as phosphoserines and trimethylated lysines is presented. The natively occurring lysine alkylation with oligo-propylenimine was, for ease of synthesis, mimicked by incorporation of spermidine via a succinic acid linker (Scheme 3-1, C). Silica precipitation activity of all modified peptides was analyzed with regard to morphology of the resulting particles and amount of precipitated silica.

3.2 Materials and methods

3.2.1 Materials

All used solvents and reagents were purchased from commercial sources and used without further purification: *N*,*N*-dimethylformamide (DMF), dichloromethane (DCM) and acetonitrile (ACN) from Biosolve. Fmoc-protected amino acids and 2-(1H-benzotriazol-1-yl)-1,1,3,3-tetramethyluronium hexafluorophosphate (HBTU) from Novabiochem. Methanol and trifluoroacetic acid (TFA) from Roth. Ammonium molybdate tetrahydrate, dibenzyl-*N*,*N*-di*iso*propylphosphoramidite $(BzlO)_2PN(i\text{-}Pr)_2$), Di*iso*propylethylamine (DIEA), 1,1'-carbonyldiimidazole (CDI), fuming HCl, 1-Hydroxybenzotriazole (HOBt), 4-chloro-7-nitro-1,2,3benzoxadiazole (NBD-Cl), 1,8-octandithiol (ODT), phenol, piperidine, spermidine, *t*-butylhydroperoxide (*t*BuOOH, 5.5 M in decane), tri*iso*propylsilane (TIS), tetramethoxysilane and tetrazole (0.45 M in ACN) from Sigma Aldrich. Succinic anhydride from VWR.

3.2.2 RP-HPLC and ion exchange chromatography

Analytical RP-HPLC analysis was performed on a Beckman (System Gold) instrument using a C4 column(150 x 4.6 mm, 5 µm particle size, Grace Vydac) at a flow rate of 1 mL/min with a gradient from 5 % to 65 % buffer B in buffer A over 30 min (buffer A: 0.1 % (v/v) TFA in ddH_2O, buffer B: 0.08 % (v/v) TFA in ACN).

For reversed phase purification of crude peptides a Varian Pro Star system was used. According to the amount and hydrophobicity of the peptides to be purified, different columns were used: C4 column (250 x 22 mm, 5 µm particle size, Protein C4, Grace Vydac), C4 column (250 x 10 mm, 5 µm particle size, Protein C4, Grace Vydac) and C18 column (250 x 10 mm, 5 µm particle size, Kromasil). Buffer A and B were used as eluents.

Ion exchange chromatography was carried out on a Beckman (System Gold) instrument using a Source 15 Q column (100 x 4.6 mm, Pharmacia Biotech). Elution of peptides from the column was achieved running a linear gradient from 0 % to 25 % of buffer D (20 mM Tris/HCl, 1 M NaCl in ddH_2O, pH 7.8) in buffer C (20 mM Tris/HCl in ddH_2O, pH 7.8) in 30

min at a flow rate of 1 mL/min. After lyophilisation of peptide containing fractions, peptides were dissolved in water and desalted following the RP-HPLC protocol described above. Detection for all chromatographic methods occurred at 214 and 280 nm wavelength.

3.2.3 Mass spectrometry

Mass spectra were acquired by electrospray ionization (ESI-MS) in positive ion mode using a LCQ-classic (Finnigan) or a LCQ-fleet (Thermo Fisher). Liquid chromatography-mass spectrometry (LC-MS) was performed on a LCQ-fleet (Thermo Fisher) connected to an UltiMate3000 Dionex HPLC. Separation was achieved using a BioBasic-4 column (150 x 2.1 mm, 5 µm particle size, Thermo Fisher) at a flow rate of 0.35 mL/min. ddH_2O (+ 0.1 % (v/v) formic acid) and ACN (+ 0.1 % (v/v) formic acid) were used as solvents. Peptide masses were detected using electrospray ionization MS in the positive mode.

3.2.4 Synthesis and purification of peptides A-F

3.2.4.1 General protocol for solid phase peptide synthesis

All peptides were synthesised manually on solid support using fluorenylmethoxycarbonyl (Fmoc) chemistry.[29] Syntheses were performed on 0.2 mmol scale using preloaded Fmoc-Leucine-Wang-polystyrene (Fmoc-Leu-Wang-PS) resin (Novabiochem). Deprotection of the N-terminal Fmoc-group was achieved by treating the resin twice with 20 % (v/v) piperidine in DMF for 3 and 7 min, respectively.

For each amino acid coupling 2.5 eq. of the corresponding Fmoc-amino acid were activated with 2.38 eq. HBTU and 5 eq. DIEA for 3 min and added to the resin for 30 min. At times coupling and deprotection reactions were checked by ninhydrin tests.[30] Between coupling and deprotection steps the peptidyl-resin was washed with DMF. Amino acid side chains were protected by base-stable groups as follows: Cys(tButhio) and Cys(tBu), Lys(Boc) and Lys(Mtt), Arg(Pbf), Ser(tBu) and Ser(Trt), Tyr(tBu). To improve synthesis yields, the pseudo-proline dipeptide Fmoc-Gly-Ser($\psi^{Me,Me}$pro)-OH was used as a building block.[31,32] After completion of peptide elongation the N-terminal Fmoc group was removed, the peptidyl resin was washed with DCM and MeOH and dried under vacuum.

Overall deprotection and cleavage of peptides from resin were achieved with 5 % TIS, 2.5 % ddH_2O and 92.5 % TFA or with a mixture of 5 % phenol, 5 % TIS, 2.5 % ODT, 5 % ddH_2O and 82.5 % TFA (10 mL/g resin) for 3 h at RT. Crude peptides were precipitated by addition of cold diethylether and subsequent centrifugation. Precipitated peptides were washed twice with ether and after removal of the supernatant dissolved in 50 % acetonitrile in water and finally lyophilized.

Calculations of yields for purified peptides are based on the synthesis scale.

3.2.4.2 Synthesis of peptide A

The unmodified silaffin R5 peptide **A** was synthesised using standard SPPS procedures as described above. Final deprotection and cleavage of the peptide from the resin was accomplished with 5 % TIS, 2.5 % ddH_2O and 92.5 % TFA. The peptide was purified by reversed phase HPLC (preparative C4 column, 10 mL/min flow rate, linear gradient from 5 % to 65 % buffer B in buffer A in 60 min). 27.9 mg of pure peptide were obtained from 100 mg (26.5 µmol) of peptidyl resin (49.8 % yield).

3.2.4.3 Synthesis of peptide B

Peptide **B** was synthesised following the general protocol using *N*-α-Fmoc-*N*-ε-trimethyl-*N*-L-lysine (Novabiochem) as building block at position 13. Peptide deprotection and cleavage from the solid support was done with 5 % TIS, 2.5 % ddH_2O and 92.5 % TFA. The crude peptide was purified via reversed phase chromatography (preparative C4 column, 10 mL/min flow rate, linear gradient from 20 % to 50 % buffer B in buffer A in 20 min) yielding 20.7 mg of peptide **B** in good purity (18.9 % yield from 194 mg (48.8 µmol) peptidyl resin).

3.2.4.4 Synthesis of peptide C

Modification of the silaffin R5 peptide with the polyamine spermidine was achieved by synthesizing the native sequence using Fmoc-Lys(Mtt)-OH at positions 4 and 16. Mtt-protecting groups were selectively removed by repeated treatment of the peptidyl resin with a solution of 1 % TFA and 1 % TIS in DCM for 2 min and subsequent washing with DCM for 1 min. 219 mg (0.05 mmol) peptidyl resin were swollen again in DMF for 1 h. A solution of 100 mg (0.5 mmol, 10 eq.) succinic anhydride and 150 µL DIEA in 1.5 mL 0.5 M HOBt in

DMF was added to the resin for 30 min. After 30 min activation of the carboxyl group with CDI (10 mL, 0.5 M in DMF), spermidine (726 mg, 5.0 mmol, 100 eq.) dissolved in a solution of HOBt (5mL, 0.5 M in DMF) was added to the resin and incubated at room temperature for 30 min. The peptidyl resin was washed and dried under vacuum. Peptide **3** was deprotected and cleaved from the resin using a mixture of 5 % phenol, 5 % TIS, 2.5 % ODT, 5 % ddH_2O and 82.5 % TFA. Pure peptide **C** was obtained after RP-HPLC purification (semipreparative C4 column, 3 mL/min flow rate, linear gradient from 5 % to 65 % buffer B in buffer A in 60 min) with a yield of 4.1 mg pure peptide from 211 mg (0.05 mmol) of peptidyl resin (3.1 % yield).

3.2.4.5 Synthesis of peptide D

Silaffin peptide **D**, carrying a single phosphorylated serine residue, was assembled following the general protocol. At position 15 the commercial available phosphoserine building block *N*-α-Fmoc-O-benzyl-L-phosphoserine (Novabiochem) was incorporated. Peptide **D** was cleaved from the resin with 5 % TIS, 2.5 % ddH_2O and 92.5 % TFA and purified by reversed phase HPLC (preparative C4 column, 10 mL/min flow rate, 20 % to 50 % buffer B in buffer A in 20 min). From 100 mg (24.9 μmol) peptidyl-resin 21.2 mg pure peptide **D** were isolated (38.8 % yield).

3.2.4.6 Synthesis of peptide E

Peptide **E** was obtained by global phosphorylation[33-35] of all seven unprotected serine-hydroxyl groups occurring in the silaffin sequence. The peptide backbone was assembled on the solid support following the general protocol and by incorporating trityl-protected serine residues (Fmoc-Ser(Trt)-OH). The N-terminal cysteine residue was Boc-protected (Boc-Cys(StBu)-OH) in order to avoid β-elimination during basic Fmoc-deprotection after post-synthetic phosphorylation on the solid support. After completion of chain elongation the Trt-protecting groups were selectively removed by repeated treatment of peptidy-resin (243 mg, 0.05 mmol) with a solution of 1 % TFA and 1 % TIS in DCM for 2 min and subsequent washing with DCM for 1 min. The peptidyl resin was placed in a suitable reaction vessel and dried under vacuum overnight. The following reactions were carried out under an argon atmosphere and with dried solvents. The peptidyl-resin was swollen in 3.6 mL dry DMF for

2 h. After addition of tetrazole (5.7 mL, 0.45 M in ACN, 2.6 mmol) and $(BzlO)_2PN(i\text{-}Pr)_2$ (0.39 mL, 1.04 mmol) the reaction vessel was gently agitated for 3 h at RT and then washed with dry DMF (5 x 10 mL). For oxidation of the intermediate phosphite ester 1.9 mL dry DMF and *t*-butyl hydroperoxide (2.4 mL, 5.5 M in decane, 13.2 mmol) were added for 1.5 h. Finally, the resin was washed with DMF and dried under vacuum. Final deprotection and cleavage of the peptide from the resin was accomplished with 5 % TIS, 2.5 % ddH_2O and 92.5 % TFA. Crude peptide was first purified by reversed phase HPLC (semipreparative C18 column, 3 mL/min flow rate, 20 % to 50 % buffer B in buffer A in 20 min) followed by ion exchange chromatography resulting in highly pure peptide **5** (0.8 mg from 0.05 mmol peptidyl resin, 0.6 % yield).

3.2.4.7 Synthesis of peptide F

A part of the unmodified peptidyl-resin (see synthesis of peptide **A**) was used for N-terminal fluorescent labelling with nitrobenzoxadiazole (NBD). Peptiyl-resin 1 (150 mg, 0.04 mmol) was swollen in DMF for 2 h. 4-chloro-7-nitrobenzofurazan (77.8 mg, 0.4 mmol, 10 eq.) and DIEA (7.0 µL, 0.04 mmol, 1 eq.) were dissolved in 400 µL DMF. The obtained solution was added to the peptidyl-resin and incubated at 37 °C for 16 h under permanent shaking. After extensive washing of the resin with DMF, DCM and MeOH the peptidyl-resin was dried under vacuum. Finally the fluorescently labelled peptide was cleaved from the resin with 5 % TIS, 2.5 % ddH_2O and 92.5 % TFA. Peptide **F** was purified by reversed phase HPLC (preparative C4, 10 mL/min flow rate, 5 % to 65 % buffer B in buffer A in 60 min, and subsequent semipreparative C18 column, 3 mL/min flow rate, 5 % to 65 % buffer B in buffer A in 60 min) yielding 3.8 mg of peptide **F** in satisfactory purity (4.2 % yield from 0.04 mmol peptidyl resin).

3.2.5 *In vitro* silica precipitation assays and microscopic analysis

Peptides to be analysed were dissolved to a final concentration of 1 mg/mL in 50 mM potassium phosphate buffer at pH 7.0. Silicic acid was generated by hydrolysis of 250 mM tetramethoxysilane in 1 mM aqueous HCl for 4 min. Silica precipitation reactions were initiated by addition of silicic acid to peptide solutions to a final concentration of 25 mM.

Reactions were incubated at RT for 30 min. Silica precipitates were collected by centrifugation (5 min, 16.873 × g) and washed twice with water. Silicic acid solutions without silaffin peptides did not lead to the formation of any precipitate. Silica precipitate collected by centrifugation was suspended in water, applied to a *Thermanox*™ coverslip (Thermo scientific) and air dried. The coverslips were placed onto sample holders and sputter coated with gold in high vacuum (Bal-Tec SCD 005). Electron micrographs were recorded with a scanning electron microscope (JEOL JSM 5900 LV) operating at 20 kV. Analysis of elemental composition was done by energy dispersive X-ray (EDX) spectroscopy (Röntec). For fluorescence microscopy, silica material was suspended in water, applied to a glass slide and coverd with a cover glass. Fluorescence micrographs were obtained using a Zeiss Axiovert 200 microscope using the oil-immersion objective.

3.2.6 Determination of silicon concentration

In vitro silica precipitation assays were performed as described in 4.1. The collected silica precipitates were dissolved in 2 M NaOH for 1 h at RT and quantified by a modified β-silicomolybdate method[36] as described by Wieneke et al.[28] Calibration curves are based on a silicon atomic absorption standard solution (Sigma Aldrich). All assays were at least performed in triplicate.

3.2.7 Particle size analysis

The statistical analysis of silica particle size distribution was done with ImageJ. For a representative number of silica particles resulting from peptides **A**, **B** and **C** the diameter was determined manually from the corresponding digital electron micrographs. Figure 3-3 shows the calculated frequency of particle diameters from peptides **A**, **B** and **C.**

3.3 Results and discussion

Peptides **A-F** were synthesized using Fmoc-based SPPS and appropriately modified building blocks (peptides **B** & **D**) or postsynthetic modification procedures (peptides **C, E** & **F**) and subsequently purified by RP-HPLC (see chapter 3.2). All synthetic peptides carry an N-terminal cysteine residue, not present in the native sequence of the R5 peptide. This addition introduces a unique thiol group and provides a site for further selective modification reactions such as controlled covalent dimerization or covalent attachment of target molecules, which will be beneficial for (bio-)technological approaches using these synthetically modified silaffin variants. In peptide **F** the fluorescence probe 7-nitro-1,2,3-benzoxadiazole (NBD) was introduced to determine peptide localization within silica structures.

Table 3-1 Synthetic silaffin R5 peptides

	Sequence	MW [Da]	Yield [%]
A	CSSKKSGSYSGSKGSKRRIL	2116.40	49.8
B	CSSKKSGSYSGSK(Me)$_3$GSKRRIL[a]	2247.66	18.9
C	CSSK(Sp)KSGSYSGSKGSK(Sp)RRIL[b]	2659.18	3.1
D	CSSKKSGSYSGSKGpSKRRIL[c]	2196.38	38.8
E	CpSpSKKpSGpSYpSGpSKGpSKRRIL[c]	2764.43	0.6
F	NBD-CSSKKSGSYSGSKGSKRRIL[d]	2279.49	4.2

[a] K(Me)$_3$ = ε-*N*,*N*,*N*-trimethyllysine; [b] K(Sp) = ε-(4-spermidine) succinyl lysine [c] pS = Phosphoserine; [d] NBD = 7-nitro-1,2,3-benzoxadiazole.

Peptide **B** contains a trimethylated lysine residue at position 13 as found in the native sequence (Scheme 3-1), but this lysine side chain does not carry an additional phosphorylated hydroxyl group at the δ-C-atom as described for native silaffins.[20,37] To mimic the unusual, native lysine alkylation with oligo-propyleneimine the polyamine spermidine was attached to the R5 peptide at two lysine side chains (peptide **C**). This mimic of a native PTM differs from native lysine alkylation with oligo-*N*-methyl-propyleneimine units by number of carbon atoms, distance between amino groups and the attachment via a succinic acid linker. Recently the synthesis of ε-dimethylated and ω-dimethyl-dipropyleneamino modified tetrapeptides (KXXK) derived from silaffin sequences was reported and their influence on

silica precipitation analyzed.[28] Here spermidine was chosen as a commercially available mimic for species-specific oligo-propyleneimine modifications since it can be easily installed on full-length silaffin R5 peptides (chapter 3.2.4.4). Peptides **D** and **E** have been prepared to focus on the effect of phosphorylation of serine residues and the contrast between single and global phosphorylation. Whereas in peptide **E** all seven serine residues are phosphorylated, peptide **d** allows analysing the influence of a single phosphoserine residue. The available set of peptides (**A-F**) represents all presently described posttranslational modifications of silaffins, either by incorporation of the native structures or by mimics, in separate peptides. This enables a systematic study of the effect of each modification on the silica precipitating activity and the resulting particle morphology.

The unmodified R5 peptide requires neutral pH for silica precipitation activity while native silaffins act at slightly acidic conditions.[18] In addition, the presence of polyvalent anions in the reaction solution is strictly required for silica precipitation activity of silaffin peptides lacking native serine phosphorylations.[20] Here, all silica precipitation assays were carried out in a phosphate buffered solution at pH 7 to ensure comparability and reproducibility. Figure 3-1 depicts electron micrographs of the resulting silica particles after addition of monosilicic acid (freshly generated from tetramethyl orthosilicate, TMOS) to solutions of peptides **A-F** at similar concentrations. Unmodified peptide **A** induces the rapid formation of highly homogenous spherical silica particles with a diameter of approximately 750 nm (Figure 3-1,A and Figure 3-3). Silica particles resulting from peptide **B** exhibit a similar morphology (Figure 3-1, B), albeit the specific activity (defined as the precipitation of pmoles silicon per min and nmoles peptide at pH 7.0) of this peptide is slightly increased in comparison to the unmodified R5 peptide **1** (Figure 3-2). This effect can be explained by the permanent positive charge arising from the trimethylated lysine residue in **B**. Native silaffins are zwitterionic peptides that can self-assemble into larger clusters. This self-assembly process is mainly driven by their PTMs[20] and based on electrostatic interactions between negatively charged phosphate moieties and positively charged protonated amino groups. Unmodified synthetic silaffin peptides have a polycationic character based on the numerous ε-amino groups of lysine residues (pK of 10.5) that are mostly protonated at neutral pH. Silaffin peptides lacking serine phosphorylations absolutely require the addition of divalent anions such as phosphate acting as ionic cross-linkers to restore silica precipitating activity.[20]

The permanent positive charge in peptide **B** increases its tendency for self-assembly in phosphate buffered solutions in comparison to peptide **A**. The ability to form larger assemblies is closely associated with the increased silicification activity of peptide **B** as the self-assembly process is a prerequisite for this activity. In addition, quaternary ammonium groups stabilise oligosilicate anions such as $Si_8O_{20}^{8-}$.[38] Controlled formation of oligosilicate species promotes silica precipitation and also contributes to an enhanced activity of peptide **B** as seen in Figure 3-2.

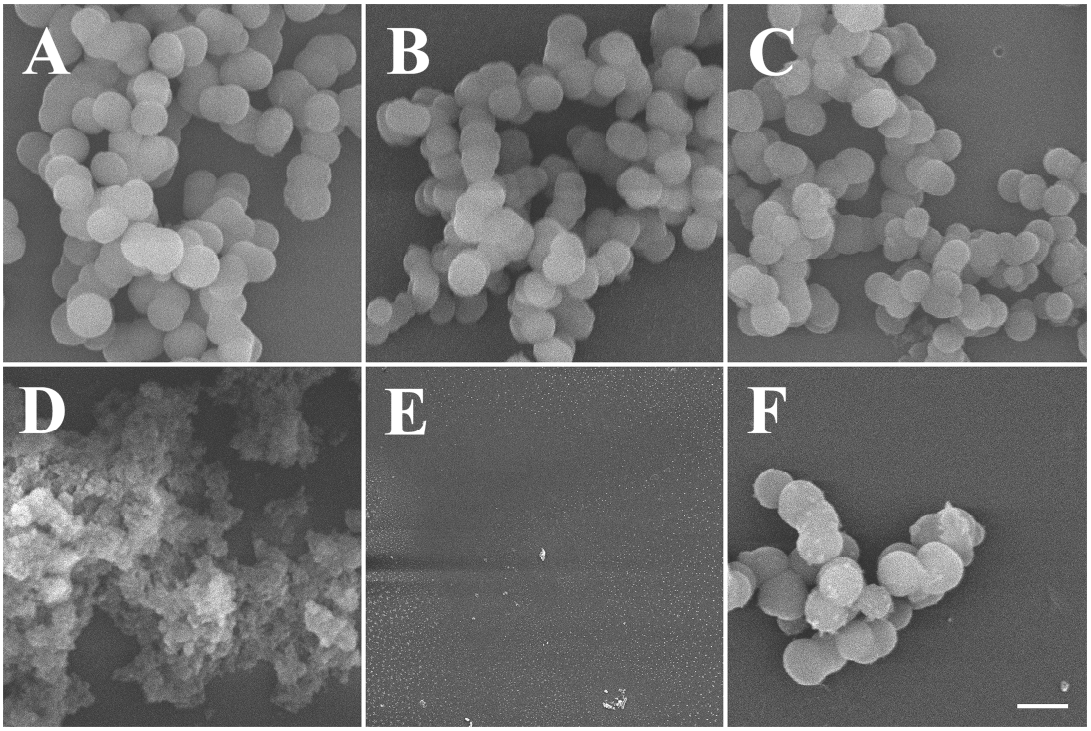

Figure 3-1 Scanning electron micrographs of silica particles resulting from [A] peptide **A**, [B] peptide **B**, [C] peptide **C**, [D] peptide **D**, [E] peptide **E** and [F] peptide **F**. Scale bar: 1 μm. All silica precipitation assays have been carried out at pH 7.0, repeated at least 3 times and have each time produced similar results. A control of silicic acid in phosphate buffer without addition of peptide shows no silica formation (data not shown).

A unique PTM found in silaffins is species-specific long-chain polyamines that attach to lysine side chains.[18,19] Generally amines and polyamines exhibit silicic acid poly-condensation activity in aqueous solution at neutral pH.[39] Acid-base catalysis facilitating the

formation of siloxane bonds has been proposed to explain this observation (Scheme 1-7).[40] This model implies the stabilisation of a transition state by two appropriately arranged amino groups within the polyamine backbone. A detailed study using synthetic polyamines, structurally based on the long-chain polyamines extracted from diatoms, clearly revealed that the morphology of silica precipitates depends on polyamine chain length, *N*-methylation and the distance between two adjacent amino groups in the polyamine backbone.[41]

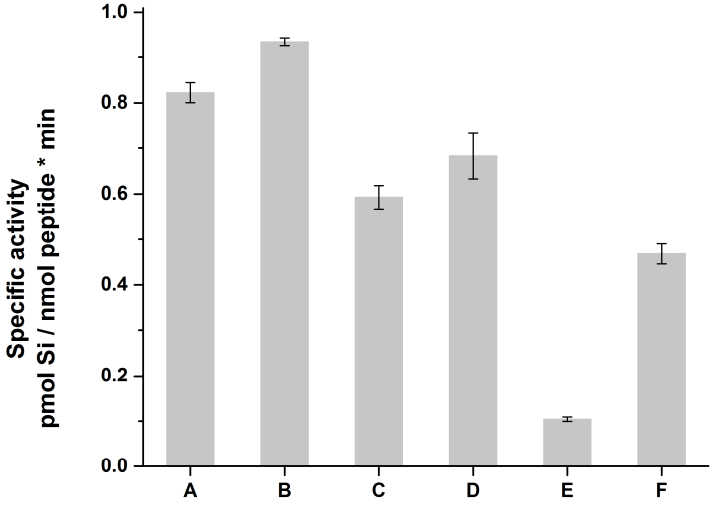

Figure 3-2 Specific silica precipitation activity of peptides **A-F** at pH 7.0 given in pmoles silicon per min and nmoles of peptide. Silicic acid in phosphate buffer without addition of peptide shows no silica formation (data not shown).

In order to mimic native poly(propyleneimine)-modifications (Scheme 3-1) in a full-length synthetic R5 peptide, we synthesised peptide **C** carrying two spermidine residues attached to succinyllysine side chains (Table 3-1). Spermidine is a naturally occurring polyamine for which silicification activity has previously been demonstrated.[42] Spherical silica particles are formed upon addition of silicic acid to a solution of peptide **C**. These particles show a distinctly inhomogeneous particle size distribution with diameters ranging between 400 and 800 nm (Figure 3-1, C and Figure 3-3) as well as a lower specific activity compared to unmodified peptide **A** (Figure 3-2).

The occurrence of different particle sizes (Figure 3-1, C) hints towards the previously described shape patterning activity of polyamines.[17,43] The decreased silica precipitation activity observed for peptide **C** could be linked to missing *N*-methylations since this

modification has been shown to accelerate silica formation.[44,45] In addition the spacing of amino groups in polyamines plays an important role as well, with a propyl spacer being a much more potent silica precipitation catalyst than butyl spacers.[41] Both the missing *N*-methylation and the improper alkyl spacer length between adjacent amino groups may contribute to the decreases silica precipitation activity of spermidine modified peptide **C**. Mimicking the native polypropylenimine modifications with spermidine even diminishes the silica precipitation activity below the value measured for unmodified peptide **A.** This finding leads to the assumption that the attachment of a rather bulky modification to lysine side chains disturbs the well-balanced arrangement of amino groups in the silaffin sequence and therefore diminishes the potency of the peptide in catalysing the polycondensation of silicic acid. The influence of lysine modifications in the context of minisilaffin was recently analysed.[28] ε,ε-dimethyl-lysine and ω,ω-dimethyl-dipropyleneamino-lysine were introduced in KXXK tetrapeptides, a short domain frequently observed in silaffins. It was shown that even short KXXK peptides carrying methylation and polyamine modifications are able to influence the morphology of silica precipitates. The results by Wieneke et al. revealed a correlation of amino acid composition of the KXXK tetrapeptides and the amount and nature of resulting silica precipitates.[28]

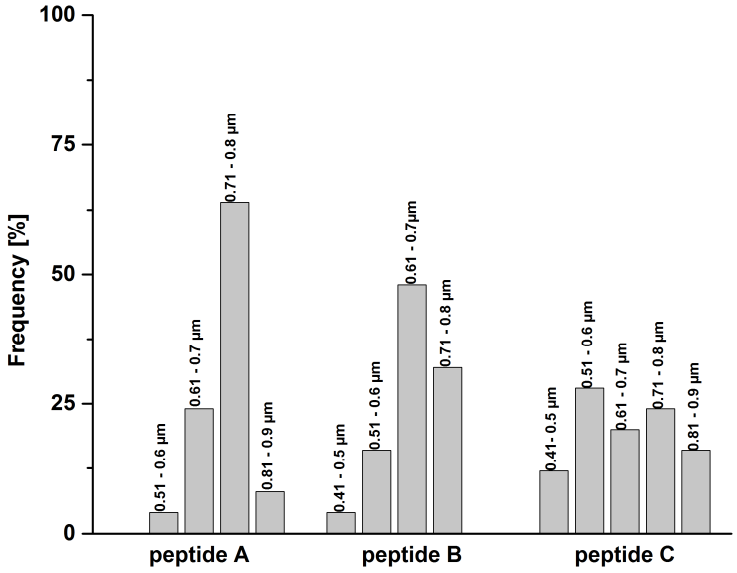

Figure 3-3 Distribution of silica particle sizes resulting from peptide **A**, **B** and **C** shown as the frequency of particle diameters

Phosphorylation of serine hydroxyl groups is the other predominant modification found in silaffin peptides. Phosphorylations provide negatively charged counter ions for cationic polyamine modifications. Without these no self-assembly of silaffin peptides would be possible due to electrostatic repulsion. Peptides **D** and **E** are aimed at deciphering the influence of phosphorylation alone. Globally phosphorylated peptide **E** exhibits almost no silica precipitation activity in a 50 mM phosphate buffered solution at pH 7.0 (Figure 3-1, E and Figure 3-2). There is also no silica formation observed in other phosphate-free buffers or plain water (data not shown). At neutral pH, with deprotonated phosphate groups, the negative charges within the peptide appear to dominate the cationic amino groups of the lysine side chains. In the absence of any additional cationic species such as polyamines, multiple phosphorylation inevitably results in electrostatic repulsion and prevents peptide self-assembly. Furthermore, the repulsion between negatively charged phosphorylated peptides and silanol groups of silicic acid abolishes formation of siloxane bonds for which the interaction between lysine ε-amino groups and silicic acid is required. These effects contribute to the dramatic loss in silica precipitation activity of peptide **E**. In contrast, a silaffin R5 variant carrying only a single serine phosphorylation (peptide **D**) maintains the ability to efficiently precipitate silica. However, the morphology of the formed silica particles is completely altered (Figure 3-1, D) in comparison to unmodified peptide **A** (Figure 3-1, A) and peptides **B** and **C** carrying cationic modifications (Figure 3-1, B and C). No well-defined spherical silica particles can be observed by electron microscopy but rather fuzzy silica material. This material appears to consist of a cluster of nanometer-sized silica particles. This observation can be explained based on the generally accepted mechanism of silica formation by polycondensation of silicic acid.[36] In the presence of peptide **D** this process seems to stop at an early stage at which only small particles consistent of highly branched polysilicic acid exist. Out of these nuclei of polysilicic acid, either by continuous polymerization with monomeric silicic acid or by fusion of small silica particles, the spherical silica particles are typically formed. However, the morphology of the silica material resulting from addition of monosilicic acid to a solution of peptide **D** (Figure 3-1, D) suggests that further growth to form distinct, spherical silica particles is inhibited. For peptide **D** electrostatic repulsion between the anionic phosphate group and silanol groups present on silica surfaces might partially preclude interaction of silaffin peptides with preformed silica surfaces. Such an

effect would hamper formation of larger silica particles. A 27 % decrease in silica precipitation activity of peptide **4** (Figure 3-2), *i.e.* a decreased amount of precipitated silica per min and nmole of peptide, is in line with this explanation. In addition, this observation is in agreement with previously published results in which glutamate as a phosphoserine mimic in the KXXK tetrapeptide motif of silaffins caused a decrease in silica particle size as well in the amount of precipitated silica.[28]

Silaffin peptides typically co-precipitate with and are incorporated into silica during the deposition processes described above.[18,21] In order to demonstrate that our synthetic peptides behave similarly we have synthesised a variant of the R5 peptide that carries a small fluorescence probe, 7-nitro-1,2,3-benzoxadiazole (NBD), attached to its N-terminal amino group (peptide **F**). This probe allows to determine peptide localisation within the formed silica structures via fluorescence microscopy. The attachment of NBD to the N-terminus of silaffin R5 peptide does not interfere with the formation of smooth spherical silica particles (Figure 3-1, F). Albeit a significant decrease in silica precipitation activity is observed (Figure 3-2), an effect that can either be explained based on electrostatic interactions due to the blocked N-terminus or by the hydrophobic nature of the fluorescent probe hampering the poly-condensation process. Fluorescence micrographs of silica particles containing peptide **F** (Figure 3-4) prove that the peptide co-precipitates and is either entrapped in the silica particles or at least tightly associated with the silica material. This finding is of interest with respect to potential (bio-) technological applications of silaffin peptides.

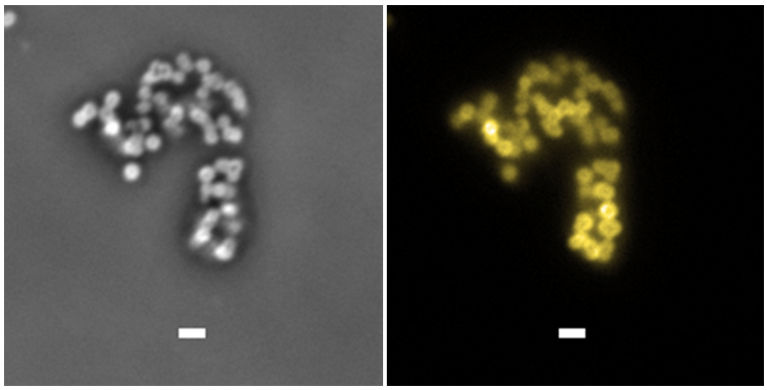

Figure 3-4 Fluorescence micrographs of silica particles resulting from peptide **F**. Left: brightfield; right: fluorescence. Scale bar 1 µm.

3.4 Conclusion

The set of synthetic silaffin peptides carrying different amino acid side chain modifications presented in this work provides a basis for defining the influence of such modifications on the *in vitro* silicification activity, on the morphology of the resulting silica material as well as on the amount of precipitated silica. The data presented here extends previous findings for modified KXXK tetrapeptides and unmodified silaffins towards differently modified full-length silaffin peptides and emphasizes nature's careful design of these biomolecules, partially based on the intricate interplay of attractive and repulsive electrostatic interactions. The well-balanced arrangement of different PTMs in a peptidic context leads to highly complex molecules that can self-assemble, mediate silicic acid polycondensation and play a major role in nano-pattering of diatom cell wall silica. This study helps to decipher the independent influence of each of the known silaffin modifications. In a next step combinations of these modifications will be analysed to further broaden our understanding of the complex function of silaffins in silica precipitation and biomineralization.

The results are a rational basis for developing modified silaffin peptides into defined silica precipitation agents and into efficient silica-anchors for a diverse set of molecules, e.g. fluorescent probes, drugs or proteins. Up to now different polycationic polymers, e.g. polyethyleneimine,[46,47] amine-terminated dendrimers,[48] poly-L-lysine-b-polyglycine block copolypeptides,[49] protamine[50] or recombinant and synthetic silaffin peptide variants[22-26] have been used to achieve biomimetic silica formation, resulting in immobilisation of proteins in silica matrices with concomitant stabilisation and mostly under retention of activity. As demonstrated above for NBD-labelled peptide **F**, coupling of such moieties to the N-terminus of a silaffin peptide will not interfere with the resulting particle morphology but leads to homogenous incorporation. Using synthetic silaffin peptides with defined modifications for immobilization of target molecules in silica material provides several advantages: The material properties can be controlled by silaffin modifications and covalent attachment of target molecules to the peptide will lead to selective and homogenous encapsulation. Furthermore, very mild conditions can be applied for the encapsulation of sensitive molecules such as enzymes and others. Here the unique thiol function provided by the N-terminal cysteine residue can be exploited as a selective attachment site.

3.5 Supplement: Analytical data for synthetic peptides A-F

Peptide A

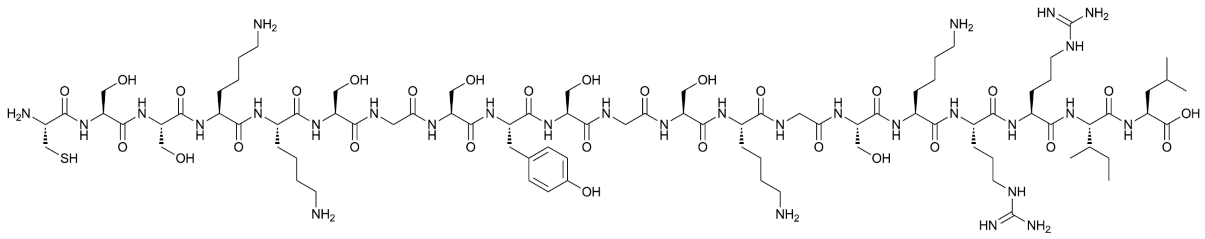

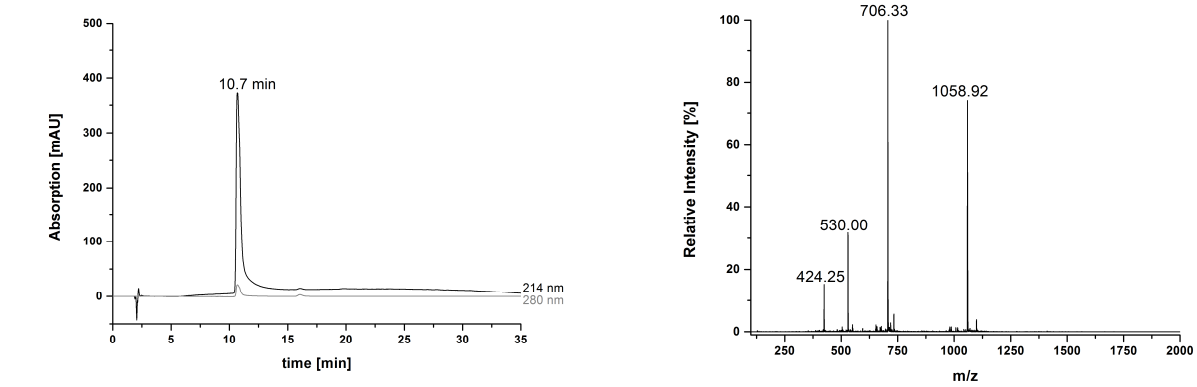

Figure 3-5 **A)** Analytical RP-HPLC chromatogram of purified peptide **A**.
B) ESI-MS of purified peptide **A**. Mass calculated for $C_{87}H_{155}N_{30}O_{29}S$: 2116.13 $[M+H]^+$, found: 1058.92 $[M+2H]^{2+}$, 706.33 $[M+3H]^{3+}$, 530.00 $[M+4H]^{4+}$, 424.25 $[M+5H]^{5+}$.

Peptide B

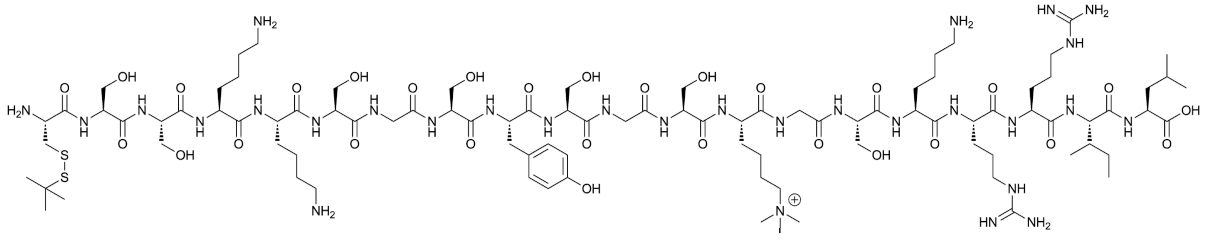

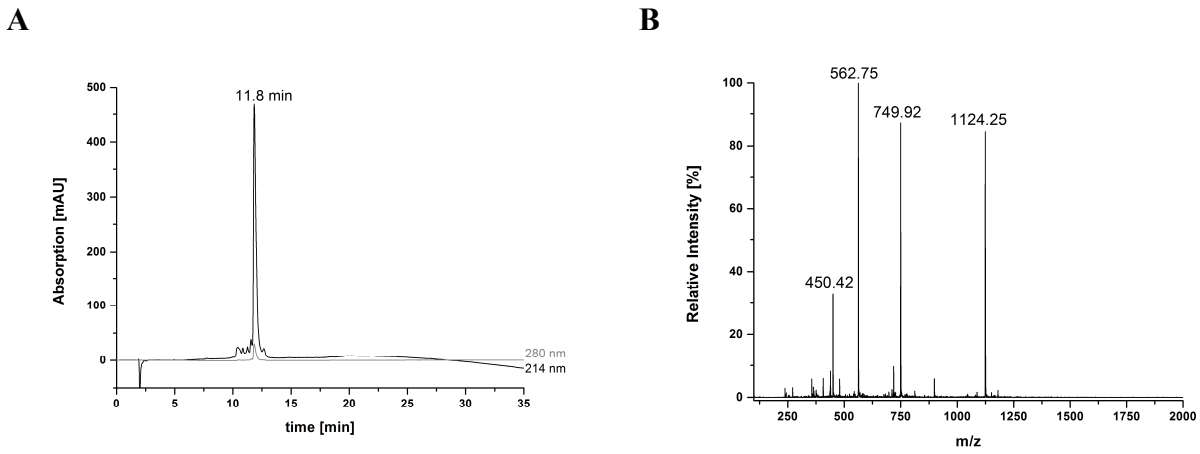

Figure 3-6 **A)** Analytical RP-HPLC chromatogram of purified peptide **B**.
B) ESI-MS of purified peptide **B**. Mass calculated for $C_{94}H_{170}N_{30}O_{29}S_2^+$: 2247.22 $[M+H]^+$, found: 1124.25 $[M+2H]^{2+}$, 749.92 $[M+3H]^{3+}$, 562.75 $[M+4H]^{4+}$, 450.42 $[M+5H]^{5+}$.

Peptide C

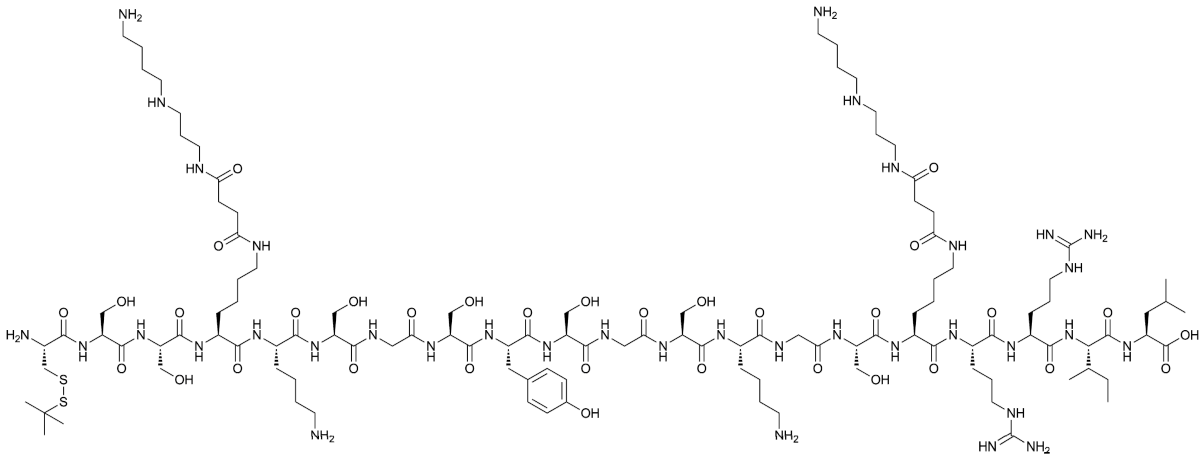

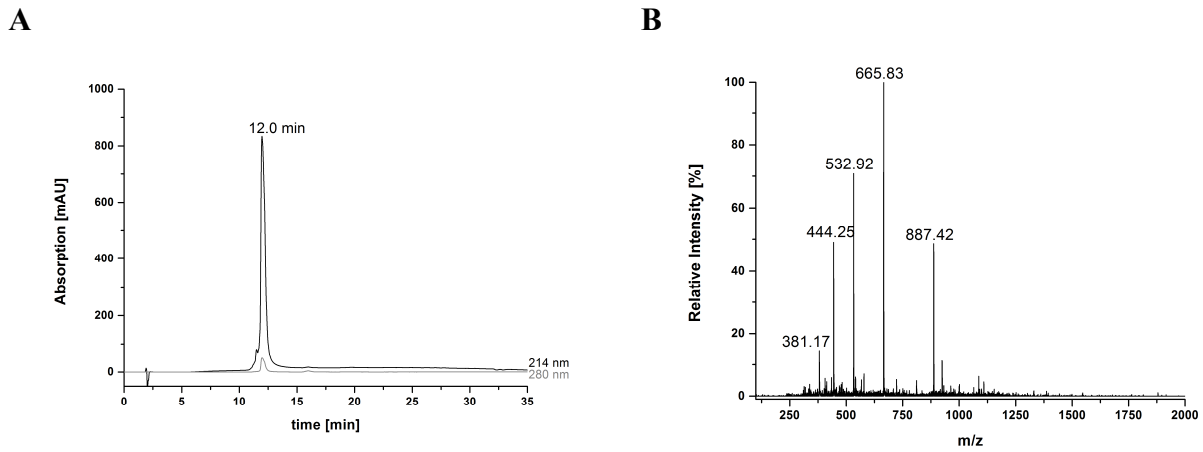

Figure 3-7 **A)** Analytical RP-HPLC chromatogram of purified peptide **C**.

B) ESI-MS of purified peptide **C**. Mass calculated for $C_{113}H_{205}N_{36}O_{33}S_2^+$: 2658.49 $[M+H]^+$, found: 887.42 $[M+3H]^{3+}$, 665.83 $[M+4H]^{4+}$, 532.92 $[M+5H]^{5+}$, 444.25 $[M+6H]^{6+}$, 381.17 $[M+7H]^{7+}$

Peptide D

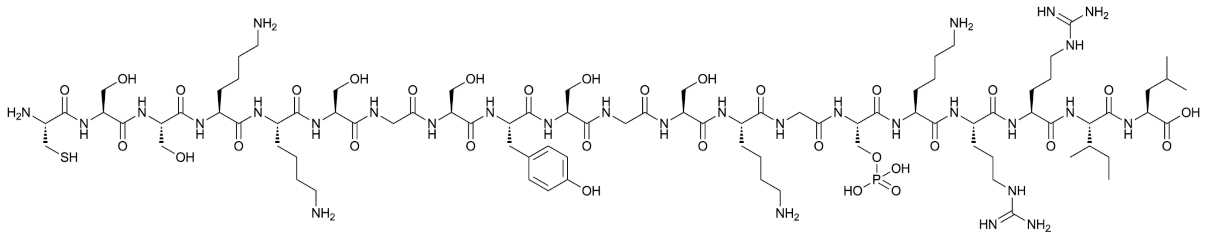

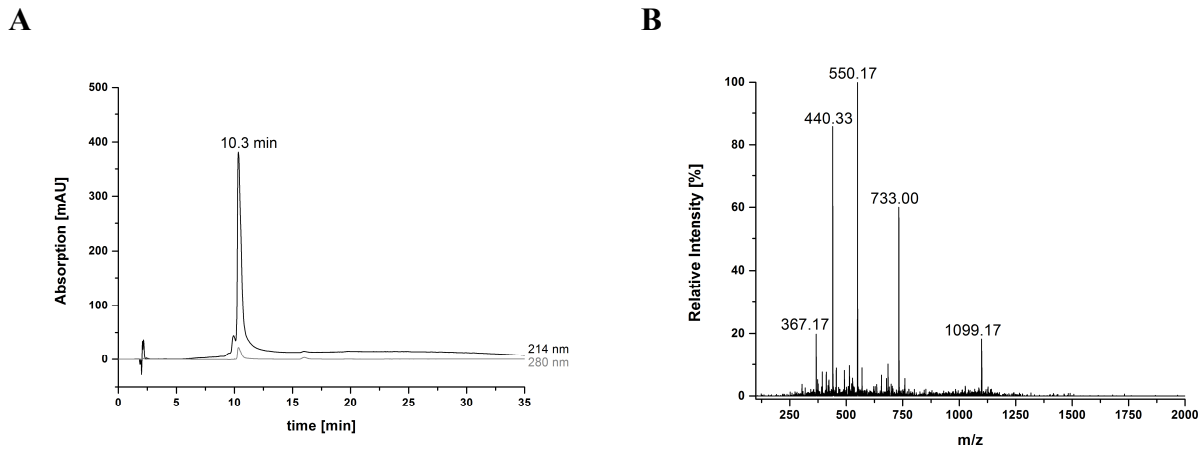

Figure 3-8 **A)** Analytical RP-HPLC chromatogram of purified peptide **D**.

B) ESI-MS of purified peptide **D**. Mass calculated for $C_{87}H_{156}N_{30}O_{32}PS$: 2196.10 $[M+H]^+$, found: 1099.17 $[M+2H]^{2+}$, 733.00 $[M+3H]^{3+}$, 550.17 $[M+4H]^{4+}$, 440.33 $[M+5H]^{5+}$, 367.17 $[M+6H]^{6+}$.

Peptide E

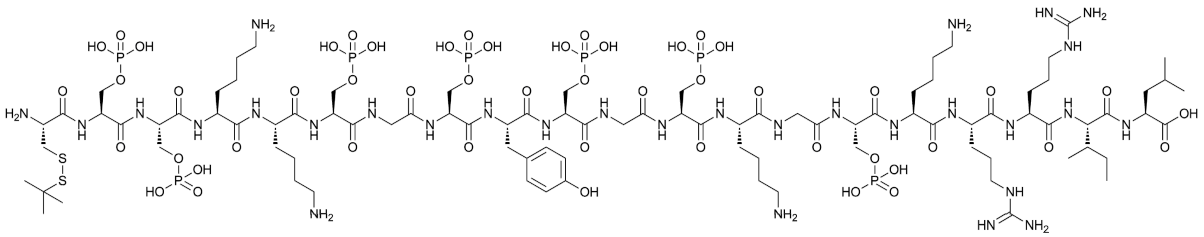

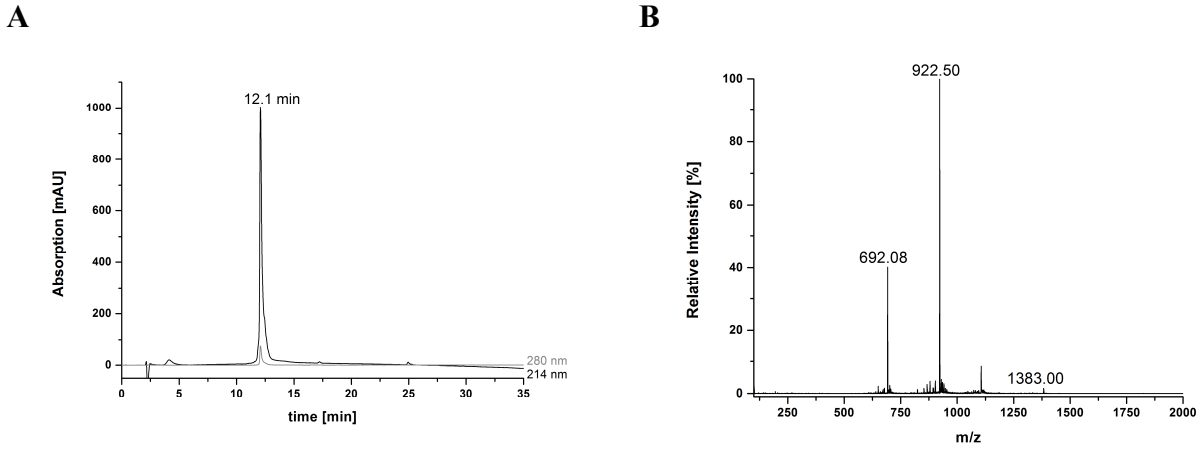

Figure 3-9 **A)** Analytical RP-HPLC chromatogram of purified peptide **E**.
B) ESI-MS of purified peptide **E**. Mass calculated for $C_{91}H_{170}N_{30}O_{50}P_7S_2$: 2763.93 $[M+H]^+$, found: 1383.00 $[M+2H]^{2+}$, 922.50 $[M+3H]^{3+}$, 692.08 $[M+4H]^{4+}$.

Peptide F

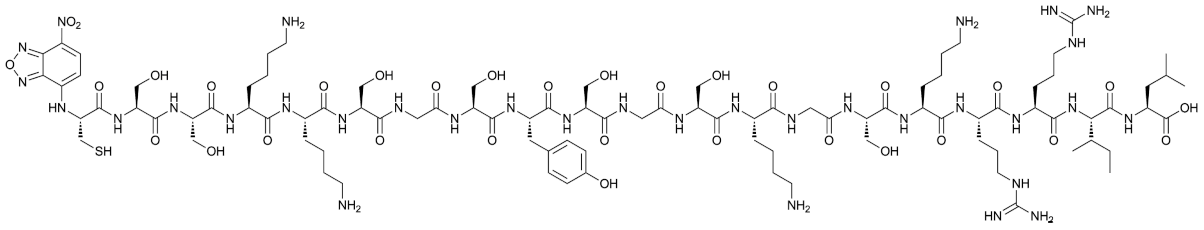

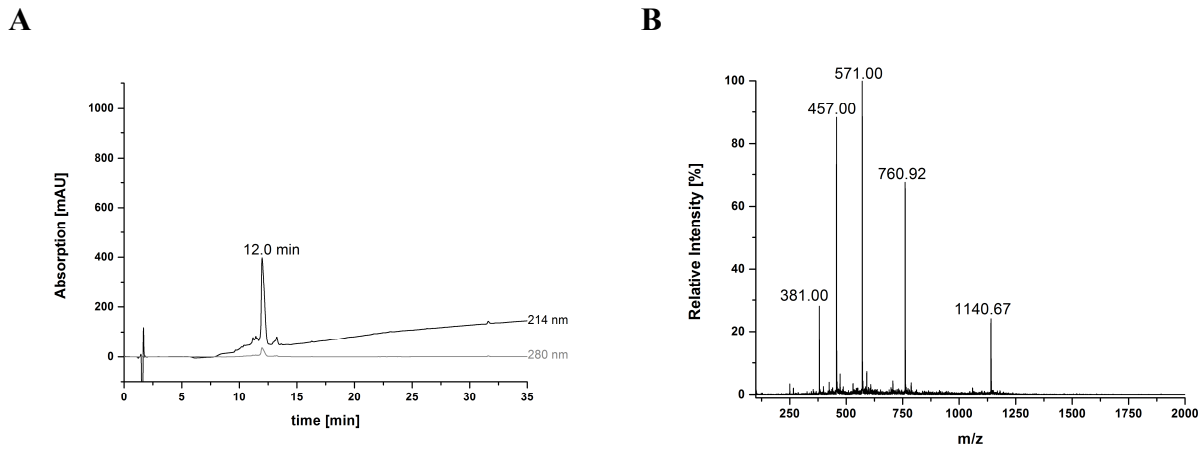

Figure 3-10 **A)** Analytical RP-HPLC chromatogram of purified peptide **F**.

B) ESI-MS of purified peptide **F**. Mass calculated for $C_{93}H_{156}N_{33}O_{32}S$: 2279.13 $[M+H]^{+}$, found: 1140.67 $[M+2H]^{2+}$, 760.92 $[M+3H]^{3+}$, 571.00 $[M+4H]^{4+}$, 457.00 $[M+5H]^{5+}$, 381.00 $[M+6H]^{6+}$

3.6 References

1 Round, F. E.;. Crawford, R. M; Mann, D. G. *The Diatoms: Biology & Morphology of the Genera;* Cambridge University Press: Cambridge, 1990.

2 Mann, S.; Webb, J.; Williams, R. J. P., Eds. *Biomineralization: Chemical and Biochemical Perspectives;* VCH: Weilheim. Germany, 1989.

3 Hildebrand, M.; Volcani, B. E.; Gassmann, W.; Schroeder, J. I. A gene family of silicon transporters. *Nature* **1997**, *385*, 688-689.

4 Del Amo, Y.; Brzezinski, M. A. The chemical form of dissolved Si taken up by marine diatoms. *J. Phycol.* **1999**, *35*, 1162-1170.

5 Hamm, C. E.; Merkel, R.; Springer, O.; Jurkojc, P.; Maier, C.; Prechtel, K.; Smetacek, V.; Architecture and material properties of diatom shells provide effective mechanical protection. *Nature* **2003**, *421*, 841-843.

6 Tacke, R. Milestones in the biochemistry of silicon: From basic research to biotechnological applications. *Angew. Chem. Int. Ed.* **1999**, *38*, 3015-3018.

7 Mann, S.; Ozin, G. Synthesis of inorganic materials with complex form. *Nature,* **1996**, *382*, 313-318.

8 Parkinson, J.; Gordon, R. Beyond micromachining: the potential of diatoms. *Trends Biotechnol,* **1999**, *17*, 190-196.

9 Sun, Q.; Vrieling, E. G.; van Santen, R. A.; Sommerdijk, N. A. J. M. Bioinspired synthesis of mesoporous silicas. *Curr. Opin. Solid State Mater. Sci.* **2004**, *8*, 111-120.

10 Kröger, N.; Bergsdorf, C.; Sumper, M. A new calcium binding glycoprotein family constitutes a major diatom cell wall component. *EMBO J.* **1994**, *13*, 4676-4683.

11 Kröger, N.; Bergsdorf, C.; Sumper, M. *Eur. J. Biochem.* 1996, **239,** 259-264.

12 Kröger, N.; Lehmann, G.; Rachel, R.; Sumper, M. Characterization of a 200 kDa diatom protein that is specifically associated with a silica-based substructure of the cell wall. *Eur. J. Biochem.* **1997**, *250*, 99-105.

13 Wenzl, S.; Hett, R.; Richthammer, P.; Sumper, M. Silacidins: Highly acidic phosphopeptides from diatom shells assist in silica precipitation in vitro. *Angew. Chem. Int. Ed.* **2008**, *47*, 1729-1732.

14 Richthammer, P.; Börmel, M.; Brunner, E.; van Pée, K. H. Biomineralization in diatoms: The role of silacidins. *ChemBioChem* **2011**, *12*, 1362-1366.

15 Davis, A. K.; Hildebrand, M. Palenik, B. A stress-induced protein associated with the girdle band region of the diatom *Thalassiosira pseudonana* (Bacillariophyta). *J. Phycol.* **2005**, *41*, 577-589.

16 Scheffel, A.; Poulsen, N.; Shian, S.; Kröger, N. Nanopatterned protein microrings from a diatom that direct silica morphogenesis. *Proc. Natl. Acad. Sci. U .S. A,* **2011**, *108*, 3175-3180.

17 Kröger, N.; Deutzmann, R.; Bergsdorf, C.; Sumper, M. Species specific polyamines from diatoms control silica morphology. *Proc. Natl. Acad. Sci. U .S. A.* **2000**, *97*, 14133-14138.

18 Kröger, N.; Deutzmann, R.; Sumper, M. Polycationic peptides from diatom biosilica that direct silica nanosphere formation *Science* **1999**, *286*, 1129-1132.

19 Kröger, N.; Deutzmann, R.; Sumper, M. Silica precipitating peptides from diatoms: The chemical structure of silaffin-1A from *Cylindrotheca fusiformis*. *J. Biol. Chem.* **2001**, *276*, 26066-26070.

20 Kröger, N.; Lorenz, S.; Brunner, E.; Sumper, M. Self-assembly of highly phosphorylated silaffins and their function in biosilica morphogenesis *Science* **2002**, *298*, 584-586.

21 Knecht, M. R.; Wright, D. W. Functional analysis of the biomimetic silica precipitating activity of the R5 peptide from *Cylindrotheca fusiformis*. *Chem. Commun.* **2003**, 3038-3039.

22 Luckarift, H. R.; Spain, J. C.; Naik, R. R.; Stone, M. O. Enzyme immobilization in a biomimetic silica support. *Nat. Biotechnol.* **2004**, *22*, 211-213.

23 Naik, R. R.; Tomczak, M. M.; Luckarift, H. R.; Spain, J. C.; Stone, M. O. Entrapment of enzymes and nanoparticles using biomimetically synthesized silica. *Chem. Commun.* **2004**, 1684-1685.

24 Marner II, W. D.; Shaikh, A. S.; Muller, S. J.; Keasling, J. D. Enzyme immobilization via silaffin-mediated autoencapsulation in a biosilica support. *Biotechnol. Prog.* **2009**, *25*, 417-423.

25 Nam, D. H.; Won, K.; Kim, Y. H.; Sang, B. I. A novel route for immobilization of proteins to silica particles incorporating silaffin domains. *Biotechnol. Prog.* **2009**, *25*, 1643-1649.

26 Choi, O.; Kim, B. C.; An, J. H.; Min, K.; Kim, Y. H.; Um, Y.; Oh, M. K.; Sang, B. I. A biosensor based on the self-entrapment of glucose oxidase within biomimetic silica nanoparticles induced by a fusion enzyme. *Enzyme Microb. Technol.* **2011**, *49*, 441-445.

27 Brott, L. L.; Naik, R. R.; Pikas, D. J.; Kirkpatrick, S. M.; Tomlin, D. W.; Whitlock, P. W.; Clarson, S. J.; Stone, M. O. Ultrafast holographic nanopatterning of biocatalytically formed silica. *Nature* **2001**, *413*, 291-293.

28 Wieneke, R.; Bernecker, A.; Riedel, A.; Sumper, M.; Steinem, C.; Geyer, A. Silica precipitation with synthetic silaffin peptides. *Org. Biomol. Chem.* **2011**, *9*, 5482-5486.

29 Atherton, E.; Sheppard, R. C. *Solid Phase Synthesis: A Practical Approach,* IRL Press at Oxford Univ. Press: Oxford, 1989.

30 Sarin, V. K.; Kent, S. B. H.; Tam, J. P.; Merrifield, R. B. Quantitative monitoring of solid-phase peptide synthesis by the ninhydrin reaction. *Analyt. Biochem.* **1981**, *117*, 147-157.

31 Haack, T.; Mutter, M.; Serine derived oxazolidines as secondary structure disrupting, solubilizing building blocks in peptide synthesis. *Tetrahedron Lett.* **1992**, *33*, 1589-1592.

32 Mutter, M.; Nefzi, A.; Sato, A.; Sun, X.; Wahl, F.; Wöhr, T.; Pseudo-prolines (psi Pro) for accessing "inaccessible" peptides. *Peptide Res.* **1995**, *8*, 145-153.

33 Perich, J.W.; Johns, R. B. Di-*t*-butyl *N*, *N*-diethylphosphoramidite and dibenzyl *N*, *N*-diethylphosphoramidite. Highly reactive reagents for the 'phosphite-triester' phosphorylation of serine-containing peptides. *Tetrahedron Lett.* **1988**, *29*, 2369-2372.

34 Andrews, D. W.; Kitchin, J.; Seale, P. W. Solid-phase synthesis of a range of O-phosphorylated peptides by post-assembly phosphitylation and oxidation. *Int. J. Peptide Protein Res.* **1991**, *38*, 469-475.

35 Otvos Jr. L.; Elekes, I.; Lee, V. M. Y. Solid-phase synthesis of phosphopeptides. *Int. J. Peptide Protein Res.* **1989**, *34*, 129-133.

36 Iler, R. K. *The Chemistry of Silica,* Wiley-Interscience: New York, 1979.

37 Nakajima, T.; Volcani, B. E. ε-N-trimethyl-L-δ-hydroxylysine phosphate and its nonphosphorylated compound in diatom cell walls. *Biochem. Biophys. Res. Comm.* **1970**, *39*, 28-33.

38 Hoebbel, D.; Garzo, G.; Engelhardt, G.; Ebert, R.; Lippmaa, E.; Alla, M. Über die Silicatanionenkonstitution in Tetraethylammoniumsilicaten und ihren wäßrigen Lösungen. *Z. Anorg. Allg. Chem.* **1980**, *465*, 15-33.

39 Mizutani, T.; Nagase, H.; Fujiwara, N.; Ogoshi, H. Silicic acid polymerization catalyzed by amines and polyamines. *Bull. Chem. Soc. Jpn.* **1998**, *71*, 2017-2022.

40 Kröger, N.; Sumper, M. In *Biomineralization;* Baeuerlein, E., Ed.; Wiley-VCH: Weinheim, Germany, 2000; p. 168.

41 Bernecker, A.; Wieneke, R.; Riedel, R.; Seibt, M.; Geyer, A.; Steinem, C. Tailored synthetic polyamines for controlled biomimetic silica formation. *J. Am. Chem. Soc.* **2010**, *132*, 1023-1031.

42 Belton, D. J.; Patwardhan, S. V.; Perry, C. C. Spermine, spermidine and their analogues generate tailored silicas. *J. Mater. Chem.* **2005**, *15*, 4629-4638.

43 Sumper, M. A phase separation model for the nanopatterning of diatom biosilica. *Science* **2002**, *295*, 2430-2433.

44 Robinson, D. B.; Rognlien, J. L.; Bauer, C. A.; Simmons, B. A. Dependence of amine-accelerated silicate condensation on amine structure. *J. Mater. Chem.* **2007**, *17*, 2113-2119.

45 Menzel, H.; Horstmann, S.; Behrens, P.; Bärnreuther, P.; Krueger, I.; Jahns, M. Chemical properties of polyamines with relevance to the biomineralization of silica. *Chem. Commun.* **2003**, 2994-2995.

46 Zamora, P.; Narváez, A.; Domínguez, E.; Enzyme-modified nanoparticles using biomimetically synthesized silica. *Bioelectrochemistry* **2009**, *76*, 100-106.

47 Neville, F.; Broderick, M. J. F.; Gibson, T.; Millner, P. A. Fabrication and activity of silicate nanoparticles and nanosilicate-entrapped enzymes using polyethyleneimine as a biomimetic polymer. *Langmuir* **2011**, *27*, 279-285.

48 Miller, S. A.; Hong, E. D.; Wright, D. Rapid and efficient enzyme encapsulation in a dendrimer silica nanocomposite. *Macromol. Biosci.* **2006**, *6*, 839-845.

49 Lai, J. K.; Chuang, T. H.; Jan, J. S.; Wang, S. S. S. Efficient and stable enzyme immobilization in a block copolypeptide vesicle-templated biomimetic silica support *Colloids Surf., B* **2010**, *80*, 51-58.

50 Haase, N. R.; Shian, S.; Sandhage, K. H.; Kröger, N. Biocatalytic nanoscale coatings through biomimetic layer-by-layer mineralization. *Adv. Funct. Mater.* **2011**, *21*, 4243-4251.

Chapter 4

Modified silaffin R5 peptides for encapsulation and release of cargo molecules from silica particles

Biomimetic silica formation has attracted increasing interest over the last decade for numerous biotechnological applications due to the favorable mild reaction conditions. Inspired from silica biogenesis in diatoms, peptide variants derived from native silaffins have been used for silica formation in vitro. Here a generally applicable route for covalently linking a cargo molecule to the R5 silaffin peptide via a disulfide linkage is established. The peptide CG12AB, a peptide ligand of the epidermal growth factor receptor, was chosen as model. The ability of such silaffin-cargo conjugates to encapsulate the cargo molecule during silaffin-mediated silica precipitation is demonstrated. Cargo release from silica material under different conditions was analyzed. The results obtained here provide a rational basis for developing engineered R5 silaffin peptides into efficient tools for silica precipitation as well as for entrapment and release of cargo molecules under physiological conditions.

The work described in this chapter was published in
Lechner, C. C.; Becker, C. F. W. *Bioorg. Med. Chem*. **2013**, *21*, 3533-3541.

DOI: 10.1016/j.bmc.2013.04.006

4.1 Introduction

Silica based nanomaterials have found broad application in biotechnological and biomedical research, for example in enzyme immobilization, drug delivery, imaging and sensing.[1-3] Since the commonly applied processes for silica syntheses require extreme conditions with respect to pH, temperature and pressure,[4] biomimetic approaches for silica formation have gained more attention in the past decade.[5] The mild reaction conditions in biomimetic silica synthesis are beneficial, especially in formation of hybrid silica materials containing sensitive biomolecules. The field of bioinspired silica formation and its applications was particularly stimulated by the quickly progressing research towards understanding the biological principles of silicification.

Amorphous silica is formed in a biomineralization process in diatoms, sponges and higher plants and is deposited as skeletal material.[6] The ornate, nano-patterned silica cell walls of diatoms are considered a paradigm for controlled silica biogenesis under mild conditions. Genomic analysis of diatoms and chemical analysis of diatom cell walls led to the identification of diverse organic macromolecules that are associated with silica formation and patterning.[7-16] Among these, species-specific long chain polyamines and silaffin peptides have been shown to be directly involved in the process of biosilica formation and of being capable to initiate silica formation from a solution of silicic acid in vitro.[15,16] All silaffin peptides show a high sequence similarity and originate from precursor polypeptides that are proteolytically processed during maturation and are extensively posttranslationally modified.[16] The major posttranslational modifications (PTMs) of silaffins are phosphorylation of serine residues, hydroxylation and phosphorylation at the δ-C-atom of lysine residues as well as methylation and alkylation with unique oligo-N-methyl-propylamine units at the ε-amino groups of lysine residues.[17,18] These PTMs have been shown to be essential for silica precipitating activity of silaffins under native conditions.[16] Nevertheless, a synthetic, unmodified silaffin variant, the R5 peptide (H-SSKKSGSYSGSKGSKRRIL-OH) is capable of triggering silica formation from monosilicic acid under specific conditions.[16,18]

The proposed mechanism for silaffin-mediated silica formation is mainly based on two key aspects: first, the silaffin variants selfassemble into larger clusters, which serve as templates

for silica formation. In case of the native, posttranslationally modified silaffin peptides, this process is driven by their zwitterionic structure. Synthetic, unmodified R5 peptides absolutely require divalent anions such as phosphate to form larger self-assemblies (Scheme 4-1).[17] Second, amino groups within the peptide facilitate formation of siloxane bonds, which results in polycondensation of silicic acid and formation of small nuclei of highly branched polysilicic acid. These nuclei continuously polymerize with monosilicic acid or nuclei of polysilicic acid aggregate, subsequently forming the typically observed spherical silica particles.[4,19] During silica formation, the silaffin peptides co-precipitate with the silica and become entrapped within or tightly associated with the silica material.[16,20]

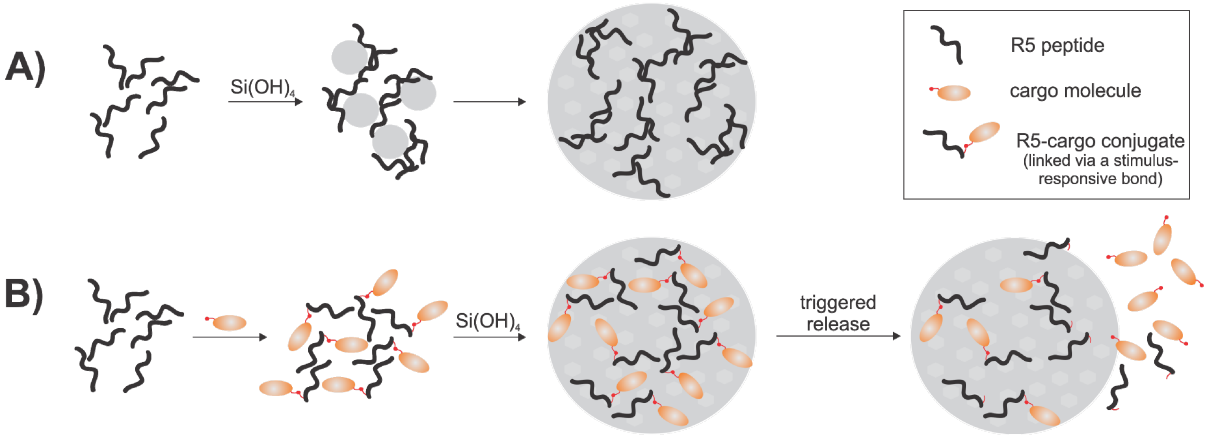

Scheme 4-1 Silica precipitation with synthetic R5 peptide and R5-cargo conjugates.

A) The R5 peptide forms self-assemblies which serve as template for the polycondensation of silicic acid mediated by the peptidic amino groups. The small particles consistent of highly branched polysilicic acid of the early stage grow further by continuous polymerization or consolidate to form the typically observed spherical silica particles. The R5 peptide becomes entrapped within the silica material in this process.

B) Covalent linkage of a cargo molecule to the R5 peptide leads to co-entrapment of the cargo into silica particles during R5-directed silica precipitation. In case of conjugation of the cargo to the R5-peptide via a stimulus-responsive bond, the release of cargo molecules from the silica particles can be triggered by external stimuli.

Based on these characteristics, several biotechnological applications of biomimetic silica formation using silaffins or silaffin-derived peptides were already established.[21-26] Most of these applications serve the purpose of enzyme encapsulation and stabilization and have been achieved by genetic fusion of a silaffin tag to the target protein or by simple co-precipitation of the protein during silaffin R5 mediated silica formation. Nevertheless, these methods lack control over silica morphology and structure, which can be achieved with silaffin R5 variants carrying different amino acid modifications (see chapter 3)

Despite all the advances in biomimetic silica formation, there is only a limited number of applications in the biomedical field yet, for example formation of hybrid material with bioactive peptides or proteins.[27,28] Current applications for drug delivery and release are mainly based on mesoporous silica nanoparticles (MSNs).[1] The production of mesoporous silica nanoparticles (MSNs) by chemical synthesis allows tuning of particle size, morphologies, and pore size.[29] The loading capacity of such synthesized silica particles is, in turn, dependent on the total pore volume and the pore diameter in relation to the chemical properties of the molecule to be encapsulated in the silica material.[30] Loading of chemically synthesized mesoporous silica nanoparticles is in general achieved by the immersion loading method, in which silica particles are soaked in a solution containing the cargo molecule for several hours.[31] By adjusting and optimizing the parameters for silica nanoparticle material formation as well as for the cargo molecule, high loading capacities can be achieved.[32] Nevertheless, obvious advantages of biomimetic formation of silica particles are the mild reaction conditions in aqueous solution at neutral pH and room temperature as well as the possibility of simultaneous encapsulation of cargos during silica formation. This is particularly beneficial for the entrapment of sensitive cargos such as biomolecules.

In chapter 3 it was demonstrated that homogeneous incorporation of a small fluorescent probe was achieved by its covalent attachment to the R5 N-terminus. This prompted the development of the synthetic R5 peptide into a reagent for simultaneous silica precipitation and direct incorporation of cargo molecules in silica particles. Modification of the R5 peptide with a cargo molecule via a covalent, but stimulus-responsive cleavable bond, enables the controlled release of cargo molecules from silica material (Scheme 4-1, B). The initial development of disulfide-linked R5-cargo conjugates offers the possibility for triggered release of the cargo from silica particles under reducing conditions. Such conditions can also

be compatible with *in vivo* release of cargo molecules from inert silica particles, for example by the native reducing agent glutathione.

To this end the concept of R5-cargo conjugate encapsulation into silica particles was proven with the cargo peptide CG12AB (H-CGYHWYGYTPQNVI-OH). CG12AB is a peptide ligand of the epidermal growth factor receptor (EGFR) initially identified via phage display.[33] Here the originally identified sequence is N-terminally elongated with glycine and cysteine. The peptide was shown to bind to EGFR with a K_D of 22 nM and to be efficiently internalized into EGFR expressing cells, but in contrast to the natural ligand EGF not to promote mitogenic activity. Since EGFR was found to be overexpressed in many tumors[34] a high affinity peptide ligand is promising as a tool for receptor-mediated cellular delivery of drugs. Here, a convenient route for the synthesis of disulfide-linked R5-cargo conjugates is described (Scheme 4-2) and the activity of R5 peptide variants and R5-cargo conjugates in biomimetic silica precipitation is explored. Loading of silica with the cargo peptide CG12AB is analyzed and the release of entrapped R5 peptide and cargo from the silica particles is investigated depending on buffer conditions such as pH and presence of reducing agents as well as incubation time.

4.2 Materials and methods

4.2.1 Materials

All solvents and chemicals were purchased in the highest available quality and were used as received: *N,N*-dimethylformamide (DMF), dichloromethane (DCM) and acetonitrile (ACN) from Biosolve (Valkenswaard, The Netherlands). Fmoc-protected L-amino acids, Fmoc-Leu-Wang resin and 2-(1*H*-benzotriazol-1-yl)-1,1,3,3-tetramethyluronium hexafluorophosphate (HBTU) from Novabiochem (Nottingham, UK). Boc-Ile-PAM resin and Boc-protected L-amino acids from Bachem (Bubendorf, Switzerland) and Orpegen (Heidelberg, Germany). Methanol and trifluoroacetic acid (TFA) from Roth (Karlsruhe, Germany). Diisopropylethylamine (DIEA), 2,2'-dithiobis(5-nitropyridine) (DTNP); L-glutathione reduced (GSH), *p*-cresol, piperidine, silicon atomic absorption standard solution, tetramethoxysilane (TMOS) tris(2-carboxyethyl)phosphine (TCEP) and triisopropylsilane (TIS) from Sigma–Aldrich (Taufkirchen, Germany). 1,4-Dithio-D,L-threitol (DTT) from Gerbu (Gaiberg, Germany). Hydrogen fluoride (HF) from Merck (Darmstadt, Germany).

4.2.2 HPLC and mass spectrometry

Analytical RP-HPLC analysis was performed on a Dionex Ultimate 3000 instrument using C4 columns (Kromasil 300-5-C4 150 × 4.6 mm, 5 µm particle size and BioBasic-4 150 × 4.6 mm, 5 µm particle size, Thermo Fisher) at a flow rate of 1 mL/min with a gradient from 5% to 65% buffer B in buffer A over 30 min (buffer A: 0.1% (v/v) TFA in ddH_2O, buffer B: 0.08% (v/v) TFA in ACN). For reversed phase purification and mass spectrometry of peptides a Waters AutoPurification HPLC/MS System was used. For analytical liquid chromatography-mass spectrometry (LC-MS) separation was achieved with a Kromasil 300-5-C4 column (50 × 4.6 mm, 5 µm particle size) at a flow rate of 1 mL/min running a linear gradient from 5% to 65% of (ACN + 0.05 % TFA) in (ddH_2O + 0.05 % TFA) in 10 min. Mass spectra were acquired by electrospray ionization (ESI-MS) operating in positive ion mode. Detection for all chromatographic methods occurred at 214 and 280 nm wavelength.

4.2.3 Peptide synthesis and purification

The sequence of the R5 peptide (R5-Cys(StBu): H-C(StBu)SSKKSGSYSGSKGSKRRIL-OH) was synthesized as described in chapter 3 using fluorenylmethoxycarbonyl (Fmoc) chemistry.[35] The side chain protecting groups were as followed: Cys(*t*Buthio), Lys(Boc) and Lys(Mtt), Arg(Pbf), Ser(*t*Bu), Tyr(*t*Bu) and Gly-Ser($\psi^{Me,Me}$pro).

Synthesis and purification of the cargo-peptide CG12AB was done by Karine Farbiarz and Manuel Brehs (Institute of Biological Chemistry, University of Vienna). The cargo-peptide CG12AB was synthesized at a 0.2 mmol scale using an S-DVB (stryrene-divinylbenzene) resin that carries an $–OCH_2$-PAM linker and was preloaded with Boc-isoleucine. The peptide sequence H-CGYHWYGYTPQNVI-OH was assembled on the solid support following an *in situ* neutralization and HBTU activation protocol for Boc (*tert*-butoxycarbonyl) chemistry.[36] Side-chain protecting groups were Asn(Xan), Cys(Trt), His(3Bom), Thr(Bzl) and Tyr(2-Br-Z). To improve synthesis yields, a double coupling cycle for Thr(Bzl) was applied. The peptide was finally deprotected and cleaved from the resin by treatment with liquid HF (10 mL/g of peptidyl resin) for 1 h at 0 °C in the presence of 10% (v/v) p-cresol. Purification of the peptide was achieved using a Kromasil 300-5-C18 column at a flow rate of 8 mL/min with a linear gradient from 5% to 45% of (ACN + 0.05% TFA) in (ddH_2O + 0.05% TFA) in 30 min yielding 16.8 mg pure peptide.

4.2.4 On resin activation of cysteine with 5-nitro-2-pyridinesulfenyl (pNpys)

From 100 mg (25 µmol) peptidyl resin (H-C(StBu)SSKKSGSYSGSKGSKRRIL-OH) the N-terminal Fmoc group was removed and resin was swollen in DMF. The *tert*-butylthio (S*t*Bu) protecting group was selectively removed on resin with a solution of 380 mg DTT (2.5 mmol, 100 equiv) in 900 µL DMF and 100 µL DIEA (0.58 mmol, 23 equiv) in 16 h. After extensive washing with DMF, the peptidyl resin was transferred to DCM and swollen for 1 h. Activation of the free thiol function of the cysteine was achieved by gently agitating the peptidyl resin in a solution of 155.2 mg DTNP (0.5 mmol, 20 equiv) in 2.25 mL DCM and 250 µL DIEA (1.45 mmol, 57.5 equiv) for 16 h. Small amounts of peptidyl resin were taken

after each step and cleaved from the resin to monitor the reactions by analytical HPLC and ESI-MS. Finally, the peptidyl resin was washed with DMF and dried under vacuum. Final deprotection and cleavage of the peptide from the resin was accomplished with 5% TIS, 2.5% ddH2O and 92.5% TFA. Crude peptide was purified by reverse phase HPLC (Kromasil 300-5-C18 column, 8 mL/min with a linear gradient from 5 to 45% of (ACN + 0.05% TFA) in (ddH_2O + 0.05% TFA) in 30 min) yielding 19.3 mg of R5-Cys(pNpys) in good purity (34.0% yield from 100 mg (25 μmol) peptidyl resin).

4.2.5 Preparation of heterodisulfide-bonded R5-CG12AB conjugate

The reaction buffer of 6 M Gdn/HCl and 200 mM NaPi pH 6 was degassed and flushed with argon. Stock solutions of peptides R5-Cys(pNPys) and CG12AB were prepared in the reaction buffer. R5-Cys(pNpys) was diluted to a final concentration of 1 mM in the reaction buffer and the heterodisulfide-formation was initiated by addition of equimolar amount of cargo-peptide CG12AB. The process of the reaction was monitored via the absorption of released 5-nitro-2-pyridinesulfenyl at 412 nm. Aliquots of 2 nmol of R5-Cys(pNpys) and cargo-peptide in the reaction buffer at time point zero and an equal volume of the reaction solution after 10 min were analyzed by HPLC. The formation of the heterodisulfide-conjugate of R5 and cargo-peptide CG12AB was verified by LC-MS analysis (not shown). The R5-CG12AB conjugate was purified by RP-HPLC (Kromasil 300-5-C18 column, 8 mL/min, linear gradient from 5% to 45% of (ACN + 0.05% TFA) in (ddH_2O + 0.05% TFA) in 30 min). Pure R5-CG12AB conjugate was analyzed by HPLC (Kromasil 300-5-C4 column 150 × 4.6 mm) and MS.

4.2.6 Silica precipitation *in vitro*

The peptides R5-Cys(SH), R5-Cys(pNpys), the cargo-peptide CG12AB and the R5-CG12AB conjugate were each dissolved in 50 mM potassium phosphate buffer at pH 7.0 to a final concentration of 470 μM. A stock solution of silicic acid was generated by hydrolysis of 250 mM tetramethoxysilane (TMOS) in 1 mM aqueous HCl for 4 min. The addition of the silicic acid to the peptide solution to a final concentration of 25 mM initiated the silica

precipitation reaction. The reaction was incubated at room temperature for 30 min, subsequently centrifuged (5 min, 16.873×g) to collect the silica precipitates and washed twice with water. Silicic acid solutions without silaffin peptides did not lead to the formation of any precipitate. For electron microscopic analysis the silica precipitates were suspended in water, applied to a Thermanox™ coverslip (Thermo scientific) and air dried. The coverslips were placed onto sample holders and sputter coated with gold/palladium in high vacuum (Leica SCD050). Electron micrographs were recorded with a scanning electron microscope (Zeiss Supra 55 VP) operating at 5 kV. To quantify the amount of precipitated silica, the collected silica precipitates were dissolved in 2 M NaOH for 1 h at room temperature. A modified β-silicomolybdate method[4] as described by Wieneke et al.[37] was applied for the quantification and all assays were performed at least in triplicate. Control experiments showed no interference of R5 and CG12AB peptides in these quantification assays. Calibration curves are based on a silicon atomic absorption standard solution.

4.2.7 Release of peptides from silica particles

Silica precipitation with different peptides and conjugates were carried out as described in 4.2.6. The formed silica precipitates were washed twice with water and pelleted by centrifugation again. To analyze the release of peptides and cargo molecules from the silica material under different conditions, the silica precipitate was resuspended in equal volumes of different buffers (PBS pH 7.4; PBS + 5 mM TCEP pH 7.4; 100 mM NaOAc, pH 5). The silica suspension was shaken at 37 °C for 1 h. Afterwards the silica was pelleted again by centrifugation (5 min, 16.873×g) and the supernatant was collected. Aliquots of equal volumes were analyzed by HPLC (Kromasil 300-5-C4 column 150 × 4.6 mm). For kinetic analyses of peptide release from silica particles, the silica was prepared as described above and the silica precipitate was suspended in buffer at pH 7.4. Aliquots of the silica suspension were centrifuged (5 min, 16.873×g) at defined time points and the supernatant buffer was analyzed for peptide content by HPLC (Kromasil 300-5-C4 column 150 × 4.6 mm). All assays were performed at least in triplicate. The amount of the released peptide was calculated from integrated areas of HPLC traces and referred to standards.

4.3 Results and discussion

4.3.1 Preparation of disulfide-linked R5-cargo conjugates

To achieve specific and efficient heterodisulfide-conjugation between two sulfhydryl-containing moieties the activation of the sulfhydryl function in one reaction partner is generally required in order to prevent formation of homodimers. The R5 peptide variant used in this study carries an N-terminal cysteine residue (Table 4-1). For solid phase peptide synthesis (SPPS) using the Fmoc/*t*Bu strategy, the cysteine sulfhydryl group was protected with *tert*-butylthio (S*t*Bu). The S*t*Bu-protecting group is compatible with peptide synthesis via both Boc- and Fmoc-strategy, but it is partially removed during HF cleavage, which follows standard Boc/Bzl-SPPS. In contrast, Cys-S*t*Bu is stable to TFA, and therefore orthogonal to all other protecting groups commonly used in Fmoc/*t*Bu strategy.[38,39] Cysteine residues with protecting groups compatible with TFA and HF treatments and that also provide activation for subsequent disulfide formation, such as 3-nitro-2- pyridinesulfenyl (Npys), can be readily incorporated during Boc/Bzl-based peptide synthesis.[40,41] However, Npys is not stable to basic conditions and therefore not suitable for Fmoc/*t*Bu-based peptide syntheses. Here the Fmoc/*t*Bu synthesis strategy is preferred since silaffins are typically highly posttranslationally modified with groups that are not stable under Boc/Bzl synthesis conditions.[16,17] Such native posttranslational as well as non-native modifications of silaffins have been shown to modulate silica precipitation activities and morphology of the resulting silica particles (chapter 3). Specifically the synthesis of natively occurring phosphorylated silaffin variants[17] could not be achieved via Boc/Bzl peptide synthesis due to the lack of suitably protected serine building blocks for post synthetic phosphorylation and due to dephosphorylation of amino acid during HF-cleavage.[42] Therefore, postsynthetic activation of the cysteine thiol function on the solid phase provides a convenient method compatible with other posttranslational modifications of silaffin or for changing position of the cysteine in the R5-sequence. In addition, our synthetic route for the preparation of R5-cargo conjugates allows installation of almost any cargo-molecule carrying a thiol group (Scheme 4-2).

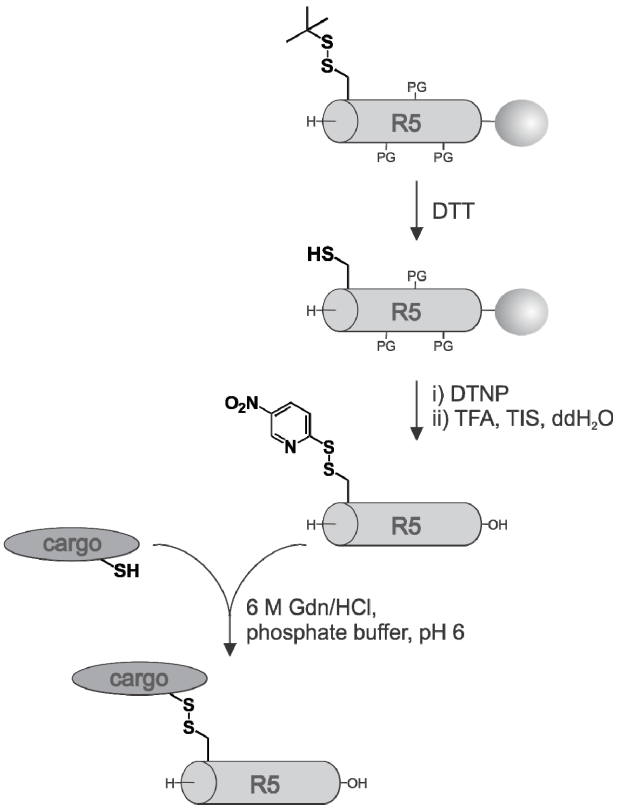

Scheme 4-2 General outline for the synthesis of disulfide-linked R5-cargo variants via on resin activation and subsequent cleavage before loading with a cargo molecule.

The S*t*Bu-protecting group of the N-terminal cysteine residue in R5 is selectively removed under mild reducing conditions using DTT. Subsequently, the now unprotected thiol group is activated as the 5-nitro-2-pyridinesulfenyl (pNpys) disulfide by treating the peptidyl resin with 2,2'-dithiobis(5-nitropyridine) (DTNP).[43] Activation of the thiol group with pNpys is superior to Npys, since unstable and cross-reactive sulfenyl halides such as Npys-Cl have to be used for postsynthetic modification. In addition, pNpys is a better leaving group compared to Npys due to increased acidity based on the nitro group in para position.[43,44] This reaction proceeds selectively and with high efficiency as verified by HPLC and ESI-MS analysis of crude intermediates (Figure 4-1 and Figure 4-2).

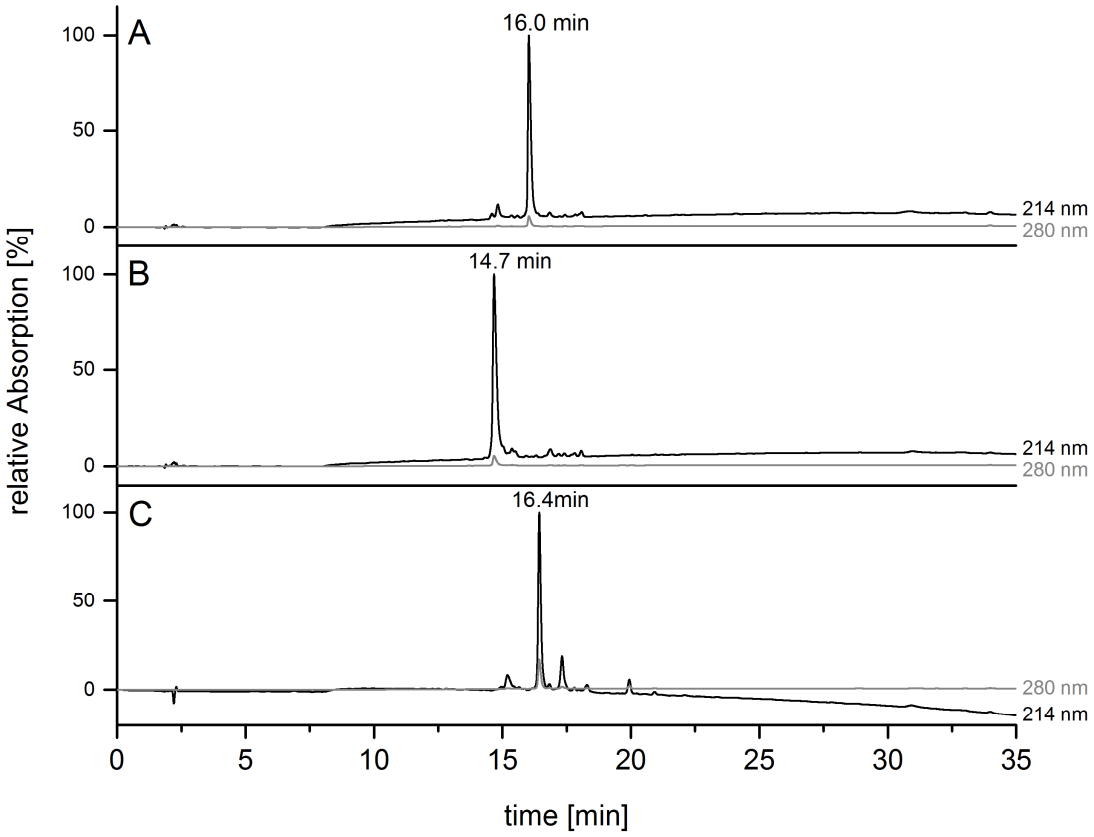

Figure 4-1 Conversion of Cys(S*t*Bu) to Cys(pNpys). Analytical RP-HPLC chromatograms of crude peptides. Reactions were carried out on the solid support. Small samples of peptidyl-resin were taken after each step and cleaved to monitor the reactions reactions (BioBasic-4 column 150 x 4.6 mm):

A) R5-Cys(S*t*Bu): H-C(S*t*Bu)SSKKSGSYSGSKGSKRRIL-OH

B) R5-Cys(SH): H-C(SH)SSKKSGSYSGSKGSKRRIL-OH

C) R5-Cys(pNpys): H-C(pNpys)SSKKSGSYSGSKGSKRRIL-OH

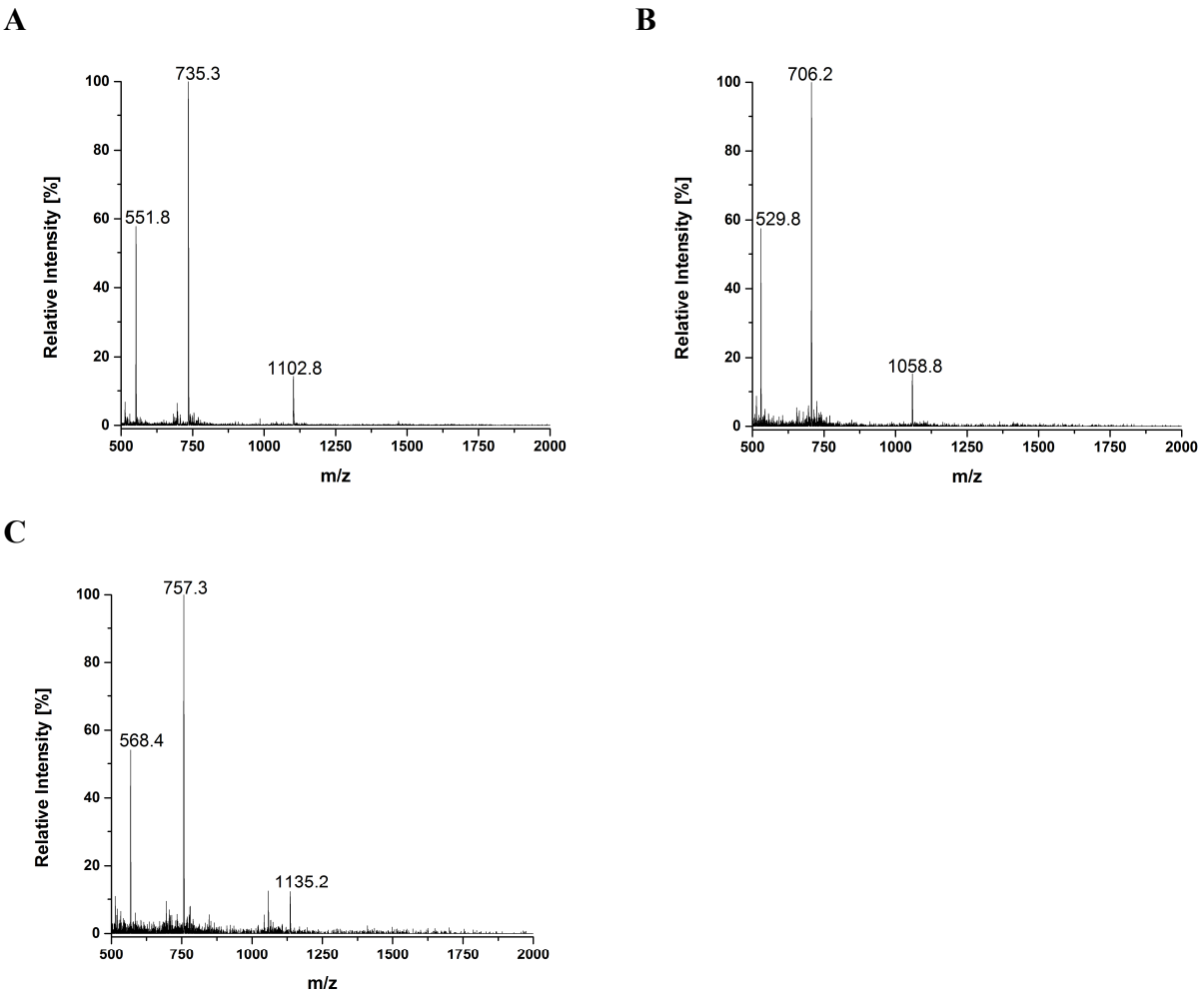

Figure 4-2 Conversion of Cys(S*t*Bu) to Cys(pNpys). ESI-MS of crude peptides. Reactions were carried out on the solid support. Small amounts of peptidyl-resin were taken after each step and cleaved to monitor reactions by ESI-MS:

A) R5-Cys(StBu): Mass calculated for $C_{91}H_{163}N_{30}O_{30}S_2^+$: 2204.2 $[M+H]^+$, found: 1102.8 $[M+2H]^{2+}$, 735.3 $[M+3H]^{3+}$, 551.8 $[M+4H]^{4+}$.

B) R5-Cys(SH): Mass calculated for $C_{87}H_{155}N_{30}O_{29}S^+$: 2116.1 $[M+H]^+$, found: 1058.8 $[M+2H]^{2+}$, 706.2 $[M+3H]^{3+}$, 529.8 $[M+4H]^{4+}$.

C) R5-Cys(pNpys): Mass calculated for $C_{92}H_{157}N_{32}O_{31}S_2^+$: 2270.1 $[M+H]^+$, found: 1135.2 $[M+2H]^{2+}$, 757.3 $[M+3H]^{3+}$, 568.4 $[M+4H]^{4+}$.

The R5 peptide with activated Cys(pNpys) was cleaved from the solid support and purified (Figure 4-3). Activation of the sulfhydryl group with DTNP would also be possible in solution or during cleavage of the peptide from the resin by adding DTNP to the cleavage

cocktail,[43,45] but on-resin activation facilitates purification and allows disulfide conjugation on the solid support. However, the on-resin formation of a mixed disulfide between the R5 peptide and the selected cargo CG12AB[33] (Table 4-1) did not work (data not shown). This observation might be caused by limited diffusion of the CG12AB-peptide into the porous resin beads. In contrast, as indicated by the successful conversion of cysteine into pNpys-activated cysteine by addition of an excess of DTNP, the disulfide-coupling of small molecules works smoothly on the solid support.

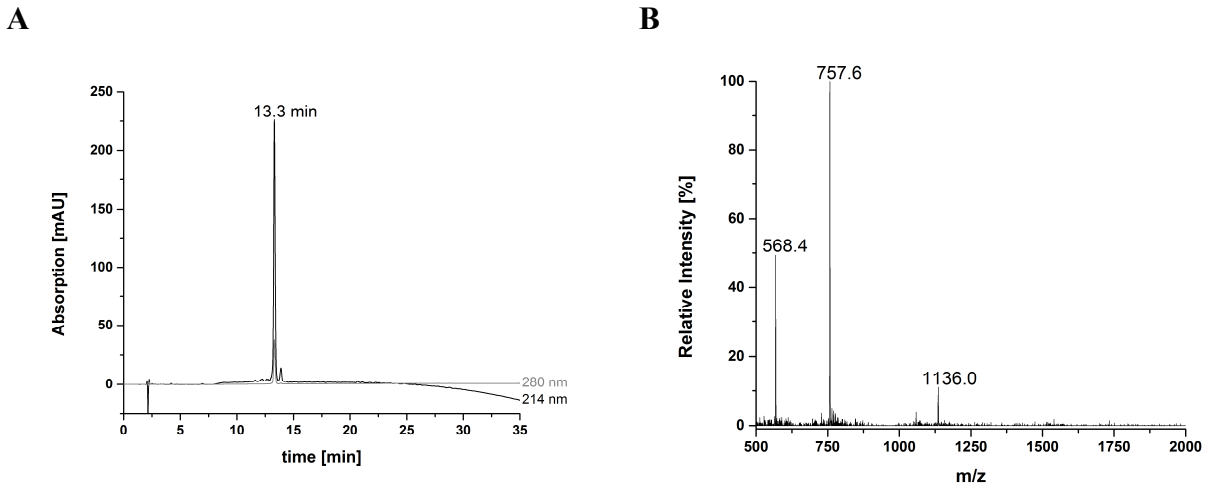

Figure 4-3 **A)** Analytical RP-HPLC chromatogram of purified R5-Cys(pNpys) (Kromasil 300-5-C4 column 150 x 4.6 mm).

B) ESI-MS of purified R5-Cys(pNpys): Mass calculated for $C_{92}H_{157}N_{32}O_{31}S_2^+$: 2270.1 $[M+H]^+$, found: 1136.0 $[M+2H]^{2+}$, 757.6 $[M+3H]^{3+}$, 568.4 $[M+4H]^{4+}$.

Table 4-1 Characteristics of peptides and peptide-conjugates

Peptide	Sequence	MW_{calc} [Da]	MW_{obs} [Da]	Spec. activity[a]	Loading efficiency[b] [%]
R5-Cys(SH)	CSSKKSGSKGSKRRIL	2115.1	2115.3	0.65 ± 0.03	32.7 ± 2.1
R5-Cys(pNpys)	C(pNpys)SSKKSGSKGSKRRIL	2269.1	2268.9	0.58 ± 0.01	24.3 ± 1.1
CG12AB	CGYHWYGYTPQNVI	1699.8	1700.0	N.d.	-
R5-CG12AB	CSSKKSGSKGSKRRIL | CGYHWYGYTPQNVI	3812.9	3813.4	0.55 ± 0.02	47.7 ± 6.5

N.d.– not detected.

[a] Specific silica precipitation activity at pH 7.0 given in pmol silicon per min and nmol of peptide.

[b] (nmol peptide in nanoparticles/nmol peptide used initially for silica precipitation)*100.

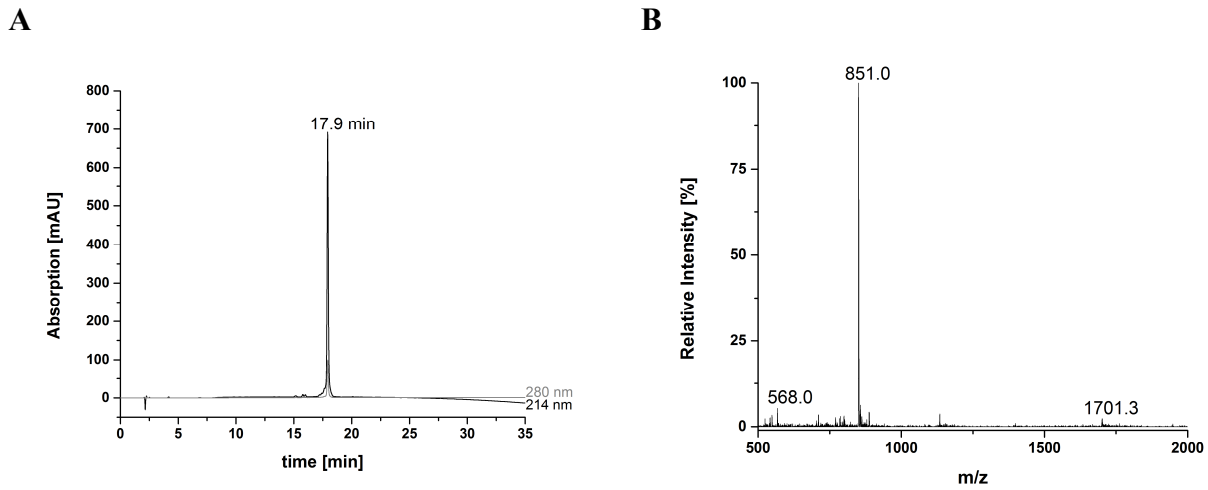

Figure 4-4 **A)** Analytical RP-HPLC chromatogram of purified cargo peptide CG12AB (H-CGYHWYGYTPQNVI-OH) (Kromasil 300-5-C4 column 150 x 4.6 mm).
B) ESI-MS of purified CG12AB peptide: Mass calculated for $C_{80}H_{106}N_{19}O_{21}S^+$: 1700.8 $[M+H]^+$, found: 1701.3 $[M+H]^+$, 851.0 $[M+2H]^{2+}$, 568.0 $[M+3H]^{3+}$.

Formation of a mixed disulfide between activated R5-Cys (pNpys) and the purified CG12AB peptide (Figure 4-4) in solution was carried out under argon atmosphere at pH 6 to prevent homodimer formation by disulfide exchange reactions. The reaction went to completion within a few minutes as monitored via the absorbance of released 5-nitro-2-pyridinesulfenyl at 412 nm (Figure 4-5) and by HPLC analysis (Figure 4-6).

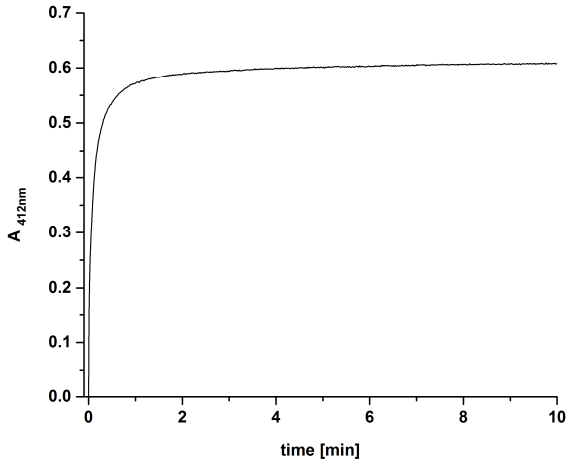

Figure 4-5 Reaction kinetic of hetero-disulfide formation between R5 and the cargo peptide CG12AB. The reaction was monitored via absorption of released 5-nitro-2-pyridinesulfenyl at 412 nm.

The disulfide-linked heterodimer of R5 and the CG12AB-peptide was selectively formed, no homodimer species were observed. Reversed phase HPLC purification gave the R5-CG12AB conjugate in high purity and with good yields of 40% after purification (Figure 4-7). All peptides and disulfide-linked peptide conjugates are summarized in Table 4-1.

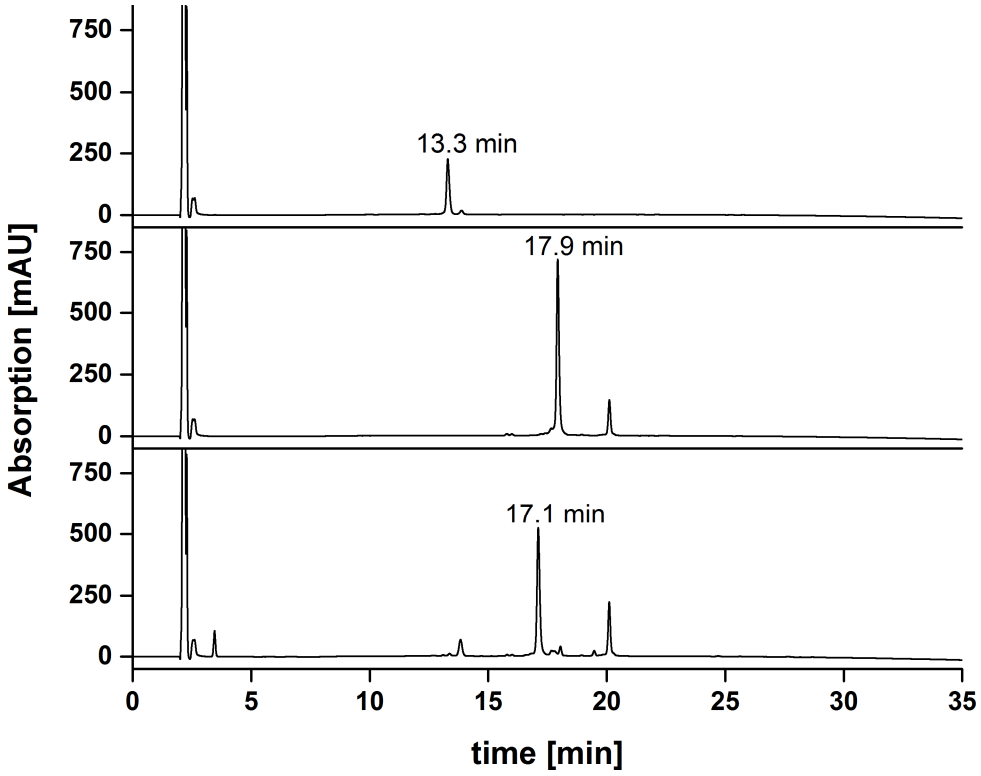

Figure 4-6 Hetero-disulfide formation between R5 and CG12AB-peptide in solution (6 M Gdn/HCl and 200 mM NaPi at pH 6) monitored via analytical RP-HPLC (Kromasil 300-5-C4 column 150 x 4.6 mm).

A) 2 nmol R5-Cys(pNpys), t = 0

B) 2 nmol CG12AB, t = 0

C) Reaction mixture, t = 10 min

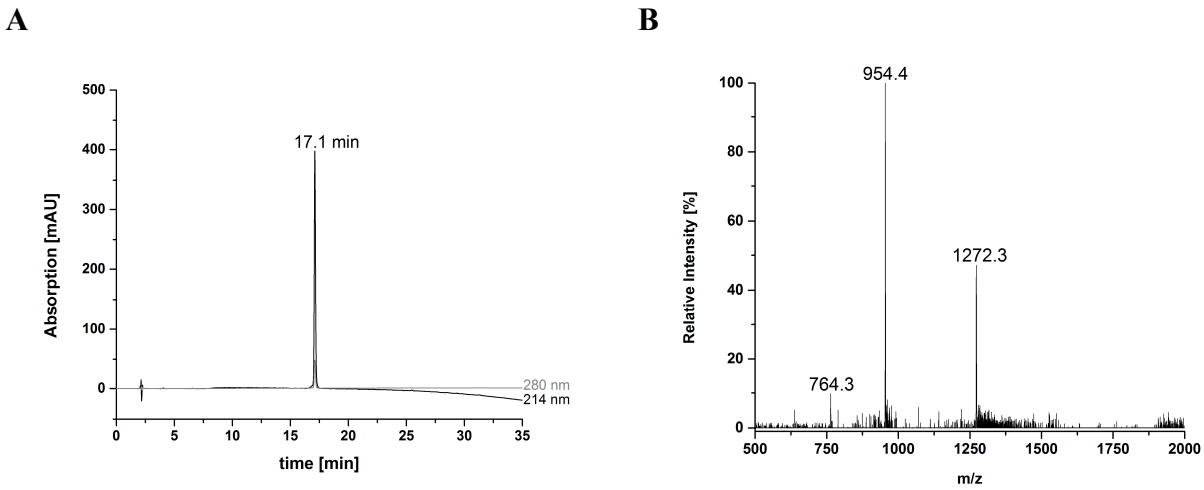

Figure 4-7 **A)** Analytical RP-HPLC chromatogram of purified R5-CG12AB conjugate (Kromasil 300-5-C4 column 150 x 4.6 mm)
B) ESI-MS of purified R5-CG12AB conjugate: Mass calculated for $C_{167}H_{258}N_{49}O_{50}S_2^+$: 3813.9 $[M+H]^+$, found: 1272.3 $[M+3H]^{3+}$, 954.4 $[M+4H]^{4+}$, 764.3 $[M+5H]^{5+}$.

4.3.2 Silica precipitation with R5-variants and R5-CG12AB conjugate

The ability of the silaffin R5 variants (with free and pNpys-modified thiol function), the peptide CG12AB and the R5-CG12AB conjugate (Table 4-1) to precipitate silica from a phosphate buffered solution of silicic acid at pH 7 was analyzed. All experiments described here have been repeated at least 3 times and always gave similar results. Figure 4-8 depicts representative scanning electron micrographs of the silica material obtained from experiments with peptides and peptide conjugates listed in Table 4-1. Control reactions carried out with silicic acid in phosphate buffer in the absence of the R5 peptide showed no silica formation. The unmodified R5 peptide leads to formation of homogenous spherical silica particles as was observed previously (chapters 2 and 3).[20,24] The average diameter of the particles was 600 nm (Figure 4-8, A) and the specific silica precipitation activity of the R5 peptide was 0.65 ± 0.03 pmol Si/ nmol peptide min (Table 4-1).

Modification of the cysteine sulfhydryl-group with 5-nitro-2- pyridinesulfenyl did not interfere with the silica precipitation activity. R5-Cys(pNpys) showed specific activity in

silica precipitation similar to R5-Cys(SH) (Table 4-1), although the silica particles resulting from R5-Cys(pNpys) induced precipitation had increased particle diameters of approximately 720 nm (Figure 4-8, B). For the CG12AB peptide alone no silica formation was observed at all (Figure 4-8, C). The R5-CG12AB peptide conjugate induced, similar to R5 and R5-Cys(pNpys), rapid formation of spherical silica particles (Figure 4-8, D). These silica spheres were even bigger, with an average diameter of 920 nm, but the specific silica precipitation activity of the R5-CG12AB conjugate was slightly decreased compared to R5-Cys(SH) (Table 4-1). Nevertheless, this result shows that conjugation of a cargo peptide, in our case the CG12AB peptide, to the R5-sequence slightly decreases the silica precipitation activity of the R5 peptide, but does not completely abolish it.

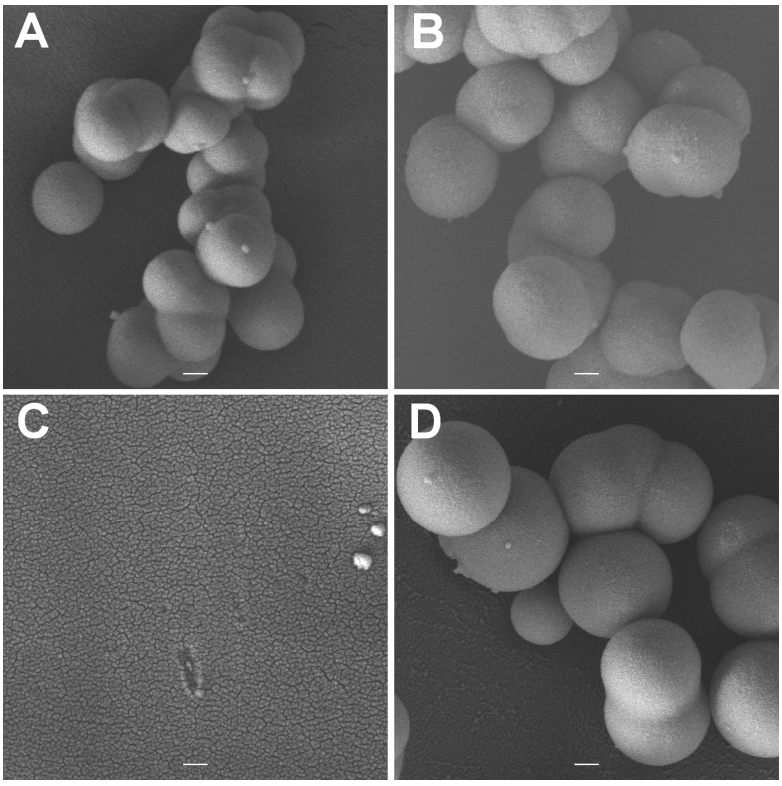

Figure 4-8 Scanning electron micrographs of silica particles resulting from (A) R5-Cys(SH), (B) R5-Cys(pNpys), (C) CG12AB, and (D) R5-CG12AB conjugate. Scale bars: 200 nm.

Since the R5 peptide is known to co-precipitate during silica formation,[16,20] the amount of peptide that is entrapped in the precipitated silica was analyzed in order to determine the loading of silica material with the different peptide species. To this end, the peptide content

in both the supernatant after silica precipitation and the silica material dissolved in 2 M sodium hydroxide was analyzed by integration and direct comparison of HPLC peak areas. Since the pNpys group is cleaved from the R5-sequence during basic treatment of the silica material, peaks corresponding to pNpys and R5-Cys(SH) were integrated and summarized for evaluation of loading of R5-Cys(pNpys). For R5-Cys(SH) (16.8 ± 1.1 nmol/nmol SiO_2, (32.7 ± 2.1%)) and R5-Cys(pNpys) (13.9 ± 0.7 nmol/nmol SiO_2, (24.3 ± 1.1%)) similar amounts of the respective peptides were loaded per nmol of precipitated SiO2. Interestingly, with 29.2 ± 4.0 nmol/nmol SiO2 (47.7 ± 6.5%), almost twice as much of R5-CG12AB conjugate was trapped in the silica material (Tables 4-1 and 4-2). In line with the proposed mechanism for silica precipitation described above, all R5-variants and -conjugates show silica precipitating activity, whereas the CG12AB peptide has no silicification activity due to the lack of lysine residues and a low tendency for self-assembly (Table 4-1). The R5-Cys(SH), R5-Cys (pNpys) and R5-CG12AB conjugate do not differ in the R5-sequence and all have the essential lysine residues that mediate the polycondensation of silicic acid. Therefore, the reason for the different loading of peptide into the silica material must be their tendency for self-assembly which is most likely influenced by electrostatic and hydrophobic interactions of the cargo-molecules attached to the R5-sequence. The very minor difference in silica precipitation efficiency in R5-Cys(SH) and R5-Cys(pNpys) indicates that the N-terminal cysteine modification with the rather small pNpys group has a negligible effect. A major difference was observed in case of the R5-CG12AB conjugate. In this conjugate, the R5-part triggers the silica precipitation and the CG12AB-cargo is believed to become entrapped within the formed silica. The R5-CG12AB conjugate shows comparable specific silica precipitating activity to the R5-Cys(SH) and R5-Cys(pNpys) (Table 4-1). Albeit a significantly increased loading of the formed silica particles (29.2 ± 4.0 nmol conjugate/nmol SiO_2) (Table 4-2) and loading efficiency (47.7 ± 6.5%) (Table 4-1) were observed. Interestingly, also the silica particles resulting from the R5-CG12AB conjugate show a distinctly enlarged average diameter of 920 nm (Figure 4-8, D) compared to the particles from R5-Cys(SH) and R5-Cys(pNpys) (Figure 4-8). These results suggest that conjugation of a bigger cargo via a disulfide-bond to the R5-sequence disturbs the proper and tight formation of self-assemblies of the R5-sequence. In addition, the sequence of the cargo peptide CG12AB has no zwitterionic character and therefore cannot assist in self-assembly

via electrostatic interactions. Formation of tight clusters of R5 peptide as templates for silica precipitation requires more R5-CG12AB conjugate, consequently resulting both in enlarged particle diameters and increased loading of particles with the R5-CG12AB conjugate.

In addition to exploring silica precipitation with the covalently linked R5-CG12AB conjugate, silica formation and cargo encapsulation using a mixture of R5 and CG12AB peptides, in which these peptides were not linked via a disulfide bond, was studied. Albeit there are several examples in the literature of such co-precipitation approaches for silica encapsulation of enzymes,[22,23] here no encapsulation of the cargo peptide CG12AB was observed. Addition of freshly generated silicic acid to a 1:1 mixture of R5 and CG12AB in phosphate buffer at pH 7 resulted in the formation of silica material, although the R5 showed reduced specific activity (0.43 ± 0.03 pmol Si/nmol peptide min). The R5 peptide becomes entrapped into the silica material during this process (23.2 ± 0.8 nmol/nmol SiO_2), but not the CG12AB peptide.

4.3.3 Controlled release of peptides from silica particles

The covalent conjugation of a cargo molecule to the R5-sequence offers the possibility of loading the silica particles coincidently with their formation. A stimulus-responsive cleavable linkage between cargo and R5 peptide enables controlled release of the entrapped cargo from the silica material. The feasibility to use engineered R5 peptide variants for biomimetic silica particle formation and cargo encapsulation was investigated. In addition, it was explored if the R5 peptide and cargo are permanently entrapped in the silica or can be selectively released.

The possibility to use silica particles formed by R5-induced precipitation as a vehicle for delivering cargo molecules depends on the stability of loaded silica particles as well as on the ability to control the release of cargo and, potentially, of R5 peptide from silica material. To test for stability and uncontrolled release of R5 and cargo the silica material was suspended in different buffer solutions, incubated at 37 °C for a specific time and the supernatant buffer was analyzed for peptide content. Silica is stable towards dissolution in aqueous media in a pH range from 1 to 8.[46] To mimic physiological conditions, PBS buffer at pH 7.4 was used

and to simulate intracellular redox conditions 5 mM TCEP was added to the solution. TCEP was chosen because this water-soluble phosphine gives rapid and quantitative reduction of the disulfide. Glutathione as the physiological reducing agent also cleaves the disulfide bonds and releases cargo molecules but leads to the formation of mixed disulfides that severely complicate quantitative analysis of peptide release (data not shown). Additionally, the peptide release from the silica material at pH 5 in sodium-acetate buffer was examined. The results for release of peptides and cargo molecules (pNpys and CG12AB) from silica material after 1 h of incubation under three different buffer conditions are summarized in Table 4-2. Notably, the pNpys group was partly cleaved from the R5-Cys(pNpys) peptide over time in PBS due to its base lability. Therefore, all peaks corresponding to R5-Cys(pNpys), R5-Cys(SH) and pNpys in HPLC analysis were considered for quantification. The comparison of all different peptide species shown in Table 4-2 reveals a distinctly altered release of entrapped peptides from silica particles depending on buffer conditions.

Table 4-2 Release of peptides from silica particles under different conditions after 1 h incubation at 37 °C

	Loading of silica with peptide[a]	**Release in NaOAc, pH 5**	**Release in PBS, pH 7.4**	**Release in PBS + TCEP, pH 7.4**	
				R5-peptide	**pNpys/CG12AB**
R5-Cys(SH)	16.8 ± 1.1	14.1 ± 0.1 [a] (84%)[b]	2.0 ± 0.3 [a] (12%)[b]	8.40 ± 0.2 [a] (50%)[b]	-
R5-Cys(pNpys)	13.9 ± 0.7	10.6 ± 0.4 [a] (76%)[b]	3.4 ± 0.3 [a] (24%)[b]	8.0 ± 1.2 [a] (58%)[b]	7.9 ± 0.3 [a] (57%)[b]
R5-CG12AB	29.2 ± 4.0	14.1 ± 0.9 [a] (48%)[b]	5.2 ± 0.3 [a] (18%)[b]	3.0 ± 0.5 [a] (10%)[b]	8.1 ± 1.2 [a] (28%)[b]

[a] Given in (nmol) peptide/(nmol) SiO_2.

[b] (%) Release of peptide from initial loading of silica with peptide.

Most obvious is the strongly increased release of peptides under acidic conditions (100 mM NaOAc, pH 5). This observation implies that neither R5 nor the cargo peptide is covalently bound to the silica material but rather entrapped in and associated to the silica material by hydrogen bonding and electrostatic interactions between peptide side chains and silanol groups. At decreased pH the lysine ε-amino groups (pK of 10.5) are protonated and the free silanol groups become protonated as well, resulting in impaired hydrogen bonding. Therefore, the R5 species were detached from the silica material at acidic pH and were

released much faster compared to neutral pH. This behavior might be of particular interest for release of cargo in acidic environments as it is found in certain cellular compartments (e.g., lysosomes) or in and around tumor cells.[47]

In PBS buffer less peptide was released from silica material. A diffusion-based release of bioactive peptides or proteins from hybrid silica material in PBS buffer was already observed in approaches for biomimetic silica formation.[27,28] Based on the loading capacity of precipitated silica with the different peptides 12% of R5-Cys(SH), 24% of R5-Cys(pNpys) and 18% of R5-CG12AB conjugate were washed out after 1 h of incubation (Table 4-2). These values increased slowly until they became constant after 6 h in PBS buffer. At that time 23% of R5-Cys(SH) and R5-Cys(pNpys) and 32% of the R5-CG12AB conjugate were released (Figure 4-9).

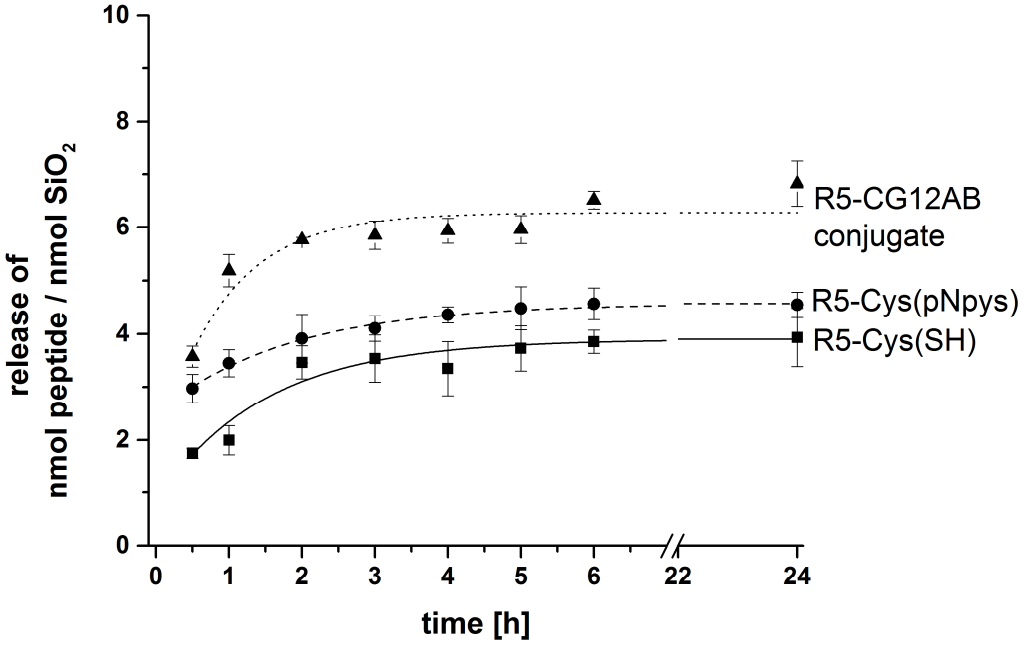

Figure 4-9 Release of peptides and peptide conjugate from silica particles in PBS, pH 7.4 at 37 °C versus time; (■) R5-Cys(SH); (●) R5-Cys(pNpys); (▲) R5-cargo conjugate.

The time course of peptide release in PBS (Figure 4-9) shows slightly faster release kinetics for R5-Cys(pNpys) and R5-CG12AB conjugate when compared to R5-Cys(SH). Silaffins consist of a peptide sequence perfectly evolved for silica precipitation activity. This implies a

tight association and interaction between peptide and silica as well as silanol groups, respectively. Native silaffins show extremely strong association to bio-silica, for example in diatoms, which requires dissolution of this silica with HF or acidic ammonium fluoride in order to release the peptides.[16,17] Besides the unique amino acid sequence of silaffins, a series of specific PTMs of these native silaffins as well as other molecules involved in silica biomineralization in diatoms contribute to this strong interaction. Synthetic R5 peptides lacking any PTM and the biological context exhibit a less tight association to silica compared to native silaffins, which leads to leaching of peptide as observed here.

The attachment of the small para-nitropyridinylsulfenyl (pNpys) moiety to synthetic R5 further decreased this tight association between peptide and silica as can be recognized by the faster and increased release of R5-Cys(pNpys) compared to R5-Cys(SH) (Figure 4-9). This effect was even more pronounced in case of the R5-CG12AB conjugate, in which the rather hydrophobic CG12AB peptide seemed to significantly lower the interaction between R5 and the silica inducing a faster and increased release of up to 32% of conjugate from the silica material.

Modification of the R5-peptide with pNpys or the cargo-peptide CG12AB via a redox-sensitive disulfide linkage not only allows the entrapment of the cargo into the precipitated silica material, but also a redox-responsive release of cargo from silica particles. Under reducing conditions (PBS + 5 mM TCEP, pH 7.4), both the release of the small pNpys from R5-Cys(pNpys) (Figure 4-10) and of CG12AB peptide from R5-CG12AB conjugate (Figure 4-11) was analyzed (Table 4-2).

In case of the R5-Cys(pNpys) peptide, a fast release of similar amounts of pNpys (7.9 ± 0.3 nmol pNpys/nmol SiO_2, 57%) and R5 peptide (8.0 ± 1.2 nmol peptide/nmol SiO_2, 58%) was observed under reducing conditions (Table 4-2 and Figure 4-10). However, for R5-CG12AB conjugate reducing conditions lead to a much more rapid release of CG12AB peptide from silica material (8.1 ± 1.2 nmol peptide/nmol SiO_2, 28%), and a delayed and decreased release of R5 peptide (3.0 ± 0.5 nmol peptide/nmol SiO_2, 10%) (Table 4-2, Figure 4-11).

This result indicates that cleavage of the disulfide bond can occur on the entrapped R5-CG12AB conjugate followed by diffusion of peptides out of the silica. Otherwise equal amounts of CG12AB and R5 peptide would be detectable. The similar fast release profiles for the small pNpys group compared to the rather hydrophobic CG12AB peptide hints

towards little influence of size and hydrophobicity on the release and diffusion. However, in case of R5-CG12AB conjugate, the CG12AB peptide seems to hamper diffusion of the cleaved R5 out of the silica. Approximately fivefold more of R5-Cys(SH) (50%) and of the R5 part cleaved from R5-Cys(pNpys) (58%, Table 4-2) is released from particles in PBS with TCEP. This result might also indicate the impaired ability of R5-CG12AB conjugate to form self-assemblies required for silica precipitation. R5-Cys(pNpys) can homogenously self-assemble as can the unmodified R5-Cys(SH), resulting in a homogenous distribution of these peptide variants in the silica material and consequently in very similar release profiles. One could speculate that R5-CG12AB conjugate forms larger clusters in a core-shell like structure, whereby the R5 forms a tight assembled core and the cargo a surrounding shell. Consequently, after reductive cleavage of the disulfide linkage between CG12AB and R5 peptide, the cargo peptide CG12AB is released rapidly, followed by a slower release of R5 peptide.

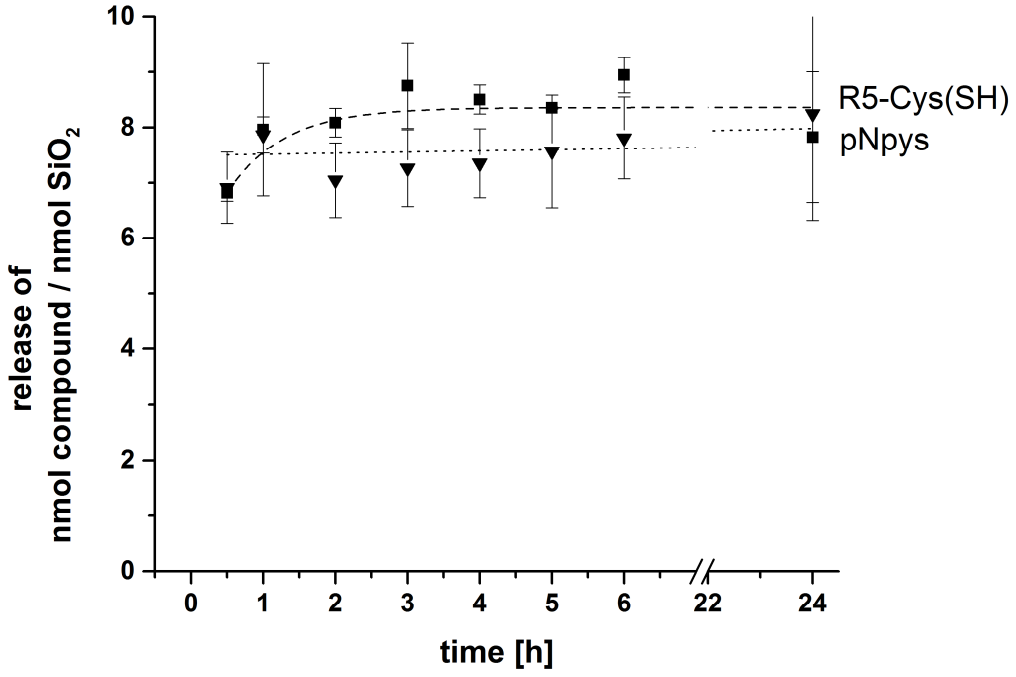

Figure 4-10 Release of (■) R5-Cys(SH) and (▼) pNpys from silica particles in PBS + 5 mM TCEP, pH 7.4 at 37 °C versus time.

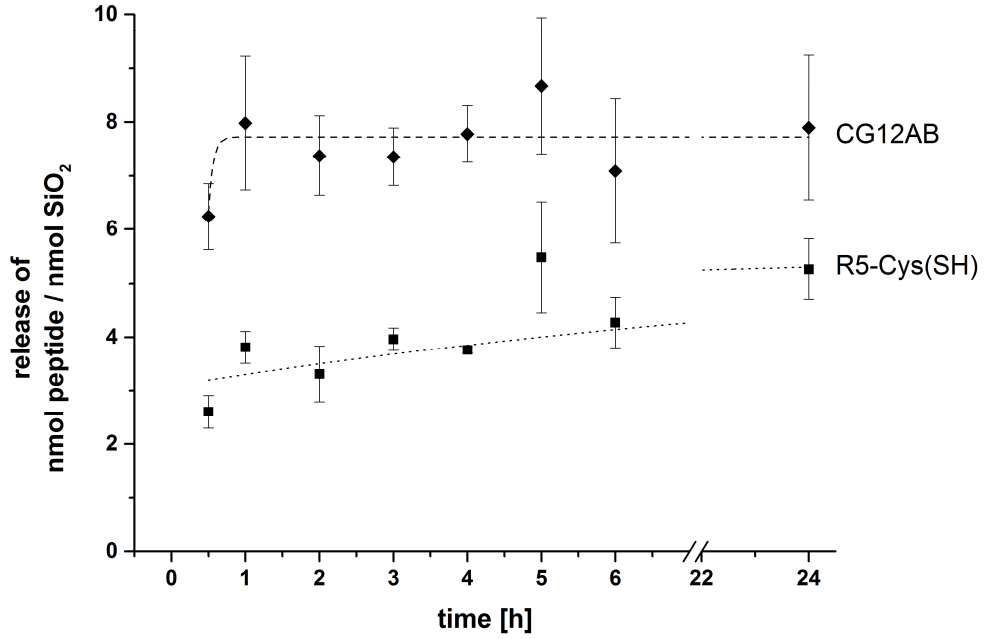

Figure 4-11 Release of (■) R5-Cys(SH) and (♦) CG12AB from silica particles in PBS + 5 mM TCEP, pH 7.4 at 37 °C versus time.

Time-dependent analyses of peptide release from silica particles in PBS buffer at neutral pH (Figure 4-9, A) showed a constant level of peptides after 6 h. At that time only 23-32% of the total amount of peptide was released from silica material. In contrast, under reducing conditions an increased release of peptide and cargos was observed (Table 4-2). Therefore, pre-incubation of silica material in PBS buffer at pH 7.4 should prevent uncontrolled release of peptides and only under reducing conditions release of peptides should be initiated again. Indeed in case of R5-CG12AB conjugate, after incubation in PBS first, reductive conditions lead to fast release (2 h) of both cargo peptide CG12AB (7.7 ± 0.2 nmol/nmol SiO_2, 26%) and R5 peptide (6.0 ± 0.4 nmol/nmol SiO_2, 28%). However, even unmodified R5-Cys(SH) (7.1 ± 0.7 nmol peptide/nmol of SiO_2) was released in TCEP containing PBS buffer, which might indicate formation of disulfide linked homodimers that can only diffuse out of the silica material after reductive cleavage.

4.4 Conclusion

As described above, the silaffin R5-sequence can be readily modified to serve as a silica precipitating agent and anchor for entrapment of covalently bound cargo molecules. Pre-incubation of this hybrid silica material in PBS buffer will result in release of low amounts of weakly associated peptide species from the silica material. The major amount of peptide will remain associated with the silica material and can partially be released by exposure to acidic and/or reducing conditions as found in certain cellular environments.

A method for preparation of covalently linked R5- cargo conjugates was established (Scheme 4-2). This strategy allows straightforward and selective conjugation of R5 with different thiol-functionalized cargo molecules, such as small (drug or fluorescent) molecules, bioactive peptides and proteins via formation of a disulfide bond. The disulfide linkage enables controlled cleavage of the R5 conjugate under reducing conditions.

Analysis of different R5-cargo conjugates reveals only minor changes in silica precipitation activity. 48% of R5-CG12AB conjugate become entrapped in the silica material during silica formation. By careful adjustment of reaction conditions, for example concentrations of peptides or silicic acid precursor, even higher loading efficiencies can be achieved. Particularly the mild one-step procedure is advantageous. In comparison, loading of mesoporous silica nanoparticles suffers from usage of organic solvents, which is not favorable for many biomolecules. The development of R5 peptides into efficient agents for encapsulation of biomolecules in silica requires a thorough understanding of the performance of R5 peptides in silica particle formation. The R5 peptide co-precipitates during silica formation, but is again released from the silica material after suspension in buffer. The diffusion-based release is highly dependent on the pH of the buffer medium, which is displayed in an increased release at acidic pH compared to neutral pH (Table 4-2). Moreover, a stimulus-responsive release of R5 peptide and the cargos pNpys and CG12AB could be observed under reducing conditions. The cargo-peptide CG12AB is rapidly cleaved from the R5-CG12AB conjugate and released from the silica material (Figure 4-11). The different release rates of CG12AB and R5 peptide in reducing buffer suggest diffusion-based release that is highly dependent on the chemical nature and size of the cargo molecule.

These findings are important for establishing a drug delivery system based on R5-induced biomimetic silica. Application of silaffin variants with different (posttranslational) modifications that are known to have different silica precipitating properties (chapter 3) might provide an additional level of control over the release of cargo molecules. In addition, further functionalization of silaffin variants or silica particles offers the possibility for targeted, site specific delivery of bioactive hybrid silica.

4.5 References

1 Slowing, I. I.; Trewyn, B. G.; Giri, S.; Lin, V. S. Y. Mesoporous silica nanoparticles for drug delivery and biosensing applications. *Adv. Funct. Mater*. **2007**, *17*, 1225-1236.

2 Li, Z.; Barnes, J. C.; Bosoy, A.; Stoddart, J. F.; Zink, J. I. Mesoporous silica nanoparticles in biomedical applications. *Chem. Soc. Rev*. **2012**, *41*, 2590-2605.

3 Betancor, L.; Luckarift, H. R. Bioinspired enzyme encapsulation for biocatalysis. *Trends Biotechnol.* **2008**, *26*, 566-572.

4 Iler, R. K. *The Chemistry of Silica*; John Wiley & Sons: New York, 1979.

5 Patwardhan, S. V. Biomimetic and bioinspired silica: recent developments and applications. *Chem. Commun*. **2011**, *47*, 7567-7582.

6 Simpson, T. L.; Volcani, B. E. *Silicon and Siliceous Structures in Biological Systems*; Springer: New York, 1981.

7 Armbrust, E.; Berges, J.; Bowler, C.; Green, B.; Martinez, D.; Putnam, N.; Zhou, S.; Allen, A.; Apt, K.; Bechner, M.; Brzezinski, M.; Chaal, B.; Chiovitti, A.; Davis, A.; Demarest, M.; Detter, J.; Glavina, T.; Goodstein, D.; Hadi, M.; Hellsten, U.; Hildebrand, M.; Jenkins, B.; Jurka, J.; Kapitonov, V.; Kröger, N.; Lau, W.; Lane, T.; Larimer, F.; Lippmeier, J.; Lucas, S.; Medina, M.; Montsant, A.; Obornik, M.; Parker, M.; Palenik, B.; Pazour, G.; Richardson, P.; Rynearson, T.; Saito, M.; Schwartz, D.; Thamatrakoln, K.; Valentin, K.; Vardi, A.; Wilkerson, F.; Rokhsar, D. The genome of the diatom *Thalassiosira pseudonana*: ecology, evolution, and metabolism.*Science* **2004**, *306*, 79-86.

8 Kröger, N.; Bergsdorf, C.; Sumper, M. A new calcium binding glycoprotein family constitutes a major diatom cell wall component. *EMBO J*. **1994**, *13*, 4676-4683.

9 Kröger, N.; Bergsdorf, C.; Sumper, M. Frustulins: domain conservation in a protein family associated with diatom cell walls. *Eur. J. Biochem*. **1996**, *239*, 259-264.

10 Kröger, N.; Lehmann, G.; Rachel, R.; Sumper, M. Characterization of a 200 kDa diatom protein that is specifically associated with a silica-based substructure of the cell wall. *Eur. J. Biochem*. **1997**, *250*, 99-105.

11 Davis, A. K.; Hildebrand, M.; Palenik, B. A stress-induced protein associated with the girdle band region of the diatom *Thalassiosira pseudonana* (Bacillariophyta). *J. Phycol.* **2005**, *41*, 577-589.

12 Wenzl, S.; Hett, R.; Richthammer, P.; Sumper, M. Silacidins: Highly acidic phosphopeptides from diatom shells assist in silica precipitation in vitro. *Angew. Chem., Int. Ed*. **2008**, *47*, 1729-1732.

13 Richthammer, P.; Börmel, M.; Brunner, E.; van Pée, K. H. Biomineralization in diatoms: the role of silacidins. *ChemBioChem* **2011**, *12*, 1362-1366.

14 Scheffel, A.; Poulsen, N.; Shian, S.; Kröger, N. Nanopatterned protein microrings from a diatom that direct silica morphogenesis. *Proc. Natl. Acad. Sci. U. S. A.* **2011**, *108*, 3175-3180.

15 Kröger, N.; Deutzmann, R.; Bergsdorf, C.; Sumper, M. Species specific polyamines from diatoms control silica morphology. *Proc. Natl. Acad. Sci. U. S. A*. **2000**, *97*, 14133-14138.

16 Kröger, N.; Deutzmann, R.; Sumper, M. Polycationic peptides from diatom biosilica that direct silica nanosphere formation *Science* **1999**, *286*, 1129-1132.

17 Kröger, N.; Lorenz, S.; Brunner, E.; Sumper, M. Self-assembly of highly phosphorylated silaffins and their function in biosilica morphogenesis. *Science* **2002**, *298*, 584-586.

18 Kröger, N.; Deutzmann, R.; Sumper, M. Silica precipitating peptides from diatoms: The chemical structure of silaffin-1A from *Cylindrotheca fusiformis*. *J. Biol. Chem*. **2001**, *276*, 26066-26070.

19 Kröger, N.; Sumper, M. In *Biomineralization*; Baeuerlein, E., Ed.; Wiley-VCH: Weinheim, Germany, 2000; p 168.

20 Knecht, M. R.; Wright, D. W. Functional analysis of the biomimetic silica precipitating activity of the R5 peptide from *Cylindrotheca fusiformis*. *Chem. Commun*. **2003**, 3038-3039.

21 Brott, L. L.; Naik, R. R.; Pikas, D. J.; Kirkpatrick, S. M.; Tomlin, D. W.; Whitlock, P. W.; Clarson, S. J.; Stone, M. O. Ultrafast holographic nanopatterning of biocatalytically formed silica. *Nature* **2001**, *413*, 291-293.

22 Luckarift, H. R.; Spain, J. C.; Naik, R. R.; Stone, M. O. Enzyme immobilization in a biomimetic silica support. *Nat. Biotechnol*. **2004**, *22*, 211-213.

23 Naik, R. R.; Tomczak, M. M.; Luckarift, H. R.; Spain, J. C.; Stone, M. O. Entrapment of enzymes and nanoparticles using biomimetically synthesized silica. *Chem. Commun*. **2004**, 1684-1685.

24 Nam, D. H.; Won, K.; Kim, Y. H.; Sang, B. I. A novel route for immobilization of proteins to silica particles incorporating silaffin domains. *Biotechnol. Prog*. **2009**, *25*, 1643-1649.

25 Marner, W. D., II; Shaikh, A. S.; Muller, S. J.; Keasling, J. D. Enzyme immobilization via silaffin-mediated autoencapsulation in a biosilica support. *Biotechnol. Prog*. **2009**, *25*, 417-423.

26 Choi, O.; Kim, B. C.; An, J. H.; Min, K.; Kim, Y. H.; Um, Y.; Oh, M. K.; Sang, B. I. A biosensor based on the self-entrapment of glucose oxidase within biomimetic silica nanoparticles induced by a fusion enzyme. *Enzyme Microb. Technol*. **2011**, *49*, 441-445.

27 Eby, D. M.; Farrington, K. E.; Johnson, G. R. Synthesis of bioinorganic antimicrobial peptide nanoparticles with potential therapeutic properties. *Biomacromolecules* **2008**, *9*, 2487-2494.

28 Sano, K.-I.; Minamisawa, T.; Shiba, K. Autonomous silica encapsulation and sustained release of anticancer protein. *Langmuir* **2010**, *26*, 2231-2234.

29 Wu, K. C.-W.; Yamauchi, Y. Controlling physical features of mesoporous silica nanoparticles (MSNs) for emerging applications. *J. Mater. Chem*. **2012**, *22*, 1251-1256.

30 Salonen, J.; Laitinen, L.; Kaukonen, A. M.; Tuura, J.; Björkqvist, M.; Heikkilä, T.; Väha-Heikkilä, K.; Hirvonen, J.; Lehto, V. P. J. Mesoporous silicon microparticles for oral drug delivery: Loading and release of five model drugs. *Controlled Release* **2005**, *108*, 362-374.

31 Charnay, C.; B'gu, S.; Tourné-Péteilh, C.; Lerner, N. D. A.; Devoisselle, J. M. Inclusion of ibuprofen in mesoporous templated silica: drug loading and release property. *Eur. J. Pharm. Biopharm*. **2004**, *57*, 533-540.

32 Zhang, Y.; Zhi, Z.; Jiang, T.; Zhang, J.; Wang, Z.; Wang, S. Spherical mesoporous silica nanoparticles for loading and release of the poorly water-soluble drug telmisartan. *J. Controlled Release* **2010**, *145*, 257-263.

33 Li, Z.; Zhao, R.; Wu, X.; Sun, Y.; Yao, M.; Li, J.; Xu, Y.; Gu, J. Identification and characterization of a novel peptide ligand of epidermal growth factor receptor for targeted delivery of therapeutics. *FASEB J*. **2005**, *19*, 1978-1985.

34 Salomon, D. S.; Brandt, R.; Ciardiello, F.; Normanno, N. Epidermal growth factor-related peptides and their receptors in human malignancies. *Crit. Rev. Oncol. Hematol*. **1995**, *19*, 183-232.

35 Atherton, E.; Sheppard, R. C. *Solid Phase Synthesis: A Practical Approach*; IRL Press at Oxford Univ. Press: Oxford, 1989.

36 Schnölzer, M.; Alewood, P.; Jones, A.; Alewood, D.; Kent, S. B. H. In situ neutralization in Boc-chemistry solid phase peptide synthesis. Rapid, high yield assembly of difficult sequences. *Int. J. Pept. Protein Res*. **1992**, *40*, 180-193.

37 Wieneke, R.; Bernecker, A.; Riedel, R.; Sumper, M.; Steinem, C.; Geyer, A. Silica precipitation with synthetic silaffin peptides. *Org. Biomol. Chem*. **2011**, *9*, 5482-5486.

38 Weber, U.; Hartter, P. S-Alkylmercapto-Gruppen zum Schutz der SH-Funktion des Cysteins, I. Synthese und Stabilität einiger S-(Alkylmercapto)cysteine. *Hoppe-Seyler's Z. Physiol. Chem*. **1970**, *351*, 1384-1388.

39 Atherton, E.; Sheppard, R. C.; Ward, P. Peptide synthesis. Part 7. Solid-phase synthesis of conotoxin G1. *J. Chem. Soc., Perkin Trans. 1* **1985**, 2065-2073.

40 Bernatowicz, M. S.; Matsueda, R.; Matsueda, G. R. Preparation of Boc-[S-(3-nitro-2-pyridinesulfenyl)]-cysteine and its use for unsymmetrical disulfide bond formation. *Int. J. Pept. Protein Res*. **1986**, *28*, 107-112.

41 Albericio, F.; Andreu, D.; Giralt, E.; Navalpotro, C.; Pedroso, E.; Ponsati, B.; Ruiz-Gayo, M. Use of the Npys thiol protection in solid phase peptide synthesis. Application to direct peptide-protein conjugation through cysteine residues. *Int. J. Pept. Protein Res*. **1989**, *34*, 124-128.

42 Otvos, L.; Elekes, I.; Lee, V. M.-Y. Solid-phase synthesis of phosphopeptides. *Int. J. Pept. Protein Res*. **1989**, *34*, 129-133.

43 Rabanal, F.; DeGrado, W. F.; Dutton, P. L. Use of 2,2′-dithiobis(5-nitropyridine) for the heterodimerization of cysteine containing peptides. Introduction of the 5-nitro-2-pyridinesulfenyl group. *Tetrahedron Lett*. **1996**, *37*, 1347-1350.

44 Ponsati, B.; Ruiz-Gayo, M.; Giralt, E.; Albericio, F.; Andreu, D. Solid-phase-mediated peptide heterodisulfide formation. *J. Am. Chem. Soc*. **1990**, *112*, 5345-5347.

45 Gosh, A. K.; Fan, E. A novel method for sequence independent incorporation of activated/protected cysteine in Fmoc solid phase peptide synthesis. *Tetrahedron Lett*. **2000**, *41*, 165-168.

46 Alexander, G. B.; Heston, W. M.; Iler, R. K. The solubility of amorphous silica in water. *J. Phys. Chem*. **1954**, *58*, 453-455.

47 Song, C. W.; Park, H. J.; Ross, B. D. In *Antiangiogenic Adnets in Cancer Therapy*; Teicher, B. W., Ed.; Humana Press: Totowa, 1998; pp 51–64.

Chapter 5

A novel route for immobilizing enzymes in silica using modified silaffin peptides

Immobilizing enzymes in silica is commonly applied to improve performance of enzymes under detrimental conditions. Inspired by silica biomineralization processes occurring in nature, approaches towards biomimetic silica formation gained increasing attention. In diatoms, complex posttranslationally modified silaffin peptides are directly involved in formation and patterning of silica cell walls. Here, modified silaffin peptides were used to establish a novel strategy for silica immobilization of target proteins. Silaffin variants carrying different modifications were covalently linked to eGFP and thioredoxin using expressed protein ligation. Covalent protein-silaffin conjugates are aimed to achieve selective immobilization of proteins while maintaining control over silica properties by choice of different silaffin peptides. Covalent eGFP- and thioredoxin-silaffin conjugates were able to precipitate silica and simultaneously lead to encapsulation of the proteins in the silica material. Silica materials with different morphologies were obtained indicating the influence of the covalently linked silaffin. With the covalent protein-silaffin conjugates, a distinctly more efficient and homogenous encapsulation of proteins in silica was achieved, which is superior to random entrapment resulting from simple co-precipitation. Analysis of protein release from silica revealed that part of the protein is set free over time. For both, the extent of entrapmentin silica and release of proteins from silica, a dependency on the silaffin variants used for silica formation became apparent. Silica-immobilized proteins were confirmed to be enzymatically active and stabilized against denaturation.

5.1 Introduction

The immobilization of functional biomolecules, such as enzymes is beneficial for diverse biotechnological and medicinal applications due to improved properties of the immobilized biomolecules. In the case of enzymes, immobilization can improve stability and activity under detrimental reaction conditions or enable recycling of these sensitive biomolecules.[1] Immobilization can be achieved by binding of enzymes to a solid support, either via covalent bonds or physical adsorption, by encapsulating them or by cross-linking enzymes into large aggregates.[2]

The latter method differs from the others by having no need for a solid support. Cross linked enzyme aggregates (CLEAs) are prepared by initially inducing protein aggregation via addition of salts, organic solvents, polymers or acids. The subsequent cross-linking of the resulting catalytically active aggregates makes them permanently insoluble and enables their use as efficient biocatalysts with improved properties.[3-5]

Physical adsorption of enzymes to a support matrix driven by hydrogen bonding or electrostatic and hydrophobic interactions is the simplest method of enzyme immobilization. However, it also poses many challenges, e.g. reaction conditions have to be carefully optimized and adjusted to minimize leaching of enzymes out of the solid material. Desorption of enzymes from solid supports can be prevented by attaching them covalently via reactive amino acid side chain functionalities to the surface. However, covalent immobilization frequently results in lowered activity of the enzymes due to conformational changes and spatial constraints.[2] Encapsulation of enzymes in a solid support, i.e. physical confinement of the enzymes in a support matrix, often reduces leaching and has less negative impact on enzyme activity.

For immobilization or encapsulation of enzymes, mesoporous silica materials have gained substantial attention as support matrix due to their convenient properties. This material provides a large surface area with uniform pore sizes, the surface silanol groups can be easily functionalized and silica has a high chemical and physical stability. Mesoporous silica nanoparticles (MSNs) are synthesized using an organic template that is removed after silica formation,[6] allowing the control of silica morphology and pore sizes by the choice of templating molecule and reaction conditions.[7,8] Therefore, pore sizes can be adjusted to be

suitable for large biomolecules such as enzymes. But the efficiency in loading of mesoporous silica materials via adsorption of an enzyme turned out to be also highly dependent on protein size and properties.[9] This inefficient and slow loading process as well as the elaborate syntheses of MSNs under harsh conditions are major drawbacks of synthetic silica materials as solid support for enzyme immobilization.

In contrast, biogenic formation of silica materials occurs under mild, physiological conditions and takes place in diatoms, sponges and higher plants.[10] The eukaryotic, unicellular diatoms are major producers of amorphous silica in aqueous habitats and have remarkably nano-structured, porous frustules composed of amorphous silica and organic matter.[10] Due to its highly regular, porous structure implicating a large surface area, diatom silica is convenient as carrier for protein immobilization. The porous silica frustules can be modified or loaded with biomolecules and thus be used in biotechnological and biomedical approaches such as immunoprecipitation, biosensing and drug delivery.[11-15]

In addition, the molecular mechanisms of silica biogenesis in diatoms were extensively investigated to gain insights into these complex processes and to establish novel routes for generating structured silica materials under mild conditions. The chemical analysis of diatom cell walls led to the discovery of numerous biomolecules, including polysaccharides,[16] long chain polyamines (LCPAs)[17,18] and diverse proteins such as frustulins,[19,20] pleuralins,[21,22] silacidins,[23,24] cingulins[25] and silaffins[26] that are associated with diatom biosilica. Among these, silaffins and LCPAs are directly involved in the silica precipitation process *in vivo* and have also been proven to be able to precipitate silica from a solution of silicic acid *in vitro*.[17,26] The silaffin peptides from the diatom *C. fusiformis* derive from a precursor polypeptide by proteolytic processing and show a high sequence similarity (repetitive units R1-R7).[26] During maturation silaffin peptides become extensively posttranslationally modified. The numerous serine hydroxyl groups are phosphorylated and the ε-amino groups of lysine residues become di- or trimethylated or alkylated with long-chain polyamines.[27,28] Additionally, hydroxylation and phosphorylation of the trimethylated lysine residues at the δ-position was observed.[28] Although these posttranslational modifications (PTMs) turned out to be essential for silica precipitating activity under native conditions (pH 5)[26] a synthetic, unmodified silaffin R5 peptide (H-SSKKSGSYSGSKGSKRRIL-OH) is also highly efficient

in precipitating silica from a solution of silicic acid at neutral pH, as long as phosphate ions are present.[26-28]

The outstanding silica precipitation activity of silaffin peptides under mild conditions enables their application in silica formation for enzyme immobilization. Several strategies for immobilization of enzymes using silaffin peptides have been developed. One approach is based on genetic manipulation of diatoms with the sequence of a target protein being genetically fused to a silaffin gene.[29] The fusion protein is produced by the diatom and becomes tightly associated with the newly formed silica frustules during silica biogenesis. The protein-containing biosilica is subsequently purified and the enzymes remain active and are considerably stabilized.[29,30] Fusion proteins comprising a target protein and the R5 sequence can also be obtained by recombinant expression in *E. coli*. However, silaffin tags produced in bacteria lack posttranslational modifications. Purified protein-silaffin chimeras can be used for *in vitro* silica precipitation resulting in auto-encapsulation of the protein during silica formation.[31-33] In another approach, synthetic silaffin R5 peptides are mixed with a solution of target enzyme without prior covalent linkage. During silaffin-mediated silica precipitation, the enzyme molecules become randomly co-entrapped in the newly formed silica material.[34,35]

Nevertheless, whereas the first method is not generally applicable, the latter methods lack control over silica morphology and properties as well as suffering from random and unspecific entrapment. Since R5 variants with different (posttranslational) modifications have been shown to trigger the formation of different silica materials (chapter 3), their application in protein immobilization would open the possibility to tailor silica properties to individual proteins. In addition, covalent linkage of the R5 peptide to the target protein should ensure an efficient and homogenous encapsulation of the protein in the silica material. However, access to such fusion proteins containing site-specifically modified R5 sequences is severely limited by means of classic biological methods such as recombinant expression in bacteria.

These limitations can be overcome by chemical synthesis of proteins. Solid phase peptide synthesis enables the facile incorporation of modified amino acids at defined positions in the peptide sequence.[36] Since routine and effective solid phase synthesis of peptides with more than 50 amino acids remains challenging, methods for the chemoselective ligation of protein

segments were developed.[37] The most common ligation method currently used is native chemical ligation (NCL).[38] This method relies on the reaction between the N-terminal cysteine of one peptide fragment with the C-terminal thioester of a second peptide. The intermediate thioester spontaneously and irreversibly rearranges via a S→N acyl transfer resulting in a stable amide linkage of the two peptide segments (Figure 5-1). The great advantages of NCL are that the reaction proceeds in aqueous solutions and results in a native peptide bond at the ligation site. Although iterative ligations using appropriately protected peptide fragments are possible,[39] the synthesis of large proteins is difficult because of variable ligation yield and complex purifications. However, the scope of NCL was widely expanded by introducing expressed protein ligation (EPL).[40]

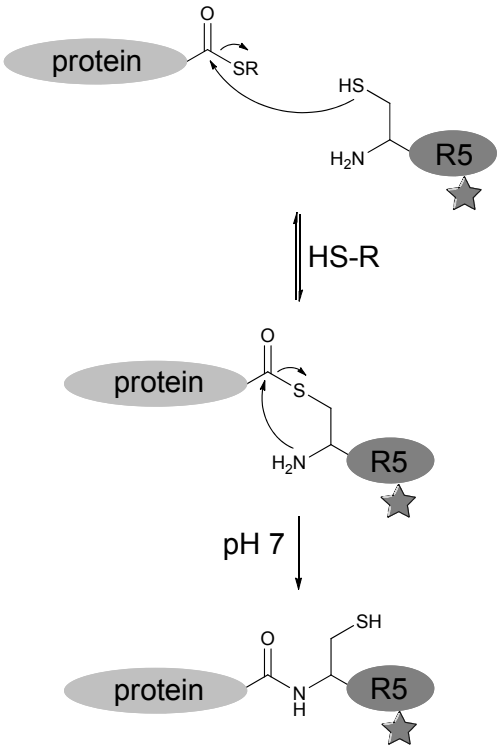

Figure 5-1 General scheme of expressed protein ligation to generate protein-silaffin R5 conjugates. The protein with a C-terminal thioester moiety selectively reacts with the N-terminal cysteine of the modified R5 peptide und forms a stable peptide bond.

EPL is based on the autocatalytic self-splicing activity of inteins. Inteins are internal protein segments that mediate a series of intramolecular rearrangements finally resulting in their own excision from a precursor protein with concomitant linkage of the flanking sequences via a

native peptide bond.[41] Fusion proteins with modified inteins that can only undergo cleavage reactions allow the generation of protein fragments with C-terminal thioester moiety or an N-terminal cysteine residue, suitable for NCL reactions. Thus, EPL elegantly combines molecular biology methods with chemical peptide synthesis and enables the site-specifically introduction of posttranslational modifications into large proteins and protein-peptide conjugates.

The aim of this work is to use EPL to generate stable conjugates between selected target proteins and modified R5 peptides. Such covalent protein-R5 conjugates should serve two purposes: The covalent attachment of the R5 peptide variants to the proteins ensures selective and efficient encapsulation of the protein in the silica matrix during silica formation. The difference to random entrapment in co-precipitation experiments is analyzed. In addition, the specific modifications of the R5 peptide will allow tailoring morphology and properties of the resulting silica material to requirements desired for specific proteins and/or applications.

The strategy of silica immobilization of proteins that are covalently conjugated to posttranslationally modified silaffin R5 peptides is exemplified with two model proteins, the enhanced green fluorescent protein (eGFP)[42] and thioredoxin (TRX).[43] The intrinsic fluorescent properties of the 28 kDa protein eGFP allow facile detection of protein localization by microscopy as well as fast assessment of proteins stability via its autofluorescence. eGFP immobilized in silica particles may be valuable for the development of stable, fluorescent (bio-) sensors.

Thioredoxins are 12 kDa proteins found in all kingdoms of life.[43] These enzymes reduce disulfide bonds in proteins by catalyzing a cysteine thiol-disulfide exchange reaction and are involved in redox-regulation and -signaling of many important biological processes.[44] Thioredoxins have proven potential in food biotechnology, e.g. since they are able to reduce disulfide bonds of allergens and thereby mitigate the allergenic response to wheat or increase the digestibility of milk.[45,46] In contrast to the cellular reducing agent glutathione, thioredoxins are also potent in reducing disulfide-containing venom neurotoxins thus rendering them inactive.[47] This suggests an application of thioredoxins as detoxifying agent or clinical antidote.

5.2 Materials and Methods

5.2.1 Materials

9-fluorenylmethoxycarbonyl (Fmoc)-protected amino acid derivatives, 2-(1*H*-benzotriazol-1-yl)-1,1,3,3-tetramethyluronium hexafluorophosphate (HBTU) and preloaded Fmoc-Leu-Wang resin were purchased from Novabiochem (Nottingham, UK). *N*,*N*-dimethylformamide (DMF), dichloromethane (DCM) and acetonitril (ACN) were obtained from Biosolve (Valkenswaard, The Netherlands). All other commonly used chemical reagents and solvents were purchased in the highest available quality from the following companies if not noted otherwise: Gerbu (Gaiberg, Germany), Invitrogen (Darmstadt, Germany), J.T. Baker (Griesheim, Germany), Merck (Darmstadt, Germany), NeoLab (Heidelberg, Germany), Omnilab (Bremen, Germany), Roth (Karlsruhe, Germany), Sigma-Aldrich (Taufkirchen, Germany) or VWR (Darmstadt, Germany).

The Wizard® Plus SV Minipreps DNA Purification System for isolation of plasmids from *E. coli* cells, DNA polymerases (*Pfu* and *Taq*), restriction enzymes (*Nco*I and *Spe*I) and the dNTP mix were purchased from Promega (Mannheim, Germany). PCR fragments were purified with QIAquick PCR Purification Kit from Quiagen (Hilden, Germany). T4 DNA ligase was obtained from Thermo Fisher Scientific (Schwerte, Germany). Alkaline phosphatase (from bovine intestinal mucosa) was from Sigma, 100 bp and 1kb DNA ladders from Invitrogen.

Chemical competent *E. coli* strains XL1-Blue, BL21(DE3) and Rosetta 2(DE3) were from Strategene and Invitrogen, respectively. Oligonucleotide synthesis and gene sequencing were performed by VBC Biotech (Vienna, Austria).

SDS-PAGE analysis was accomplished with 15 % SDS gels according to Laemmli[48] or with precast gradient gels (8-16 % polyacrylamide) from Peqlab (Erlangen, Germany). The LMW-SDS marker kit was from GE Healthcare (Freiburg, Germany). Gels were stained with Coomassie Brilliant Blue R-250.

Centrifugal filtrations units were from Millipore (Amicon Ultra-15) or from Sartorius (Vivaspin 500), Zeba™ Spin Desalting Columns were from Thermo Fisher Scientific.

Recombinant DNaseI was purchased from Roche (Mannheim, Germany).

5.2.2 Instrumentation

The MJ Mini Thermal Cycler for PCR, the chamber for horizontal DNA electrophoresis and the Mini-Protean II system for SDS-PAGE were from Biorad (München, Germany).
UV-Vis absorption measurements were carried out using an Amersham Biosciences Ultrospec 2100 pro (Freiburg, Germany) system or a NanoDrop 2000c from Peqlab.
E. coli cells were lysed using a microfluidizer manufactured by Constant Systems (Warwick, England).
Sedimentations were accomplished in Avanti J25 and J26XP centrifuges and rotors (JA-10, JA-8.1000 and JA-25.50) from Beckman Coulter, (Krefeld, Germany).
Purifications of proteins were done using Äkta Prime FPLC systems and HisTrap™ HP columns from GE Healthcare.
Analytical reversed phase HPLC was performed on a Dionex Ultimate 3000 instrument using C4 columns (Kromasil 300-5-C4, 150×4.6 mm, 5 µm particle size and BioBasic-4, 150×4.6 mm, 5 µm particle size, Thermo Fisher).
ESI-MS analysis was conducted with a LCQ-fleet (Thermo Fisher Scientific) and with a Waters AutoPurification HPLC/MS system (3100 Mass Detector, 2545 Binary Gradient Module, 2767 Sample Manager and 2489 UV/Visible Detector), respectively. For LC-MS separation was achieved using C4 columns (Kromasil 300-5-C4, 50×4.6 mm, 5 µm particle size and BioBasic-4 150 x 2.1 mm, 5 µm particle size, Thermo Fisher).
Electron micrographs were recorded with the scanning electron microscopes Zeiss Supra 55 VP operating at 5 kV and JEOL JSM 5900 LV operating at 20 kV, respectively. Samples were sputter coated in high vacuum with gold in a Bal-Tec SCD 005 system or with gold/palladium using a Leica SCD050 sputter coater.
Fluorescence micrographs were obtained using a Zeiss Axiovert 200 microscope.
A Genios plate reader from Tecan (Männedorf, Switzerland) equipped with filters (excitation 485 nm; emission 535 nm) was used for measurements of eGFP fluorescence. Absorbance measurements in multiwell format were carried out with a Synergy Mx plate reader from Biotek (Bad Friedrichshall, Germany).

5.2.3 Peptide synthesis

Peptides **A-D** were synthesized on solid phase using 9-fluorenylmethoxycarbonyl (Fmoc)-chemistry[49] and purified as described in chapter 3.

5.2.4 HPLC and mass spectrometry

Analytical RP-HPLC analyses were carried at a flow rate of 1 mL/min with buffer A (0.1% (v/v) TFA in ddH_2O) and buffer B (0.08% (v/v) TFA in ACN) as mobile phase. Separation was achieved running linear gradients from 5 % to 65 % buffer B in buffer A over 30 min.
When LC-MS was performed with the LCQ-fleet connected to an UltiMate3000 Dionex HPLC, a flow rate of 0.35 mL/min was applied and the TFA in buffer A and buffer B was replaced with 0.1 % (v/v) formic acid. For analytical LC-MS analyses with the Waters AutoPurification HPLC/MS system, the flow rate was 1 mL/min, linear gradients were 5-65% buffer B in 10 min and the buffers contained 0.05 % (v/v) TFA. Mass spectra were acquired using electrospray ionization in the positive mode.

5.2.5 Cloning of Thioredoxin (TRX)-GyrA-H6-CBD fusion protein

The plasmid pBad202 coding for a hispatch-thioredoxin gene was a kind gift from Henning Mootz (University of Münster, Germany). Using pBad202 as template, the thioredoxin gene was amplified via PCR using the following primers (recognition sequences for restriction enyzmes are shown in italic):

forward primer 5’ - CACCAT*CCATGG*GATCTGATAAAATTATTCATCTG - 3’

reverse primer 5’ - TACCAC*ACTAGT*GCATCTCCCGTGATGCAATATTCCGC AAATTTTCCAGAGCCGGCCAGGTTAGCG- 3’

For cloning of the thioredoxin sequence (TRX) in frame with the GyrA intein in a pTXB3 plasmid, the forward primer contains an *Nco*I recognition sequence and a *Spe*I restriction site was introduced in the reverse primer. With the reverse primer the additional amino acid sequence KFAEY (underlined) was introduced to the C-terminus of the thioredoxin.

Purified PCR product and the pTXB3 vector were both digested with *Nco*I and *Spe*I. Linearized pTXB3 was treated with alkaline phosphatase for 1 h at 37 °C to remove phosphate groups from the 5' end and subsequently purified. Finally, the PCR insert and the vector were incubated with T4 DNA ligase overnight at 22 °C. The ligation mixture was transformed into *E. coli* XL1-Blue using the heat shock method and bacteria were grown on selective medium. From positive clones, the plasmids were isolated and the correct sequence of the resulting TRX-GyrA-His_6-CBD fusion construct in pTXB3 was confirmed by gene sequencing.

5.2.6 Protein expression and purification

A pTXB3 expression plasmid coding for the eGFP-GyrA-His_6-CBD fusion protein was already available (pTXB3-eGFP-GyrA-His_6-CBD).[50] The eGFP-GyrA-His_6-CBD fusion protein was expressed with *E. coli* BL21 (DE3) cells. 4 L dYT medium containing ampicillin (100 µg/mL) as selection marker were inoculated from an overnight pre-culture to an OD_{600} of 0.1 and shaken at 37 °C. Protein expression was induced with 1 mM IPTG during log-phase (OD_{600} = 0.6-0.8) and cell cultures were incubated at 25 °C for 20 h at 150 rpm. Subsequently, cells were harvested by centrifugation (6000 rpm at 4 °C, 15 min). The cell pellet was resuspended in lysis buffer (PBS, 1 mM EDTA, pH 7.4) followed by cell lysis with a microfluidizer. The lysat was incubated with DNAse I and 10 mM $MgCl_2$ at 4 °C for 1 h and afterwards centrifuged at 18000 rpm for 1 h at 4 °C. The supernatant was immediately loaded on a 5 mL HisTrap™ HP column (GE Healthcare), previously equilibrated with PBS buffer, and washed with washing buffer (50 mM Na phosphate, 250 mM NaCl, 20 mM imidazole, pH 8). The protein was finally eluted with elution buffer (10 mM Na phosphate, 100 mM NaCl, 250 mM imidazole, pH 8). Using centrifugal filter units (Amicon Ultra-15, MWCO 10K), the protein solution was concentrated and the buffer was exchanged to PBS, pH 7.4. Cleavage of the GyrA-intein was initiated by addition of 250 mM MESNa and the protein solution was incubated overnight at 4 °C. The intein thiolysis reaction was followed by SDS-PAGE. Subsequently, excess thiol was removed with centrifugal filter units (Amicon Ultra-15, MWCO 10K) and the protein solution was applied to a second 5 mL HisTrap™ HP column, equilibrated in PBS, to remove the cleaved GyrA-

His_6-CBD protein and uncleaved fusion protein. The flow-through of the column was collected and concentrated with an Amicon Ultra-15 spin column (MWCO 10K). Protein concentration was determined by the method of Bradford[51] and calculated on the basis of a calibration line obtained with BSA. The purified eGFP-MESNa thioester protein was flash frozen in small aliquots and stored at -80 °C.

An eGFP variant with free carboxyl function at the C-terminus was kindly provided by Dr. Martin Haslbeck (TU München).

For expression of the TRX-GyrA-His_6-CBD fusion protein, the cloned plasmid described above was transformed into *E. coli* Rosetta 2 cells. An overnight culture was used to inoculate 4 L dYT medium supplemented with ampicillin (100 µg/mL) and chloramphenicol (30 µg/mL). Expression and purification of the protein followed the same protocol as described for the eGFP-GyrA-His_6-CBD construct. After cleavage of the GyrA-intein with 250 mM MESNa (20 h, 4 °C), the buffer was exchanged to PBS, pH 7.4 using centrifugal filter units (Amicon Ultra-15, MWCO 3K). The TRX-thioester protein was purified with a 5 mL HisTrap™ HP column running a linear gradient from 0-50 % elution buffer (10 mM Na-phosphate, 100 mM NaCl, 250 mM imidazole, pH 8) in PBS buffer in 90 min. Protein-containing fractions were analyzed by SDS-PAGE. Pure fractions were combined and transferred into PBS buffer using centrifugal filter concentrators (Amicon Ultra-15, MWCO 3K). Concentration of the protein solution was determined by UV-absorbance at 280 nm and calculated using the molar extinction coefficient for reduced thioredoxin. Thioredoxin-MESNa thioester was shock frozen and stored at -80 °C.

5.2.7 DTT-mediated hydrolysis of TRX-MESNa thioester

To prepare thioredoxin protein with free carboxyl function at the C-terminus, the recombinant TRX-Mesna α-thioester was hydrolyzed. 1 mM TRX-SR in 100 mM Tris/HCl, 5 mM TCEP, pH 8 was incubated with 200 mM DL-1,4-Dithiothreitol (DTT) under shaking (400 rpm) for 24 h at 37 °C. Completion of hydrolysis of the C-terminal thioester was confirmed with LC-MS. After desalting and buffer exchange to 50 mM potassium phosphate with Zeba Spin Desalting Columns (MWCO 7K) protein solutions were concentrated with

Vivaspin ultrafiltration spin columns (MWCO 3K) and protein concentrations were measured via UV-absorbance at 280 nm.

5.2.8 Expressed protein ligation

The recombinant eGFP-Mesna α-thioester and peptides **A-D** were ligated to obtain four variants of semisynthetic eGFP-R5 conjugates. 250 µM eGFP-Mesna thioester and 1.25 mM peptides **A-D** were dissolved in 100 mM Tris buffer at pH 8. Ethanethiol (2 % v/v) was added and the reaction was incubated under shaking (350 rpm) for 20 h at RT. The reactions were monitored by SDS-PAGE (15 % Laemmli) and LC-MS analysis. Removal of excess peptide and exchange of buffer to 50 mM postassium phosphate pH 7 was achieved with ultrafiltration spin columns (MWCO 10K).

Ligation of recombinant TRX-Mesna thioester (250 µM) with peptides **A-D** (1.25 mM) was carried out in 100 mM Tris buffer pH 8 containing 5 mM TCEP and 1 % (v/v) thiophenol. The reaction was shaken at 700 rpm and 30 °C for 24 h. Occurring precipitates were pelleted by centrifugation for 5 min at 14000 rpm. The supernatant was collected and buffer exchange and removal of excess peptide was achieved with Zeba Spin Desalting Columns (MWCO 7K). Ligation reactions were analyzed by SDS-PAGE (8-16 % polyacrylamide gradient gel), LC-MS and HPLC. After concentration of protein solutions with ultrafiltration spin columns (MWCO 3K), protein concentrations were measured via UV-absorbance at 280 nm.

5.2.9 Silica precipitation assays

All silica precipitation assays were carried out in 50 mM potassium phosphate buffer at pH 7. Stock solutions of peptides **A-D**, proteins and protein-conjugates were prepared in 50 mM potassium phosphate buffer, pH 7. A solution of silicic acid was freshly generated from 250 mM TMOS in 1 mM HCl for exactly 4 min before each assay.

Precipitation of silica from solutions of silicic acid with peptides **A-D** was carried out as described in chapter 3. Briefly, peptides were diluted in phosphate buffer to a final concentration of 470 µM. With addition of 25 mM silicic acid (final concentration), the silica precipitation reaction was initiated. After 30 min incubation at RT, silica precipitates were

collected by centrifugation (5 min, 14000 rpm). The silica precipitates were washed twice with ddH_2O. Silica precipitation assays using eGFP- and TRX-R5 conjugates, eGFP-OH and TRX-OH were carried out in exact the same manner using 470 µM of each protein. In Co-precipitation experiments, 470 µM eGFP-OH or TRX-OH were mixed with equimolar amounts of peptides **A-D** prior to initiation of silica precipitation by addition of silicic acid. Control experiments that were conducted without silicic acid or a R5 peptide variant in the reaction solution did not lead to formation of any precipitate. All assays were carried out at least in triplicate.

5.2.10 Scanning electron microscopy and fluorescence microscopy

For scanning electron microscopic analysis the silica precipitates were resuspended in water, transfered to a Thermanox™ coverslip and air dried. These coverslips were placed onto appropriate sample holders of the respective scanning electron microscope. The samples derived from silica precipitation with eGFP-peptide conjugates or co-precipitation experiments with eGFP and R5 peptides were sputter coated with gold in high vacuum (Bal-Tec SCD 005). Subsequently, the electron micrographs were recorded with the JEOL JSM 5900 LV scanning electron micrograph operating at 20 kV. Silica precipitates from experiments with TRX were sputter coated with gold/palladium in high vacuum (Leica SCD050) and analyzed at 5 kV with the Zeiss Supra 55VP scanning electron microscope.
Fluorescence micrographs of eGFP containing samples were recorded with a Zeiss Axiovert 200 microscope using the oil immersion objective.

5.2.11 Quantification of precipitated silica

The amount of precipitated silica was quantified by a modified β-silicomolybdate assay.[52,53] The silica precipitates were washed twice with water and subsequently incubated for 1 h at RT in 2 M NaOH to dissolve the silica. To 40 µl of this solution with dissolved silica, 160 µl of ultrapure water and 800 µl of a molybdate solution (1.35 ml 37% HCl, in 40.3 ml ddH_2O mixed with a solution of 774.2 mg $(NH_4)_6Mo_7O_{24} \times 4\ H_2O$ in 9.7 ml ddH_2O, pH adjusted to 1.12 with 2 M NaOH) were added. The absorbance of this solution was measured at 370 nm

against a blank of 40 µl NaOH, 160 µl ddH_2O and 800 µl molybdate solution. The amount of silicon was calculated based on a calibration curve obtained with a silicon atomic absorption standard solution. Control experiments showed no interference of R5 peptides in these quantification assays. However, since the TRX protein showed interaction with the molybdate, the absorption of different dilutions of TRX mixed with molybdate solution was measured and used for normalization. All assays for quantification were carried out at least in triplicate.

5.2.12 Stability of silica immobilized eGFP against denaturation with SDS

Silica precipitations with eGFP-peptide conjugates and co-precipitations with eGFP and the different peptides **A-D** were carried out as described above. The obtained silica material was carefully washed with water to remove unspecifically bound and precipitated eGFP. Subsequently, the silica was resuspended in buffer (50 mM Tris/HCl, pH 6.5). Measurement of eGFP fluorescence was carried out on a Genios plate reader device equipped with an excitation filter for 485 nm and an emission filter for 535 nm. After measuring the initial fluorescence of the individual samples, a SDS solution (5% SDS in 50 mM Tris/HCl, pH 6.5) was added to a final concentration of 0.5% SDS to initiate protein denaturation. The decrease in fluorescence of eGFP was monitored over time for 5 min. Control and reference experiments were carried out using non-silica immobilized eGFP. Both, the stability of eGFP in 50 mM Tris/HCl buffer, pH 6.5 over measurement time was confirmed and the denaturation of free eGFP in buffer solution upon addition of 0.5% SDS was followed. All experiments and measurements were carried out in triplicate. The relative fluorescence retained after 5 min treatment with 0.5% SDS for each sample was calculated based on the fluorescence of the initial measurements.

5.2.13 Quantification of loading of silica with TRX and release of TRX from silica

To quantify the amount of TRX-protein and -conjugates that were entrapped in the silica material, the silica precipitation experiments were carried out as described above.

Subsequently, the silica materials were dissolved in 2 M NaOH for 1 h. The protein content in this solution was analyzed by HPLC. The peak areas of the resulting HPLC traces were integrated and the amount of protein was calculated based on references with known protein concentration.

To analyze the release of proteins from the silica material, the silica material collected after precipitation was resuspended in PBS buffer pH 7.4. This silica suspension was shaken at 37 °C over a period of 3 days in 24 h cycles. After each 24 h cycle, silica suspensions were centrifuged for 5 min to precipitate the silica. The supernatant buffer was analyzed for protein content by HPLC. For the next 24 h cycle, fresh PBS buffer was added.

The amounts of released proteins were calculated from integrated areas of HPLC traces and referred to standards. All assays and HPLC analyses were performed in triplicate

5.2.14 Determination of enzyme activity of TRX and silica immobilized TRX

Enzymatic activity of thioredoxin was determined based on the method introduced by A. Holmgren.[54] In the presence of DTT, thioredoxin catalyzes the reduction of disulfide bonds of insulin resulting in precipitation of the insulin B chain. The time course of insulin reduction was monitored by absorption at 650 nm.

A stock solution of insulin (1 mM) was prepared in TRX-assay buffer (PBS, 2 mM EDTA, pH 7.4). Insulin could be completely dissolved by adjusting the pH to 2-3 with 1 mM HCl and remained soluble after fast dilution into TRX-assay buffer at pH 7.4. Activity assays were performed with 10 µM TRX and 100 µM insulin in TRX-assay buffer at RT. Reactions were initiated by addition of 2 mM DTT and absorption at 650 nm was monitored for 20 min. For determination of activity of silica immobilized TRX, the amount of silica material was resuspended in TRX-assay buffer that corresponds to 10 µM silica immobilized protein in the final assay volume. All assays as well as control experiments without DTT or TRX in the reaction mixture were carried out in triplicate.

Thioredoxin activity can be quantified by comparing the rate of increase of absorption at 650 nm within the linear range ($\Delta A_{650} \times min^{-1}$).

5.3 Results and discussion

Expressed protein ligation[40] offers the possibility to generate conjugates comprising almost any target protein and R5 peptides with defined modifications. The resulting protein-peptide conjugates are supposed to initiate the formation of silica resulting in concomitant encapsulation of the protein in the silica material. In addition, the different R5 peptide variants in these conjugates should enable control over silica morphologies and properties.

For initial experiments and proof of concept, eGFP was chosen because of its fluorescent properties, which allow direct detection of silica immobilization. Next, the strategy was expanded to an active enzyme in order to test for preservation of activity after silica immobilization. Thioredoxin was chosen because this enzyme can be readily obtained by recombinant expression in *E. coli*[55,56] and has numerous possible applications in biotechnology and medicine.[45-47]

eGFP and TRX were generated with a C-terminal thioester moiety to enable ligation with synthetic silaffin peptides **A-D** via a native peptide bond. The obtained eGFP- and TRX-silaffin conjugates were used for *in vitro* silica precipitation. Subsequently, the obtained protein-silica composites were analyzed towards silica morphology as well as stability and activity of the encapsulated proteins.

5.3.1 Generation of eGFP and TRX with a C-terminal MESNa thioester moiety

To generate a variant of eGFP with a C-terminal thioester moiety, the protein was expressed in fusion with the GyrA intein encoded by a pTXB3 vector.[57,58] The pTXB3 plasmid was modified to contain an additional hexahistidine tag between the GyrA intein and chitin-binding domain (CBD), which allows affinity purification on Ni-NTA resin.[50]

In the pTXB3 vector, the asparagine at the C-terminus of the *Mxe* GyrA intein is mutated to alanine to prevent cleavage at this splice junction.[58] The initial N-S acyl shift at the N-terminal cleavage site can still occur and the intermediate thioester can be trapped by

exogenous thiols resulting in cleavage of the intein and release of the N-terminal target protein with C-terminal thioester moiety. However, the efficiency of this cleavage reaction is affected by the protein context of the cleavage site, especially by the amino acid directly preceding the intein.[59,60] In order to achieve high efficiency of thiol-mediated cleavage of the *Mxe* GyrA intein, additional amino acids including the tyrosine preceding the *Mxe* GyrA intein in its native protein context (KFAEY) were introduced to the C-terminus of eGFP as well as TRX during cloning of the GyrA-His_6-CBD fusion constructs.

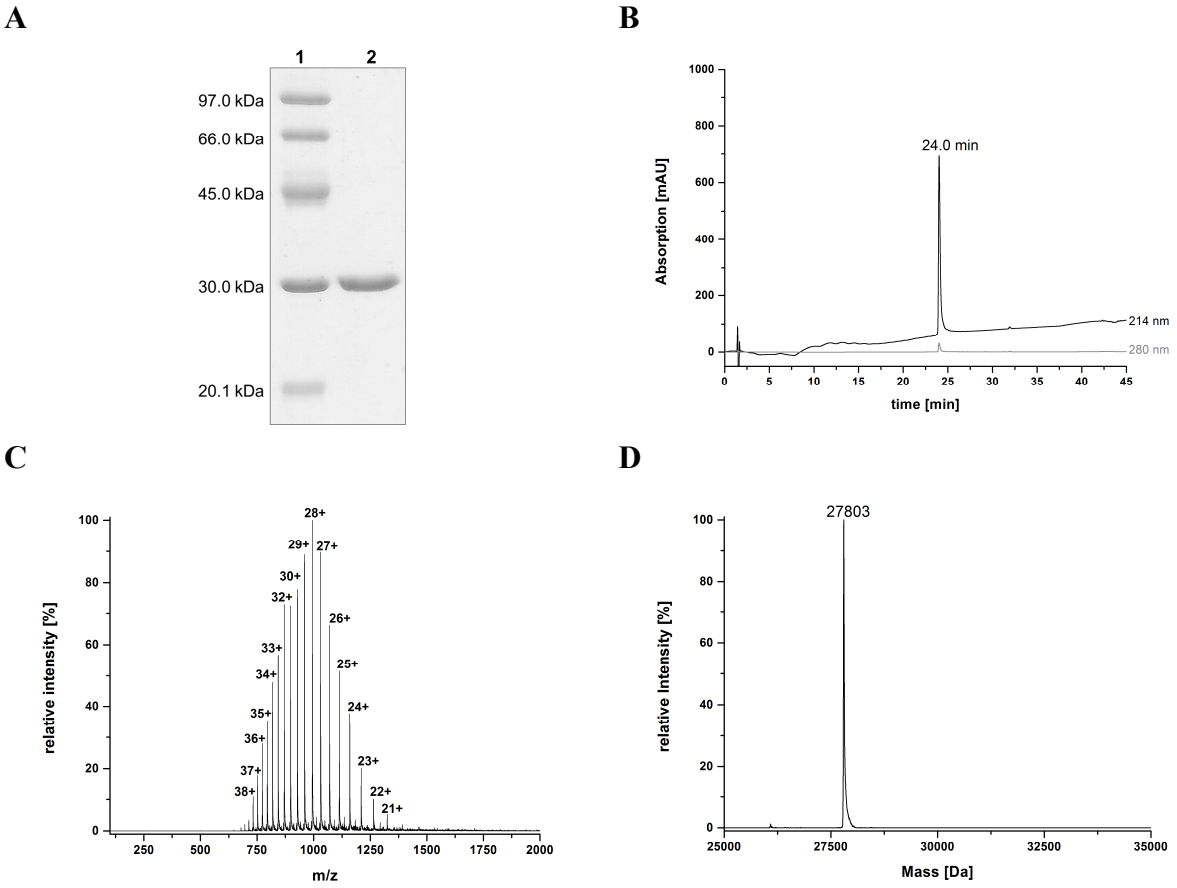

Figure 5-2 Purification of eGFP with a C-terminal MESNa thioester moiety.
A) Coomassie-stained SDS-PAGE gel (15%) of purified eGFP-MESNa thioester. Lane 1: LMW marker; Lane 2: purified eGFP-MESNa thioester.
B) HPLC chromatogram of analytical LC-MS analysis of purified eGFP-MESNa thioester.
C) Mass spectrum of the peak at 24.0 min from analytical LC-MS analysis of purified eGFP-MESNa thioester.
D) Deconvoluted mass spectrum. Calculated mass: 27797 Da; observed mass: 27803 Da.

After expression and purification of the eGFP-GyrA-His_6-CBD fusion protein, cleavage of the intein was induced by addition of MESNa resulting in the production of eGFP with a C-terminal thioester. The eGFP-MESNa thioester protein was separated from GyrA-His_6-CBD and uncleaved fusion protein with a second Ni-NTA affinity column. Typically, 3.3 mg of eGFP-MESNa thioester were obtained from 1 liter of *E. coli* culture. Analysis of the eGFP-thioester protein with SDS-PAGE (Figure 5-2, A) and analytical LC-MS (Figure 5-2) proved the high purity of the protein. The observed mass resulting from LC-MS analysis (27803 Da) fits the calculated mass of eGFP with a C-terminal MESNa thioester (27797 Da) and revealed that no hydrolysis of the thioester occurred during purification.

In contrast to the eGFP-GyrA-His_6-CBD fusion protein, expression of the TRX-GyrA-His_6-CBD construct did not succeed using *E. coli* BL21(DE3) (data not shown). Although the *trx* gene, which was amplified from the pBAD202 plasmid, originates from *E. coli*,[56] it contains some codons (GGA, CCC) that are infrequently used and can cause translational problems in *E. coli*.[61] Therefore, the expression strain was changed to *E. coli* Rosetta 2(DE3). The Rosetta strains are relatives of BL21 expression strains, but they supply tRNAs for several rare codons to enhance expression. Using *E. coli* Rosetta 2(DE3), the TRX-GyrA-His_6-CBD fusion protein was successfully expressed. In addition, lowering the incubation temperature during protein expression from 37°C to 25°C increased the amount of soluble protein and reduced the deposition in inclusion bodies.

The thioredoxin used in this study is a variant of the wildtype *E.coli* thioredoxin in which several amino acids are mutated to histidines. As a result of the thioredoxin fold, these histidines form a patch on the surface with the capacity to bind to nickel ions immobilized on a NTA resin.[56] Therefore, the TRX-MESNa thioester was eluted from the second Ni-NTA affinity column following the cleavage of the TRX-GyrA-His_6-CBD fusion protein with a gradient of increasing imidazole. Nevertheless, SDS-PAGE analysis of purified TRX-MESNa thioester (12.7 kDa) showed minor impurities at higher molecular weights (Figure 5-3, A). The observed bands in the range of 25-30 kDa could originate from GyrA-His_6-CBD protein (29.1 kDa) which could not be efficiently separated from the TRX-thioester protein. Alternatively, the TRX-MESNa protein might form disulfide-linked homodimers as observed previously,[62,63] that are not readily reduced with the β-mercaptoethanol present in the sample

preparation buffer for SDS-PAGE. From 1 liter *E. coli* culture, on average 12 mg TRX-MESNa thioester protein were obtained.

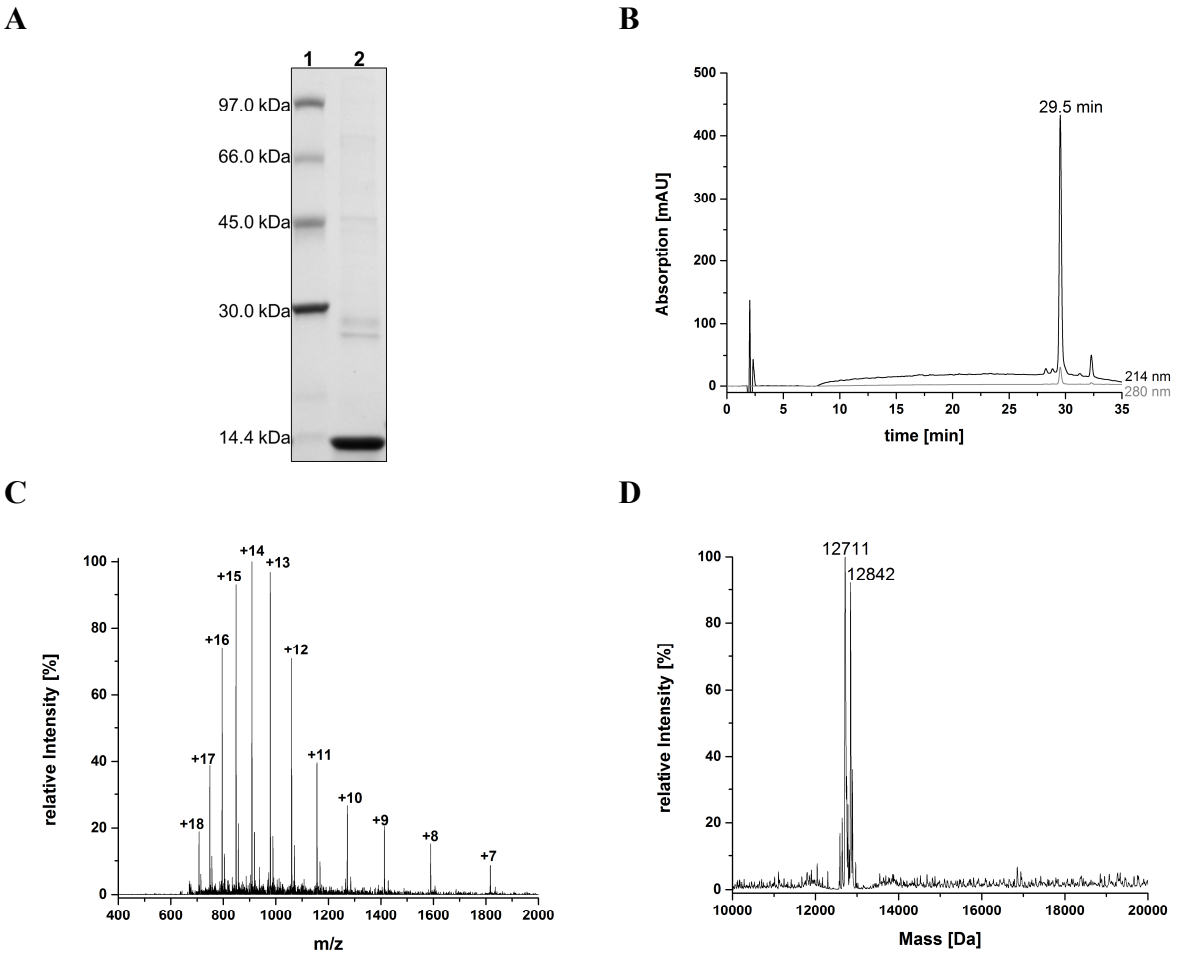

Figure 5-3 Purification of TRX with a C-terminal MESNa thioester moiety.
A) Coomassie-stained SDS-PAGE gel (8-16%) of purified TRX-MESNa thioester. Lane 1: LMW marker; Lane 2: purified TRX-MESNa thioester.
B) Analytical HPLC chromatogram of purified TRX-MESNa thioester.
C) Mass spectrum of purified TRX-MESNa thioester.
D) Deconvoluted mass spectrum. Calculated mass for reduced TRX-MESNa thioester: 12712 Da; observed masses: 12711 Da; 12842 Da.

SDS-PAGE and HPLC analysis (Figure 5-3, A and B) show adequate purity. Before HPLC- and MS-analysis, protein samples were reduced for 5 min with TCEP to avoid mixtures of oxidized and reduced protein species. In the mass spectrum corresponding to the main peak from the HPLC chromatogram (29.5 min) a major species with a mass of 12711 Da is

observed which fits to the calculated mass of 12712 Da of the reduced TRX-MESNa thioester protein (Figure 5-3, C and D). The mass spectrum revealed a second protein species with a molecular weight of 12842 Da, which corresponds most likely to a thioredoxin-MESNa variant with an N-terminal methionine residue resulting from incomplete removal of methionine from the recombinant protein by endogenous *E. coli* methionine aminopeptidase.[64] Since this TRX-variant with an N-terminal methionine residues will not interfere with TRX function in following experiments, the TRX-MESNa thioester protein was not further purified.

5.3.2 Expressed protein ligation of eGFP and TRX proteins with peptides A to D

The silaffin variants **A** to **D** were synthesized using Fmoc-SPPS and purified as described in chapter 3 (Table 5-1). Each peptide variant was provided with a cysteine residue at the N-terminus. Peptide **A** is the unmodified silaffin R5 sequence, peptide **B** contains a trimethylated lysine residue at position 13 (Table 5-1). In peptide **C**, the polyamine spermidine was attached to two lysine side chains (Table 5-1) and peptide **D** carries a single phosphoserine residue at position 15 in the peptide sequence (Table 5-1). The cysteinyl peptides **A-D** can undergo a native chemical ligation with the eGFP- and TRX-MESNa thioester proteins resulting in stable protein-peptide conjugates.

Table 5-1 Synthetic silaffin R5 peptides used in expressed protein ligation reactions

	Sequence	modifications
A	CSSKKSGSYSGSKGSKRRIL	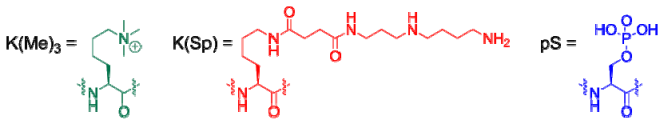
B	CSSKKSGSYSGSK(Me)$_3$GSKRRIL	
C	CSSK(Sp)KSGSYSGSKGSK(Sp)RRIL	
D	CSSKKSGSYSGSKGpSKRRIL	

The eGFP protein with C-terminal MESNa thioester was ligated to peptide variants **A** to **D** using ethanethiol as additive to promote thioester exchange and ligation reactions. Different thiol additives (thiophenol, ethanethiol, MESNa) for *in situ* transthioesterification were

analyzed regarding their effect on catalyzing the ligation reaction. Thiophenol and ethanethiol showed similar high efficiency (data not shown) and ethanethiol was chosen since ligation mixtures with thiophenol showed tendency for precipitation due to formation of a symmetrical disulfide derivative of thiophenol. The ligation mixtures containing ethanethiol were incubated at room temperature for 20 h and subsequently analyzed with SDS-PAGE and LC-MS. The gel shows that eGFP-peptide conjugate bands are distinctly shifted to higher molecular weights compared to the eGFP-MESNa thioester protein indicating successful ligation (Figure 5-4). The ligation of eGFP with peptides **A** to **D** was further confirmed by LC-MS analysis (Figure 5-19 to 5-22). The observed masses for the eGFP-peptide conjugates are in good agreement with the calculated masses (Table 5-2). The minor peaks in the HPLC chromatograms at higher retention times could be assigned to hydrolyzed eGFP thioester protein (Figure 5-19 to 5-22). The ligation reactions gave satisfactory yields between 66-80% as calculated from integrated peak areas of HPLC traces.

Table 5-2 eGFP-peptide conjugates

protein	+	peptide	→	conjugate	$MW_{calc.}$	$MW_{obs.}$	ligation yield
eGFP-MESNa		**A**		eGFP-**A**	29772 Da	29776 Da	80%
		B		eGFP-**B**	29815 Da	29818 Da	66%
		C		eGFP-**C**	30227 Da	30230 Da	68%
		D		eGFP-**D**	29852 Da	29856 Da	69%

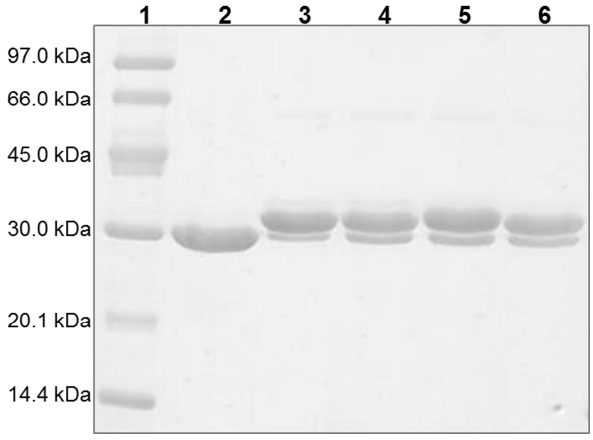

Figure 5-4 Coomassie-stained SDS-PAGE gel (15%) of EPL reaction between eGFP-MESNa thioester and peptides **A** to **D**.
Lane 1: LMW marker; Lane 2: purified eGFP-MESNa thioester; Lane 3: eGFP-**A**; Lane 4: eGFP-**D**; Lane 5: eGFP-**C**; Lane 6: eGFP-**B**.

Accordingly, the purified TRX-MESNa thioester was used in expressed protein ligation reactions with peptides **A** to **D** (Table 5-1) to yield the corresponding TRX-peptide conjugates (Table 5-3). These reactions were performed at 30 °C with thiophenol as ligation mediator. Thiophenol was chosen here as ligation mediator because higher yields of ligation product were obtained in comparison to usage of ethanethiol as ligation additive (data not shown). 5 mM TCEP were added to the reaction solution to keep the protein sulfhydryl groups permanently reduced. SDS-PAGE analysis of the EPL reactions after 24 h reveals the appearance of new bands at higher molecular weights compared to the TRX-thioester protein that correspond to the ligation products (Figure 5-5). All reactions proceeded very efficiently and yielded 91-98% of ligation products (Table 5-3).

Table 5-3 TRX-peptide conjugates

protein	+	peptide	→	conjugate	$MW_{calc.}$	$MW_{obs.}$	ligation yield
TRX-MESNa		**A**		TRX-**A**	14688 Da	14684 Da	98%
		B		TRX-**B**	14731 Da	14724 Da	91%
		C		TRX-**C**	15143 Da	15139 Da	91%
		D		TRX-**D**	14768 Da	14763 Da	95%

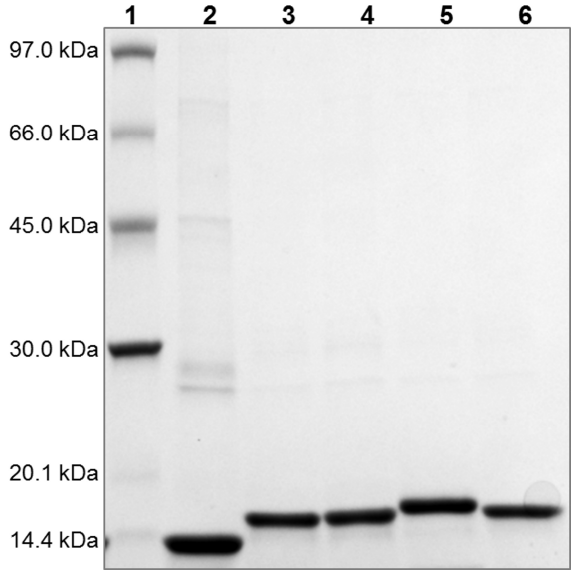

Figure 5-5 Coomassie-stained SDS-PAGE gel (8-16%) of EPL reaction between TRX-MESNa thioester and peptides **A** to **D**.
Lane 1: LMW marker; Lane 2: purified TRX-MESNa thioester; Lane 3: TRX-**A**; Lane 4: TRX-**B**; Lane 5: TRX-**C**; Lane 6: TRX-**D**.

Excess of peptides and ligation additives were removed from crude ligation mixtures prior to HPLC and LC-MS analysis. The HPLC chromatograms of the ligation reactions each showed only one major peak (Figure 5-23 to 5-26). Mass spectrometric analysis gave evidence that the ligation reactions resulted in the corresponding TRX-peptide conjugates. The observed mass for the reduced TRX-**A** conjugate (14684 Da) is in good agreement with the calculated mass of 14688 Da (Figure 5-23). This holds also true for the conjugates that were obtained by ligation of TRX with modified peptide variants **B**, **C** and **D** (Table 5-3 and Figure 5-24 to 5-26). However, deconvolution of the acquired mass spectra revealed the occurrence of traces of hydrolyzed TRX-thioester protein with the calculated mass of 12589 Da in each sample (Figure 5-23 to 5-26) although not visible on SDS-PAGE (Figure 5-5). In addition to the major peaks corresponding to the TRX-peptide conjugates, each spectrum shows another protein species with a mass difference of +131 Da related to the respective TRX-peptide conjugates. This mass difference was already observed in the TRX-MESNa thioester preparation (Figure 5-3) and derives from an additional N-terminal methionine. Since the TRX-peptide conjugates were obtained in excellent yields (> 90%) with only minor byproducts, they were used without purification for further experiments. Only excess peptide **A** to **D** used in the ligation reaction was removed to avoid their influence on silica precipitation.

5.3.3 Silica precipitation with eGFP-peptide conjugates

The synthetic silaffin R5 peptide variants **A** to **D** have been shown to be able to initiate the precipitation of silica from a solution of silicic acid (see chapter 3). Moreover, the particular amino acid side chain modifications turned out to have direct influence on the morphology of the resulting silica precipitates. Whereas the unmodified R5 peptide **A** and the variant with the trimethylated lysine (peptide **B**) induce formation of spherical silica particles with homogenous size distribution, peptide **C** carrying the polyamine modification leads to silica particles with a variable size distribution. Completely altered silica morphology, comprising clusters of nano-sized silica spheres, was observed with peptide **D** (Figure 3-1).

Stable conjugates between target proteins (eGFP and TRX) and silaffin R5 variants carrying the defined (posttranslational) modifications were generated using EPL (chapter 5.3.2). In this way, the specific characteristics in silica precipitation of the peptide variants should be transferred to the protein-peptide conjugate and enable formation of silica precipitates with distinct properties.

Prior to silica precipitation experiments with the eGFP-peptide conjugates (Table 5-2), excess peptide used in the ligation reaction was removed to ensure the observed results originate exclusively from the covalently bound peptides. The silica precipitation experiments were carried out using exactly the same procedure applied for R5 peptides **A** to **D**. All eGFP-peptide conjugates showed silica precipitating activity. The resulting silica precipitates that already exhibited an intense green color were analyzed by scanning electron and fluorescence microscopy. The scanning electron micrographs are depicted in Figure 5-6. Depending on which eGFP-peptide conjugate was used, distinct morphologies of the silica precipitates were observed. eGFP-**A,** comprising the eGFP sequence and the unmodified R5-sequence, induces formation of homogenous spherical silica particles with diameters of approximately 1 µm (Figure 5-6, A). Such spherical silica particles of homogenous size distribution were also observed with the unmodified peptide **A** alone, but in that case the average diameter was only 750 nm (Figure 3-1).

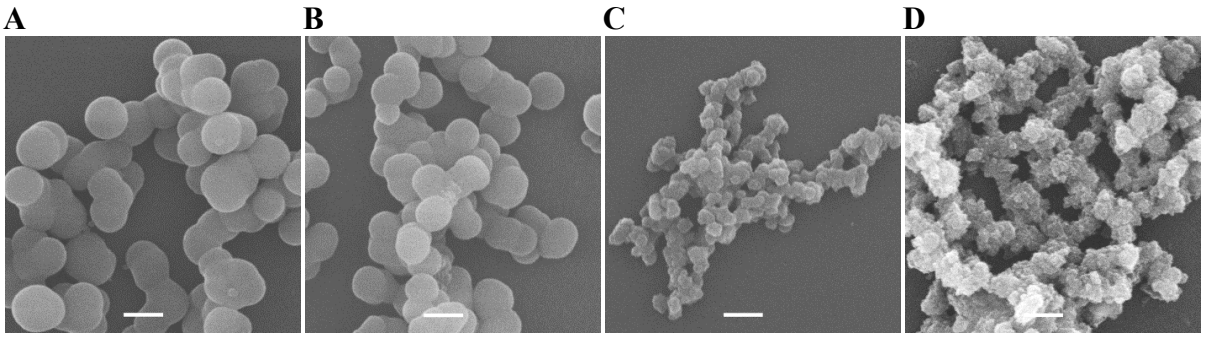

Figure 5-6 Scanning electron micrographs of silica particles resulting from silica precipitation with eGFP-peptide conjugates. Scale bars 1 µm.
A) eGFP-**A** conjugate; B) eGFP-**B** conjugate; C) eGFP-**C** conjugate; D) eGFP-**D** conjugate.

Using eGFP-**B**, spherical silica particles were obtained as well (Figure 5-6, B), but the average diameter (850 nm) is slightly decreased compared to the particles resulting from eGFP-**A**. This result correlates well with the silica particles derived from peptide **B** with a trimethylated lysine residue (Figure 3-1). Most of the silica particles do not appear as separated spheres, but are often interconnected.

The R5 peptide variant with spermidine units attached to two lysine side chains (peptide **C**, table 5-1) induces the formation of spherical silica particles with a rather inhomogeneous size distribution (Figure 3-1). The silica material resulting from the eGFP-**C** conjugate seems to be composed of highly connected small spherical silica particles (Figure 5-6, C). This silica morphology does not much resemble the silica spheres with variable size distribution observed using peptide **C** (Figure 3-1), but it distinctly differs from the large, homogenous silica spheres obtained with eGFP-**A** and -**B** conjugates (Figure 5-6, A-C). Also the eGFP-**D** conjugate, including the R5 peptide with the single phosphoserine residue, leads to silica material of rather unstructured morphology. The silica precipitate appears to be composed of nanometer-sized silica particles aggregating into clusters of larger spheres (Figure 5-6, D). Similar fuzzy silica material was observed with peptide **D** (Figure 3-1) and is assumed to arise from the electrostatic interactions of the phosphate group with the silicic acid and silica during the process of silica formation. Remarkably, this effect of the phosphate group is still very much pronounced if the short peptide **D** (2.2 kDa) is coupled to the much larger eGFP (27.6 kDa).

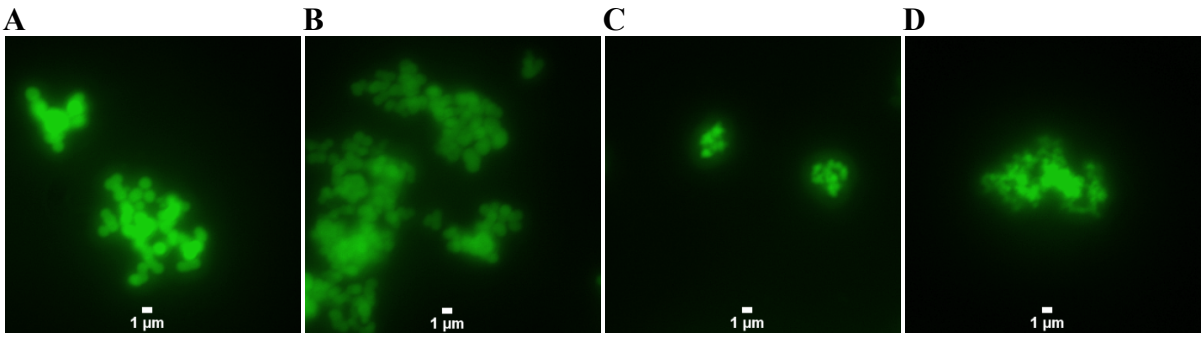

Figure 5-7 Fluorescence micrographs of silica particles resulting from silica precipitation with eGFP-peptide conjugates. Scale bars 1 µm.
A) eGFP-**A** conjugate; B) eGFP-**B** conjugate; C) eGFP-**C** conjugate; D) eGFP-**D** conjugate.

Due to the intrinsic fluorescence properties of eGFP, the silica materials prepared with eGFP-peptide conjugates were also analyzed by fluorescence microcopy (Figure 5-7). These silica particles showed a bright green fluorescence. No background fluorescence outside the silica material was observed. Also silica particles derived from R5 peptide only without containing eGFP showed no intrinsic fluorescence (data not shown). Therefore, eGFP could be clearly localized to be entrapped in the silica particles or at least to be tightly associated to the silica material.

Together, electron and fluorescence microscopic analysis of the silica materials obtained from eGFP-peptide conjugates (Table 5-2) indicate that covalent attachment of silaffin peptides **A-D** to eGFP results in specific and homogenous incorporation of the protein into the silica material (Figure 5-6 and 5-7). This finding becomes even clearer if the results obtained from the eGFP-peptide conjugates are compared to experiments based on simple co-precipitation of eGFP with peptide **A** to **D**. In the co-precipitation experiments, eGFP and the respective R5 peptides **A-D** were mixed in equimolar amounts in phosphate buffer and silica precipitation was initiated by addition of silicic acid. eGFP and peptides were not covalently tethered and an eGFP variant with a free carboxy group at the C-terminus were used instead of the eGFP-MESNa thioester to avoid *in situ* ligation between the two molecules. The resulting silica precipitates were in turn analyzed by electron and fluorescence microscopy (Figure 5-8 and 5-9).

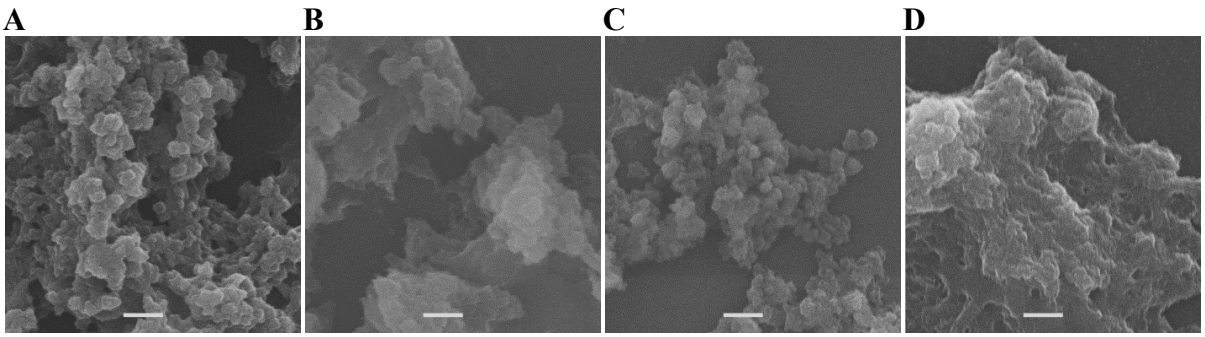

Figure 5-8 Scanning electron micrographs of silica material resulting from silica co-precipitation with eGFP and peptide variants. Scale bars 1 µm.
A) eGFP-OH and peptide **A**; B) eGFP-OH and peptide **B**; C) eGFP-OH and peptide **C**; D) eGFP-OH and peptide **D**.

The electron micrographs show rather unstructured silica materials. In silica material resulting from co-precipitation of eGFP with peptide **A** and **C**, indications for spherical silica particles, as observed with peptides **A** and **C** only, are visible (Figure 5-8, A and C). In contrast, co-precipitation of eGFP with peptides **B** and **D** leads to unstructured silica material with nanometer-sized substructures (Figure 5-8, B and D).

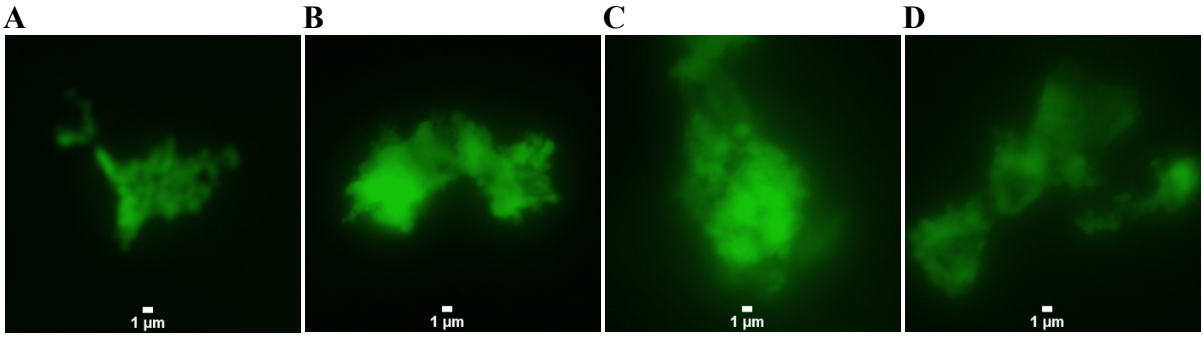

Figure 5-9 Fluorescence micrographs of silica material resulting from silica co-precipitation with eGFP and peptide variants. Scale bars 1 µm.
A) eGFP-OH and peptide **A**; B) eGFP-OH and peptide **B**; C) eGFP-OH and peptide **C**; D) eGFP-OH and peptide **D**.

Fluorescence micrographs of these silica materials show a broad distribution of eGFP fluorescence, indicating that eGFP is associated to the silica (Figure 5-9). However, since the fluorescence is not as distinct compared to the silica obtained with the eGFP-peptide conjugates (Figure 5-7), the protein seems to be rather randomly distributed over the silica material and not specifically entrapped. Thus the R5 peptide variants in the co-precipitation mixture initiate the polycondensation of silicic acid and during the silica formation process, the eGFP co-precipitates with the silica and becomes randomly entrapped.
Interestingly, the presence of eGFP in the co-precipitation mixture appears to disturb proper silica precipitation activity of all peptide variants. Control experiments revealed that eGFP itself induces precipitation of silica from a solution of silicic acid and becomes associated to the silica during this process (Figure 5-10). But the silica material shows no clearly structured morphology (Figure 5-10, A). Silica precipitation activity of eGFP is reasonable since the protein contains numerous positively and negatively charged amino acids.[65] Particularly lysine residues exposed to the surface of the β-barrel structure of the protein[66,67]

might promote silicic acid polycondensation reactions resulting in unspecific silica precipitation.

Therefore, it is assumed that in the co-precipitation experiments the eGFP contributes to silica precipitation. But the protein seems to interfere with the silica precipitation activity of the R5 peptide variants. Besides the presence of lysine residues in the R5 peptide sequence, the self-assembly of the peptides is prerequisite for silica precipitation activity. It is possible that the eGFP impairs proper self-assembly of the R5 peptide variants and hence hampers the formation of silica with well-defined structures.

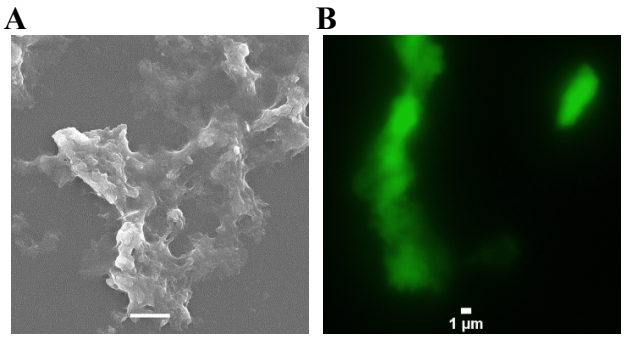

Figure 5-10 Scanning electron micrograph (A) and fluorescence micrograph (B) of silica material resulting from silica precipitation with eGFP. Scale bars 1 µm.

In the silica co-precipitation experiments, equimolar amounts of eGFP and the corresponding peptide were used. If the molar ratio of eGFP is decreased while the amount of peptide **A** is kept constant, the morphology of the silica precipitate can be steered again towards the homogenous silica spheres (data not shown). This observation proves the interference of eGFP with proper activity of the R5 peptide during co-precipitation of silica.

In contrast, in the context of the covalent eGFP-peptide conjugates, the ability of the R5 peptide variants **A-D** to exert their silica precipitation is preserved. This phenomenon was already observed with the covalent linkage of a cargo molecule to the cysteine of R5 peptide **A** via a disulfide bond (chapter 4). In this case, silica precipitation with the R5-cargo conjugates was successful and led to incorporation of the conjugate into the silica material, whereas co-precipitation with peptide **A** and the cargo resulted in silica precipitation initiated by peptide **A**, but the cargo was not simultaneously incorporated in the silica material. Therefore, it is assumed that the success of silica immobilization of target molecules via co-

precipitation during silica formation is probably highly dependent on the chemical nature of the molecule that should be entrapped in the silica.

In summary, comparison of the morphologies of silica materials resulting from silica precipitation with eGFP-peptide conjugates and co-precipitation of eGFP and peptides **A-D** clearly illustrates the superior control over silica structures using conjugates where the R5 peptide variants **A-D** are covalently linked to eGFP.

Immobilization of eGFP in the silica matrix is aimed to result in stabilization of the protein as described before for other immobilization strategies.[29,68] GFP exhibits a remarkably high stability against heat, pH-changes, proteases and denaturants due to its compact β-barrel fold.[69,70] Yet at pH 6.5, GFP was shown to be sensitive to denaturation by SDS.[71] Thus, the effect of enhanced stability of eGFP caused by silica immobilization using modified R5 peptides **A-D** was investigated by analyzing denaturation of eGFP with 0.5% SDS at pH 6.5. Denaturation was simply followed by the decrease in fluorescence since GFP fluorescence is related to correct folding of the protein and is lost upon denaturation.[72] The results of retained fluorescence after 5 min incubation with 0.5% SDS at pH 6.5 are summarized in Table 5-4.

Table 5-4 Stability of silica immobilized eGFP against treatment with 0.5% SDS at pH 6.5

sample	**relative fluorescence retained after 5 min**
eGFP in solution	10 ± 4 %
eGFP-A	62 ± 5 %
eGFP-B	64 ± 3 %
eGFP-C	74 ± 10 %
eGFP-D	82 ± 10 %
eGFP + A (Co-precipitation)	66 ± 3 %
eGFP + B (Co-precipitation)	54 ± 3 %
eGFP + C (Co-precipitation)	94 ± 10 %
eGFP + D (Co-precipitation)	77 ± 8 %

eGFP is rapidly denatured by 0.5% SDS when present in buffer at pH 6.5. The fluorescence rapidly drops to 10% of the initial fluorescence (Figure 5-11). Without addition of the denaturant SDS, eGFP is stable and remains fluorescence (data not shown). Compared to free eGFP in buffer, the silica immobilized eGFP is greatly stabilized against denaturation with SDS (Table 5-4).

Figure 5-11 exemplifies the decrease in fluorescence intensity after addition of SDS to silica samples derived from eGFP-**A** conjugate and co-precipitation with eGFP and peptide **A**. The time-resolved fluorescence measurement reveals an initial fast drop in fluorescence, while afterwards eGFP-fluorescence remains constant and does not decrease significantly. As a result of silica immobilization, in both samples more than 60% of eGFP fluorescence is retained after 5 min incubation with SDS (Table 5-4, Figure 5-12).

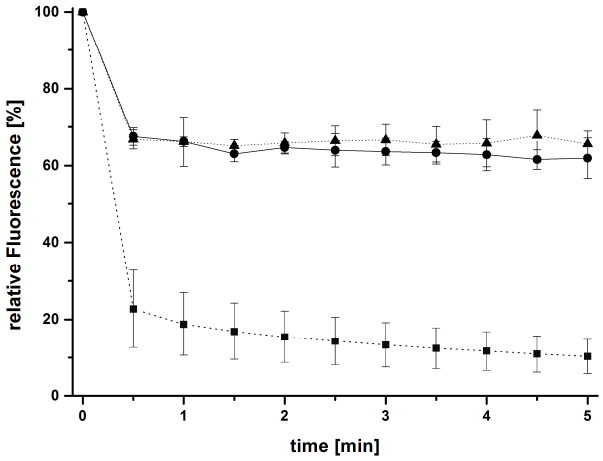

Figure 5-11 Decrease in eGFP-fluorescence after addition of 0.5% SDS at pH 6.5 over time. **(●)** silica material resulting from eGFP-**A** conjugate, (▲) silica material resulting from co-precipiation of eGFP and peptide **A**, (■) eGFP in solution.

These observations suggest that eGFP exposed to the surface of the silica material is rapidly denatured after addition of SDS. Since the residual protein is not denatured by SDS, it is most likely tightly enclosed by the silica. The eGFP encapsulated in the amorphous silica resulting from *in vitro* precipitation mediated by the R5 peptide variants **A-D** is protected against denaturation. The silica is presumably porous and SDS can enter these pores and denature the eGFP. However, the SDS-concentration used here (0.5% (w/v), 17.3 mM) is above the critical micelle concentration (cmc) of SDS. The cmc of SDS in pure water at 25 °C is 8.2 mM, and is even reduced in Tris buffer.[73,74] The size of SDS micelles is reported to be approximately 18 Å.[75] The SDS molecules that are assembled in micellar structures are unable to diffuse into the porous silica materials and to exert their denaturing effect on eGFP. This hints towards a pore size of this silica material of less than 1.8 nm.

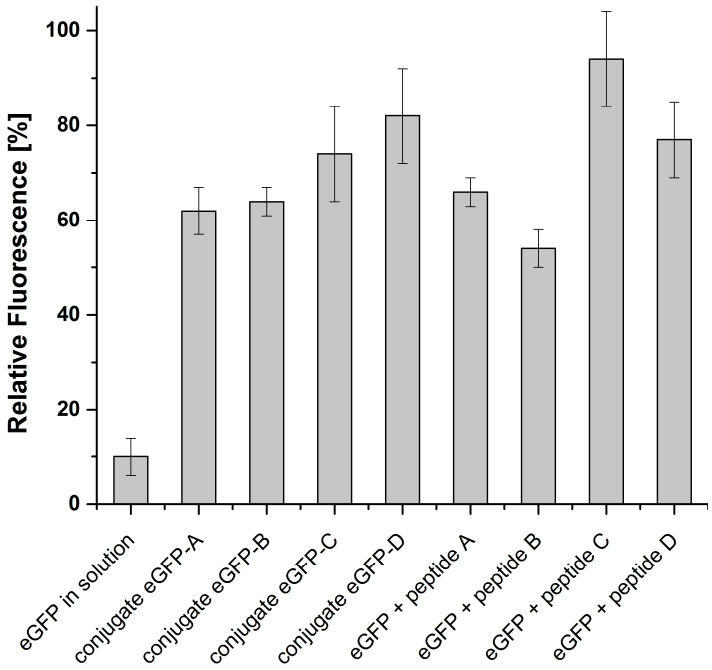

Figure 5-12 Stability of silica immobilized eGFP against treatment with 0.5% SDS at pH 6.5

Using the novel strategy for silica immobilization of proteins with modified R5 peptides **A-D**, the stabilization of eGFP against denaturation with SDS was clearly demonstrated (Table 5-4). Although the differences in stabilization between co-precipitation and the use of eGFP-peptide conjugates are not significant, a direct influence of the different peptide variants could be observed. With the unmodified peptide **A** and the variant **B** containing the trimethylated lysine residue, similar stabilization of silica-immobilized eGFP could be achieved (Table 5-4). These peptide variants also both result in spherical silica particles of homogenous size distribution. On the other hand, with peptides **C** and **D**, having a spermidine or a phosphoserine modification, greater stabilization was achieved (Table 5-4). In contrast to the homogenous silica spheres resulting from peptide **A** and **B**, peptide **C** induces the formation of inhomogenously sized silica spheres and peptide **D** leads to bulky silica material composed of silica nano-particles (Figure 3-1). Therefore, the peptide modifications might not only influence the morphology of the silica materials, but also their physical properties such as pore size. In consequence, this might reflect the different stabilization effects for eGFP by the different peptide variants.

5.3.4 Silica precipitation with TRX-peptide conjugates

Once efficient silica immobilization of proteins using modified silaffin R5 peptides was proven with eGFP, the method was applied to immobilization of the enzyme thioredoxin in order to generate a stabilized biocatalyst. Stable conjugates of TRX and the peptide variants **A** to **D** were obtained by expressed protein ligation (Table 5-3). Excess peptides and other ligation additives were removed from the crude ligation mixtures prior to silica precipitation experiments. The morphologies of the resulting silica precipitates were investigated with scanning electron microscopy (Figure 5-13).

All TRX-peptide conjugates were able to initiate precipitation of silica from a solution of silicic acid. The TRX-**A** conjugate induced the formation of large silica spheres with diameters exceeding 1 µm (Figure 5-13 A). The silica particles do not show the homogenous size distribution of silica material obtained with peptide **A** and the eGFP-**A** conjugate (Figures 3-1 and 5-6). The particles are connected to each other and appear to grow closely fused to each other and to separate later on. The spherical silica particles resulting from TRX-**B** present a much more narrow size distribution (Figure 5-13 B). This silica morphology correlates well with silica particles obtained from peptide **B** carrying the trimethylated lysine residue.

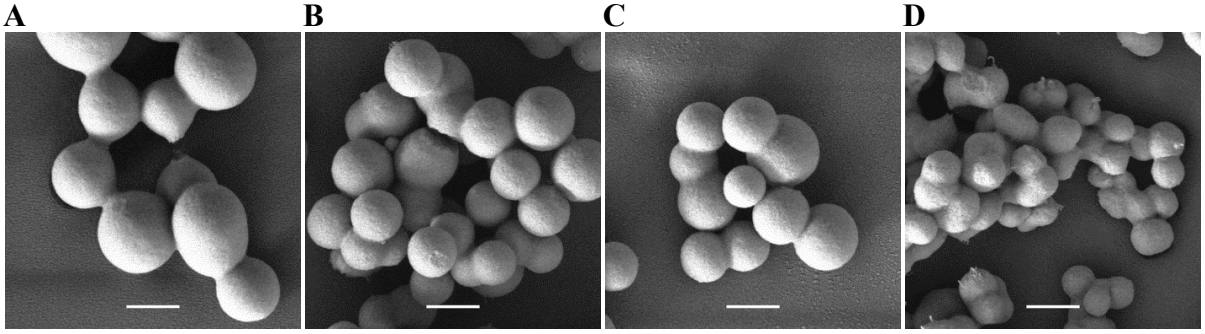

Figure 5-13 Scanning electron micrographs of silica particles resulting from silica precipitation with TRX-peptide conjugates. Scale bars 1 µm.
A) TRX-**A** conjugate; B) TRX-**B** conjugate; C) TRX-**C** conjugate; D) TRX-**D** conjugate.

Similar to the inhomogeneously sized silica spheres resulting from peptide **C** (spermidine modification), the TRX-**C** conjugate induces formation of spherical silica particles with an inhomogeneous size distribution (Figure 5-13 C). The single phosphoserine residue in peptide **D** influences silica most dramatically. The resulting silica material appeared to be composed of small, nanometer-sized silica spheres (Figure 3-1). With the TRX-**D** conjugate, spherical silica particles were observed (Figure 5-13 D). However, the single particles are not well-definec and nicely shaped as observed for the other TRX-peptide conjugates. The morphology of this silica material clearly differs from silica obtained with peptide **D** or with the eGFP-**D** conjugate (Figure 3-1 and 5-6).

Quantification of the amount of precipitated silica proved that the specific silica precipitation activities of the TRX-peptide (**A** to **D**) conjugates were in the same range as observed for unmodified peptide **A** (0.71 ± 0.02 pmol Si/nmol peptide*min) (Table 5-5). Hence the covalent conjugation of a protein five times bigger than the R5 peptide tags does not interfere with the silica precipitation activity. Expressed protein ligation to generate the TRX-peptide conjugates resulted in the covalent linkage of the R5 peptide tags to the C-terminus of the TRX protein. According to the crystal structure the carboxy-terminus of the TRX protein is not involved in secondary structures or buried in the inner core of the protein.[76] The amino acids KFAEY were C-terminally added to the TRX sequence to ensure proper intein cleavage, to provide additional motility of the C-terminus ant to obtain higher ligation yields. Therefore, the R5-peptide tags are stably, but flexibly attached to TRX. In this way, the R5 peptide variants **A** to **D** can self-assemble to exert their specific silica precipitation activity. At the same time the TRX-moiety of the conjugate is kept at distance and precluded from interfering with silica precipitation.

According to the co-precipitation experiments with eGFP and peptides **A** to **D**, silica co-precipitation was also carried out with TRX. To ensure no *in situ* ligation during silica precipitation, the thioester moiety at the C-terminus of the TRX was hydrolyzed with DTT (Figure 5-27). This TRX variant with a free carboxyl function was used for co-precipitation experiments in equimolar amounts with peptides **A** to **D**. In all co-precipitation experiments using TRX and peptide variants **A**-**D**, precipitated silica material was observed (Figure 5-14). The most unstructured silica precipitates is apparently composed of small silica nano-spheres or amorphous silica, but no large silica spheres were observed. Activity of the R5 peptide in

silica precipitation is proposed to be based on the lysine-amino groups that facilitate polycondensation of silicic acid molecules. This results in the formation of small nuclei of highly branched poly-silicic acid, which further grow by continuous polymerization with silicic acid molecules or aggregate into larger spheres. The observed silica material from co-precipitation of TRX with peptides **A** to **D** most likely represents the small silica spheres occurring in the early stage of the silica precipitation process. The TRX protein itself shows no activity in precipitating silica from a solution of silicic acid, but if the TRX protein is also present in the reaction solution but not covalently tethered to the R5 peptide variants, the peptides are hampered to further mediate the silica precipitation process in order to produce the µm-sized silica spheres observed with the TRX-peptide conjugates (Figure 5-13).

During co-precipitation with TRX, the silaffin variants **A** to **D** also show a markedly reduced specific silica precipitation activity in comparison to peptides **A-D** (Figure 3-2) or the respective TRX-peptide conjugates (Table 5-5). Consequently, the presence of TRX in co-precipitation assays does not only alter the morphology of the silica material typically obtained from peptides **A-D** but it also reduces the amount of precipitated silica. If TRX is present in the reaction solution, it seems to unspecifically interact with the R5 peptide variants and impair proper self-assembly and silica precipitation activity of the peptides. In contrast, covalently attached TRX does not influence the silica precipitation of R5 peptides in terms of amount and morphology of resulting silica material (Figure 5-13, Table 5-5).

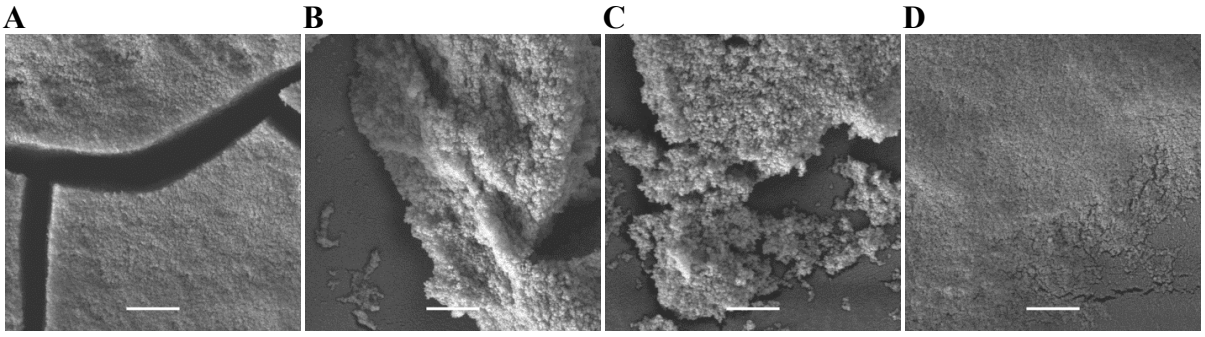

Figure 5-14 Scanning electron micrographs of silica particles resulting from silica co-precipitation with TRX and peptide variants. Scale bars 1 µm.
A) TRX and peptide **A**; B) TRX and peptide **B**; C) TRX and peptide **C**; D) TRX and peptide **D**.

Table 5-5 Characteristics of silica precipitation with TRX-peptide conjugates and co-precipitation of TRX with peptides **A** to **D**

	spec. activity[a]	loading of silica with TRX or conjugate[b]	loading efficiency[c] [%]
TRX-**A**	0.76 ± 0.02	16.8 ± 2.4	37.5 ± 5.4
TRX-**B**	0.71 ± 0.01	12.3 ± 0.4	26.5 ± 0.8
TRX-**C**	0.69 ± 0.06	14.3 ± 0.3	31.3 ± 0.7
TRX-**D**	0.82 ± 0.12	15.3 ± 1.5	33.5 ± 3.4
TRX + **A** (Co-precipitation)	0.54 ± 0.03	8.8 ± 1.0	16.8 ± 2.0
TRX + **B** (Co-precipitation)	0.65 ± 0.03	13.1 ± 0.3	28.8 ± 0.6
TRX + **C** (Co-precipitation)	0.54 ± 0.01	9.1 ± 0.1	17.0 ± 0.3
TRX + **D** (Co-precipitation)	0.46 ± 0.03	4.1 ± 0.8	6.8 ± 1.3

[a] Specific silica precipitation activity at pH 7.0 given in pmol silicon per min and nmol peptide or TRX-peptide conjugate

[b] Given in (nmol) protein/(nmol) SiO_2

[c] (nmol protein in nanoparticles/nmol protein used initially for silica precipitation) *100

As confirmed with both model proteins, eGFP and TRX, covalent conjugation of the protein to the respective R5 sequence is superior to co-precipitation in order to achieve effective and homogenous encapsulation of the protein in a silica matrix.

The entrapment of TRX in the silica particles could not be proven by fluorescence microscopy as for eGFP-conjugates. Therefore, loading of silica with TRX and TRX-peptide conjugates was determined by dissolution of silica and subsequently analyzing the protein content with HPLC. The amount of protein content in the silica material is also important as reference for determining activity of silica encapsulated enzymes.

The R5 peptides co-precipitate during silica formation and become entrapped within the silica material.[26,77] Using peptide **A**, typically 32.7 ± 2.1 % of peptide initially used for silica precipitation become entrapped within the silica particles (Table 4-1 and 4-2). In total 16.8 ± 1.1 nmol of peptide **A** are loaded per nmol of precipitated SiO_2. Silica precipitation with the covalently linked TRX-peptide conjugates resulted in comparable amounts of encapsulated proteins (Table 5-5). During silica formation with TRX-peptide conjugates, roughly one third of the initially supplied protein becomes entrapped except for TRX-**B**. This conjugate consisting of TRX and peptide **B** with the trimethylated lysine residue shows slightly decreased loading efficiency compared to the other conjugates despite exhibiting similar silica precipitation activity (Table 5-5). This effect might be due to the permanent

positive charge arising from the trimethylated lysine that impairs association with the newly formed silica by electrostatic repulsion.

In contrast, if the TRX was not covalently linked to the peptides **A-D**, distinctly decreased amounts of TRX were encapsulated in the silica material (Table 5-5). During co-precipiation of TRX and peptide **A**, with 8.8 ± 1.0 nmol/nmol SiO_2 (32.7 ± 2.1 %), only half as much of TRX became associated with the silica when compared to TRX-**A** conjugate. Least TRX was encapsulated in silica when the protein was co-precipitated in presence of peptide **D**. With 4.1 ± 0.8 nmol/nmol SiO_2, only 6.8 ± 1.3 % of TRX initially present in the reaction solution was trapped in the silica material. Interestingly, in co-precipitation with peptide **B**, almost similar amounts of TRX were achieved per nmol of precipitated SiO_2 compared to TRX-**B** conjugate. Whereas positively charged peptide **B** prevented proper loading of TRX-**B**, the increased activity of peptide **B** in silica precipitation (Figure 3-2) might contribute to more efficient loading of protein during co-precipitation of silica.

These results emphasize that a highly efficient encapsulation of target proteins in silica material can be achieved by covalent attachment to the R5 peptide and its variants. Whereas all TRX-peptide conjugates result in comparable and efficient protein encapsulation, the loading efficiency during co-precipitation is highly dependent on the nature of the peptide variant (Table 5-5). In addition, the efficacy of silica immobilization of a protein by co-precipitation with R5 peptides is certainly also depending on the nature of the protein. As demonstrated in chapter 4, immobilization of the cargo peptide CG12AB during co-precipitation with R5 was not successful whereas a disulfide linked R5-cargo conjugate showed efficient loading of silica. There are several examples in the literature of successful co-precipitation for silica encapsulation of enzymes, but a very high molar excess of R5 peptide is needed in order to achieve high yields of immobilization.[34,35] In contrast, covalent protein-R5 conjugates lead to efficient protein encapsulation with equimolar ratios of protein and R5 peptide.[31]

5.3.5 Release of TRX and TRX-peptide conjugates from silica material

TRX becomes entrapped in the silica material during R5 peptide mediated silica formation and loading of the silica was determined (Table 5-5). However, the entrapped proteins and peptides are no covalently bound to the silica material, but association of the proteins to the silica relies on electrostatic interactions and hydrogen bonding between peptide side chains and silanol groups. The R5 peptide has been shown to be partly released from silica depending on pH and buffer conditions (chapter 4).

In other approaches of hybrid silica formation with bioactive molecules, uncontrolled, diffusion-based release of an encapsulated antimicrobial peptide or apoptotic protein from the silica materials was observed.[78,79] Consequently, it was analyzed if TRX is permanently entrapped in the silica or if the protein is gradually released from silica. To investigate release of TRX, the hybrid silica materials were suspended in PBS buffer and incubated at 37 °C over a period of 3 days in 24 h cycles. After each 24 h cycle, the supernatant was separated from the silica material and analyzed for protein content by HPLC. The silica material was resuspended in fresh PBS buffer for the next 24 h cycle.

The highest rate of protein release is observed in the first 24 hours for all TRX-silica hybrid materials (Table 5-6, Figure 5-15). In the second and third 24 hour cycles, considerably less protein leaks from the silica material or no release at all can be detected any more. Comparison of the TRX-peptide (**A** to **D**) conjugates reveals a slightly increased release of TRX-**B**. Based on the initial loading capacity, almost half of TRX-**B** conjugate (42 %) is washed out after 3 days (Figure 5-15). TRX-**B** differs from the other conjugates by the trimethylated lysine residue in the R5 peptide moiety. This positive charge may impair electrostatic interactions and hydrogen bonding between the protein conjugate and the silica material and therefore cause a reduced affinity of TRX-**B** to the silica. Another potential explanation for the increased release of TRX-**B** compared to the other conjugates would be based on the size of the pores. Different R5 peptide variants (**A** to **D**) influence the morphology of the resulting silica material and have an effect on the properties of the silica materials such as pore size. However, the existence of enlarged pores in the silica material resulting from peptide **B** is not consistent with the amount of released TRX from silica material obtained by co-precipitation of TRX and peptide **B** (Table 5-6). Here only half as

much of TRX is released after three days (21 %) compared to the TRX-**B** conjugate (42 %, Figure 5-15). In this case, the TRX is not covalently bound to peptide **B** and is independently released.

Table 5-6 Release of TRX-peptide conjugates and TRX from silica material after incubation in PBS (pH 7.4) at 37 °C for repeatedly 24 h cycles. After each 24 h cycle, the supernatant was separated and exchanged with fresh buffer.

	1st 24 h cycle	**2nd 24 h cycle**	**3rd 24 h cycle**
TRX-**A**	3.48 ± 0.12 [a] (21 %)[b]	1.53 ± 0.09 [a] (9 %) [b]	0.85 ± 0.07 [a] (5 %) [b]
TRX-**B**	2.78 ± 0.06 [a] (23 %) [b]	1.51 ± 0.09 [a] (12 %) [b]	0.87 ± 0.07 [a] (7 %) [b]
TRX-**C**	2.54 ± 0.05 [a] (18 %) [b]	1.09 ± 0.05 [a] (8 %) [b]	0.68 ± 0.02 [a] (5 %) [b]
TRX-**D**	2.31 ± 0.02 [a] (15 %) [b]	0.95 ± 0.07 [a] (6 %) [b]	0.65 ± 0.03 [a] (4 %) [b]
TRX + **A** (Co-precipitation)	1.20 ± 0.06 [a] (14 %) [b]	0.57 ± 0.20 [a] (6 %) [b]	n.d.
TRX + **B** (Co-precipitation)	1.72 ± 0.11 [a] (13 %) [b]	0.65 ± 0.13 [a] (5 %) [b]	0.38 ± 0.23 [a] (3 %) [b]
TRX + **C** (Co-precipitation)	2.13 ± 0.13 [a] (23 %) [b]	0.69 ± 0.25 [a] (8 %) [b]	0.32 ± 0.10 [a] (4 %) [b]
TRX + **D** (Co-precipitation)	0.36 ± 0.05 [a] (9 %) [b]	n.d.	n.d.

[a] Given in (nmol) protein/(nmol) SiO_2

[b] (%) Release of TRX-peptide conjugate from initial loading of silica with peptide

n.d. = not detectable

During co-precipitation with the different peptides **A** to **D**, distinctly decreased amounts of TRX were encapsulated in the silica material (Table 5-5). Comparing the silica materials resulting from these silica co-precipitations, most TRX is released from silica material obtained with spermidine-modified peptide **C** (35 % of initially loaded protein after 3 days, Figure 5-15). Polyamines have been shown to have a shape patterning effect during silica formation.[17,80] The increased release of TRX might be indicative for a different substructure and pore size of the silica material resulting from spermidine-modified peptide **C**. The slightly decreased release of TRX-**C** conjugate hints towards a more tight binding of peptide **C** to the silica material, since the native PTMs of silaffins such as the long-chain polyamines contribute to a strong interaction of the peptides with the biosilica.

The lowest amount of released protein was observed from silica material with phosphorylated peptide **D**, both from silica obtained with TRX-**D** or by co-precipitation of TRX and peptide **D** (Table 5-6, Figure 5-15). The single phosphoserine residue in peptide **D** also mostly influenced the morphology of silica precipitates (Figure 3-1, Figure 5-13). The

cluster of small silica-nanospheres commonly observed with phosphorylated peptide **D** might contribute to a tight entrapment of TRX in the silica material.

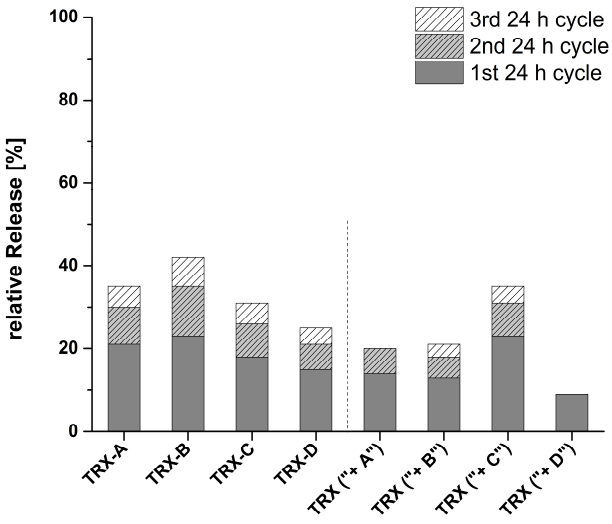

Figure 5-15 Relative release of TRX-peptide conjugates and TRX from silica material after incubation in PBS for 3 days in cycles of 24 hours. The labels TRX-**A**, TRX-**B**, TRX-**C** and TRX-**D** represent the corresponding TRX-peptide conjugates, TRX (+"X") marks the co-precipitation experiments with the different peptides.

From all silica materials analyzed, less than half of the initially encapsulated TRX-peptide conjugates or TRX is released even after three days incubation in PBS buffer at 37 °C (Figure 5-15). Thus probably only the protein that is unspecifically associated to the silica material or is located in the outer regions of the silica material is released whereas protein that is tightly enclosed in the particle core remains entrapped.

5.3.6 Activity of silica immobilized TRX

Thioredoxins (TRX) are the major cellular protein disulfide isomerases and contain a dithiol/disulfide active site (CGPC). *In vivo*, the cysteine disulfide of TRX is reduced to the dithiol form by electrons from NADPH via a thioredoxin reductase.[43]

The *in vitro* assay for thioredoxin activity is based on the reduction of insulin catalyzed by thioredoxin in the presence of dithiothreitol (DTT).[54] The disulfide in the CGPC active site motif of TRX (TRX-S_2) is rapidly reduced by DTT resulting in free sulfhydryl groups (TRX-$(SH)_2$). Subsequently, TRX-$(SH)_2$ catalyzes an thiol-disulfide exchange reaction with insulin (Figure 5-16). Reduction of the interchain disulfide bonds of insulin results in the precipitation of the insulin B chain. The rate of insulin reduction can be monitored as the increase of turbidity at 650 nm caused by insulin B chain aggregation.[81]

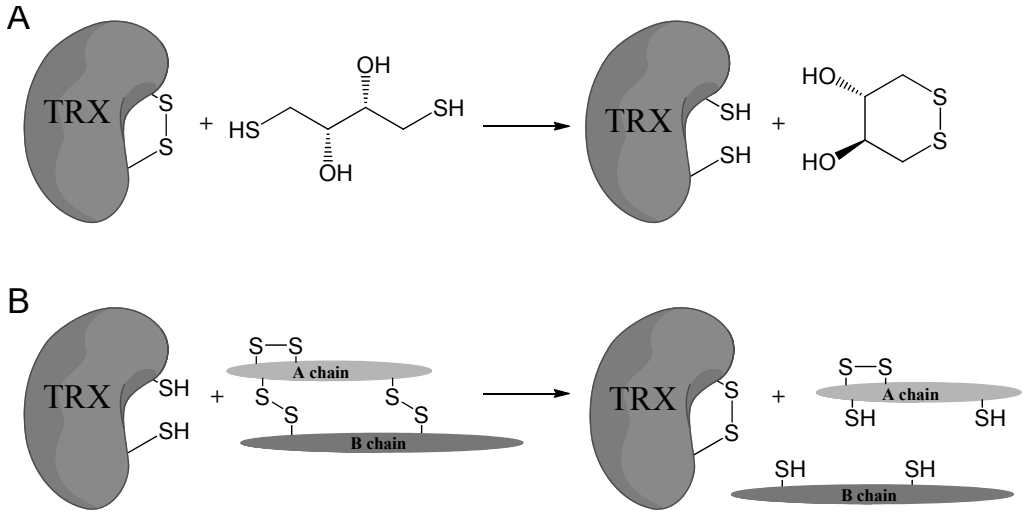

Figure 5-16 Schematic illustration of insulin-based thioredoxin assay.[54]

A) TRX-S_2 is rapidly reduced by DTT.

B) TRX-$(SH)_2$ reduces the interchain disulfide bridges of insulin resulting in precipitation of the insulin B-chain.

Notably, DTT does not cause detectable reduction of insulin and precipitation of the B chain within 20 min (Figure 5-17, A). However, insulin reduction by DTT followed by aggregation of the B chain could be observed with prolonged incubation times. Therefore, all measurements for determination of thioredoxin activity were restricted to 20 min. The rate of insulin B chain precipitation measured as ΔA_{650}/min was used as parameter for quantitation and comparison of thioredoxin activity of the different protein variants.

The catalytic reduction of insulin by the TRX variants was initiated by the addition of DTT. After initial formation of TRX-$(SH)_2$, the catalytically active enzyme reduced the interchain disulfide bonds of insulin. Precipitation of the insulin B chain causing the increase in

absorption at 650 nm could be observed after a few minutes. The TRX variants with the MESNa thioester moiety or with free carboxyl group at the C-terminus (TRX-OH) both showed similar activity in reduction of the interchain disulfide bonds of insulin (Figure 5-17, A; Table 5-7).

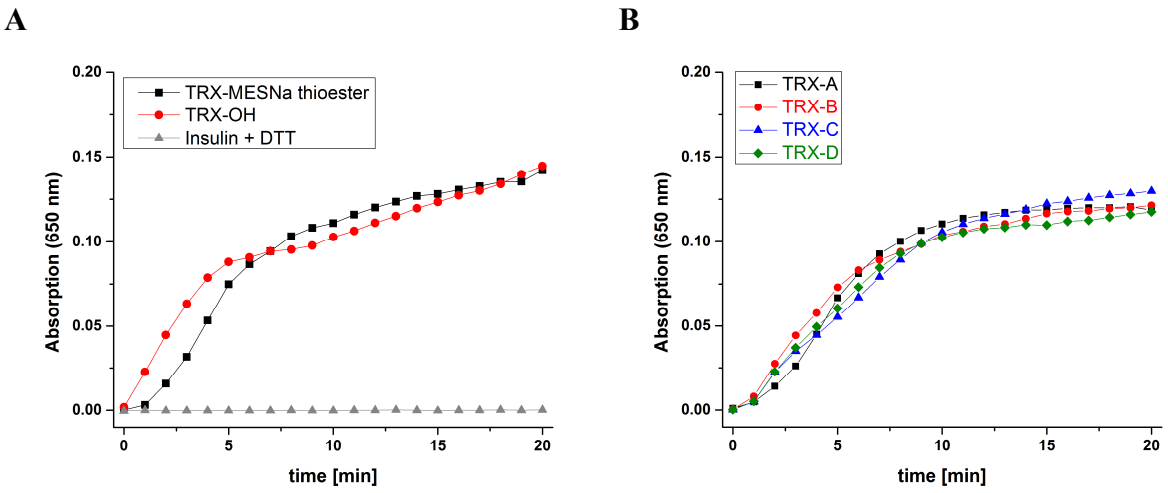

Figure 5-17 TRX and TRX-peptide conjugate catalyzed reduction of insulin by DTT.

A) Activity of TRX variants with a C-terminal MESNa thioester (black squares) or free carboxyl group (red circles). DTT did not cause reduction of insulin (grey triangles).

B) Activity of TRX-peptide conjugates: TRX-**A** (black squares), TRX-**B** (red circles), TRX-**C** (blue triangles) and TRX-**D** (green rhombus).

For the thioredoxin-MESNa thioester, turbidity could be observed typically after a delay time of 2 min. With TRX-OH, precipitation of insulin B chain was detected after a shorter delay time. This is reasonable since the TRX with free C-terminus was obtained by treatment of the TRX-thioester protein with an excess of DTT to hydrolyze the C-terminal thioester moiety. Thus, TRX-OH was already in the reduced form and did not require initial activation.

Chemoselective ligation of the differently modified silaffin peptides **A** to **D** to the C-terminus of TRX via expressed protein ligation did not abolish enzymatic activity of TRX. The TRX-peptide conjugates (**A** to **D**) showed very good activity in reduction of the disulfide bonds in insulin (Figure 5-17, B). However, the silaffin-tags slightly interfere with TRX activity as observed in reduced rates of insulin reduction (Table 5-7). Besides a generally reduced

relative specific activity (given as $\Delta A_{650} \times min^{-1}/\mu g$ protein) of the TRX-peptide conjugates in comparison to the TRX-MESNa thioester and TRX-OH protein, also a distinct difference between the individual conjugates became apparent. The conjugates TRX-**A** comprising the unmodified silaffin R5 peptide **A** or TRX-**B** containing peptide **B** with the trimethylated lysine residue showed highest activity in insulin reduction among the conjugates. In contrast, the spermidine-modification in TRX-**C** and the phosphoserine residue in TRX-**D** had a greater influence on enzymatic activity (Table 5-7).

Table 5-7 Activity of TRX and TRX-peptide conjugates in reduction of insulin by DTT at pH 7.4. Rate of insulin reduction by thioredoxin is given as $\Delta A_{650} \times min^{-1}$ in the linear range of increase of absorption.

	delay time	**$\Delta A_{650} \times min^{-1}$**	**relative specific activity[a]**
TRX-MESNa thioester	2 min	$(19.8 \pm 1.2) \times 10^{-3}$	1.6×10^{-3}
TRX-OH	1 min	$(18.7 \pm 0.7) \times 10^{-3}$	1.5×10^{-3}
TRX-**A** conjugate	2 min	$(17.6 \pm 3.1) \times 10^{-3}$	1.2×10^{-3}
TRX-**B** conjugate	2 min	$(15.0 \pm 1.9) \times 10^{-3}$	1.0×10^{-3}
TRX-**C** conjugate	2 min	$(11.0 \pm 1.7) \times 10^{-3}$	0.7×10^{-3}
TRX-**D** conjugate	2 min	$(12.6 \pm 3.1) \times 10^{-3}$	0.9×10^{-3}

[a] Calculated as $\Delta A_{650} \times min^{-1}$ in the linear range of increase of absorption / µg protein

As described above, the TRX-peptide conjugates were used for silica precipitation resulting in encapsulation of the proteins in the resulting silica material. Additionally, co-precipitation of TRX during silica formation with different peptides **A-D** was carried out and for both cases, loading of the silica material with protein was determined (Table 5-5). Based on these loadings of silica with protein, a respective amount of silica with encapsulated TRX or TRX-peptide conjugate was used to test for activity in order to achieve comparability to activity of TRX in solution.

Activity of TRX after silaffin-mediated immobilization in silica could be observed for all variants, but distinct differences in the activity profiles became apparent (Figure 5-18, Table 5-8). In contrast to free TRX and TRX-conjugates in buffer solution (Figure 5-17), longer delay times until detectable precipitation of insulin B chain were observed (Figure 5-18, A). This is most likely caused by the silica, which acts as a physical barrier and limits fast diffusion of DTT and insulin during enzymatic reaction. For the silica immobilized TRX-conjugates, insulin B chain precipitation could be observed after 5 to 7 min (Table 5-8). After

this prolonged delay time, the silica encapsulated TRX-peptide conjugates showed high rates of insulin reduction detected as $\Delta A_{650} \times min^{-1}$. This increased activity may be caused by an added affinity of the substrate to the silica and resulting spatial proximity of enzymes and substrate. Least active among the silica immobilized TRX-silaffin conjugates was silica immobilized TRX-**C** (Table 5-8). Also TRX-**C** conjugate in buffer showed decreased enzymatic activity compared to the other TRX-peptide conjugates (Table 5-7). The distinctly altered activity of TRX-**C** conjugated and silica immobilized TRX-**C** is indicative for a negative influence of the spermidine modification in peptide **C** on TRX activity.

Table 5-8 Activity of silica immobilized TRX and TRX-peptide conjugates in reduction of insulin by DTT at pH 7.4. Rate of insulin reduction by thioredoxin is given as $\Delta A_{650} \times min^{-1}$ in the linear range of increase of absorption.

	delay time	**$\Delta A_{650} \times min^{-1}$**	**relative specific activity[a]**
TRX-**A**	5 min	$(35.5 \pm 9.4) \times 10^{-3}$	2.4×10^{-3}
TRX-**B**	5 min	$(39.1 \pm 10.9) \times 10^{-3}$	2.7×10^{-3}
TRX-**C**	7 min	$(19.2 \pm 2.2) \times 10^{-3}$	1.3×10^{-3}
TRX-**D**	7 min	$(43.8 \pm 5.3) \times 10^{-3}$	3.0×10^{-3}
TRX + **A** (Co-precipitation)	12 min	$(11.3 \pm 2.9) \times 10^{-3}$	0.9×10^{-3}
TRX + **B** (Co-precipitation)	14 min	$(12.3 \pm 2.6) \times 10^{-3}$	1.0×10^{-3}
TRX + **C** (Co-precipitation)	8 min	$(9.4 \pm 2.9) \times 10^{-3}$	0.7×10^{-3}
TRX + **D** (Co-precipitation)	15 min	$(7.5 \pm 2.3) \times 10^{-3}$	0.6×10^{-3}

[a] Calculated as $\Delta A_{650} \times min^{-1}$ in the linear range of increase of absorption / µg protein

If TRX was immobilized in silica by co-precipitation with the differently modified silaffin peptides, distinctly altered silica morphologies were obtained (Figure 5-14). Also distinctly less protein became entrapped in the silica material during the co-precipitation process (Table 5-5). Nevertheless, to ensure comparability of enzymatic activities, a respective amount of silica with co-precipitated TRX based on the loading of silica with TRX (Table 5-5) was used for activity assays.

Activity of co-precipitated TRX could only be observed after much longer delay times (Figure 5-18, B). Precipitation of the insulin B chain occuring after reduction of insulin disulfide bridges by TRX co-precipitated with peptides **A**, **B** and **D** became visible only after 12-15 min. This suggests that the enzyme is tightly entrapped in the silica material. Either diffusion of substrates to the encapsulated TRX is severely limited or TRX enzyme activity is

restricted by the silica materials. Silica materials resulting from co-precipitation of peptides **A-C** with TRX appeared to be clusters composed of small silica particles (Figure 5-14). This distinctly different morphology of the silica material in contrast to the spherical particles resulting from TRX-peptide conjugates may account for impaired activity of TRX. Eventually, the TRX entrapped in this silica material is spatially constrained and therefore, enzymatic activity is impaired.

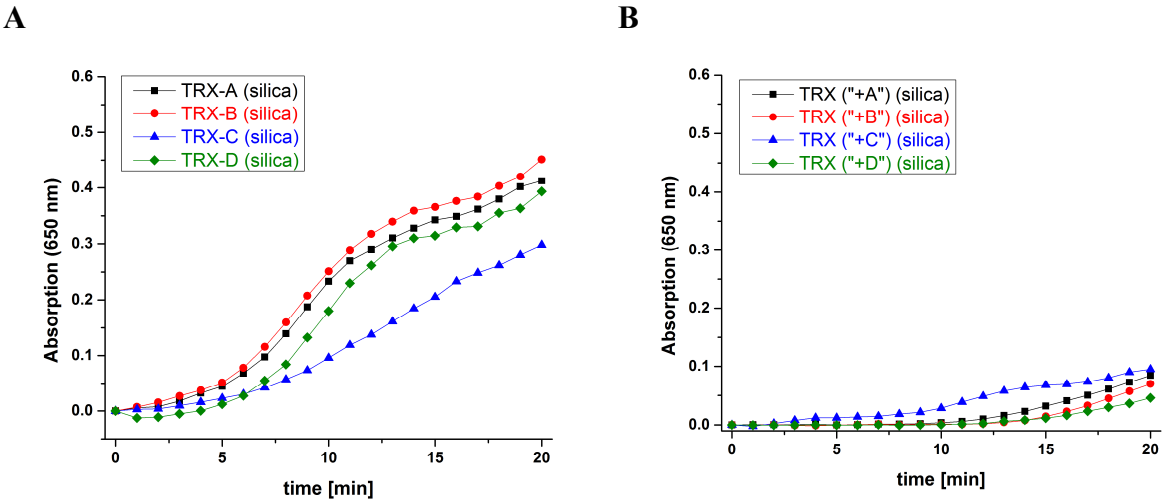

Figure 5-18 Activity of silica immobilized TRX variants in reduction of insulin by DTT.

A) Activity of silica immobilized TRX-peptide conjugates immobilized in silica: Silica-immobilized TRX-**A** (black squares), Silica-immobilized TRX-**B** (red circles), Silica-immobilized TRX-**C** (blue triangles) and Silica-immobilized TRX-**D** (green rhombus).

B) Activity of silica immobilized TRX after co-precipitation during silica formation with different peptides: TRX immobilized in silica resulting from peptide **A** (black squares), TRX immobilized in silica resulting from peptide **B** (red circles), TRX immobilized in silica resulting from peptide **C** (blue triangles) and TRX immobilized in silica resulting from peptide **D** (green rhombus).

For TRX co-precipitated with peptide **C**, shorter delay times could be detected (Figure 5-18, B). With this silica material, also distinctly increased release of TRX from the silica material could be observed over time (Figure 5-15). Enzymatic activity of TRX was monitored only for 20 min to ensure that reduction of insulin is not caused by DTT. Faster release of TRX

from silica material resulting from peptide **C** could be the reason for a shorter delay time for enzymatic activity of this material.

In conclusion, with the covalent TRX-silaffin conjugates not only a more efficient and homogenous encapsulation of the proteins in the silica material was achieved but also improved enzymatic activities. Investigations towards release of proteins from the silica materials (Table 5-6, Figure 5-15) and enzymatic activity of encapsulated proteins (Table 5-8, Figure 5-18) revealed a clear influence of the differently modified silaffin peptides that were used for silica formation. The influence of the silaffin variants opens the possibility to adjust silica properties to the requirements in different applications by the choice of silaffin peptides. Using the differently modified silaffin variants, entrapment and release rates of proteins from hybrid silica materials as well as enzymatic activity of entrapped proteins can be controlled. This opens the possibility to use differently modified silaffin peptides for efficient formation of hybrid protein-silica materials that can be developed into systems for sustained release of proteins from silica or into efficient biocatalysts, especially when introducing more complex modification patterns as found in native silaffins.

5.4 Conclusion

Silaffin peptides are a powerful tool for efficient silica formation under mild conditions. Several strategies for enzyme immobilization using silaffins were already reported.[31-35] Nevertheless, these methods are limited by random, unspecific entrapment of proteins and lack control over silica properties. However, differently modified silaffins were shown to influence silica morphology (chapter 3). Therefore, these modified silaffin peptides were used to achieve immobilization of enzymes in silica materials with defined properties by covalently attaching them to two different proteins.

Expressed protein ligation proved to be an efficient strategy to generate stable protein-silaffin conjugates. Differently modified silaffin variants are accessible via SPPS and once the peptides are synthesized, they can be readily ligated to various proteins. Using EPL, stable eGFP- and thioredoxin-silaffin conjugates were obtained in high yields.

The eGFP- and thioredoxin-silaffin conjugates were analyzed towards their silica precipitation activities. With both protein-silaffin conjugates highly efficient and homogenous encapsulation of the proteins in the resulting silica material was achieved. In addition different morphologies of the silica materials resulting from different protein-silaffin conjugates indicate the influence of the covalently linked silaffin. If eGFP or TRX were not covalently linked to the silaffin variants, random and less efficient co-precipitation of the proteins during silica formation was observed.

Detailed analyses of the amount of TRX that was encapsulated in the silica material under the different conditions revealed a higher loading of silica with protein using the covalent protein-silaffin conjugates. It was found that parts of the entrapped proteins were released from silica material over time. TRX retained its enzymatic activity after immobilization and eGFP was demonstrated to be stabilized against denaturation with SDS. The rates of entrapment, release as well as enzymatic activity of TRX, turned out to be dependent on the silaffin variants used for silica formation.

The results described here demonstrate that covalent attachment of silaffins to target proteins is a valuable method to achieve efficient and homogenous encapsulation of target proteins in silica materials. In addition, it was proven that conjugation with differently modified silaffin peptides influences the properties of the resulting silica material as well as the activity of the

encapsulated enzyme. These findings provide a rational basis for the development of modified silaffin peptides into efficient agents for precipitation of silica and the simultaneous encapsulation of proteins. The properties of the silica material can be tailored to the requirements of a given enzyme in order to achieve reasonable stabilization and activity for the desired applications.

5.5 Supplementary analytical data

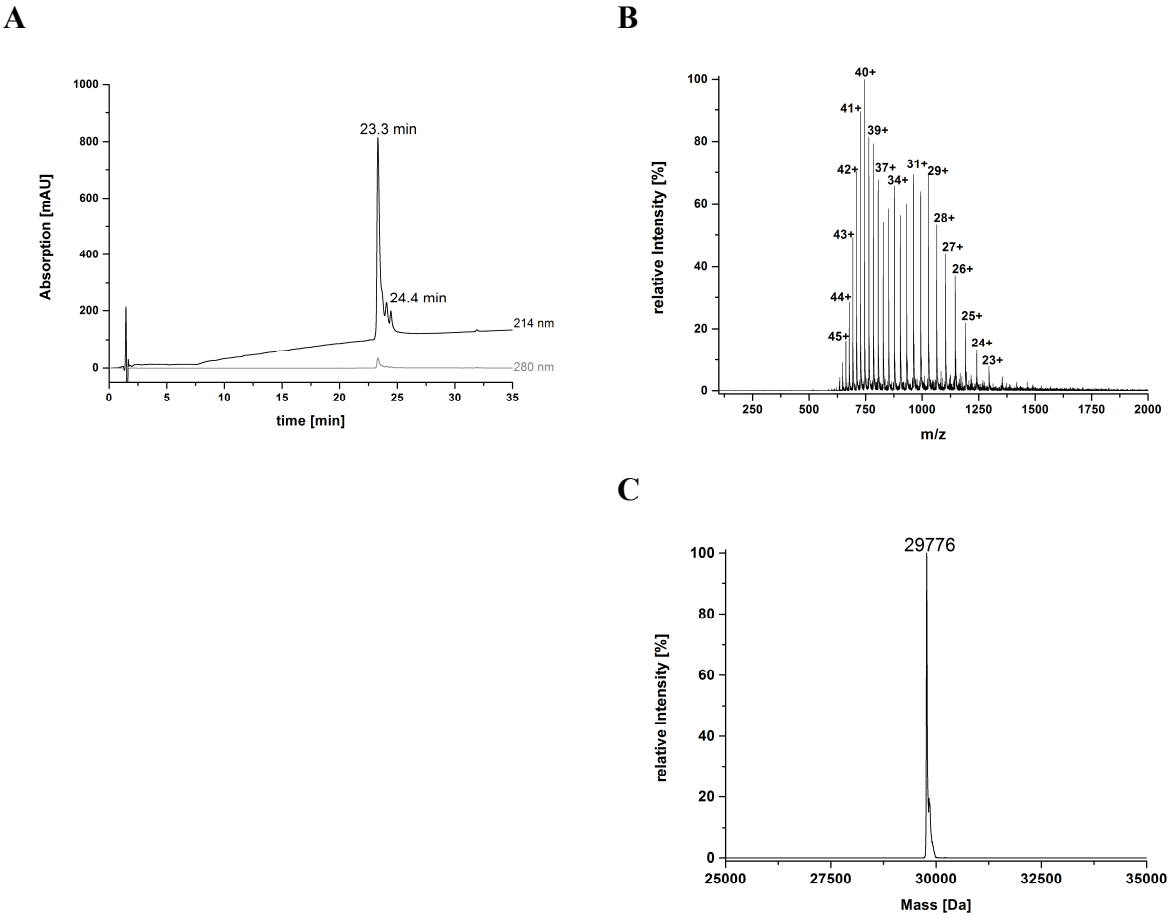

Figure 5-19 Analysis of eGFP-**A** conjugate.
A) HPLC chromatogram of analytical LC-MS analysis of eGFP-**A** conjugate.
B) Mass spectrum of the peak at 23.3 min from analytical LC-MS analysis of eGFP-**A**.
C) Deconvoluted mass spectrum. Calculated mass: 29772 Da; observed mass: 29776 Da.

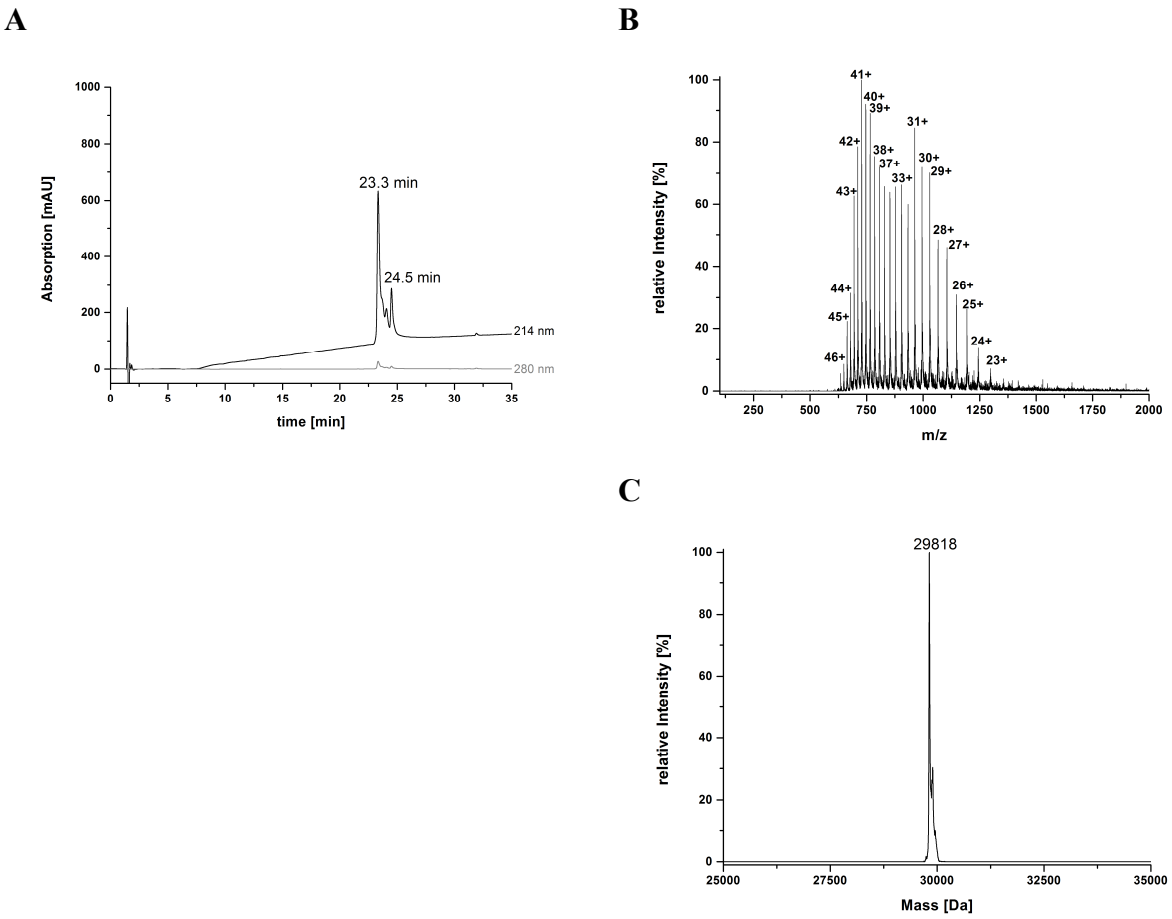

Figure 5-20 Analysis of eGFP-**B** conjugate.
A) HPLC chromatogram of analytical LC-MS analysis of eGFP-**B** conjugate.
B) Mass spectrum of the peak at 23.3 min from analytical LC-MS analysis of eGFP-**B**.
C) Deconvoluted mass spectrum. Calculated mass: 29815 Da; observed mass: 29818 Da.

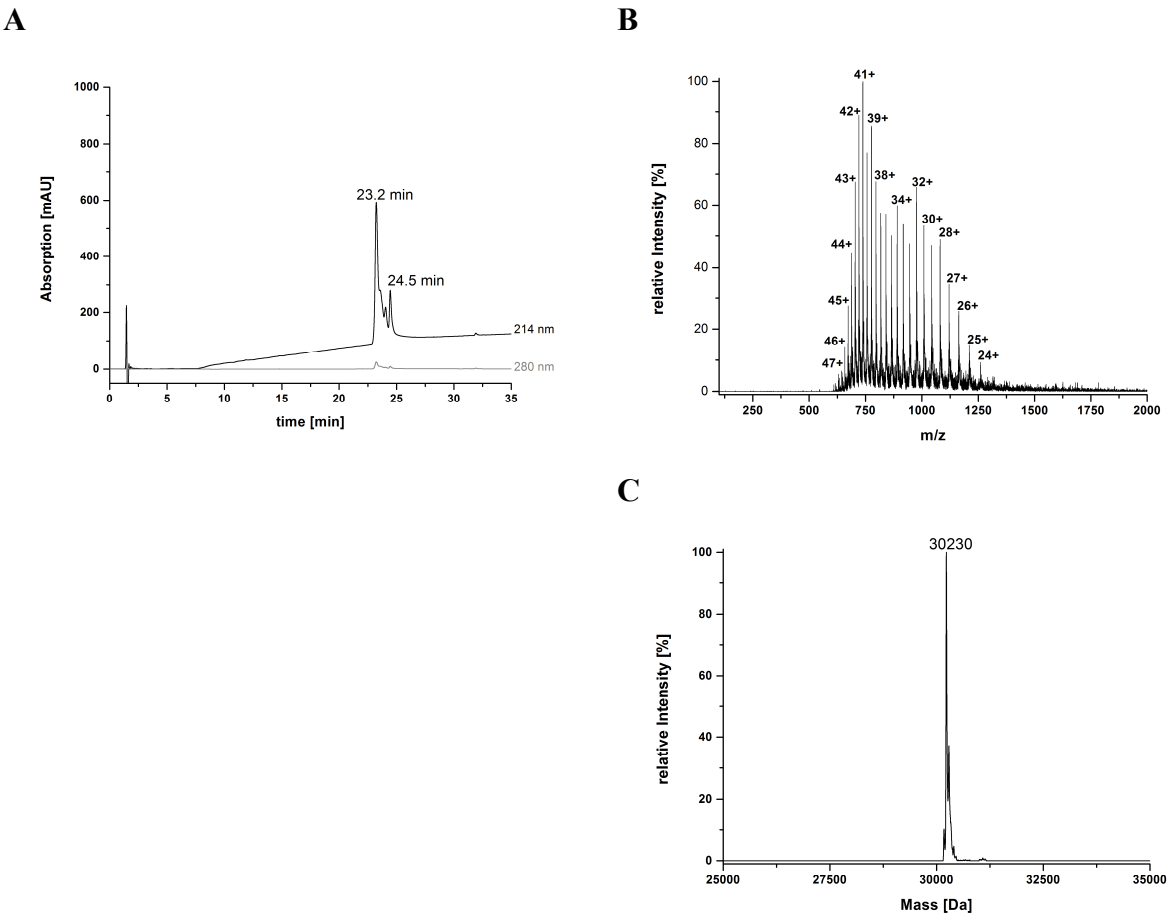

Figure 5-21 Analysis of eGFP-**C** conjugate.
A) HPLC chromatogram of analytical LC-MS analysis of eGFP-**C** conjugate.
B) Mass spectrum of the peak at 23.2 min from analytical LC-MS analysis of eGFP-**C**.
C) Deconvoluted mass spectrum. Calculated mass: 30227 Da; observed mass: 30230 Da.

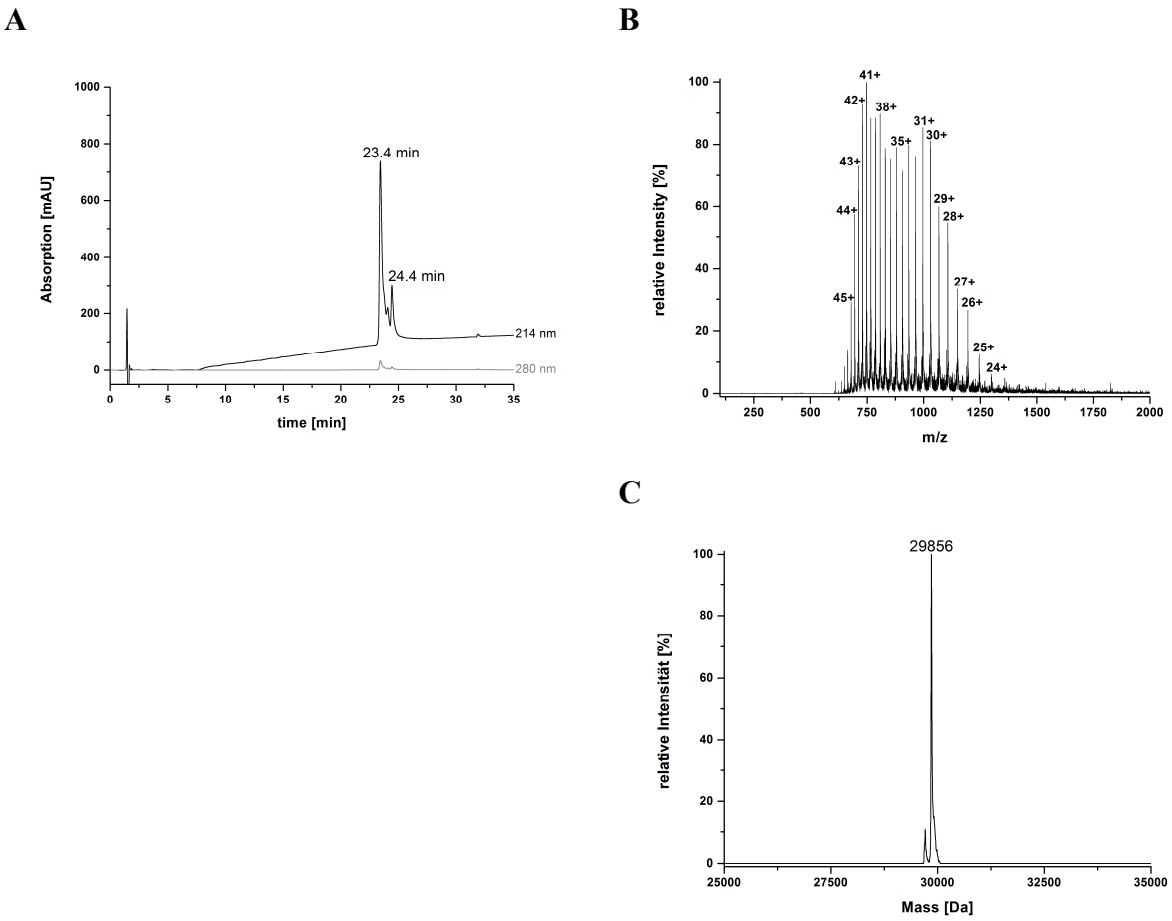

Figure 5-22 Analysis of eGFP-**D** conjugate.
A) HPLC chromatogram of analytical LC-MS analysis of eGFP-**D** conjugate
B) Mass spectrum of the peak at 23.4 min from analytical LC-MS analysis of eGFP-**D**.
C) Deconvoluted mass spectrum. Calculated mass: 29852 Da; observed mass: 29856 Da.

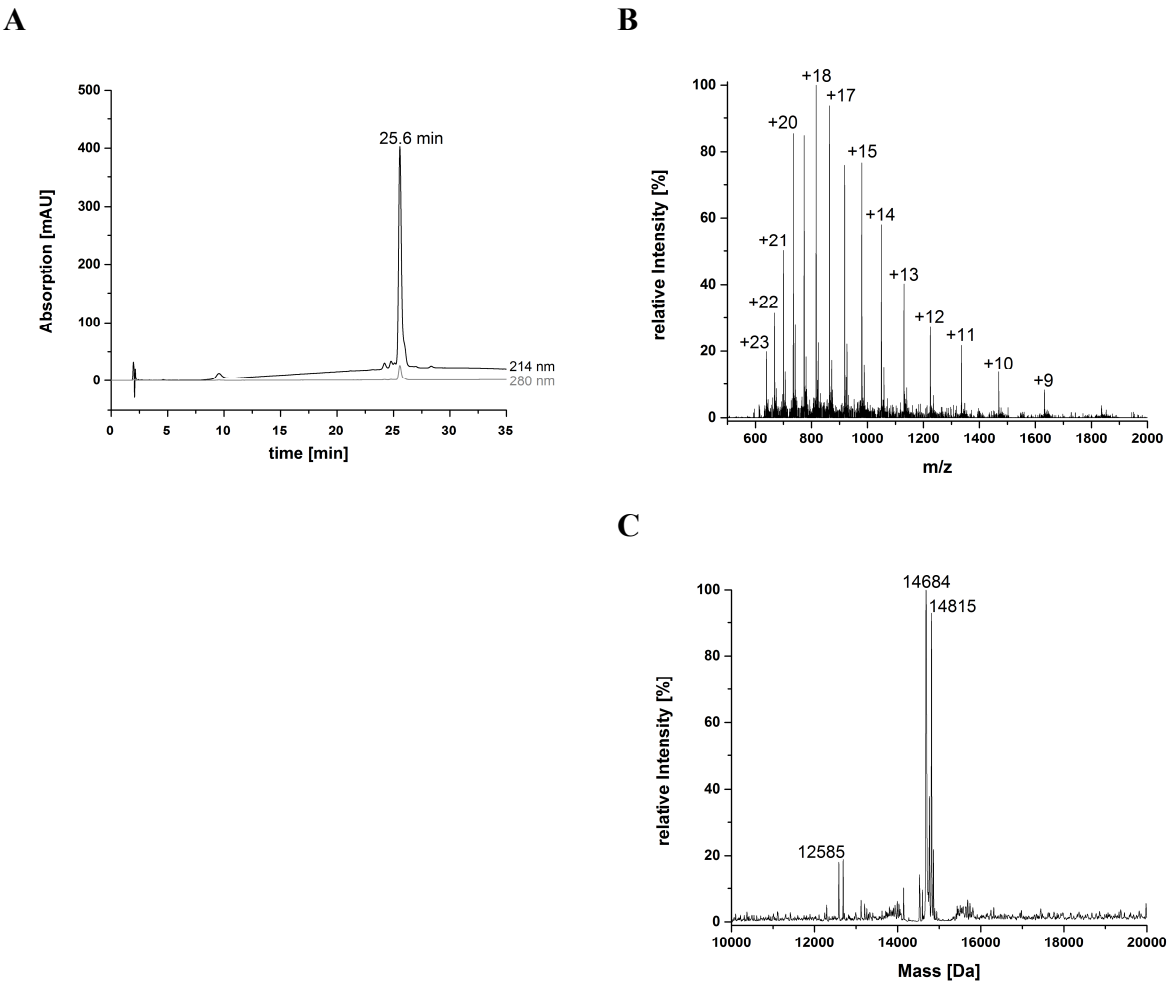

Figure 5-23 Analysis of TRX-**A** conjugate.
A) Analytical RP-HPLC chromatogram of TRX-**A** conjugate
B) Mass spectrum of analytical LC-MS analysis of TRX-**A**.
C) Deconvoluted mass spectrum. Calculated mass for TRX-**A**: 14688 Da; observed masses: 14684 Da; 14815 Da; 12585 Da.

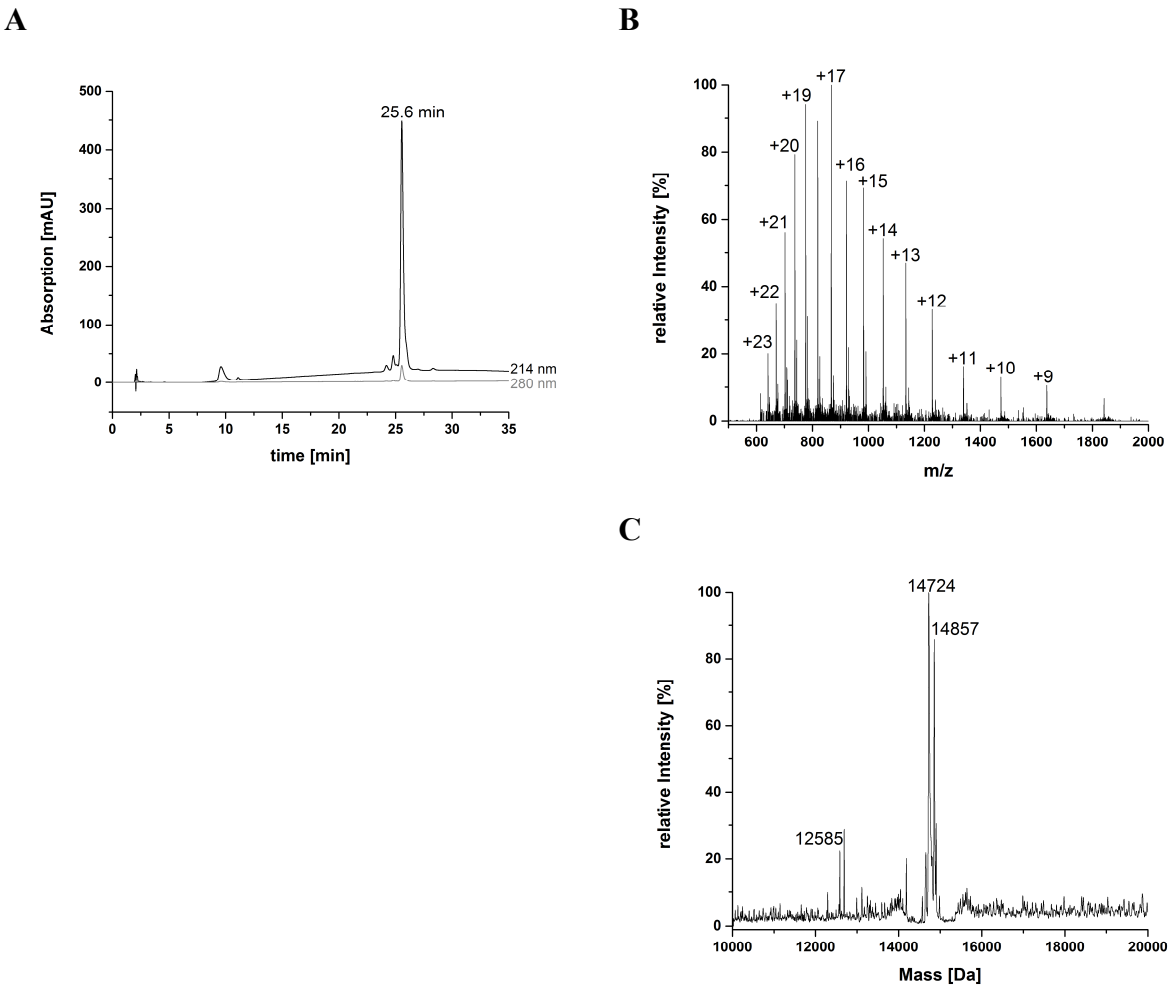

Figure 5-24 Analysis of TRX-**B** conjugate.
A) Analytical RP-HPLC chromatogram of TRX-**B** conjugate.
B) Mass spectrum of analytical LC-MS analysis of TRX-**B**.
C) Deconvoluted mass spectrum. Calculated mass for TRX-**B**: 14731 Da; observed masses: 14724 Da; 14857 Da; 12585 Da.

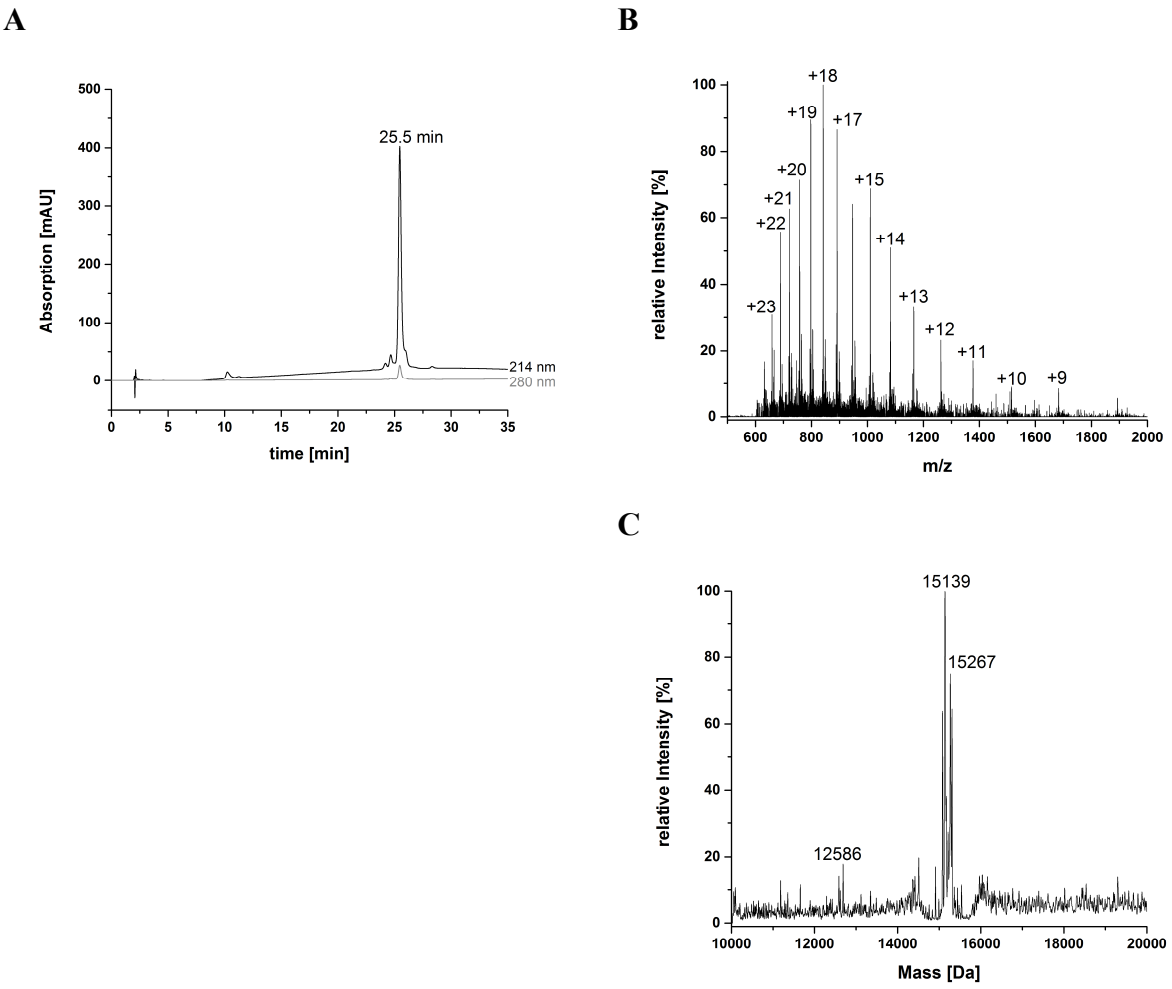

Figure 5-25 Analysis of TRX-**C** conjugate.
A) Analytical RP-HPLC chromatogram of TRX-**C** conjugate
B) Mass spectrum of analytical LC-MS analysis of TRX-**C**.
C) Deconvoluted mass spectrum. Calculated mass for TRX-**C**: 15143 Da; observed masses: 15139 Da; 15267 Da; 12586 Da.

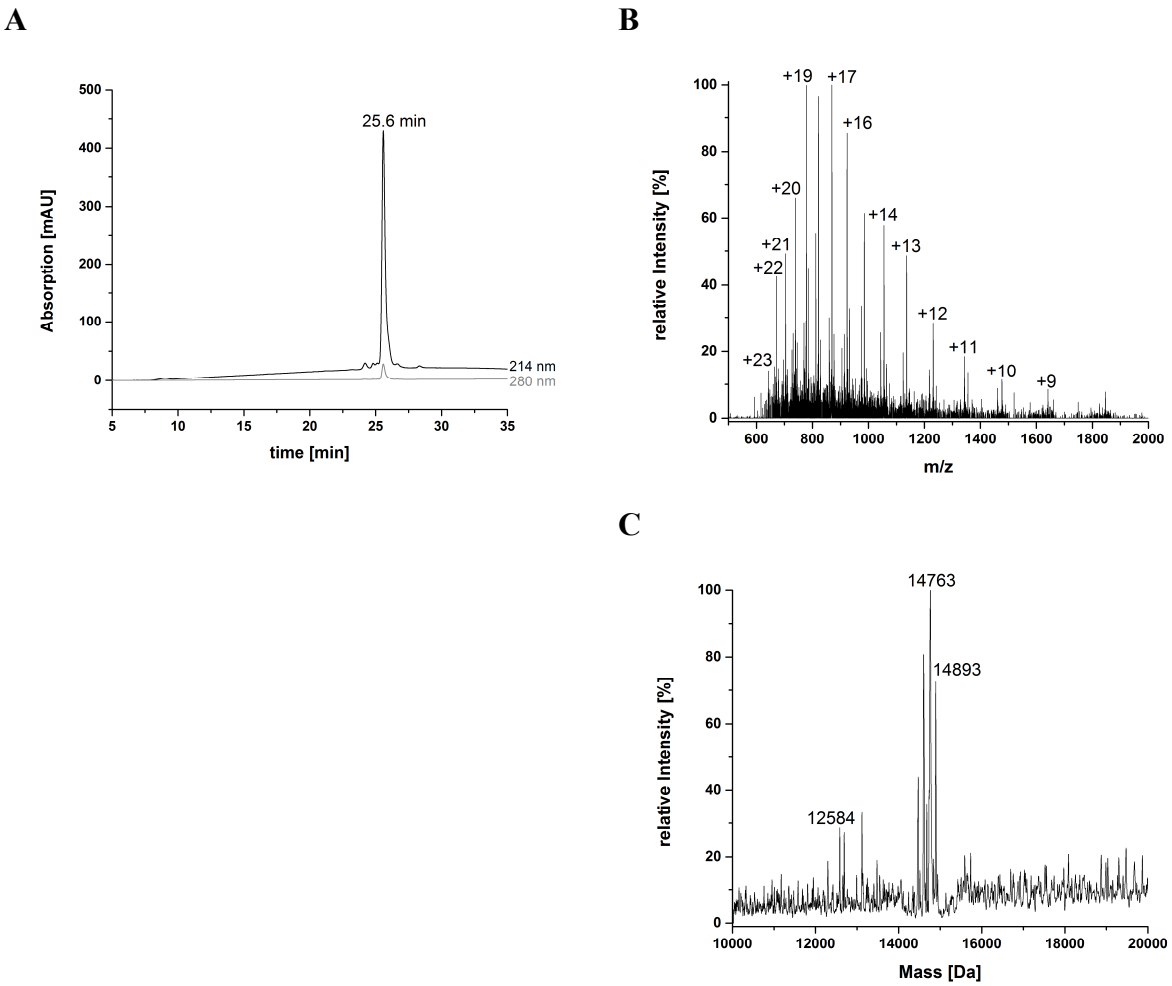

Figure 5-26 Analysis of TRX-**D** conjugate.
A) Analytical RP-HPLC chromatogram of TRX-**D** conjugate
B) Mass spectrum of analytical LC-MS analysis of TRX-**D**.
C) Deconvoluted mass spectrum. Calculated mass for TRX-**D**: 14768 Da; observed masses: 14763 Da; 14893 Da; 12584 Da.

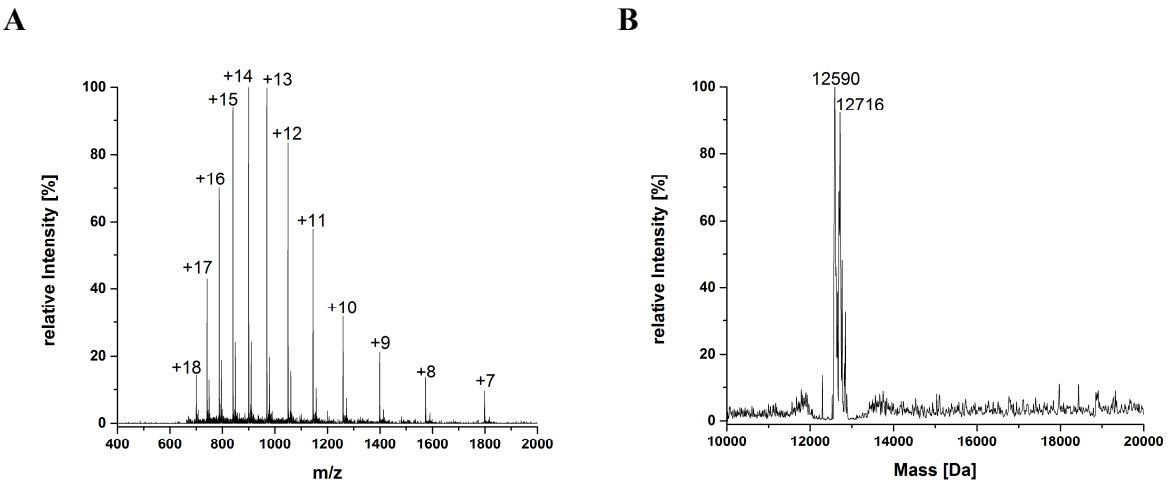

Figure 5-27 Hydrolysis of C-terminal MESNa thioester moiety from TRX.
A) Mass spectrum of analytical LC-MS analysis of TRX after hydrolysis C-terminal MESNa thioester.
B) Deconvoluted mass spectrum. Calculated mass: 12589 Da; observed masses: 12590 Da; 12716 Da.

5.6 References

1 Bornscheuer, U. T. Immobilizing enzymes: How to create more suitable biocatalysts. *Angew. Chem. Int. Ed*. **2003**, *42*, 3336-3337.

2 Tran, D. N.; Balkus Jr, K. J. Perspective of recent progress in immobilization of enzymes. *Acs Catal.* **2011**, *1*, 956-996.

3 Cao, L.; van Rantwijk, F.; Sheldon, R. A. Cross-linked enzyme aggregates: a simple and effective method for the immobilization of penicillin acylase. *Org. Lett.* **2000**, *2*, 1361-1364.

4 Schoevaart, R.; Wolbers, M. W.; Golubovic, M.; Ottens, M.; Kieboom, A. P. G.; van Rantwijk, F.; van der Wielen L. A.; Sheldon, R. A. Preparation, optimization, and structures of cross-linked enzyme aggregates (CLEAs). *Biotechnol. Bioeng.* **2004**, *87*, 754-762.

5 Matijošytė, I.; Arends, I. W.; de Vries, S.; Sheldon, R. A. Preparation and use of cross-linked enzyme aggregates (CLEAs) of laccases. *J. Mol. Catal. B: Enzym.* **2010**, *62*, 142-148.

6 Kresge, C. T.; Leonowicz, M. E.; Roth, W. J.; Vartuli, J. C.; Beck, J. S. Ordered mesoporous molecular sieves synthesized by a liquid-crystal template mechanism. *Nature* **1992**, *359*, 710-712.

7 Wan, Y.; Zhao, D. On the controllable soft-templating approach to mesoporous silicates. *Chem. Rev.* **2007**, *107*, 2821-2860.

8 Wu, K. C. W.; Yamauchi, Y. Controlling physical features of mesoporous silica nanoparticles (MSNs) for emerging applications. *J. Mater. Chem.* **2012**, *22*, 1251-1256.

9 Diaz, J. F.; Balkus Jr, K. J. Enzyme immobilization in MCM-41 molecular sieve. *J. Mol. Catal. B: Enzym.* **1996**, *2*, 115-126.

10 Simpson, T. L.; Volcani, B. E. *Silicon and Siliceous Structures in Biological Systems*, Springer:New York, 1981.

11 De Stefano, L.; Larnberti, A.; Rotiroti, L.; De Stefano, M. Interfacing the nanostructured biosilica microshells of the marine diatom *Coscinodiscus wailesii* with biological matter. *Acta Biomater*. **2008**, *4*, 126-130.

12 Townley, H. E.; Parker, A. R.; White-Cooper, H. Exploitation of diatom frustules for nanotechnology: Tethering active biomolecules. *Adv. Funct. Mater*. **2008**, *18*, 369-374.

13 Gale, D. K.; Gutu, T.; Jiao, J.; Chang, C. H.; Rorrer, G. L. Photoluminescence detection of biomolecules by antibody-functionalized diatom biosilica. *Adv. Funct. Mater*. **2009**, *19*, 926-933.

14 Aw, M. S.; Simovic, S.; Addai-Mensah, J.; Losic, D. Silica microcapsules from diatoms as new carrier for delivery of therapeutics. *Nanomedicine* **2011**, *6*, 1159-1173.

15 Bariana, M.; Aw, M. S.; Kurkuri, M.; Losic, D. Tuning drug loading and release properties of diatom silica microparticles by surface modifications. *Int. J. Pharm.* **2013**, *443*, 230-241.

16 Brunner, E.; Richthammer, P.; Ehrlich, H.; Paasch, S.; Ueberlein, S.; van Pee, K. H. Chitinbased organic networks - An integral part of cell wall biosilica from the diatom *Thalassiosira pseudonana*: *Angew. Chem. Int. Ed*. **2009**, *48*, 9724-9727.

17 Kröger, N.; Deutzmann, R.; Bergsdorf, C.; Sumper, M. Species-specific polyamines from diatoms control silica morphology. *Proc. Natl. Acad. Sci. U. S. A* **2000**, *97*, 14133-14138.

18 Sumper, M.; Brunner, E.; Lehmann, G. Biomineralization in diatoms: characterization of novel polyamines associated with silica. *FEBS Lett.* **2005**, *579*, 3765-3769.

19 Kröger, N.; Bergsdorf, C.; Sumper, M. A new calcium-binding glycoprotein family constitutes a major diatom cell wall component. *EMBO J.* **1994**, *13*, 4676-4683.

20 Kröger, N.; Bergsdorf, C.; Sumper, M. Frustulins: domain conservation in a protein family associated with diatom cell walls. *Eur. J. Biochem.* **1996**, *239*, 259-264.

21 Kröger, N.; Lehmann, G.; Rachel, R.; Sumper, M. Characterization of a 200-kDa diatom protein that is specifically associated with a silica-based substructure of the cell wall. *Eur. J. Biochem.* **1997**, *250*. 99-105.

22 Kröger, N.; Wetherbee, R. Pleuralins are involved in theca differentiation in the diatom *Cylindrotheca fusiformis*. *Protist* **2000**, *151*, 263-273.

23 Wenzl, S.; Hett, R.; Richthammer, P.; Sumper, M. Silacidins: highly acidic phosphopeptides from diatom shells assist in silica precipitation in vitro. *Angew. Chem. Int. Ed*. **2008**, *47*, 1729-1732.

24 Richthammer, P.; Börmel, M.; Brunner, E.; van Pée, K. H. Biomineralization in diatoms: the role of silacidins. *ChemBioChem*, **2011**, *12*, 1362-1366.

25 Scheffel, A.; Poulsen, N.; Shian, S.; Kröger, N. Nanopatterned protein microrings from a diatom that direct silica morphogenesis. *Proc. Natl. Acad. Sci. U. S. A* **2011**, *108*, 3175-3180.

26 Kröger, N.; Deutzmann, R.; Sumper, M. Polycationic peptides from diatom biosilica that direct silica nanosphere formation. *Science* **1999**, *286*, 1129-1132.

27 Kröger, N.; Deutzmann, R.; Sumper, M. Silica-precipitating peptides from diatoms. The chemical structure of silaffin-A from *Cylindrotheca fusiformis*. *J. Biol. Chem.* **2001**, *276*, 26066-26070.

28 Kröger, N.; Lorenz, S.; Brunner, E.; Sumper, M. Self-assembly of highly phosphorylated silaffins and their function in biosilica morphogenesis. *Science* **2002**, *29*, 584-586.

29 Poulsen, N.; Berne, C.; Spain, J.; Kröger, N. Silica immobilization of an enzyme through genetic engineering of the diatom *Thalassiosira pseudonana*. *Angew. Chem. Int. Ed*. **2007**, *46*, 1843-1846.

30 Sheppard, V. C.; Scheffel, A.; Poulsen, N.; Kröger, N. Live diatom silica immobilization of multimeric and redox-active enzymes. *Appl. Environ. Microbiol*. **2012**, *78*, 211-218.

31 Nam, D. H.; Won, K.; Kim, Y. H.; Sang, B. I. A novel route for immobilization of proteins to silica particles incorporating silaffin domains. *Biotechnol. Progr*. **2009**, *25*, 1643-1649.

32 Marner, W. D.; Shaikh, A. S.; Muller, S. J.; Keasling, J. D. Enzyme immobilization via silaffin-mediated autoencapsulation in a biosilica support. *Biotechnol. Progr*. **2009**, *25*, 417-423.

33 Choi, O.; Kim, B. C.; An, J. H.; Min, K.; Kim, Y. H.; Um, Y.; Oh, M. K.; Sang, B. I. A biosensor based on the self-entrapment of glucose oxidase within biomimetic silica nanoparticles induced by a fusion enzyme. *Enzyme Microb. Technol*. **2011**, *49*, 441-445.

34 Luckarift, H. R.; Spain, J. C.; Naik, R. R.; Stone, M. O. Enzyme immobilization in a biomimetic silica support. *Nat. Biotechnol*. **2004**, *22*, 211-213.

35 Naik, R. R.; Tomczak, M. M.; Luckarift, H. R.; Spain, J. C.; Stone, M. O. Entrapment of enzymes and nanoparticles using biomimetically synthesized silica. *Chem. Commun*. **2004**, 1684-1685.

36 Merrifield, R. B. Solid phase peptide synthesis. I. The synthesis of a tetrapeptide. *J. Am. Chem. Soc*. **1963**, *85*, 2149-2154.

37 Hackenberger, C. P.; Schwarzer, D. Chemoselective ligation and modification strategies for peptides and proteins. *Angew. Chem. Int. Ed.* **2008**, *47*, 10030-10074.

38 Dawson, P. E.; Muir, T. W.; Clark-Lewis, I.; Kent, S. B. Synthesis of proteins by native chemical ligation. *Science* **1994**, *266*, 776-779.

39 Raibaut, L.; Ollivier, N.; Melnyk, O. Sequential native peptide ligation strategies for total chemical protein synthesis. *Chem. Soc. Rev.* **2012**, *41*, 7001-7015.

40 Muir, T. M.; Sondhi, D.; Cole, P. A. Expressed protein ligation: A general method for protein engineering. *Proc. Natl. Acad. Sci. U. S. A* **1998**, *95*, 6705-6710.

41 Noren, C. J.; Wang, J.; Perler, F. B. Dissecting the chemistry of protein splicing and its applications. *Angew. Chem. Int. Ed.* **2000**, *39*, 450-466.

42 Yang, T. T.; Cheng, L.; Kain, S. R. Optimized codon usage and chromophore mutations provide enhanced sensitivity with the green fluorescent protein. *Nucleic Acids Res.* **1996**, *24*, 4592-4593.

43 Holmgren, A. Thioredoxin. *Annu. Rev. Biochem.* **1985**, *54*, 237-271.

44 Arnér, E. S.; Holmgren, A. Physiological functions of thioredoxin and thioredoxin reductase. *Eur. J. Biochem.* **2000**, *267*, 6102-6109.

45 Buchanan, B. B.; Adamidi, C.; Lozano, R. M.; Yee, B. C.; Momma, M.; Kobrehel, K.; Ermel, M.; Frick, O. L. Thioredoxin-linked mitigation of allergic responses to wheat. *Proc. Natl. Acad. Sci. U. S. A.* **1997**, *94*, 5372-5377.

46 del Val, G.; Yee, B. C.; Lozano, R. M.; Buchanan, B. B.; Ermel, R. W.; Lee, Y. M.; Frick, O. L. Thioredoxin treatment increases digestibility and lowers allergenicity of milk. *J. Allergy Clin. Immunol.* **1999**, *103*, 690-697.

47 Lozano, R. M.; Yee, B. C.; Buchanan, B. B. Thioredoxin-linked reductive inactivation of venom neurotoxins. *Arch.Biochem.Biophys.* **1994**, *309*, 356-362.

48 Laemmli, U. K. Cleavage of structural proteins during the assembly of the head of bacteriophage T4. *Nature* **1970**, *227*, 680-685.

49 Atherton, E.; Sheppard, R.C. *Solid Phase Synthesis: A Practical Approach*, IRL Press at Oxford Univ. Press, Oxford. 1989.

50 Chu, N. K.; Olschewski, D.; Seidel, R.; Winklhofer, K. F.; Tatzelt, J.; Engelhard, M.; Becker, C. F. Protein immobilization on liposomes and lipid-coated nanoparticles by protein trans-splicing. *J. Pept. Sci.* **2010**, *16*, 582-588.

51 Bradford, M. M. A rapid and sensitive method for the quantitation of microgram quantities of protein utilizing the principle of protein-dye binding. *Anal. Biochem.* **1976**, *72*, 248-254.

52 Iler, R. K. *The Chemistry of Silica*, Wiley: New York, 1979.

53 Wieneke, R.; Bernecker, A.; Riedel, R.; Sumper, M.; Steinem, C.; Geyer, A. Silica precipitation with synthetic silaffin peptides. *Org. Biomol. Chem*. **2011**, *9*, 5482-5486.

54 Holmgren, A. Thioredoxin catalyzes the reduction of insulin disulfides by dithiothreitol and dihydrolipoamide. *J. Biol. Chem.* **1979**, *254*, 9627-9632.

55 LaVallie, E. R.; DiBlasio, E. A.; Kovacic, S.; Grant, K. L.; Schendel, P. F.; McCoy, J. M. A thioredoxin gene fusion expression system that circumvents inclusion body formation in the *E. coli* cytoplasm. *Nat. Biotechnol.* **1993**, *11*, 187-193.

56 Lu, Z.; DiBlasio-Smith, E. A.; Grant, K. L.; Warne, N. W.; LaVallie, E. R.; Collins-Racie, L. A.; Follettie, M. T.; Williamson, M. J.; McCoy, J. M. Histidine Patch Thioredoxins: Mutant forms of thioredoxin with metal chelating affinity that provide for convenient purifications of thioredoxin fusion proteins. *J. Biol. Chem.* **1996**, *271*, 5059-5065.

57 Chong, S.; Mersha, F. B.; Comb, D. G.; Scott, M. E.; Landry, D.; Vence, L. M.; Perler, F. B.; Benner, J.; Kucera, R. B.; Hirvonen, C. A.; Pelletier, J. J.; Paulus, H.;

Xu, M. Q. Single-column purification of free recombinant proteins using a self-cleavable affinity tag derived from a protein splicing element. *Gene* **1997**, *192*, 271-281.

58 Evans, T. C.; Benner, J.; Xu, M. Q. Semisynthesis of cytotoxic proteins using a modified protein splicing element. *Protein Sci*. **1998**, *7*, 2256-2264.

59 Telenti, A.; Southworth, M.; Alcaide, F.; Daugelat, S.; Jacobs, W. R.; Perler, F. B. The *Mycobacterium xenopi* GyrA protein splicing element: Characterization of a minimal intein. *J.Bacteriol.* **1997**, *179*, 6378-6382.

60 Southworth, M. W.; Amaya, K.; Evans, T. C.; Xu, M. Q.; Perler, F. B. Purification of proteins fused to either the amino or carboxy terminus of the *Mycobacterium xenopi* gyrase A intein. *Biotechniques* **1999**, *27*, 110-114.

61 Chen, D.; Texada, D. E. Low-usage codons and rare codons of *Escherichia coli*. *Gene Ther. Mol. Biol.* **2006**, *10*, 1-12.

62 Holmgren, A.; Söderberg, B. O.; Eklund, H.; Brändén, C. I. Three-dimensional structure of *Escherichia coli* thioredoxin-S2 to 2.8 A resolution. *Proc. Natl. Acad. Sci. U. S. A.* **1975**, *72*, 2305-2309.

63 Gleason, F. K.; Lim, C. J.; Gerami-Nejad, M.; Fuchs, J. A. Characterization of *Escherichia coli* thioredoxins with altered active site residues. *Biochemistry* **1990**, *29*, 3701-3709.

64 Ben-Bassat, A.; Bauer, K.; Chang, S. Y.; Myambo, K.; Boosman, A.; Chang, S. Processing of the initiation methionine from proteins: properties of the *Escherichia coli* methionine aminopeptidase and its gene structure. *J. Bacteriol.* **1987**, *169*, 751-757.

65 Prasher, D. C.; Eckenrode, V. K.; Ward, W. W.; Prendergast, F. G.; Cormier, M. J. Primary structure of the *Aequorea victoria* green-fluorescent protein. *Gene* **1992**, *111*, 229-233.

66 Ormö, M.; Cubitt, A. B.; Kallio, K.; Gross, L. A.; Tsien, R. Y.; Remington, S. J. Crystal structure of the *Aequorea victoria* green fluorescent protein. *Science* **1996**, *273*, 1392-1395.

67 Yang, F.; Moss, L. G.; Phillips, G. N. J. The molecular structure of green fluorescent protein. *Nat. Biotechnol*. **1996**, *14*, 1246-1251.

68 Cao, A.; Ye, Z.; Cai, Z.; Dong, E.; Yang, X.; Liu, G.; Deng, X.; Wang, Y.; Yang, S. T.; Wang, F.; Wu, M.; Liu, Y. A facile method to encapsulate proteins in silica nanoparticles: encapsulated green fluorescent protein as a robust fluorescence probe. *Angew. Chem. Int. Ed.* **2010**, *49*, 3022-3025.

69 Nagy, A.; Malnasi-Csizmadia, A.; Somogyi, B.; Lorinczy, D. Thermal stability of chemically denatured green fluorescent protein (GFP): A preliminary study. *Thermochim. Acta* **2004**, *410*, 161-163.

70 Penna, T. C.; Ishii, M.; Junior, A. P.; Cholewa, O. Thermal stability of recombinant green fluorescent protein (GFPuv) at various pH values. *Appl. Biochem. Biotechnol.* **2004**, *113-116*, 469-483.

71 Alkaabi, K. M.; Yafea, A.; Ashraf, S. S. Effect of pH on thermal-and chemical-induced denaturation of GFP. *Appl. Biochem. Biotechnol.* **2005**, *126*, 149-156.

72 Bokman, S. H.; Ward, W. W. Renaturation of Aequorea green-fluorescent protein. *Biochem. Biophys. Res. Commun.* **1981**, *101*, 1372-1380.

73 Williams, R. J.; Phillips, J. N.; Mysels, K. J. The critical micelle concentration of sodium lauryl sulphate at 25 C. *Trans. Faraday Soc.* **1955**, *51*, 728-737.

74 Esposito, C.; Colicchio, P.; Facchiano, A.; Ragone, R. Effect of a weak electrolyte on the critical micellar concentration of sodium dodecyl sulfate. *J. Colloid Interface Sci.* **1998**, *200*, 310-312.

75 Almgren, M.; Swarup, S. Size of sodium dodecyl sulfate micelles in the presence of additives. 3. Multivalent and hydrophobic counterions, cationic and nonionic surfactants. *J. Phys. Chem.* **1983**, *87*, 876-881.

76 Katti, S. K.; LeMaster, D. M.; Eklund, H. Crystal structure of thioredoxin from *Escherichia coli* at 1.68 Å resolution. *J. Mol. Biol.* **1990**, *212*, 167-184.

77 Knecht, M. R.; Wright, D. W.; Functional analysis of the biomimetic silica precipitating activity of the R5 peptide from *Cylindrotheca fusiformis*. *Chem. Commun*. **2003**, 3038-3039.

78 Eby, D. M.; Farrington, K. E.; Johnson, G. R. Synthesis of bioinorganic antimicrobial peptide nanoparticles with potential therapeutic properties. *Biomacromolecules* **2008**, *9*, 2487-2494.

79 Sano, K. I.; Minamisawa, T.; Shiba, K. Autonomous silica encapsulation and sustained release of anticancer protein. *Langmuir* **2010**, *26*, 2231-2234.

80 Sumper, M. A phase separation model for the nanopatterning of diatom biosilica. *Science* **2002**, *295*, 2430-2433.

81 Sanger, F. Fractionation of oxidized insulin. *Biochem. J.* **1949**, *44*, 126-128.

Abbreviations

°C	degree Celsius
Å	Angström
ACN	acetonitrile
ATP	adenosine triphosphate
Boc	*tert*-butyloxycarbonyl
bp	base pairs
BSA	bovine serum albumin
Bzl	benzyl
C. fusiformis	*Cylindrotheca fusiformis*
C. gracilis	*Chaetoceros gracilis*
CBD	chitin binding domain
CDI	1,1'-carbonyldiimidazole
cDNA	complementary deoxyribonucleic acid
CLEA	cross linked enzyme aggregates
cmc	critical micelle concentration
d	day(s)
Da	Dalton
DCM	Dichloromethane
ddH_2O	double distilled water
DIEA	Diisopropylethylamine
DMF	N,N-dimethylformamide
DNA	deoxyribonucleic acid
DNaseI	deoxyribonuclease I
dNTP	deoxyribonucleotide triphosphate
DTNP	2,2'-dithiobis(5-nitropyridine)
DTT	1,4-Dithio-D,L-threitol
dYT	double yeast tryptone
E. coli	*Escherichia coli*
E. zodiacus	*Eucampia zodiacus*
EDTA	ethylenediaminetetraacetic acid

EDX	energy dispersive X-ray
EGF	epidermal growth factor
eGFP	enhanced green fluorescent protein
EGFR	epidermal growth factor receptor
EPL	expressed protein ligation
eq	equivalent(s)
ER	endoplasmatic reticulum
ESI	electrospray ionization
ESI-MS	electrospray ionization-mass spectrometry
Fmoc	Fluorenylmethoxycarbonyl
Gdn/HCl	guanidinium hydrochloride
GRAS	generally recognized as safe
GSH	glutathione (reduced)
h	hour(s)
HBTU	2-(1*H*-benzotriazol-1-yl)-1,1,3,3-tetramethyluronium hexafluorophosphate
HF	hydrogen fluoride
His_6	hexahistidine tag
HOBt	1-Hydroxybenzotriazole
HPLC	high performance liquid chromatography
IPTG	isopropyl-ß-D-thiogalactopyranoside
$K(Me)_3$	epsilon-N,N,N-trimethyllysine
K(Sp)	epsilon-(4-spermidine)succinyllysine
kbp	kilobase pairs
K_D	dissociation constant
kDa	kilo dalton
kV	kilo volt
LC-MS	liquid chromatography-mass spectrometry
LCPA	long chain polyamine
LMW	low molecular weight
M	relative molecular mass

MCM	Mobile Crystalline Material
MESNa	sodium 2-mercaptoethanesulfonate
min	minute(s)
MS	mass spectrometry /mass spectrum
MSN	mesoporous silica nanoparticle
Mtt	Methyltrityl
MW	molecular weight
MW_{calc}	calculated molecular weight
MW_{obs}	observed molecular weight
MWCO	Molecular weight cut off
Mxe	*Mycobacterium xenopii*
NADPH	Nicotinamide adenine dinucleotide phosphate hydrogen
NaOAc	sodium acetate
NaPi	sodium phosphate
NBD	7-nitro-2,1,3-benzoxadiazole
NCL	native chemical ligation
Ni-NTA	nickel-nitrilotriacetic acid
Npys	3-nitro-2-pyridinesulfenyl
OD_{600}	optical density at 600 nm
ODT	1,8-octanedithiol
PAA	Polyallylamine
PAM	Phenylacetamidomethyl
PBS	phosphate buffered saline
PCR	polymerase chain reaction
PEI	Polyethyleneimine
PG	protecting group
PLA	poly-L-arginine
PLL	poly-L-lysine
pNpys	5-nitro-2-pyridinesulfenyl
PPI	Polypropyleneimine
pS	Phosphoserine

PTM	posttranslational modification
R5	unmodified, repetitive unit 5 from silaffin $1A_1$
RP	reversed phase
RP-HPLC	reversed phase-high performance liquid chromatography
rpm	revolutions per minute
RT	room temperature
S. turris	*Stephanopyxis turris*
SBA	Santa Barbara Amorphous
SDS	sodium dodecylsulfate
SDS-PAGE	sodium dodecylsulfate-polyacrylamide gel electrophoresis
SDV	silica deposition vesicle
S-DVB	styrene-divinylbenzene
SEM	scanning electron microscopy
SERS	surface enhanced raman spectroscopy
SIT	silicic acid transporter protein
SPPS	solid phase peptide synthesis
S*t*Bu	*tert*-butylthio
T. pseudonana	*Thalassiosira pseudonana*
*t*Bu	*tert*-butyl
TCEP	tris(2-carboxyethyl)phosphine
TFA	trifluoroacetic acid
TIS	Triisopropylsilane
TMOS	Tetramethoxysilane
tpSilxp	silaffin precursor polypeptides from *T. pseudonana*
tpSTK1	serine/threonine kinase from *T. pseudonana*
Tris	tris(hydroxymethyl-)aminomethane
Trt	Trityl
TRX	Thioredoxin
UV	Ultraviolet
v/v	volume per volume
Vis	Visible

w/v	weight per volume
ε	extinction coefficient

One- and three letter code of the 20 canonical amino acids

Alanine	A	Ala
Arginine	R	Arg
Asparagine	N	Asn
Aspartic acid	D	Asp
Cysteine	C	Cys
Glutamine	Q	Gln
Glutamic acid	E	Glu
Glycine	G	Gly
Histidine	H	His
Isoleucine	I	Ile
Leucine	L	Leu
Lysine	K	Lys
Methionine	M	Met
Phenylalanine	F	Phe
Proline	P	Pro
Serine	S	Ser
Threonine	T	Thr
Tryptophan	W	Trp
Tyrosine	Y	Tyr
Valine	V	Val

Acknowledgment

At first, I would like to thank Prof. Christian Becker for giving me the opportunity to work on this exciting and very fruitful project. I am very grateful for his excellent supervision, all the support and independency in pursuing my own ideas I experienced during my thesis.

In addition, I would also like to express my gratitude to the members of my thesis committee, Prof. Dr. Dr. h. c. Bernhard Rieger, Prof. Dr. Aymelt Itzen and Prof. Dr. Michael Groll.

I appreciate the financial support from the Institute of Silicon Chemistry, TUM and the Wacker Chemie AG. I would like to acknowledge Dr. Manfred Amann for the regular meetings and helpful discussions.

I am grateful to Prof. Dr. Sevil Weinkauf and Dr. Marianne Hanzlik (Institute of Electron Microscopy, TUM) and Dr. Stephan Puchegger (Faculty Center for Nanostructure Research, University of Vienna) for giving me access to and assistance with the electron microscopes.

I want to thank Susanne Hilber and Michaela Cherrier for their invaluable help with all administrative matters.

Thanks to all my current and former colleagues of the Becker lab, for the support, discussions, practical help and the good atmosphere in and outside of the lab. In particular, many thanks to Katja and Manuel for their continuous effort to keep the labs and equipment running.

Special and cordial thanks to my “MPAT”-girls, my Bro and my “L-office” mates, for your continuous encouragement, support and friendship. I couldn’t have done it without you.
Many thanks also to my friends and roommates. Thank you for listening, giving me helpful advice and supporting me through all the years.

Finally, but most importantly, I would like to thank my family, all of you: My parents Friedrich and Brigitte, my grandparents, my brother Christian with Nadja, Samia and Evelyn, my sister Claudia with Julian and Anna, and Nico. You made my smile even at difficult times. Thanks for your faith in me, your encouragement and unconditional support during all the years!

Publications

Peer-reviewed articles

1. Lechner, C. C.; Becker, C. F. W. Modified silaffin R5 peptides enable encapsulation and release of cargo molecules from biomimetic silica particles. *Bioorg. Med. Chem*. **2013**, *21*, 3533-3541.
2. Lechner, C. C.; Becker, C. F. W. Exploring the effect of native and artificial peptide modifications on silaffin induced silica precipitation. *Chem. Sci*. **2012**, *3*, 3500-3504.

Manuscripts in preparation

1. Lechner, C. C.; Becker, C. F. W. A sequence-function analysis of silica precipitating silaffin R5 peptide.
2. Lechner, C. C.; Becker, C. F. W. Silica immobilization of an enzyme using chemically modified silaffin peptides.

Conference contributions

1. Lechner, C. C.; Becker, C. F. W. Silica precipiating silaffin peptides: Versatile tools for biotechnological applications. 5th Chemical Protein Synthesis Meeting 2013, Vienna, Austria. Poster presentation (Poster Presentation Prize).
2. Lechner, C. C.; Becker, C. F. W. Silica precipiating silaffin peptides: Versatile tools for biotechnological applications. 2nd Austrian Peptide Symposium 2013, Vienna, Austria. Oral and poster presentation (Best Poster Award).
3. Lechner, C. C.; Becker, C. F. W. Complex modified silaffin peptides: Versatile tools for efficient enzyme immobilization. In *Peptides 2012*, Proceedings of the 32nd European peptide symposium, Athens, Greece, September 2-7, 2012; Kokotos, G., Constantinou-Kokotou V., Matsoukas J., Eds.; pp. 330-331.
4. Lechner, C. C.; Becker, C. F. W. Complex modified silaffin peptides: Versatile tools for efficient enzyme immobilization. 32nd European Peptide Symposium 2012, Athens, Greece. Poster presentation.

5. Lechner, C. C.; Becker, C. F. W. Immobilization of biomolecules by silaffin-directed biomineralization. 1st Munich Forum on Functional Materials 2011, Garching, Germany. Poster presentation.
6. Lechner, C. C.; Becker, C. F. W. Immobilization of biomolecules by silaffin-directed biomineralization. 10th German Peptide Symposium 2011, Berlin, Germany. Poster presentation.
7. Lechner, C. C.; Becker, C. F. W. Immobilization of biomolecules by silaffin-directed biomineralization. 4th Conference on Probing Protein Function through Chemistry 2009, Schloss Ringberg Tegernsee, Germany. Poster presentation.

Declaration

I, Carolin Lechner, hereby declare that I independently prepared the present thesis, using only the references and resources stated. This work has not been submitted to any examination board yet. Parts of this work have been or will be published in scientific journals.

Hiermit erkläre ich, Carolin Lechner, dass ich die vorliegende Arbeit selbständig verfasst und keine anderen als die angegebenen Quellen und Hilfsmittel verwendet habe. Die Arbeit wurde noch keiner Prüfungskommission vorgelegt. Teile dieser Arbeit wurden bzw. werden in wissenschaftlichen Journalen veröffentlicht.

Wien, 01.10.2013

Carolin Lechner